Reconstructing Mid-Late Holocene Climate and Environmental Change in Antarctica using Glycerol Dialkyl Glycerol Tetraethers (GDGTs) and Pigments in Lake Sediments

Louise Claire Foster

Submitted in Accordance with the Requirements for the Degree of Doctor of Philosophy

School of Geography, Politics and Sociology

August 2015

Abstract

Assessing the impact of past phases of natural warming on climatically sensitive areas, such as Antarctic and sub-Antarctic regions, will help us better understand the impact that climate warming may have in the future. In recent decades, the Antarctic Peninsula has been one of the fastest warming regions on Earth, warming at a rate of 3.4 °C per century, five times the global mean. Several phases of marked environmental change have occurred on the Antarctic Peninsula during the mid-late Holocene nonetheless, to date quantitative temperature reconstructions of terrestrial climates are not possible.

GDGTs are one of few existing quantitative temperature proxies and recent developments of their use in lakes indicates their potential as a temperature proxy. Prior to application the relationship between GDGT-composition and several environmental factors, such as temperature, pH and conductivity, in Antarctic and sub-Antarctic lakes was assessed. Temperature explained a statistically significant independent control on the composition of branched GDGTs in the lakes and a new regional Antarctic and sub-Antarctic GDGT-temperature calibration was developed. Within this calibration, GDGT-IIIb was a statistically significant component indicating its importance in these environments.

Applying the new GDGT-temperature calibration to sediment cores from Fan Lake, South Georgia and Yanou Lake, South Shetland Islands allowed the quantitative reconstruction of past temperatures during the Mid to Late-Holocene. The reconstructions showed varied temperatures throughout the records, evidencing the mid-Holocene warm period, and potentially the Medieval Climate Anomaly and Little Ice Age. Neither record, however, reconstructed the recent rapid warming seen in the glacial meltwater and instrumental records. A comparison of Fan Lake and Yanou Lake with other records from Antarctica and Chile showed periods of coherence between records alongside periods of inconsistency. This comparison also enabled potential changes in the PFZ to be considered, suggesting a more poleward position of the PFZ during warmer climates.

Acknowledgements

First and foremost, I would like to thank my supervisors, both at Newcastle University and the British Antarctic Survey (BAS); Dr. Stephen Roberts, Dr. Emma Pearson, Prof. Stephen Juggins and Prof. Dominic Hodgson for their invaluable help, support, knowledge and discussions over the last three and a half years. I would also like to thank an additional supervisor Dr. Kathryn (Kate) Manzo for her pastoral support.

I would like to thank Emma for her time and patience whilst I learnt how to extract and analyse GDGTs and Steve J for his invaluable input as I learnt how to use R. I would also like to thank both Steve R and Dominic for their complete and ongoing support throughout my PhD, particularly during my many visits to BAS and following my move to Cambridge to write up.

My sincerest gratitude goes to Dr. Helen Talbot and Frances Sidgwick for their unfailing determination to run the GDGT samples on the LCMS despite a multitude of problems they have encountered over the last three years. I would also like to thank all the technical staff at both Newcastle University and BAS who have helped with the laboratory work. I must also thank the administrative and support staff at both Newcastle University and BAS for their help and advice and the Natural Environment Research Council (NERC) for funding my PhD.

There are a wealth of others whom without their generous donation of Antarctic lake sediment samples or data from previously undertaken analysis my thesis would not have been possible. Thanks go to Dr. Elie Verleyen, Dr. Krystyna Saunders, Dr. Emma Hocking, Wim Van Nieuwenhuyze and many others who either provided sediments or were involved in the field campaigns during which samples were collected. Also thanks go to Wim Van Nieuwenhuyze for making his Fan Lake pigment and diatom data available and Prof. Melanie Leng for running the carbon isotope analysis.

On a personal note I would like to thank all of my friends, office mates at both Newcastle and BAS and my many housemates for their support and friendship. I can’t name you all but two people in particular who must be thanked are Becky Hair and Kathryn Lacey. Becky your friendship and support during my first year in Newcastle was invaluable, as was your role in getting me back into the swimming pool – you’ve no idea how important that was! Kathryn, likewise, for the last two years your

friendship, support and encouragement has been truly amazing despite your ridiculously busy schedule you've always had time to listen.

Special thanks go to my Mum, Dad and brother who have all been a rock to me not only throughout my PhD but also every step of the way to this point. My final thanks go to my husband William, who has spent literally hundreds of hours on the train travelling between Plymouth and Newcastle visiting me during my time in Newcastle, that's not to say I haven't done the same! But William, your love, support and encouragement has been truly invaluable over the last seven years, especially during the tough times when you have picked me up again and helped me get through, so thank you.

Table of Contents

List of Figures

Chapter 4

Chapter 6

Chapter 7

Chapter 8

List of Tables

Chapter 9

Chapter 1: Introduction

Summary

This chapter first summarises the aims and objectives of the thesis and how these aims will be achieved. The chapter then gives an introduction to the current climate of Antarctica, specifically the Antarctic Peninsula, and why an understanding of past climates is needed here. Proxy archives available to reconstruct past climates are also introduced briefly, with more details found in Chapter 4. Finally, the thesis structure is outlined.

1.1. Rationale

Parts of the Southern Ocean and the Antarctic Peninsula (Fig. 1.1) are among the fastest warming regions on Earth, with temperatures on the Antarctic Peninsula increasing at a rate of 3.4 °C per century, five times the global mean (Hodgson *et al*., 2006b; Heroy *et al*., 2008). In addition, over the last 50 years meteorological records from the Antarctic Peninsula show an even more accelerated increase in temperature of 1.09 °C per decade in austral winter months (Barnard *et al*., 2014). Nevertheless, the detailed history of Antarctic climate change is only partly known (Wagner *et al*., 2011) yet, the effects of such warming are evidenced through an acceleration in the intensity and duration of summer melting by up to 74% since 1950 (Vaughan, 2006), the recession of snowfields and glaciers (Cook *et al*., 2005), and a reduction in the duration of sea-ice cover (Parkinson, 2002). Recent warming has also been linked to the retreat (and/or collapse) of several ice shelves including the Larsen Ice Shelf A and B on the Antarctic Peninsula that have both collapsed since 1995 (Roberts *et al*., 2008). To gain a better understanding of the mechanisms related to on-going ice retreat and sea level rise due to climatic changes a knowledge of past change is indispensable (Wagner *et al*., 2011).

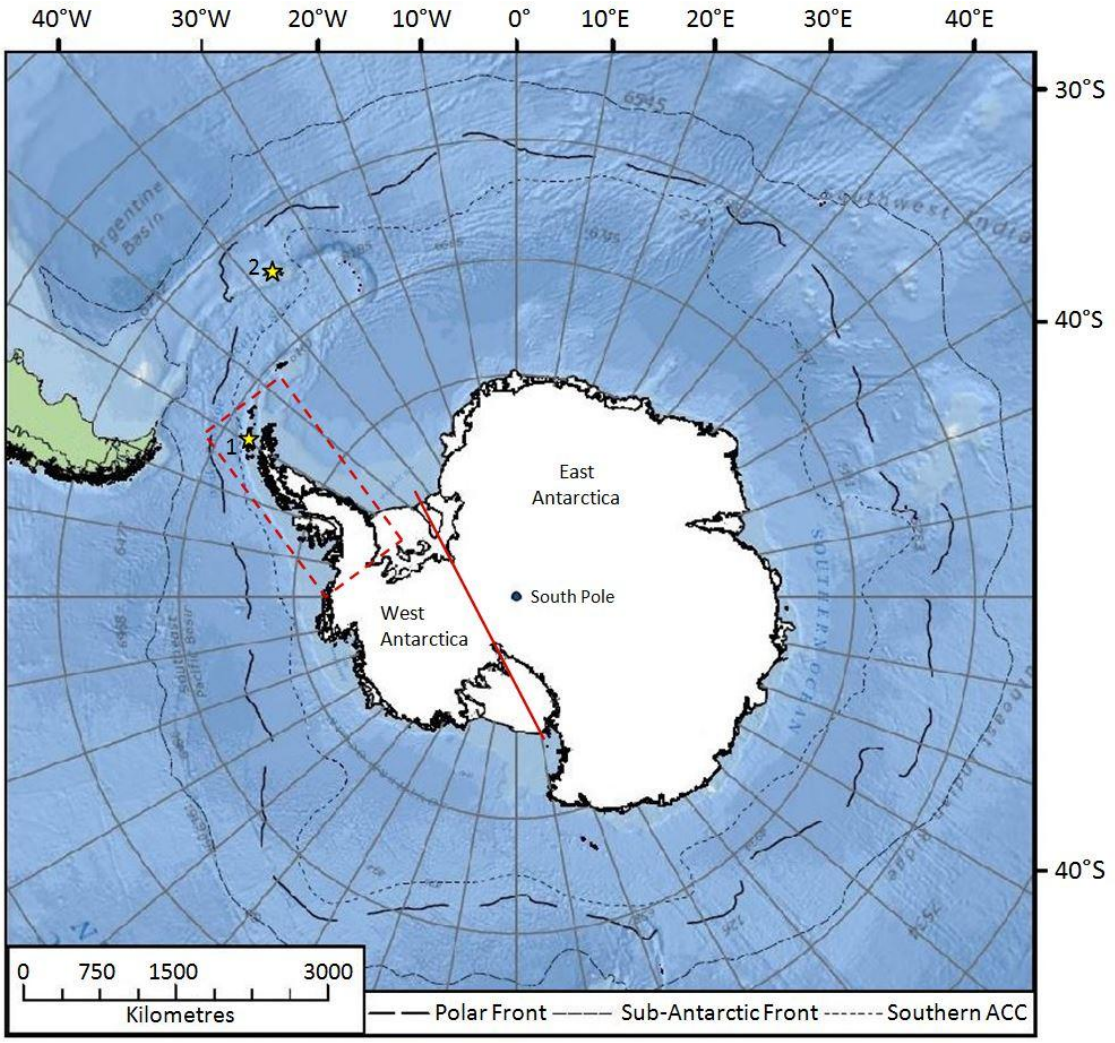

Figure 1.1: Map of Antarctica showing the division between West and East Antarctica. The red box indicates the Antarctic Peninsula. The location of the South Shetland Islands (1) and South Georgia (2) are highlighted with yellow stars.

The climates of the Antarctic Peninsula and the sub-Antarctic islands of the Southern Ocean are strongly influenced by the position and strength of the Polar Frontal Zone (PFZ; Fig. 1.1) which encircles Antarctica forming a key climatic barrier between Antarctica and the mid-latitudes. Therefore, long-term changes in the position of the PFZ are crucial to understanding climate change in Antarctica and how Antarctica and the Southern Ocean influence both regional and global climates. Within the region of the PFZ the Antarctic Peninsula and sub-Antarctic islands such as South Georgia (54°S, 36°W) are of particular interest. Birnie (1990) suggests that understanding environmental change in these areas is important for three reasons. Firstly, their location within the oceanic zone of the Southern Ocean provides much needed terrestrial data for the area. Second, their position relative to the Southern Westerly Winds (SWW) permits a typical representation of global atmospheric and oceanic circulation. Finally, the

location of the islands provide an ideal place to study the climatic connections between temperate and polar environments in the Southern Hemisphere (Clapperton *et al*., 1989; Birnie, 1990; Rosqvist and Schuber, 2003; Van der Putten *et al*., 2009).

One advantage of studying these environments is that, due to a limited amount of human impact during the Holocene, natural rather than anthropogenic climatic changes can be assessed (Jones *et al*., 2000). Nonetheless, the palaeoenvironmental record for these regions lacks a reliable temperature proxy for terrestrial environments, which has hampered reconstructions with previous work based on qualitative reconstructions (e.g., Björck *et al*., 1991; 1993; 1996; Jones *et al*., 2000; Rosqvist and Schuber, 2003). The aim of this research is to provide the first quantitative temperature reconstruction from lake sediment cores for the mid-late Holocene, the last c. 6000 years. The mid-late Holocene is of particular interest as evidence of several climatic shifts, including the mid-Holocene warm period between c. 4500 and 2500 cal yr B.P., have been recorded on the Antarctic Peninsula and sub-Antarctic Islands (e.g., Rosqvist and Schuber, 2003; Van der Putten *et al*., 2004; Bentley *et al*., 2009; Mulvaney *et al*., 2012; Strother *et al*., 2015) but currently the amplitude of this warming is unknown. A quantitative temperature reconstruction based on glycerol dialkyl glycerol tetraethers (GDGTs) will give an understanding of the amplitude of the mid-Holocene warm period and enable the recent warming seen on the Antarctic Peninsula to be put in to perspective.

1.2. Research Objectives

1. Develop the use of glycerol dialkyl glycerol tetraethers (GDGTs) as indicators of palaeotemperature in Antarctic lakes.
2. Reconstruct changes in mid-late Holocene temperatures in Antarctic lakes.
3. Compare records along the Polar Frontal Zone (PFZ) transect to reconstruct changes in the position of the PFZ during the Holocene and how variations in the PFZ relate to climatic changes.
4. Compare temperature records from Antarctic Lakes with indicators of primary productivity to identify if temperature is the main driver of primary productivity in these environments.

To address these aims the GDGT composition of surface samples (top 0-2 cm) from 32 lakes across Antarctica, the sub-Antarctic Islands and Chile are analysed to determine the primary control on GDGT composition. An Antarctic and sub-Antarctic GDGT-temperature calibration is developed in Chapter 6 based on the relationship between

individual GDGT compounds and temperature. In Chapter 7 and 8 the new Antarctic and sub-Antarctic GDGT-temperature calibration is applied to two sediment cores from Fan Lake, South Georgia and Yanou Lake, South Shetland Islands respectively. A comparison between these two palaeotemperature records and other palaeoenvironmental records is made in Chapter 9 allowing an assessment of changes in the PFZ during the mid-late Holocene. Finally, comparing the GDGT-temperature record with pigments, and other proxies of primary productivity i.e. diatoms and total organic carbon (TOC) content, is done to determine if temperature is the main driver of primary productivity in Fan Lake and Yanou Lake, also in Chapter 9.

1.3. Proxies used to reconstruct palaeoenvironments

The reconstruction of past climate variability is imperative for predicting future responses to climatic change based on climatic models (e.g., Powers *et al*., 2004; Hatté *et al*., 2009; Goosse *et al*., 2010). The addition of palaeoenvironmental data to existing climatic models will not only help validate these models, but also provide new model parameters which will improve their accuracy. Proxy records often used to gather qualitative and quantitative climate reconstructions include; pollen (e.g., Björck *et al*., 1991; Reuss *et al*., 2010; Strother *et al*., 2015), foraminifera (e.g., Jian *et al*., 1999; Pudsey *et al*., 2006; Chapori *et al*., 2015), pigments (e.g., Vincent *et al*., 1993; Squier *et al*., 2002; Hodgson *et al*., 2005; Fernandez-Carazo *et al*., 2013), diatoms (e.g., Spaulding *et al*., 1997; Esposito *et al*., 2006; Watcham *et al*., 2011), chironomids (e.g., Larocque *et al*., 2001; van Asch *et al*., 2011; Reinemann *et al*., 2014) and lipid biomarkers (e.g., Niemann *et al*., 2012; Woltering *et al*., 2014; Heyng *et al*., in press). Changes in pollen indicate changes in vegetation type or cover which can be linked to changes in climatic conditions (Björck *et al*., 1991; Liew *et al*., 2006; Hatté *et al*., 2009; Strother *et al*., 2015). Alternatively, the chemical composition of a foraminiferal test can be used as an indicator of climate (Jian *et al*., 1999; Pudsey *et al*., 2006; Chapori *et al*., 2015). However, when foraminifera or diatoms, for example, are no longer preserved biomarkers can provide an additional means to identify the presence of these organisms in the past (Castañeda and Schouten, 2011). Biomarkers are individual compounds, or compound classes, preserved in sediments which can be traced to a source organism, group of organisms, or to a particular process, e.g., photosynthesis (Peters *et al*., 2005; Castañeda and Schouten, 2011). Therefore, biomarkers allow the identification of certain algal groups or other microorganisms when they are no longer present as intact fossils or microfossils (Castañeda and Schouten, 2011).

One example of a lipid biomarker group are glycerol dialkyl glycerol tetraethers (GDGTs). GDGTs are one of few existing quantitative temperature proxies. The development of GDGTs as a temperature proxy can be found in Chapter 4. GDGTs have previously been successfully used to reconstruct past temperature changes in oceans (Schouten *et al*., 2002), soils (e.g., Weijers *et al*., 2006b; 2007a; Peterse *et al*., 2012) and lake sediments (e.g., Blaga *et al*., 2010; Powers *et al*., 2010; Pearson *et al*., 2011; Loomis *et al*., 2012; Woltering *et al*., 2014). Nevertheless, to date, these methods have not been widely applied especially in high latitude lacustrine environments due to poor performance of the GDGT-temperature calibrations at lower temperatures (Shanahan *et al.* 2013; Colcord *et al.* 2015). Another example is pigments which can also be used to reconstruct past environments in lake sediments. The identification of individual pigments or pigment groups can be used to infer specific environmental conditions such as water depth (e.g., Cantonati *et al*., 2014), allochthonous organic matter input (e.g., Buchaca and Catalan, 2007) lake acidification (e.g., Leavitt *et al*., 1999) and climatic changes (e.g., Reuss *et al*., 2010; Sterken *et al*., 2012). A combination of all of these proxies enables well evidenced palaeoenvironmental reconstructions to be made.

1.4. Thesis Structure

Chapter 2 gives a detailed background into the current knowledge of Holocene climate change from a global scale to more regional specific reconstructions. Current understanding of the changes in the PFZ during the Holocene are also outlined. Chapter 3 introduces Antarctica, the different regions of the Antarctic studied and the reasons the surface and two downcore sites were chosen. Chapter 4 focuses on GDGTs and pigments, the two main methods in this research, the development of both proxies and previous applications. Chapter 5 details the methodologies used, including those for GDGTs, pigments and other techniques previously undertaken on the cores. Chapters 6 to 8 are the results and discussion chapters. Chapter 6 contains the development of the Antarctic and sub-Antarctic GDGT-temperature calibration model from the surface sediments. Chapter 7 contains the results of the application of the new GDGT-temperature calibration at Fan Lake and compares the reconstruction with other data from Fan Lake and previous palaeoclimate reconstructions from South Georgia. Chapter 8 focuses on Yanou Lake and the GDGT-temperature reconstruction in relation to other Yanou Lake records and those from elsewhere on the South Shetland Islands. Chapter 9 contains a wider discussion comparing Fan Lake and Yanou Lake to one another and to

other palaeoclimate records from elsewhere in Antarctic and Chile. A comparison between GDGT-temperatures and productivity is also made in Chapter 9. Finally, Chapter 10 concludes the research revisiting the aim and objectives, highlighting key findings and possible future research.

Chapter 2: A Summary of Holocene Climate Change from a Global to Regional Scale

Summary

This chapter provides a review of the current knowledge of Holocene climates, the last 11,700 years. Firstly, on a global scale and then more regionally specific on the Antarctic Peninsula, South Georgia and the South Shetland Islands where previous research indicates warmer conditions at c. 9600 cal. yr B.P., between 4500 and 2800 cal. yr B.P. and since 500 cal. yr B.P. interspersed with colder conditions. The final section of the chapter focuses on the PFZ and SWW and how changes in their position could influence climate thus influencing Holocene climates.

2.1. Holocene Global Climates

Much Quaternary research to date has focused on climatic change particularly during the last glacial and interglacial periods. As a consequence multiple climatic events have been identified during the last 20000 years. Shakun and Carlson (2010) list four Northern Hemisphere climatic events; Heinrich Event 1 (c. 17500 – 16000 cal. yr B.P.), Oldest Dryas cold period (c. 18000-14700 cal. yr B.P.), Bølling/Allerød warm period (c. 14700 – 12900 cal. yr B.P.) and Younger Dryas cold period (c. 12900 – 11700 cal. yr B.P.) and one Southern Hemisphere climatic event, the Antarctic Cold Reversal (c. 15000 – 13000 cal. yr B.P.). The Bølling/Allerød warm period and Antarctic Cold Reversal indicate an antiphase in the temperature of the two hemispheres known as the thermal bipolar seesaw (Brown *et al*., 2007). This thermal bipolar seesaw is thought to be influenced by the redistribution of heat as a consequence of changes in oceanic currents, such as a weakening Atlantic Meridional Overturning Circulation (Shakun and Carlson, 2010). Therefore, although these climatic events are pre-Holocene they give an insight into how the two hemispheres are coupled.

High resolution of records during the Holocene, the last 11,700 years, has enabled the identification of smaller, more frequent, climatic changes compared to lower resolution records of the last glacial period (Mayewski *et al*., 2004). Evidence for climatic variability has been found in various archives, including ice (e.g., Stenni *et al*., 2010; Masson-Delmotte *et al*., 2011; Mulvaney *et al*., 2012; Sime *et al*., 2013), lacustrine (e.g., Hodgson *et al*., 2005; Bertrand *et al*., 2008; Strother *et al*., 2015) and marine cores (e.g., Leventer *et al*., 2006; Michalchuk *et al*., 2009; Krossa *et al*., 2015), in both

Hemispheres. Studying 50 globally distributed palaeoclimate records, Mayewski *et al*. (2004) found evidence of six periods of rapid climate change, during the Holocene at, c. 9000 – 8000, 6000 – 5000, 4200 – 3800, 3500 – 2500, 1200 – 1000, and 600 – 150 cal. yr. B.P. In 73 globally distributed proxy records, Marcott *et al*. (2013) found evidence of an early Holocene warming between c. 10000 and 5000 cal. yr B.P. followed by a cooling of around 0.7 °C during the mid to late Holocene, c. 5000 cal. yr B.P. to present. The palaeoclimate reconstructions of nine Southern Hemisphere records from Mayewski *et al*. (2004) are illustrated in Figure 2.1.

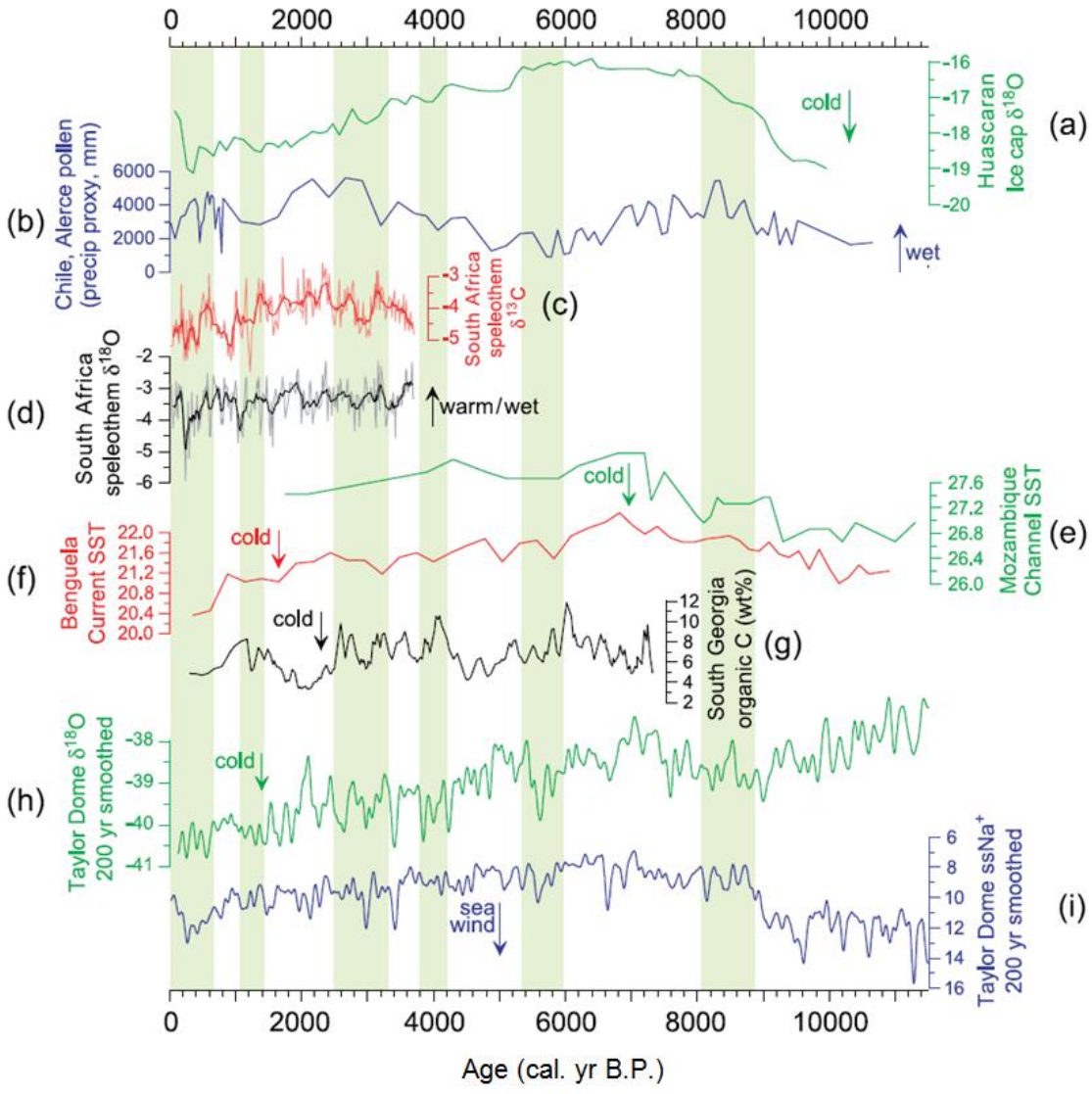

Figure 2.1: Southern Hemisphere climate records arranged by latitude. The green columns indicate periods of rapid climate change. Figure taken from Mayewski *et al*. (2004) where details of individual datasets can be found.

While global trends can be inferred, variations when comparing regions, or even the hemispheres, are often seen (Fig 2.2). For example, as temperatures in the North Atlantic indicate a period of cooling of 2 °C from c. 7000 to 100 cal. yr B.P., a slight warming of c. 0.4°C was recorded in the low latitudes between c. 11000 and 5000 cal. yr B.P. followed by more stable climatic conditions (Marcott *et al*., 2013). Marcott *et al*. (2013) also present evidence of a c. 0.4 °C cooling between c. 11000 and 7000 cal. yr B.P. in the Southern Hemisphere after which temperature remained relatively constant until strong multi-centennial variability was recorded post c. 2500 cal. yr B.P. Global climate reconstructions therefore appear to be heavily skewed by the larger temperature changes seen in the North Atlantic as there are relatively few Holocene climate records from Southern Hemisphere compared with the Northern Hemisphere. Marcott *et al*. (2013) used 11 Southern Hemisphere, 33 low latitudes and 29 Northern Hemisphere records and only nine of 50 records from Mayewski *et al*. (2004) were of Southern Hemisphere origin.

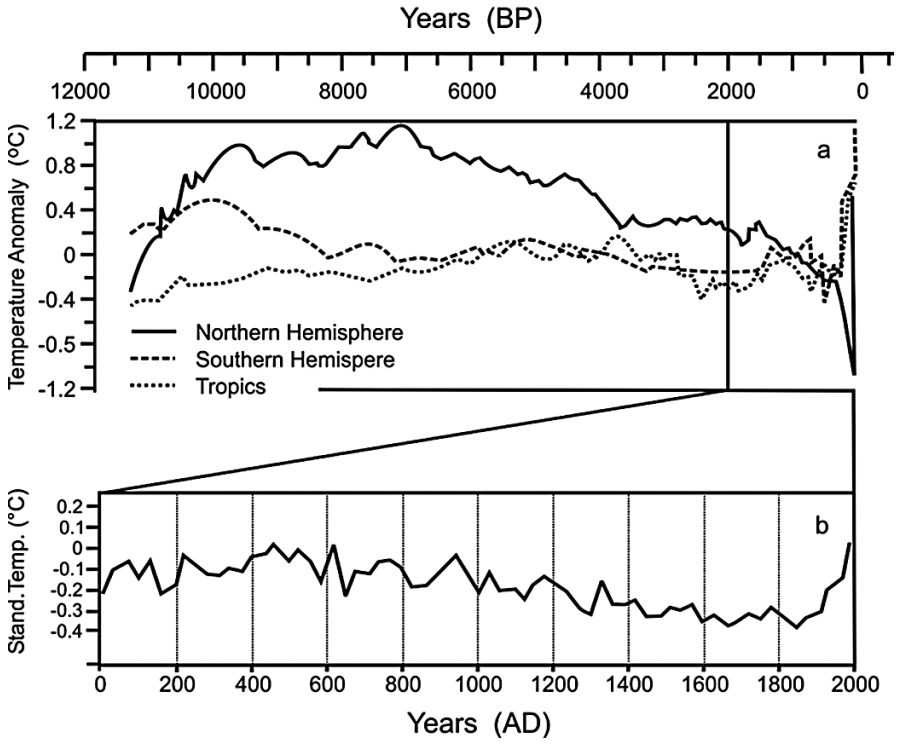

Figure 2.2: Reconstructions of average Holocene climates; a) average Holocene temperatures from the Northern Hemisphere (solid), Southern Hemisphere (dashed) and the tropics (dotted), b) 30 year averaged global temperatures for the last 2000 years. Figure taken from Wanner *et al*. (2014).

Palaeoclimate records from the high-latitudes of the Southern Hemisphere, south of 60°S, not only show evidence of climate optima during both the early and mid Holocene but also indicate that the region has undergone a linear decrease in

temperature of 1 °C between c. 9000 cal. yr B.P. and present (Renssen *et al*., 2005). Within these records, the greatest cooling, of more than 1.5 °C, occurred in the Bellingshausen Sea between 70 and 120°W and over the Atlantic sector of the Southern Ocean between 0 and 30°E (Renssen *et al*., 2005). Renssen *et al*. (2005) also state that, throughout continental Antarctica, this cooling trend varies between 1 °C in West Antarctic and less than 0.5 °C on East Antarctica indicating a differential between the climates of the two regions. However, these cooling trends are punctuated by periods of relatively warm conditions on the Antarctic Peninsula and sub-Antarctic Islands e.g. the early Holocene climate optimum between c. 11000 and 9000 cal. yr B.P. (Bentley *et al*., 2005; 2009; Heroy *et al*., 2008) and the mid-Holocene warm period between c. 4500 and 2500 cal. yr B.P. (e.g., Rosqvist and Schuber, 2003; Van der Putten *et al*., 2004; Bentley *et al*., 2009; Mulvaney *et al*., 2012; Strother *et al*., 2015).

To delimit these periods of abrupt climate change a large amount of evidence has been collected. One commonly used approach to environmental reconstructions is the analysis of pollen and macrofossil species distributions; however, these are relatively sparse in Antarctica. Stable isotopes, pigments and diatoms can also be used to reconstruct changes in glacial extent (e.g., Moreno *et al*., 2010), marine and lake ice cover (e.g., Yoon *et al*., 2000; Milliken *et al*., 2009) and relative sea level to be reconstructed (e.g., Hall, 2010; Watcham *et al*., 2011). Nonetheless, as well as reconstructing when climate changed it is equally important to determine the mechanisms behind these changes. Renssen *et al*. (2005) argue this stating it is imperative to understand the mechanisms forcing such changes to consider projected climatic variations. One forcing mechanism of global and regional trends is thought to be orbital variations (Mayewski *et al*., 2004) which has been suggested due to the cyclic nature of well documented event intervals of about 2800 – 2000 and 1500 years (Bond *et al.,* 1997; Wanner *et al*., 2008). On an Antarctic Peninsula and sub-Antarctic island scale, the position and strength of the PFZ is thought to be closely related to climate, see Section 2.3 for details.

2.1.1. Early Holocene

After the last glacial maximum (c. 22000 – 19000 cal. yr B.P.) and the Younger Dryas (c. 12900 – 11700 cal. yr B.P.), the early Holocene (c. 11700 – 8000 cal. yr B.P.) is characterised by climatic warming with a cooling event affecting the Northern Hemisphere at c. 8200 cal. yr B.P. (e.g., Tinner and Lotter, 2001; Thomas *et al*., 2007).

This early Holocene warming is seen in pollen and charcoal evidence from Sayram Lake in northern Xinjiang, China which is indicative of a warm and dry climate prior to c. 9600 cal. yr B.P. (Jiang *et al*., 2013). Bentley *et al*. (2005) also recorded a period of retreat of the George VI Ice Shelf on the Antarctic Peninsula between c. 10000 and 8000 cal. yr B.P. consistent with the early Holocene climate optimum and Birks *et al*. (2014) saw evidence of rapid warming following the Younger Dryas from c. 11500 cal. yr B.P. to a maximum at c. 9700 cal. yr B.P. on Andøya, northern Norway.

Following the early Holocene climate optimum, northern hemisphere climate reconstructions indicate a period of general cooling between 9000 and 8000 cal. yr B.P. evidenced through major ice rafting and strengthened atmospheric circulation over the North Atlantic and Siberia (Mayewski *et al*., 2004). A rapid cooling of c. 6 °C in an ice core from Greenland was reconstructed at c. 8200 cal. yr B.P. as well as cooling in ice cores from Kilimanjaro by Thompson *et al*. (2002) and dry, cold conditions on the Loess Plateau in China between 12000 and 8500 cal. yr B.P. (Tan *et al*., 2015).

In the Southern Hemisphere, in particular in Antarctica, marine and lacustrine records show the complex nature of Holocene climates (Renssen *et al*., 2005), with East and West Antarctica experiencing different conditions (Mayewski *et al*., 2004). Early Holocene austral summer temperatures were cooler than present in the East Antarctic by up to 0.5 °C but as much as 1.5 °C warmer in West Antarctica (Renssen *et al*., 2005). Nevertheless, as well as being recorded on the Antarctic Peninsula (Bentley *et al*., 2009), the early Holocene thermal optimum is well documented in isotopic evidence in East Antarctic ice cores between c. 12000 and 9000 cal. yr B.P. (e.g. Masson *et al*., 2000; Masson-Delmotte *et al*., 2011). Renssen *et al*. (2005) also noted a differential between the Southern Ocean and continental land mass temperatures, in that the ocean winter temperatures were 3.5 °C higher but the continental temperatures only 0.5 °C warmer. This oceanic-continental differential could explain why West Antarctica, with a greater coastline to landmass ratio, thus greater oceanic influence, warmed at a faster rate.

2.1.2. Mid Holocene

During the mid-Holocene (8000 – 4000 cal. yr B.P.), the orbital forcing that drove the warming of the early Holocene weakened causing the Intertropical Convergence Zone to shift southwards causing a cooling trend over the Northern Hemisphere and weakening of the Afro-Asian summer monsoon causing aridity in subtropical Africa

and Asia (Wanner *et al*., 2008). In the Northern Hemisphere there was a period of abrupt climate change between 6000 and 5000 cal. yr B.P. causing North Atlantic ice rafting events (Bond *et al*. 1997), strengthened westerly winds over the North Atlantic and Siberia (Meeker and Mayewski, 2002) and alpine glacier advance (Mayewski *et al*., 2004). In northern Xinjiang, China, pollen evidence from Sayram Lake also suggests a wetter, colder climate between ca. 5500 and 3400 cal. yr B.P. (Jiang *et al*., 2013). Nevertheless, Tan *et al*.'s (2015) pollen, organic matter and $\delta^{13}C$ derived reconstruction saw evidence of wetter but warmer conditions between 8500 and 3100 cal. yr B.P. on the Loess Plateau to the south east of Xinjiang.

Mayewski *et al*. (2004) summarise the mid-Holocene in the Southern Hemisphere as a period of generally lower temperatures, superimposed on a long-term trend of increasing summer insolation, during which time New Zealand glaciers advance and southern Africa sea surface temperatures were generally cool. In Antarctica, ice and lacustrine sediment records indicate conditions as warm as, or warmer than, present (e.g., Bentley *et al*., 2009; Stenni *et al*., 2010; Mulvaney *et al*., 2012) which Mayewski *et al*. (2004) correlate to increased southern summer insolation. In addition, during the mid-Holocene there was a second climatic optimum in Antarctica (e.g., Rosqvist and Schuber, 2003; Van der Putten *et al*., 2004; Bentley *et al*., 2009; Mulvaney *et al*., 2012; Strother *et al*., 2015) during which time Renssen *et al*. (2005) suggest temperatures could have increased to 3 °C above the preindustrial mean in West Antarctica. However, the timing of the mid-Holocene warm period is spatially variable recorded between 7000 and 5000 cal. yr B.P. in the Ross Sea terminating earlier than in East Antarctica, 3000 cal. yr B.P. (Renssen *et al*., 2005). Nevertheless, several different timings for the mid-Holocene warm period have been proposed for East Antarctica; 4000 to 3000 cal. yr B.P. (Roberts *et al*., 2004) and 8500 to 6000 cal. yr B.P. (Wagner *et al*., 2007). On the Antarctic Peninsula the mid-Holocene warm period occurred between c. 4500 and 2800 cal. yr B.P. (Bentley *et al*., 2009). The different timing of the mid-Holocene warm period gives an insight into the complexity of Holocene temperature evolution in and around Antarctica.

2.1.3. Late Holocene

During the late Holocene, 4000 cal. yr B.P. to present, Mayewski *et al*. (2004) describes widespread generally warmer conditions punctuated with cold events. Marcott *et al*. (2013) recorded the coolest late Holocene temperatures in the North Atlantic during the

Little Ice Age (LIA) c. 200 cal. yr B.P. Nevertheless, the general climatic trend throughout the last 1500 years is of unprecedented warming (Marcott *et al*., 2013). This trend has been noted on a global scale with Wanner *et al*. (2008) stating that global mean temperatures are thought to have been higher since 1990 than any other time over the last 1000 years.

In the Northern Hemisphere, the late Holocene was characterised by warming during the Medieval Climate Anomaly (MCA) between c. 1100 and 700 cal. yr B.P. and the cooling of the LIA between c. 500 and 100 cal. yr B.P. (Mann *et al*., 2009; Ljungqvist, 2010; Diaz *et al*., 2011). A multiproxy approach by Ljungqvist (2010) using marine, lake and ice cores and speleothems suggests that during the MCA temperature could have increased to temperatures comparable with twentieth century warming. While during the LIA colder conditions have been inferred from higher water levels in Lake Estanya, northeast Spain (Morellón *et al*., 2011) while Larocque and Smith (2003) identified period of glacial advance through dating moraine-building episodes at Mount Waddington, Canada. Despite the LIA, Mayewski *et al*. (2004) indicated that, since 600 cal. yr. B.P. climatic changes have been the fastest and strongest onset of any in the Holocene, possibly with the exception of the warming c. 8200 cal. yr B.P.

In the Southern Hemisphere conditions during the late Holocene were similar to those of the mid Holocene (Mayewski *et al*., 2004). In many records the mid-Holocene warm period extends into the late Holocene terminating as late as c. 2500 cal. yr B.P. (e.g., Rosqvist and Schuber, 2003; Van der Putten *et al*., 2004; Bentley *et al*., 2009; Mulvaney *et al*., 2012; Strother *et al*., 2015). Renssen *et al*. (2005) also found evidence of a maximum warming occurring between 5000 and 3000 cal. yr B.P. along the East Antarctic coastline in marine and lacustrine cores. Bentley *et al*. (2009) also show evidence of the MCA between c. 1200 and 600 cal. yr B.P. and recent rapid warming since 1950 AD on the Antarctic Peninsula. In addition, the LIA is also evidenced in some marine records from the Antarctic Peninsula between c. 500 and 100 cal. yr B.P. (e.g., Shevenell *et al*., 1996; 2011). Although, recent warming has been identified in some West Antarctic meteorological data records from East Antarctica show little or no evidence of warming (Turner *et al*., 2005a).

2.2. Holocene Climates in Antarctica

2.2.1. Antarctic Peninsula

Climate proxy records from the Antarctic Peninsula indicate that this has been an area which has undergone marked climatic variability over the Holocene (Noon *et al*., 2003), with some of the most rapid periods of climatic warming in recent history (Taylor *et al*., 2001; Michalchuk *et al*., 2009). During the twentieth century the Antarctic Peninsula has undergone period of ice shelf retreat and collapse (Bentley *et al*., 2005) with an area of more than 14,000 km^2 disappearing within the past two decades (Hodgson *et al*., 2006b). Nevertheless, the past few decades have not been the only time during the Holocene when there have been periods of ice shelf retreat or collapse. Most notably, lake sediment archives indicate that around 9595 cal. yr. B.P. the George VI Ice Shelf (GVI-IS), which is present today, was absent but reforming once again about 7945 cal. yr. B.P. (Bentley *et al*., 2005). This is indicative of a warmer climate implying that the present-day ice shelf retreat is not unprecedented and has occurred previously in the Holocene (Hodgson *et al*., 2006b). Furthermore, as the GVI-IS is present today it may be that at the time of collapse the climate was warmer than present. In fact Smith *et al*. (2007) found that prior to the collapse of GVI-IS lake environments were similar to present in that they were perennially ice-covered, fresh water dominated, largely unproductive and contained locally derived sediment.

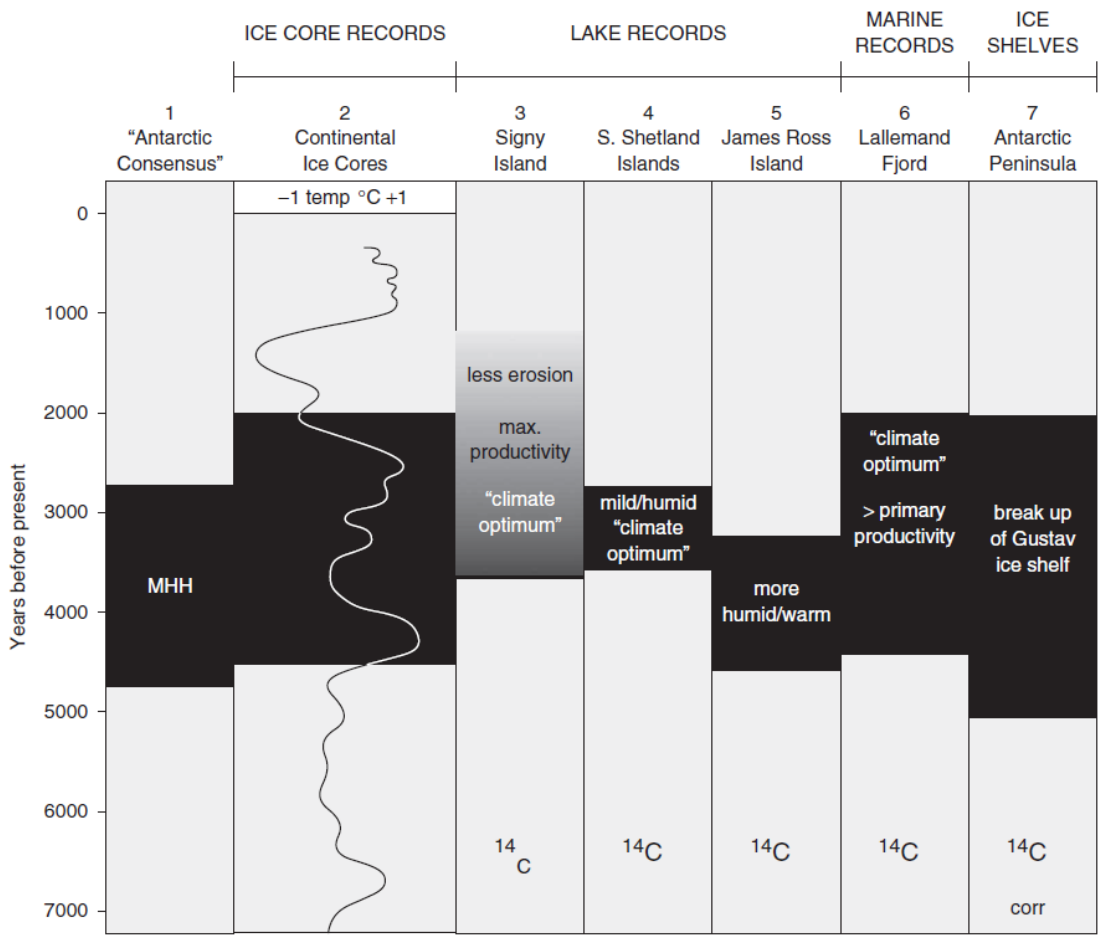

Figure 2.3: A 7000 year climate synthesis of Antarctic Peninsula records showing the variation in the timing of the mid-Holocene warm period in the region. Figure taken from Bentley *et al*. (2009) where details of individual datasets can be found.

Evidence of another warm period during the mid-Holocene is well documented on the Antarctic Peninsula (Fig. 2.3). Hodgson *et al*. (2013) reconstruct warmer conditions in diatom and $\delta^{13}C$ and macrofossil evidence from lake records in Marguerite Bay between c. 6200 and 2030 cal. yr B.P. In the Firth of Tay Michalchuk *et al*. (2009) also identified a period of glacial retreat and less extensive sea ice cover between 4500 – 3500 cal. yr B.P. and in lakes from the Prince Gustav Channel, north-eastern Antarctic Peninsula Sterken *et al*. (2012) reconstructed warmer conditions between c. 3170 and 2120 cal. yr B.P. Following the mid-Holocene period, Neoglacial conditions were reconstructed in Marguerite Bay by Hodgson *et al*. (2013) from c. 2630 cal. yr B.P. in Narrows Lake and c. 2030 cal. yr B.P. in Col Lake 1. A period of climatic deterioration was also evident in the Prince Gustav Channel between c. 2120 and 540 cal. yr B.P. (Sterken *et al*., 2012). Nevertheless, there is some evidence of the MCA, seen through a reduction in total organic carbon in Lallemand Fjord (Domack *et al*., 2003), and LIA, evidenced in organic content and GDGT records from Palmer Deep (Shevenell *et al*., 1996; 2011).

The last 500 years on the Antarctic Peninsula have been characterised as a period of general warming. Hodgson *et al*. (2013) saw increased sedimentation rates and increased organic content in Col Lake 1 and Narrows Lake after c. 400 and 410 cal. yr B.P. respectively, which they infer as a period of warming. In addition, Sterken *et al*. (2012) saw large ecological changes in top c. 5 cm of a lake core from Prince Gustav Channel suggesting climatic warming since c. 540 cal. yr B.P.

2.2.2. South Shetland Islands

The South Shetland Islands lay to the north of the Antarctic Peninsula and south of the Antarctic Convergence at 62 – 63°S, 58 – 61°W. They are thus ideally located for documenting the nature and timing of climatic fluctuations in Antarctica (Hall, 2010). Nevertheless, like much of Antarctica, there have been relatively few studies and therefore there is little data concerning climate change in this region. Most of the research on the South Shetland Islands has focused on the mapping of the glacial history of the islands which indirectly relates to relative climates over time. Although relative sea level curves are well documented for the Ross Sea region of Antarctica, they are uncommon for the Antarctic Peninsula region (Hall, 2010). Hence, Watcham *et al*. (2011) focus on the use of lake sediments and identifying the marine-freshwater transitions to measure relative sea level (RSL) during the Holocene in the South Shetland Islands thus creating a RSL curve for the area.

Watcham *et al*. (2011) successfully used diatom records to reconstruct periods of marine and freshwater influence within lake sediments from Yanou, Long, Ardley and Belén Lakes on the King George Island of the South Shetland Islands. Watcham *et al*. (2011) reconstructed deglaciation to have occurred between c. 11,000 and 9000 cal. yr. B.P. leading to a RSL highstand. Evidence of this highstand comes from the presence of marine diatoms within the sediment cores from Ardley and Belén Lakes (Watcham *et al*., 2011). Marine diatoms are present in Long Lake until 7360 cal. yr. B.P. and Yanou until 7200 cal. yr. B.P. at which time they become isolated from the sea indicating a decrease in the RSL (Watcham *et al*., 2011).

Terrestrial palaeoclimate records for the South Shetland Islands are predominantly based on the work of Björck *et al*. (1991; 1993) who qualitatively analysed palaeoenvironmental change in Midge Lake and Lake Åsa on Livingstone Island. They reconstructed a mid-Holocene warm period through peaks in sediment accumulation, pollen concentration and changes in diatom assemblage between c. 3200 and 2700 and

3000 and 2700 cal. yr B.P. respectively. A period of climatic deterioration followed the mid-Holocene warm period in both records punctuated by a brief warm period at c. 2000 cal. yr B.P. in Midge Lake (Björck *et al*., 1991; 1993). Evidence of recent warming on the South Shetland Islands is limited due to the low resolution nature of previous archives, however, although Björck *et al*. (1991; 1993) reported milder conditions in core top samples. Further details regarding the evidence of mid-late Holocene climate change on the South Shetland Islands can be found in Chapter 8, Section 8.1.

2.2.3. South Georgia

South Georgia is located in the southern Atlantic Ocean c. 1300 km east of the Falkland Islands (Roberts *et al*., 2010). Current palaeoclimate records for South Georgia are based on palynological and sedimentological data from Fan Lake, on Annenkov Island to the south of South Georgia (Strother *et al*., 2015) and macrofossil records from lakes on the north of the island at Tønsberg Peninsula and Kanin Point, at Stromness Bay (Van der Putten *et al*. 2004; 2009) and reconstruction of glacial extent from organic content in Block Lake (Rosqvist and Schuber, 2003).

The Holocene climate of South Georgia has been one of gradual warming and deglaciation. Rosqvist *et al*. (1999) use lake sediments from the Tønsberg Peninsula, Stromness Bay to provide a minimum date of deglaciation of 18,600 cal. yr. B.P. on South Georgia. Hence during the Holocene the general climatic trend in South Georgia has been one of deglaciation, although there have been multiple millennial-scale climatic features superimposed upon this trend. Mid-late Holocene palaeoclimatic reconstructions show evidence of warm periods such as the mid-Holocene warm period between c. 4500 and 2600 cal. yr B.P. (e.g., Rosqvist and Schuber, 2003; Van der Putten *et al*., 2004; Strother *et al*., 2015) and MCA at c. 800 cal. yr B.P. (e.g., Clapperton *et al*., 1989; Strother *et al*., 2015; Van Nieuwenhuyze *et al*., in prep) interspersed with colder conditions after the mid-Holocene warm period from c. 2500 cal. yr B.P. (e.g., Birnie, 1990; Rosqvist and Schuber, 2003; Van der Putten *et al*., 2009; Strother *et al*., 2015) and during the LIA (Van Nieuwenhuyze *et al*., in prep). Further details regarding the evidence of mid-late Holocene climate change on South Georgia can be found in Chapter 7, Section 7.1.1.

2.3. The Polar Frontal Zone

The Polar Frontal Zone (PFZ) encircles Antarctica forming a key climatic barrier between Antarctica and the mid-latitudes (Fig. 1.1). The Antarctic PFZ can be considered as both an atmospheric and oceanic entity. The atmospheric Polar Front is the boundary between the polar cell (60 – 90°S) and the Ferrel Cell (30 – 60°S) which includes the Southern Westerly Winds (SWW) whereas, the oceanic Polar Front forms the southern boundary of the PFZ along the northern edge of the Antarctic Circumpolar Current (ACC). Trathan *et al*. (1997) describe the oceanic form of the PFZ as being a phenomenon in which cold, northward flowing surface waters of the Antarctic sink below the warm, saline sub-Antarctic waters. Abbott *et al*. (2001) further define the PFZ as a complex set of meandering jets, which appear to enhance primary productivity. Fig. 2.4 shows the position of the different components of the oceanic PFZ as it passes through the Drake Passage between the Antarctic Peninsula and southern Chile. Noon *et al*. (2003) define the atmospheric PFZ as a circumpolar low-pressure trough which influences temperature, air pressure, wind, precipitation and sea-ice distribution.

Whether the PFZ is considered an oceanic or atmospheric phenomenon, both ocean and atmospheric circulations are linked through ocean surface waters and both play a key role in climate. For example, the intensity of the SWW means that they not only have a strong impact on the atmospheric circulation but also on oceanic circulation, in particular the ACC (Anderson *et al*., 2009; Hodgson and Sime, 2010; Moreno *et al*., 2010). As a consequence of wind-driven upwelling, the SWW influence the carbon balance between the ocean and atmosphere (Hodgson and Sime, 2010) and are thought to play a key role in global atmospheric CO_2 variations (Fletcher and Moreno, 2011; 2012). As well as influencing the ocean-atmosphere carbon balance, the SWW also affect the climate of the Southern Hemisphere landmasses south of 30°S (Fletcher and Moreno, 2012).

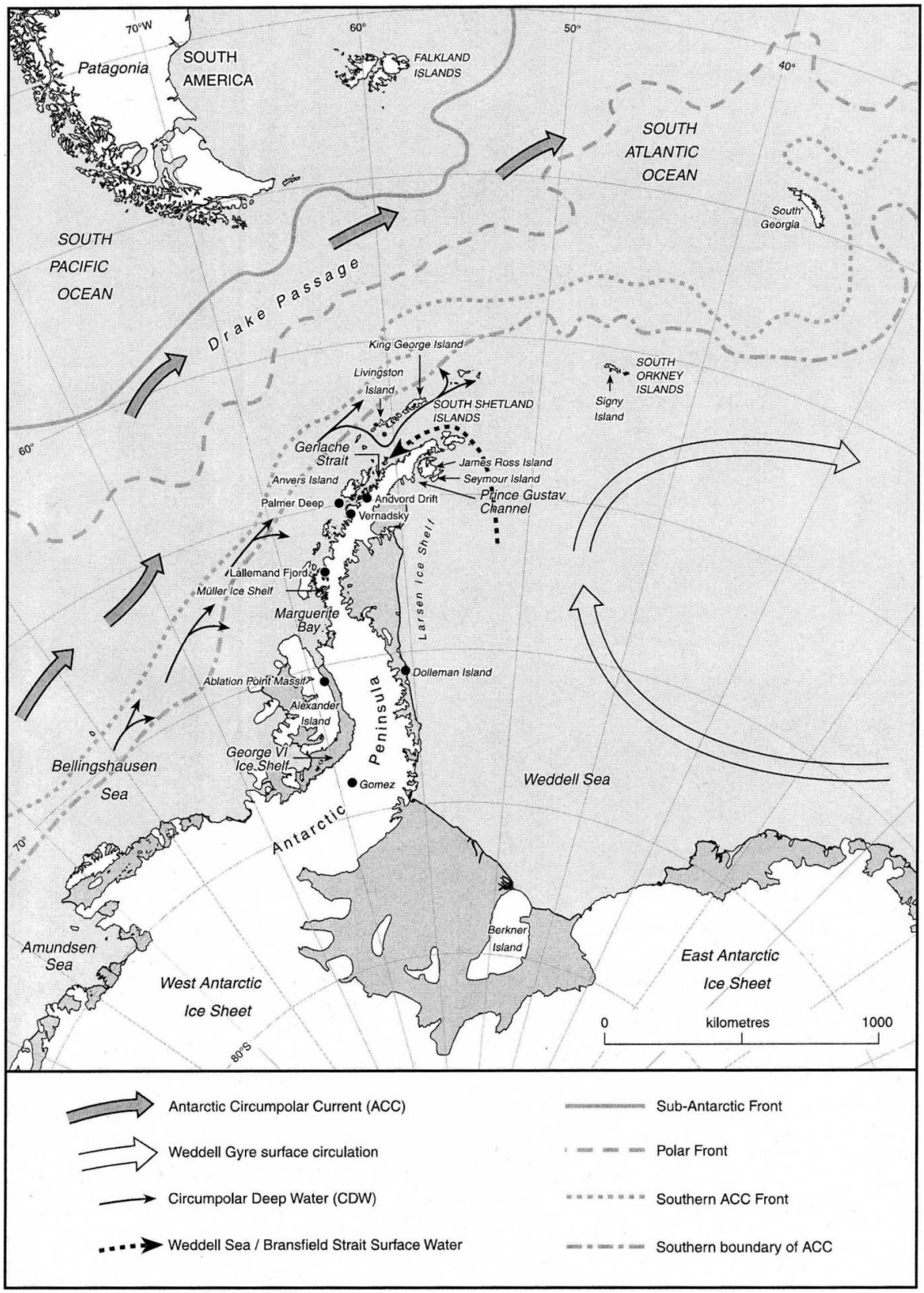

Figure 2.4: The position of the oceanic circulation around the Antarctic Peninsula and through Drakes Passage (Bentley *et al.*, 2009).

2.3.1. The Atmospheric Polar Frontal Zone

The atmospheric PFZ is influenced heavily by the SWW. The SWW are the strongest time-averaged oceanic winds in the world (Hodgson and Sime, 2010) travelling from west to east in middle latitudes between the high pressure systems of the subtropics and low pressure of the poles (Toggweiler, 2009). The SWW are driven by this equator to pole pressure and thermal gradient and variations in this gradient lead to changes in the intensity and latitudinal position of the wind belt (Fletcher and Moreno, 2011). As a consequence, the winds influence the globe between 30 and 60°S (Noon *et al*., 2003; Böning *et al*., 2008; Moreno *et al*., 2010; Fletcher and Moreno, 2011) with their core centred between about 50 and 55°S (Lamy *et al*., 2010). Therefore, the South Orkney Islands (Noon *et al*., 2003), South Georgia (Rosqvist and Schuber, 2003) and Chile (Lamy *et al*., 2010) are prone to their influence, along with most landmasses south of about 30°S (Fletcher and Moreno, 2012), thus are perfectly located to reconstruct past changes in the strength and position of the wind belt (Lamy *et al*., 2010; Shevenell *et al*., 2011).

Changes in strength and position of the SWW occur seasonally due to changes in sea surface temperature (Lamy *et al*., 2010) as well as over much larger decadal and centennial time scales. For example, during present-day winters the SWW expand northward between 33 to 40°S and the wind intensity in the core decreases (Lamy *et al*., 2010). Alternatively, during the summer the wind belt contracts latitudinally and becomes intensified over the southernmost tip of Chile (Lamy *et al*., 2010). Similar patterns can be seen in the position of the SWW during millennial scale cold and warm periods. For example, terrestrial records from 41 to 52°S reveal nearly synchronous multimillennial trends in moisture derived from the SWW over the last 14,000 years (Fletcher and Moreno, 2011).

2.3.2. The Oceanic Polar Frontal Zone

The oceanic PFZ is heavily influenced by the ACC, driven in part at least by the SWW (Böning *et al*., 2008) providing a connection between the atmospheric and ocean system. Nevertheless, the ACC is a broad meandering feature composed of narrow, coherent jets moving eastward and northern eastwards as it passes the South Orkney Islands (Abbott *et al*., 2001; Noon *et al*., 2003) and is a dominant feature of Southern Hemisphere circulation, providing a connection between surface and deep ocean waters (Böning *et al*., 2008). The path of the ACC is influenced by topography although local

bathymetry is also thought to influence its path on a smaller scale by influencing the movement of individual jets (Trathan *et al*., 1997). Thus, the position of the oceanic PFZ which is influenced by the flow of deep waters of the ACC is in fact, in part, governed by bathymetry (Trathan *et al*., 1997). Nevertheless, the position of the ACC also appears to vary seasonally with the degree of meandering more intense during late spring and early summer, possibly linked to solar radiation (Abbott *et al*., 2001).

2.3.3. Climatic Implications

Changes in the intensity and location of the SWW impact not only regional but also global climates due to their influence on deep-ocean circulation and changes in atmospheric CO_2 (Rojas *et al*., 2009). Therefore, a detailed understanding of the SWW and how and why they shift is paramount. Knowledge of the link between atmospheric CO_2 and the SWW in the past will help improve future projections regarding both atmospheric CO_2 and variations in the SWW. The SWW are thought to have strengthened and shifted poleward over the past 50 years, possibly in response to warming from rising concentrations of atmospheric CO_2 (Toggweiler, 2009). A similar phenomenon appears to have happened around 17 ka at the end of the LGM, as the earth warmed, atmospheric CO_2 increased and the SWW shifted towards Antarctica (Fig. 2.5; Toggweiler, 2009). This, in turn, caused a positive feedback as the further poleward the SWW move the more CO_2 is released thus increasing temperatures and so on (Toggweiler, 2009). Nevertheless, when investigating the timing of the upwelling of silica, Anderson *et al*. (2009) suggested that the shift of the SWW occurred prior to the increase in CO_2. Therefore, a greater knowledge as to how this complex system works is vital to understand the ocean-atmosphere carbon balance which has the potential to influence global temperatures and clarify the relationship between changes in the SWW and CO_2 release.

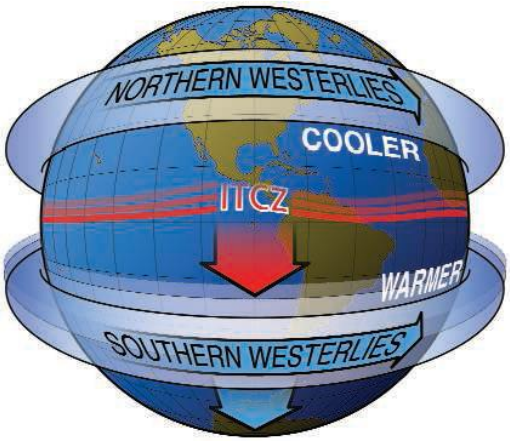

Figure 2.5: Conceptual model of the southern movement of the ITCZ and SWW at the end of the last ice age. Figure taken from Toggweiler (2009)

Research regarding changes in the SWW has been undertaken extensively with several theories considering how and why these shifts occur. Nonetheless, although there is agreement that the wind belt does appear to shift latitudinally over time, there is debate as to whether this is actually a movement of the whole wind belt or purely an expansion of the belt. One simplified model of the SWW suggests that the wind belt moves towards the equator during cold periods, exerting strong control on Southern Ocean upwelling (Hodgson and Sime, 2010). This was also found by Putman *et al*. (2010) who suggest that shifts in the position of the wind belt and variations in their intensity are partly responsible for the environmental changes in the region of the SWW during the last glacial termination and the Holocene. Alternatively, Lamy *et al*. (2010) suggest that rather than an equatorial shift the SWW expand and contract latitudinally. Nevertheless, Anderson *et al*. (2009) do note a southward displacement and intensification of the SWW in recent decades. Much of the uncertainty between whether the wind belt purely shifts latitudinally or simply expands and contracts stems from the fact that most of the evidence collected in assessing the movement of the SWW is proxy data from terrestrial origin but there are limited terrestrial locations within the Southern Ocean therefore data is limited.

Understanding why these movements of the SWW occur is just as complex as assessing how they move. Two conditions are thought to have contributed to an increase in Southern Ocean overturning during the deglaciation after the LGM (Anderson *et al*., 2009). Firstly, Watson and Naveira Garabato (2006) suggested increased heat fluxes to the ocean due to the rising air temperatures as a cause while Toggweiler *et al*. (2006) attributed a poleward shift in the SWW to increases in northward Ekman transport of

surface waters. Anderson *et al*. (2009) propose a combination of these conditions to explain two pulses of silica in their three marine sediment cores which they infer as periods of increased upwelling, increased CO_2 and warming conditions. These two periods of rapid warming in Antarctica coincide with two well-documented cold events in the Northern Hemisphere, Heinrich Event 1 (HE1) and the Younger Dryas (YD) (Anderson *et al*., 2009). During these events vast discharges of iceberg and glacial meltwater into the North Atlantic weakened the thermohaline circulation (THC) overturning causing cooling of the Northern Hemisphere and warming the Southern Hemisphere (Toggweiler, 2009). This in turn impacted global atmospheric circulation and it is hypothesised that the ITCZ shifted south as did the SWW (Toggweiler, 2009). Evidence for this shift in the ITCZ during HE1 and the YD can be seen in proxy data from Africa (Brown *et al*., 2007; Tierney and Russell, 2007), Asia (Wang *et al*., 2001) and South America (Peterson *et al*., 2000; Wang *et al*., 2004; Placzek *et al*., 2006). Anderson *et al*. (2009) also saw evidence of increased sea surface temperatures (SST) off the coast of Chile during HE1 and the YD which can be attributed to a poleward shift of the SWW. Therefore, it appears that the mechanism behind these changes in the position of the SWW was intense Northern Hemisphere cooling leading to changes in global atmospheric circulation and a southward shift in the SWW (Anderson *et al*., 2009).

2.3.4. The Polar Frontal Zone during the Holocene

During the Holocene the PFZ, SWW and ACC have not only changed position but have also shown variation in their strength. Lamy *et al*. (2010) base their analysis of the position of the SWW belt during the Holocene on three marine sediment cores, one lacustrine record and a peat-bog pollen record. Their data indicated that during the early Holocene the SWW were strong but with a weak northern margin (Lamy *et al*., 2010). The intensification of the core coincides with widespread warming of the Southern Hemisphere mid-latitudes evidenced in SST records offshore of central and northern Chile (Lamy *et al*., 2010).

The early Holocene warm period is thought to relate to an intensification of the SWW (Mayewski *et al*., 2004) during which time Hodgson and Sime (2010) state that the SWW were situated at around 50°S over the ACC and south of Campbell Island. When SSTs began to cool the SWW intensified and moved northward being positioned over Campbell Island (Hodgson and Sime, 2010). It is not known if changes in SST are

driving the SWWs or vice versa. Hodgson and Sime (2010) suggest that the cooling SST but terrestrial warming was due to an increase in poleward airflow bringing in atmospheric heat that warmed the land. Therefore, Hodgson and Sime (2010) suggest that the position of the SWWs alone may influence climate.

Although Lamy *et al*. (2010) agree that the SWW influence climate, they suggest that it is the expansion and contraction of the wind belt which affects climate, in particular on the northern side, rather than a change in position of the SWW. They showed that in Chile the amount of precipitation relates to such changes in SWW, evidenced in records from coastal shelves, lake sediments and peat bogs. In the mid-Holocene the drier conditions of western Chile indicate that the SWW are likely to have shifted poleward. Nevertheless, by the late Holocene Chile had become more humid as a result of the SWW moving north again (Wagner *et al*., 2007). The late Holocene reconstruction of the SWW and their influence on climate has become more complex due to the intensification of the El Nino and Southern Oscillation (ENSO) over the last 2000 – 1000 years (Cane, 2005). Finally, the SWW also moves seasonally, with the northern margin of the wind belt expanding towards the equator during a modern Southern Hemisphere winter, whilst in the summer it contracts (Hodgson and Sime, 2010). Therefore, this must also be considered when reconstructing changes in the position of the SWW and climate.

2.4. Conclusions

This chapter has summarised Holocene climates both on a global scale and in the Antarctic and sub-Antarctic regions. The Holocene began with a period of deglaciation at the end of the last glacial period around 11,700 cal. yr B.P. During the Holocene there have been many climatic changes both widespread changes such as the early Holocene climatic optimum c. 10000 to 8000 cal. yr B.P. to more regionally specific climatic fluctuations. On a global scale these climatic reconstructions have been made through the collation of proxy records from various archives including ice, lacustrine, marine and peat cores. Following the early Holocene climate optimum, the general global trend is of period of climatic deterioration which terminates with the mid-Holocene warm period between c. 5000 and 3000 cal. yr B.P. Once again, this is followed by a period of colder conditions with a general consensus of warming commencing again during the last 500 years. Some records also indicate the presence of warmer conditions during the MCA and colder climates during the LIA.

Many of the global trends in climate can be seen in records from Antarctica, although often not in all records as opposing climates in West and East Antarctica are not uncommon. On the Antarctic Peninsula, and Southern Ocean sub-Antarctic Islands to the north of the peninsula such as South Georgia, the mid-Holocene warm period is generally seen between c. 4500 and 2500 cal. yr B.P. however, the specific timing depends on the locality of the record. Nevertheless, although the mid-Holocene warm period has been recognised in many archives, the amplitude of the warming is unknown as most records are qualitative reconstructions of climate. Warming was also evident, though less widespread, in some Antarctic records during the MCA at c. 800 cal. yr B.P. These warm periods are interspersed with, cold Neoglacial conditions recorded between c. 2500 and 500 cal. yr B.P. on the Antarctic Peninsula, after which recent warming is evidenced in some high resolution records.

The PFZ plays a key role in the climates of Antarctica, forming a barrier between it and the mid-latitudes. During warm periods the PFZ extends polewards increasing the intensity of the SWW and during colder periods it occupies a more northerly position. Nevertheless, whether this change in the PFZ is a shift in position or a latitudinal extension of the core is still being debated.

Chapter 3: Study Area and Site Information

Summary

This chapter contains an introduction to Antarctica and the sub-Antarctic Islands. The location, climate and geology of each region studied are outlined and details of the lakes within the region are given. The chapter includes maps and satellite imagery of the regions and their lakes. The chapter concludes with a description of the site selection process for both the surface material studied in Chapter 6 when developing the GDGT-temperature calibration and two core sites, Fan Lake and Yanou Lake, at which the GDGT-temperature calibration is applied to reconstruct mid-late Holocene temperatures, Chapters 7 and 8 respectively.

3.1. Antarctica

Antarctica (Fig. 3.1) is the fifth largest continent which together with its summer sea ice has an area of 14 million km^2; about 10% of the Earth's land surface (Bockheim and Hall, 2002; Chown and Convey, 2007; Summerhayes, 2009). Antarctica is the highest, driest, windiest and coldest continent, with the lowest recorded temperature on Earth, -89.2 °C, at Russia's Vostok Station (Summerhayes, 2009). The continent of Antarctica includes ice sheets, floating ice shelves and areas of fast ice with only about 0.33% exposed rock and soil (Chown and Convey, 2007; Summerhayes, 2009). Topographically the land surface of Antarctica rises rapidly from the coast and has the highest mean elevation of any continent at around 2200 m (Summerhayes, 2009).

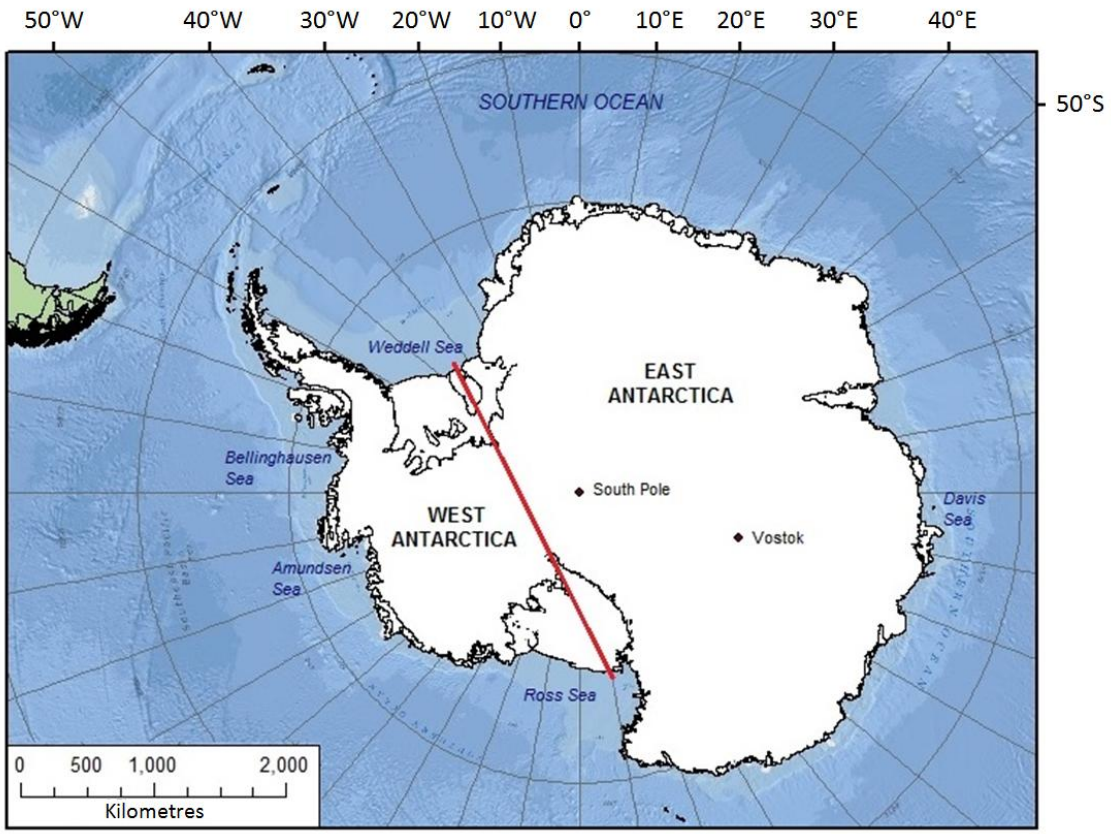

Figure 3.1: Map of Antarctica showing the division of West and East Antarctica and other key locations including Vostok Station.

Antarctica is divided into, East Antarctica and West Antarctica (Fig. 3.1), bisected by the Transantarctic Mountains (Bockheim and Hall, 2002). The Transantarctic Mountains are the largest mountain range in Antarctica running from the Ross Sea to the Weddell Sea and rising to 4528 m a.m.s.l. (Summerhayes, 2009; Verleyen *et al*., 2011). The East Antarctic Ice Sheet (EAIS) and West Antarctic Ice Sheet (WAIS) comprise 90% of the world's total glacial ice (Bockheim and Hall, 2002; Verleyen *et al*., 2011). Despite the vast amounts of glacial ice there are still rivers, streams and lakes found in the ice free regions of Antarctica and the sub-Antarctic islands and underneath or above the ice sheets. The rivers and lakes have varying physical and chemical characteristics.

3.1.1. West Antarctica

West Antarctica (Fig. 3.2), the smaller of the two 'halves' of continental Antarctica, is an archipelago buried by 2.3 million km^2 of glacial ice from the WAIS (Bockheim and Hall, 2002). West Antarctica is made up of Marie Byrd Land, Ellsworth Land and Palmer Land as well as multiple ice shelves including the Ronne Ice Shelf, Ross Ice Shelf, Larsen Ice Shelf and George VI Ice Shelf. Topographically the mean elevation of

West Antarctica is around 850 m which is lower than the mean average for the whole continent (Summerhayes, 2009). Nevertheless West Antarctica does include the highest Antarctic mountain, Mount Vinson in the Ellsworth Mountains (78°35'S, 85°25'W) at 4892 m elevation (Summerhayes, 2009).

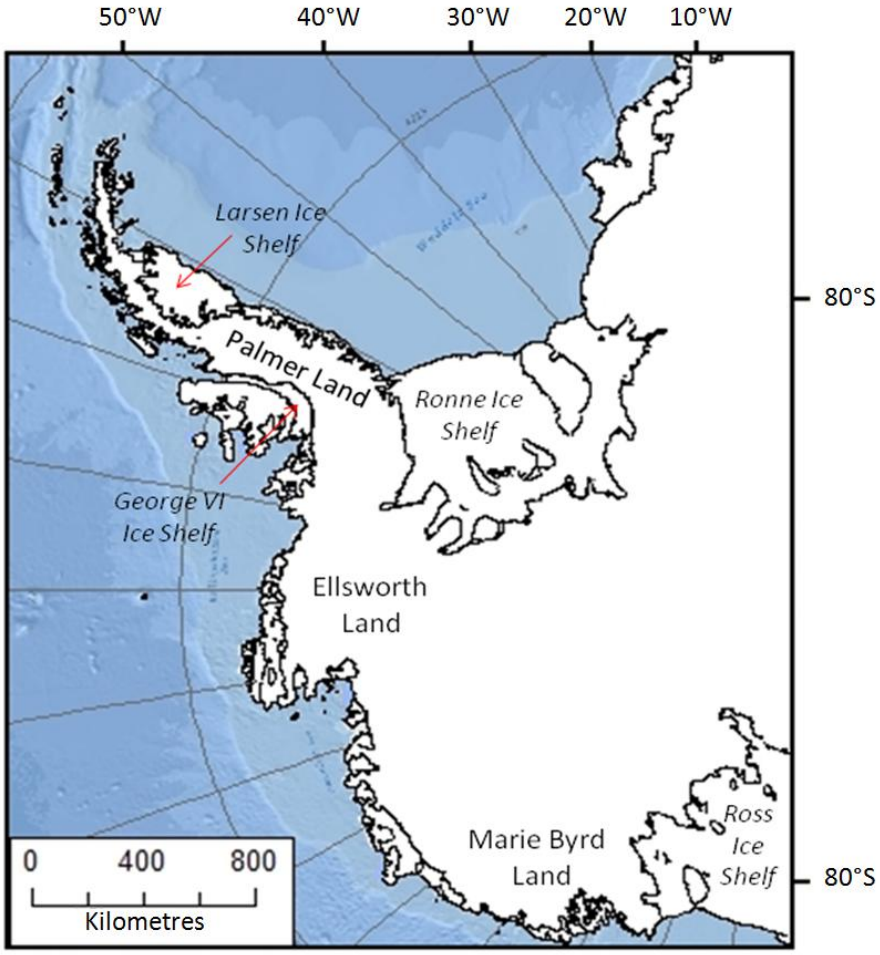

Figure 3.2: Map of West Antarctica showing the locations of Palmer Land, Ellsworth Lane, Marie Byrd Land, the Larsen Ice Shelf, George VI Ice Shelf, Ronne Ice Shelf and the Ross Ice Shelf.

3.1.1.1. The Antarctic Peninsula

The Antarctic Peninsula (AP) is 1250 km long extending north towards South America to which it is geologically comparable (Bentley *et al*., 2009). The AP consists of Palmer Land and Graham Land, which contain a chain of mountains less than 250 km wide with maximum elevations of around 3500 m a.m.s.l. (Bentley *et al*., 2009), and several peripheral islands such as Alexander Island, Beak Island and the South Shetland Islands (Fig. 3.3). Geologically the AP is composed of plutonic and volcanic rocks (Bentley *et al*., 2005) which project substantially further north than the rest of the continent.

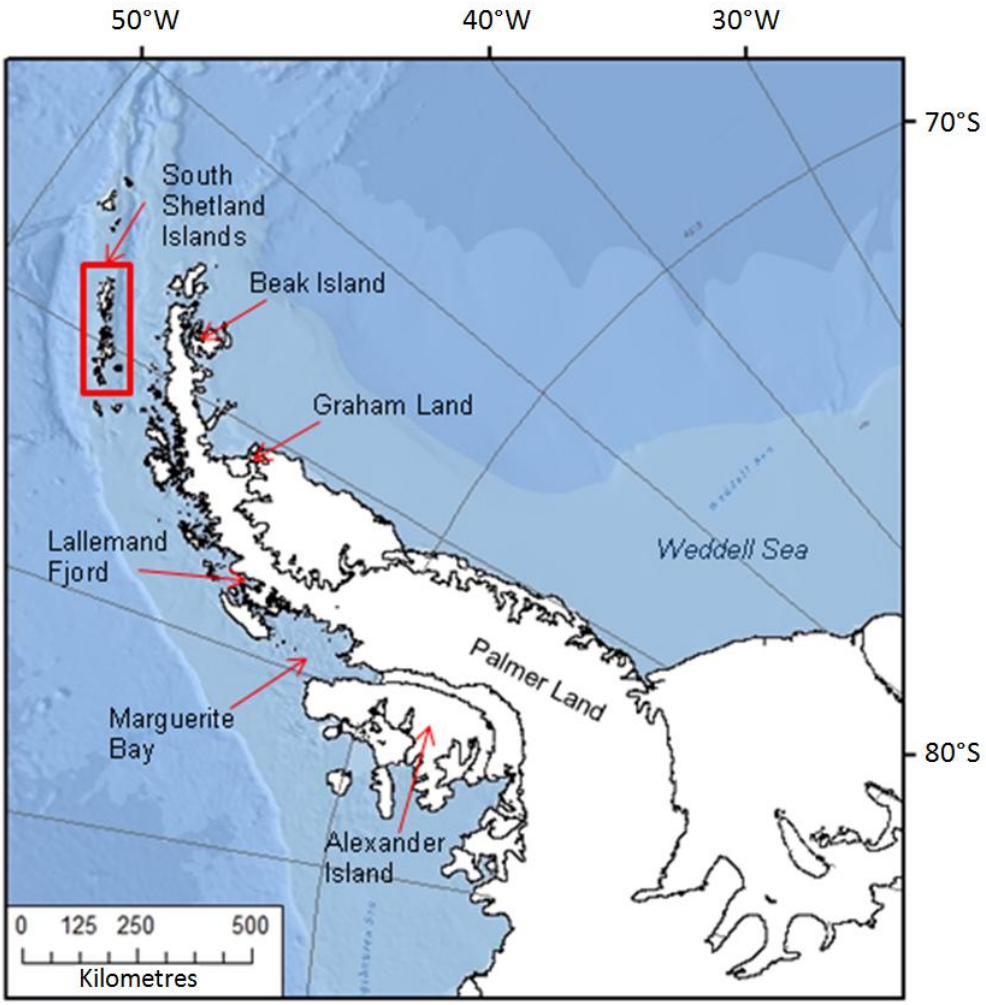

Figure 3.3: Map of the Antarctic Peninsula showing the location of the South Shetland Islands, Beak Island, Graham Land, Lallemand Fjord, Marguerite Bay, Alexander Island and Palmer Land.

It is heavily glaciated (Pritchard and Vaughan, 2007) with outlet glaciers terminating in the oceans on both the west and eastern sides of the peninsula (Bentley *et al*., 2009). These glaciers have sculpted the coastline of the AP leaving it highly convoluted with copious islands, bays, fjords and a series of embayments often interconnected by channels which are sometimes as deep as 900 m (Ducklow *et al*., 2007). Nonetheless, there are a few extensive ice-free areas where terrestrial palaeoenvironmental records from the Holocene have also been preserved (Bentley *et al*., 2009). These ice-free areas include the northeast peninsula (James Ross Island), South Shetland Islands, eastern Alexander Island (Ablation Point Massif) and the coastline around Marguerite Bay (Bentley *et al*., 2009). There are also a number of smaller ice-free areas on ridges between outlet glaciers and on nunataks.

The AP is climatically atypical of the Antarctic continent (Bentley *et al*., 2009), with a mean annual temperature of -3.7 °C at Rothera (67°34'S, 68 °08'W) in 2014 (Met READER, 2015). The AP is also one of the three fastest-warming regions on Earth at 3.4 °C per century (Vaughan *et al*., 2003; Pritchard and Vaughan, 2007). This recent rate of warming has led to increased summer melting by up to 74% since 1950 (Vaughan, 2006), the recession of snowfields and glaciers (Cook *et al*., 2005), the loss of several ice shelves (Pritchard and Vaughan, 2007) and a reduction in the duration of sea-ice cover (Parkinson, 2002).

The climate regime of the AP differs on the west and east of the peninsula, due to the strong marine influence on the western side which is exposed to the SWW (Bentley *et al*., 2009). As a consequence the west side receives relatively warm, moist air masses from mid-latitudes and is the only area of Antarctica where there is a negative correlation between winter temperatures, measured at Faraday / Vernadsky, and the extent of sea-ice (Bentley *et al*., 2009). The east side of the AP has a much colder and drier climate due to the northwards extension of cold continental air masses from the Antarctic interior into the Weddell Sea embayment (Bentley *et al*., 2009).

On the AP there are numerous lakes including Narrows Lake on Pourquoi-Pas Island in Marguerite Bay to the west of the AP (Hodgson *et al*., 2013). Pourquoi-Pas Island is separated from Blaiklock Island by The Narrows which is a constricted channel, less than 1 km in width, often full of floating icebergs and brash ice (British Antarctic Survey, 2008). Narrows Lake (67°36.054'S, 67°12.449'W) is a 6.1 m deep lake occupying a typical isolation basin setting which is partly ice-covered during the summer months (British Antarctic Survey, 2003). In January 2003 the summer surface lake temperature at Pourquoi-Pas lake was 3.7 °C.

Other AP lakes include Viewpoint lakes on Trinity Peninsula and Beak lakes on Beak Island, both to the north-eastern side of the AP. Viewpoint (63°33'S, 57°24'W) is a rocky headland consisting of small bedrock ridges and depressions, the latter are often the location of lakes and ponds (British Antarctic Survey, 2006). There are multiple lakes on Viewpoint including ice-covered, clear water and turbid lakes determined by their drainage network and proximity to upstream glaciers (British Antarctic Survey, 2006). Viewpoint 7 (63°33.136'S, 57°24.582'W) is one of the largest lakes at 15 m water depth located within a bedrock depression at 134 m elevation (British Antarctic Survey, 2006). In January 2006 the summer surface lake temperature at Viewpoint 7

was 4.5 °C. Adjacent to Trinity Peninsula is Beak Island (63°36’ S, 57°20' W), a remnant volcano in Prince Gustav Channel, on which there are six lakes and ponds. The largest of these six lakes is Beak 1 (63°36'38" S, 57°20'20" W) with a depth of 24 m and spot surface water temperature of 4.8 °C in January 2006 (Sterken *et al*., 2012).

3.1.1.2. Alexander Island

Alexander Island (Fig. 3.3) is a large glaciated island (c. 400 by 80 km) situated in Marguerite Bay to the west of the AP between 68.7° and 72.6°S (Roberts *et al*., 2009; Johnson *et al*., 2012). It is separated from the AP by the George VI Sound (Johnson *et al*., 2012). The island is predominantly ice-covered with sporadic exposed nunataks and a few notable ice-free areas including the Ablation Point Massif (Roberts *et al*., 2009; Johnson *et al*., 2012). Geologically, unlike the AP, Alexander Island is composed of sedimentary rocks (Bentley *et al*., 2005). Due to the location of Alexander Island and its proximity to the AP, Alexander Island is climatically comparable to the west side of the AP and strongly influenced by the SWW.

There are two epishelf lakes on the east coast of Alexander Island, Moutonnée Lake and Ablation Lake, both of which are tidal, stratified water bodies (Bentley *et al*., 2005). The freshwater layers in both lakes are retained by presence of the George VI Ice Shelf (GVI-IS), which impounds them in embayments on the coast of Alexander Island. Consequently if the ice shelf disappears the lakes become marine embayments with changes in ecology and sedimentology (Smith *et al*., 2007). Bentley *et al*. (2005), Smith *et al*. (2007) and Roberts *et al*. (2008; 2009) used this knowledge along with lake sediment cores to indicate periods of ice-shelf presence and absence.

Moutonnée Lake (70°52.123'S, 68°19.635'W) has a depth of 55 m and spot surface water temperature of 0.0 °C in November 2001 (British Antarctic Survey, 2002). The lake catchment contains mainly bedrock to the south and reworked glacial sediments to the west (Roberts *et al*., 2009) with the catchment glaciers currently roughly 2 km up the valley from the lake (Roberts *et al*., 2008). The GVI-IS is grounded on a partially submerged bedrock sill damming the embayment (Smith *et al*., 2007; Roberts *et al*., 2008; 2009). The lake has a limited hydraulic connection to seawater in George VI Sound (Roberts *et al*., 2008; 2009). Currently the lake is capped by 2 to 3 m of ice but, during the summer, a narrow moat, about 2 m wide, forms around the landward shoreline (Smith *et al*., 2007).

3.1.1.3. The South Shetland Islands

The South Shetland Islands (Fig. 3.4) are a 500 km long island arc in the maritime sub-Antarctic located between 61 and 63°S, and 54 to 62°W around 160 km north of the AP across the Bransfield Strait (Fretwell *et al*., 2010; Watcham *et al*., 2011). The South Shetland Islands (SSIs) include King George Island and Livingston Island and form an arc with a length of around 230 km but never more than 35 km wide (Fretwell *et al*., 2010; Watcham *et al*., 2011).

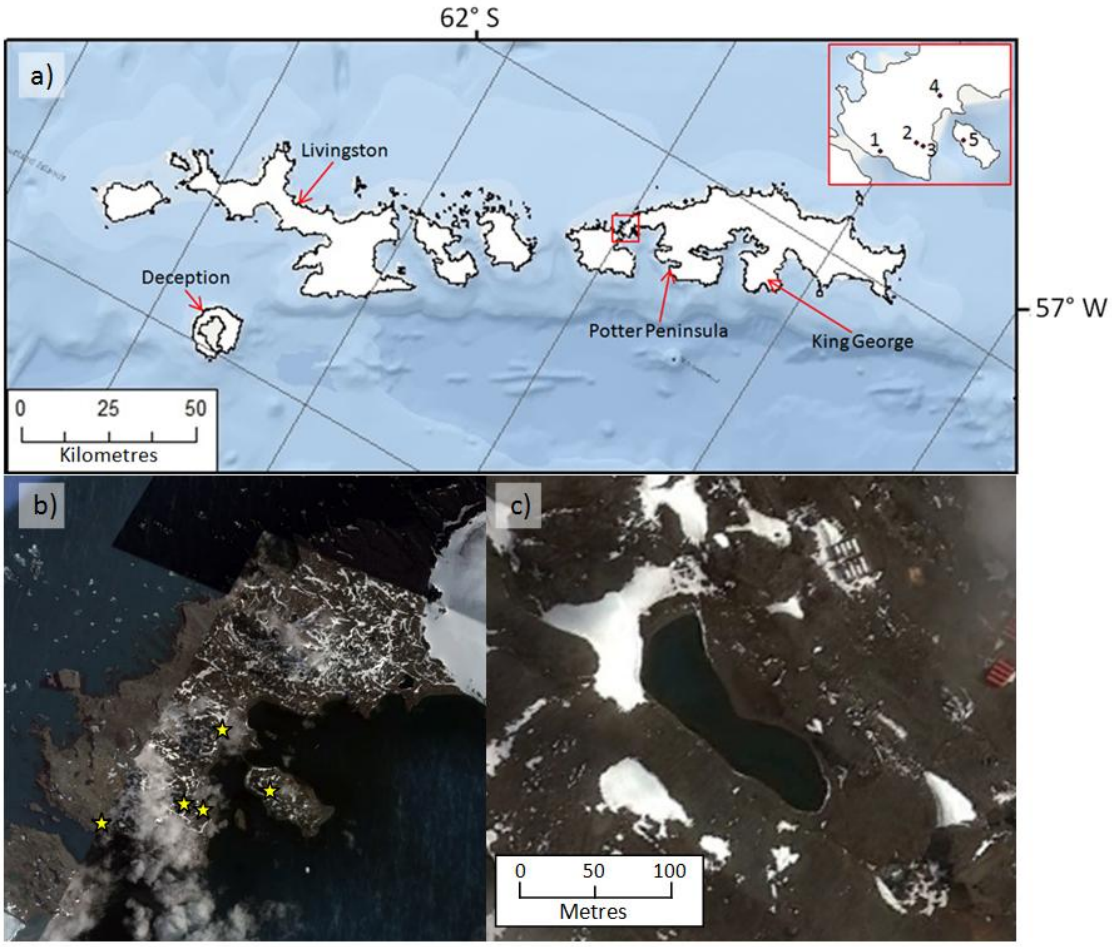

Figure 3.4: a) Map of the South Shetland Islands indicating the Fildes Peninsula, red box, where the lakes used in this research are located. The location of these lakes is shown in the insert; 1) Belén, 2) Gaoshan, 3) Yanou, 4) Long and 5) Ardley. b) Satellite image of the Fildes Peninsula, the yellow stars indicate the location of the 5 lakes identified in (a). c) Satellite image of Yanou Lake showing its proximity to snow patches and catchment vegetation. Satellite images edited from Google Earth images.

The islands have a sub-polar maritime climate regime and are the warmest location in the AP region (Heroy *et al*., 2008). Being on the western side of the AP their climate regime is characterised by higher precipitation than that of the eastern AP (Heroy *et al*.,

2008). The mean annual temperature at Bellingshausen station on Fildes Peninsula, King George Island, in 2014 was -2.3 °C (Met READER, 2015).

The Islands are still extensively covered by ice caps, permanent snowfields and ice domes which descend into ice cliffs (Fretwell *et al*., 2010; Watcham *et al*., 2011). Nevertheless there are some ice-free areas in some of the low-lying peninsulas (Fretwell *et al*., 2010), one of the largest examples of which is the Fildes Peninsula on King George Island, measuring 38 km^2 (Watcham *et al*., 2011). At these ice-free locations vegetation such as mosses and lichens occur on the wet valley floors, drained slopes, dry soils and on rock surfaces (Björck *et al*., 1993).

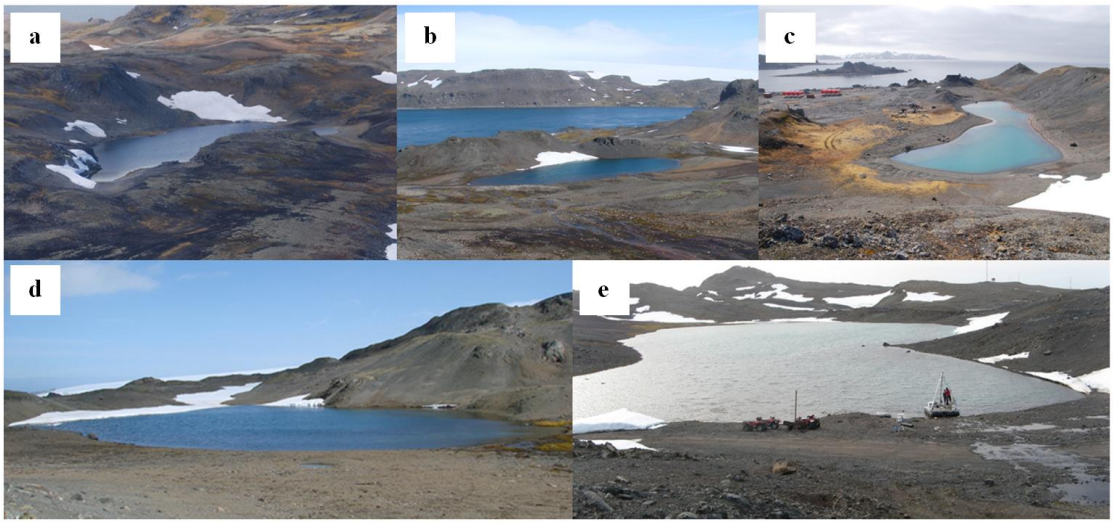

Figure 3.5: Pictures of the King George Island lakes; a) Ardley, b) Belén, c) Yanou, d) Gaoshan and e) Long. Taken by Stephen Roberts.

There are many lakes on the SSIs including Ardley, Belén, Gaoshan, Long and Yanou Lakes which range from 14.5 to 34.5 m a.m.s.l. (Watcham *et al*., 2011). Ardley, Belén, Gaoshan, Long and Yanou Lakes (Fig. 3.5) are all freshwater lakes situated on Fildes Peninsula, King George Island, with maximum depths of 6.1 m, 7.0 m, 7.0 m, 5.6 m and 5.3 m and spot summer surface water temperatures of 0.07 °C, 3.78 °C, 4.37 °C, 6.38 °C and 3.05 °C respectively between November 2006 and January 2007 (British Antarctic Survey, 2008). All five lakes have yellow-green moss in their catchments that in some cases have been disturbed by human activity at local research stations (British Antarctic Survey, 2008). The geology of the catchments for the five lakes on Fildes Peninsula is predominantly andesite with some basalt also present (British Antarctic Survey, 2008). Long Lake has a more complex catchment geology with heavily eroded distinct purple, possibly andesitic, volcanic lavas and agglomerate outcrops on the western shore.

Potter Peninsula (62°14’ S, 58°39’ W) is also ice free during the summer with patches of snow and ice common throughout the year (Vinocur and Pizarro, 2000; Vinocur and Maidana, 2010). The Peninsula has a number of lakes, shallow lakes, ponds and streams (Vinocur and Maidana, 2010) including Matias Lake (62°14’42.07" S, 58°39’52.16" W) and GPS Lake 15 (62°14’ 26.02" S, 58°40’ 39.47" W) which have maximum depths of 5.6 m and 2.2 m and spot summer surface water temperatures of 1.4 °C and 0.3 °C measured in November 2011. Matias Lake is formed within a ‘Neoglacial’ moraine and during the summer connects with Lago Rudy forming the second largest permanent water body on Potter Peninsula. Geologically, Potter Peninsula is dominated by a Lower Tertiary basaltic and andesite lavas and tuffs and Quaternary neoglacial moraines and marine sediments (Del Valle *et al*., 2002).

3.1.2. East Antarctica

East Antarctica (Fig. 3.6) is a highly elevated region capped by 10.2 million km^2 of glacial ice in the form of the EAIS (Bockheim and Hall, 2002) which drains directly into the Southern Ocean between 15°W and 150°E (Verleyen *et al.*, 2011). Lakes in East Antarctic are generally confined to ice-free oases and archipelagos surrounding the continent (Verleyen *et al.*, 2003).

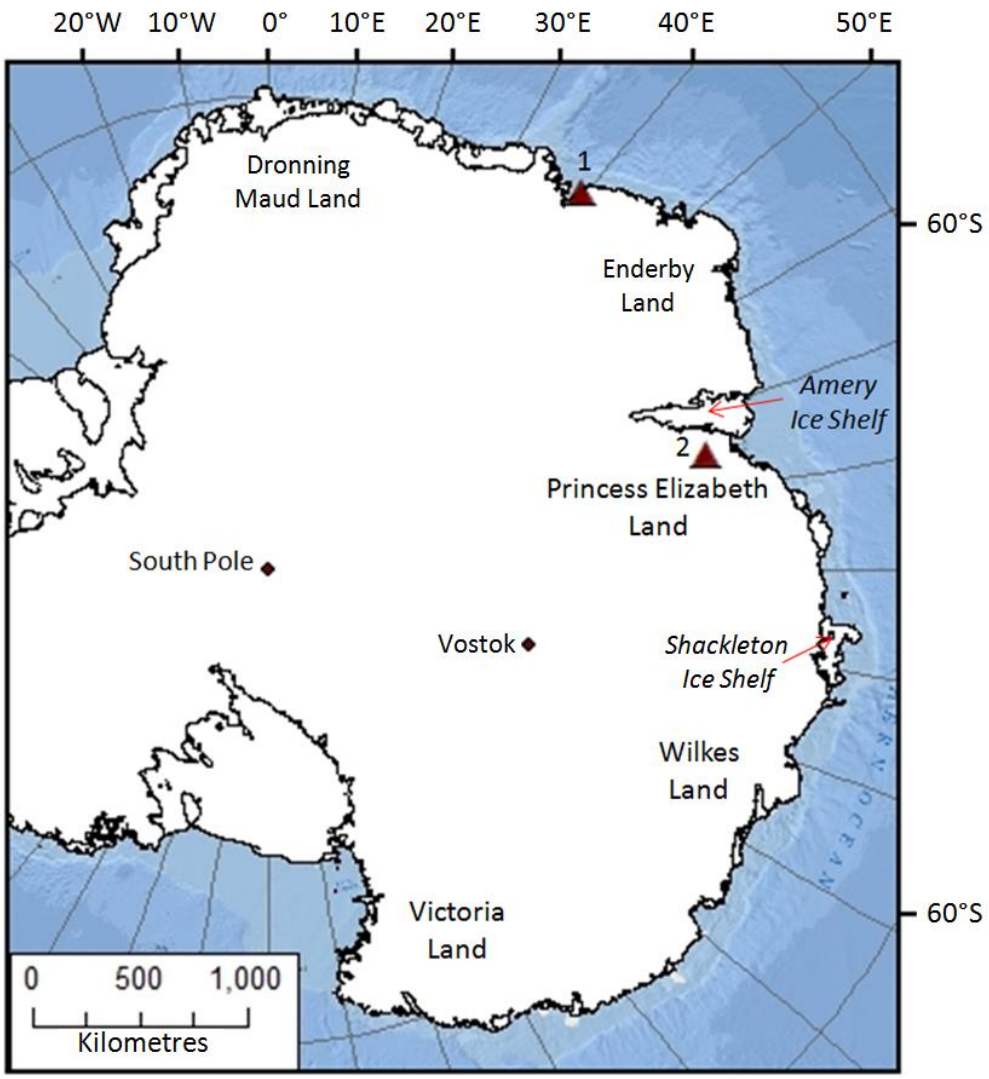

Figure 3.6: Map of East Antarctica showing key locations and the lake regions studied; 1) Syowa Oasis Lakes and 2) Larsemann Hills Lakes. Larsemann Hills contains 4 studied lakes; Progress, Heart, Reid and Pup Lagoon and Syowa Oasis contains 5 studied lakes; Mago Ike and 4 West Ongul lakes.

3.1.2.1. Syowa Oasis

The Syowa Oasis (Fig. 3.6) is located at 69°70’S, 39°40’E includes eight ice-free regions, Ongul Islands, Langhovde, Breivagnipa, Skarvsness, Skallen, Berrodden, Rundvagshetta, and Strandnibba which are thought to have been ice-free for about 20,000 years (Kimura *et al*., 2010; Sasaki *et al*., 2010; Verleyen *et al*., 2012). Skarvsness and Langhovde are the two largest peninsulas, located approximately 40 and 20 km south of Syowa Station, 69°00'S, 39°35'E, respectively (Kimura *et al*., 2010). The mean annual air temperature at the Syowa station in 2014 was -11.2 °C (Met READER, 2015).

There are hundreds of lakes in the Syowa Oasis with over 100 lakes in Skarvsness and Langhovde alone of which most are ice-free for about two months during the Antarctic summer (Sasaki *et al*., 2010). Mago Ike is located at 69°28'27.42"S, 39°36'42.87"E on the Skarvsness Peninsula with a maximum depth of 5.8 m and spot summer surface temperature of 9.9 °C in January 2007. Lakes are also found on East and West Ongul Islands (Verleyen *et al*., 2012). Both islands have multiple water bodies on them although on East Ongul these are mainly small ephemeral ponds and shallow lakes whereas West Ongul has some larger and deeper lakes, up to 11 m depth (Verleyen *et al*., 2012). These are the four lakes from the West Ongul Islands which are including in this study WO2, WO3, WO6 (Higashi-ura Ike) and WO8 (Nishi Ike) (Fig. 3.7) with maximum depths of 2.2 m, 2.1 m, 5.0 m and 6.0 m and spot surface water temperatures of 8.3 °C, 3.8 °C, 6.5 °C and 9.1 °C respectively in January 2007 (British Antarctic Survey, 2007).

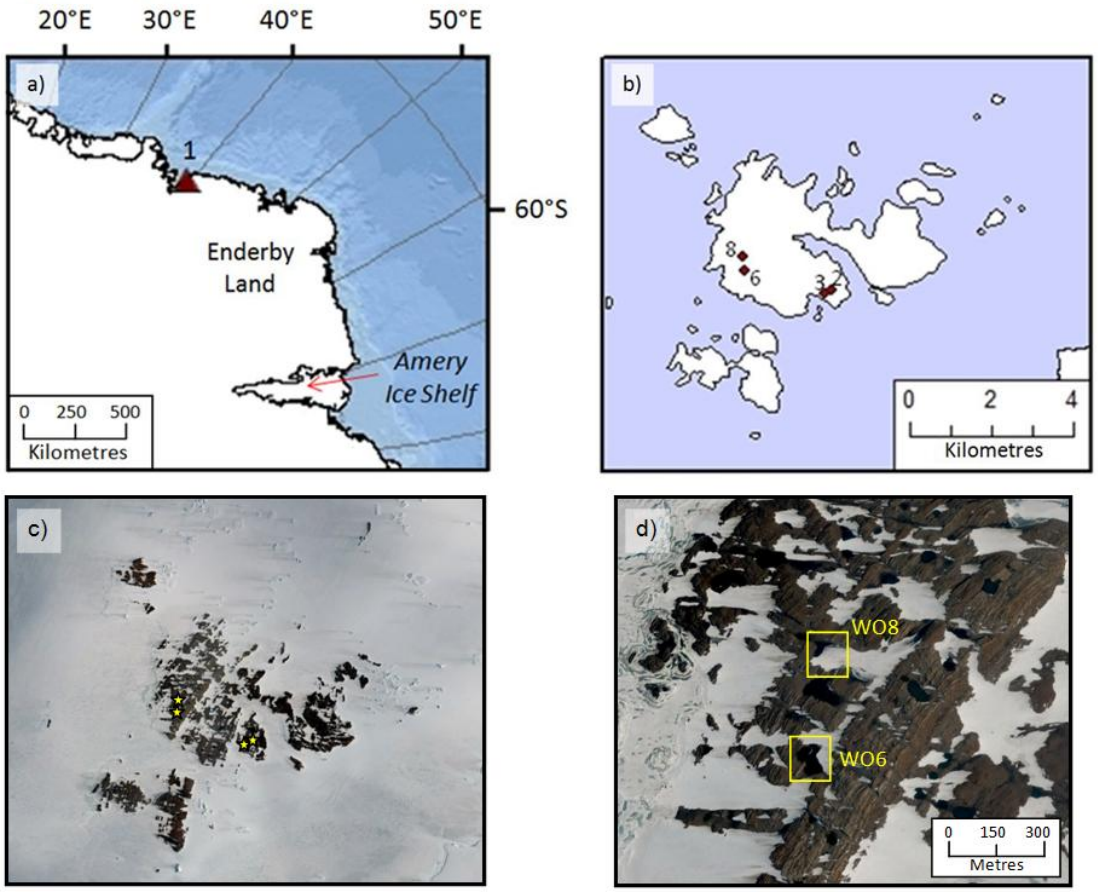

Figure 3.7: Map of the West Ongul Lakes a) Red triangle represents the location of West Ongul Island in East Antarctica; b) Location of Lakes WO2, WO3, WO6 and WO8 on West Ongul Island; c) Satellite image of West Ongul Island, the yellow stars indicate the lakes in (b); d) Satellite image of WO6 and WO8 and their catchments. Satellite images edited from Google Earth images.

3.1.2.2. Princess Elizabeth Land

Princess Elizabeth Land includes the Amery Ice Shelf and the Larsemann Hills located at 69°23'S, 76°53'E. The Larsemann Hills are an ice-free oasis made up of a series of rocky peninsulas and islands (Gillieson, 1991; Hodgson *et al*., 2001; Verleyen *et al*., 2003; 2011; 2012). At 50 km^2 (Verleyen *et al*., 2003; 2011; 2012) the Larsemann Hills (Fig. 3.6) is the second largest ice-free oasis found along East Antarctica's 5000 km of coastline (Hodgson *et al*., 2001). The region comprises two main peninsulas, Stornes and Broknes, as well as numerous scattered offshore islands (Hodgson *et al*., 2001; Verleyen *et al*., 2003; 2012). The geology of the region is granite and gneiss (Gillieson, 1991) and the highest elevations are around 180 m a.m.s.l. (Hodgson *et al*., 2001). The mean annual air temperature at the Davis station at 68.6 S, 78.0 E was -10.0 °C in 2014 (Met READER, 2015).

Lake sediments in the Larsemann Hills contain a great diversity of biological and physical markers such as pigments and diatoms from which past environments can be inferred (Hodgson *et al*., 2001). Within the region there are over 150 freshwater lakes ranging from small ephemeral ponds to larger water bodies (Gillieson, 1991; Hodgson *et al*., 2001; Verleyen *et al*., 2003). Including Progress Lake which has an area of 10 ha and depth of 38 m (Hodgson *et al*., 2001). In contrast, Pup lagoon is a smaller water body on the Strones Peninsula with an area of 1.0 ha and a maximum depth of 4.6 m (Hodgson *et al*., 2001; Verleyen *et al*., 2003; Sabbe *et al*., 2004). Other Larsemann Hills lakes include Heart Lake and Lake Reid which have an area of 5.0 ha and 5.5 ha and maximum depth of 4.5 m and 4.0 m respectively (Hodgson *et al*., 2001; Verleyen *et al*., 2003; Sabbe *et al*., 2004). Most lakes in this region are at least partially ice-free if not completely ice-free in the summer months, between December and February and covered with about 2 m of ice for the remainder of the year (Hodgson *et al*., 2001).

3.1.3. Sub-Antarctic Islands

South Georgia, Marion Island, Macquarie Island and Campbell Island are just four of many sub-Antarctic Islands (Fig. 3.8). Their oceanic setting means that they provide key locations for terrestrial climatic reconstructions within an oceanic environment, thus these islands are key locations for understanding the impact of the Antarctic Circumpolar Current and Southern Westerly Wind belt on Southern Hemisphere climates (McGlone *et al.*, 2010).

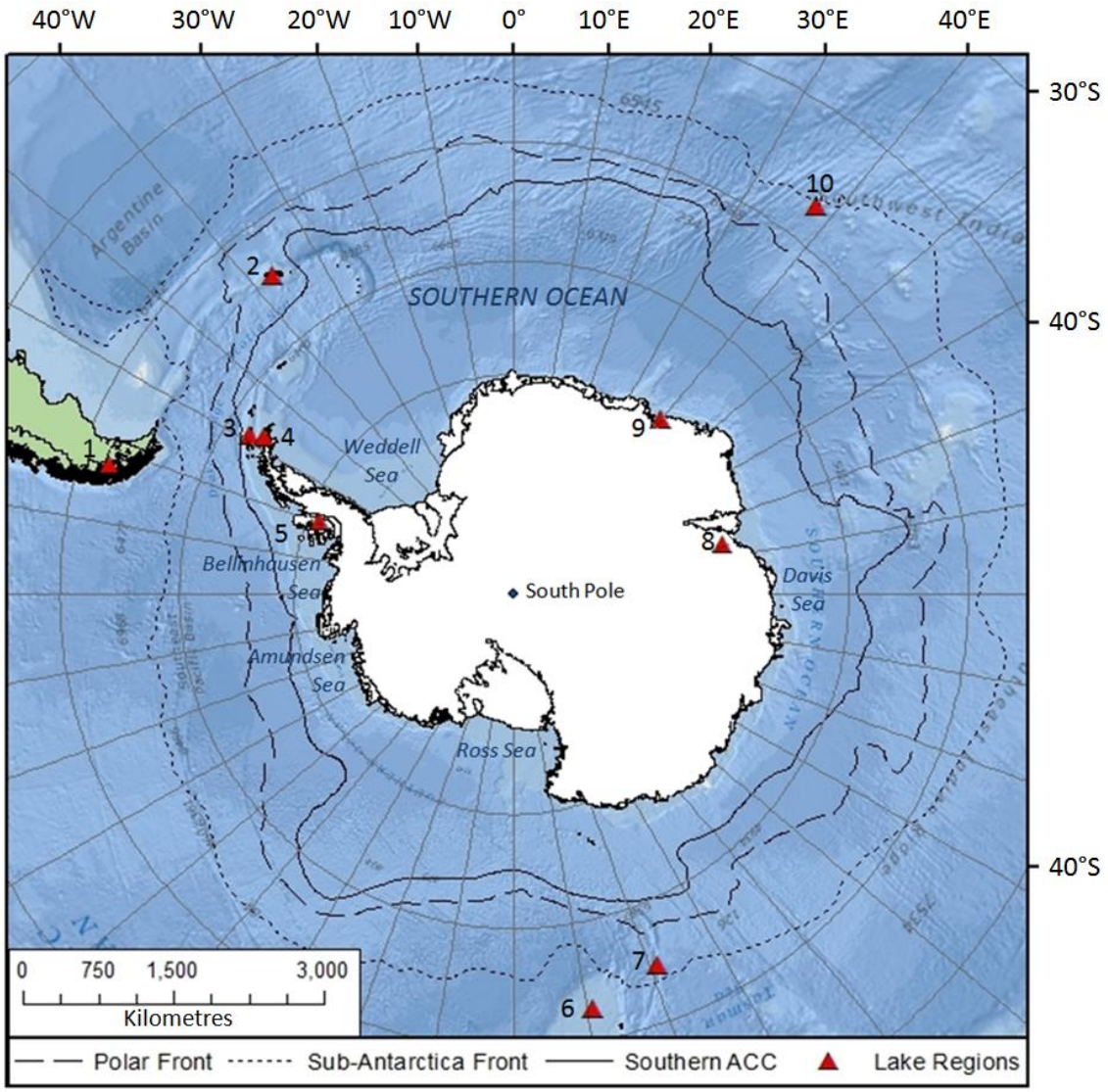

Figure 3.8: Map of Antarctica showing the location of all of the lake regions studied including the sub-Antarctic Islands; 1) Chile, 2) South Georgia, 3) South Shetland Islands, 4) Trinity Peninsula, 5)Alexander Island, 6) Campbell Island, 7) Macquarie Island, 8) Larsemann Hills, 9) Syowa Oasis and 10) Marion Island.

3.1.3.1. South Georgia

South Georgia (Fig. 3.9) is a heavily glaciated sub-Antarctic island (Roberts *et al*., 2010) located between 54 and 55°S, and 36 to 38°W (Bentley *et al*., 2007). The island is situated 350 km south of the Antarctic Convergence (Rosqvist and Schuber, 2003) and approximately 1300 km east of the Falkland Islands (Roberts *et al*., 2010). Around South Georgia there are also multiple smaller islands including Bird Island and Annenkov Island. South Georgia itself is approximately 170 km long and varies between 2 and 40 km in width (Bentley *et al*., 2007). The island is dominated by a mountain chain comprising the Salvesen and Allardyce Ranges which rise to 2960 m a.m.s.l. (Rosqvist and Schuber, 2003; Bentley *et al*., 2007; Gordon *et al*., 2008). These

mountains provide a barrier to the prevailing SWW (Gordon *et al*., 2008) thus the climates on either side of the range are different.

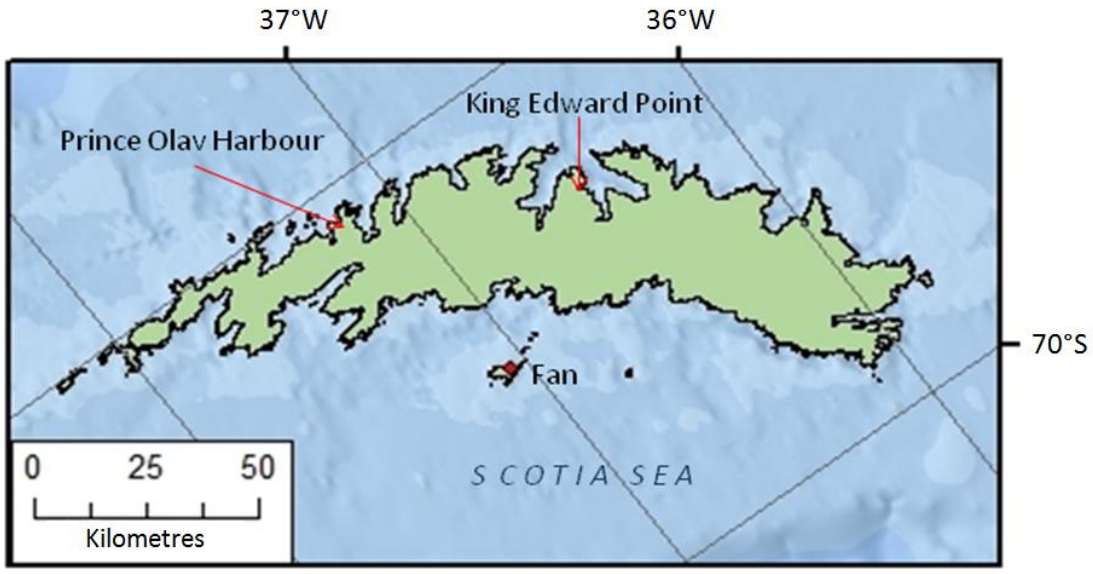

Figure 3.9: Map of the South Georgia highlighting key locations in particular Fan Lake, located on Annenkov Island.

South Georgia is located in the north-eastern Scotia Sea about 1500 km north of the northern tip of the AP and 1800 km east of South America. The Island also lies just south of the present day position of the Polar Frontal Zone (PFZ) and about 5°N of the average limit of winter sea ice (Rosqvist and Schuber, 2003; Bentley *et al*., 2007) locating it in a particularly climatically sensitive area (Roberts *et al*., 2010). Nevertheless during exceptional winters the sea ice limit can extend north of the island (Bentley *et al*., 2007). More than half of the island is covered in permanent snow and ice (Rosqvist and Schuber, 2003; Gordon *et al*., 2008), with the permanent snowline generally about 300 m above sea level on the southwest and between 450 and 600 m on the northeast (Gordon *et al*., 2008). Many glaciers descend to sea level particularly on the exposed southwest side of the island (Rosqvist and Schuber, 2003).

The main influences on the climatic regime of South Georgia are the position of the PFZ and the SWW (Rosqvist and Schuber, 2003). As a consequence the climate is cool, moist and windy with a strong maritime influence (Bentley *et al*., 2007; Gordon *et al*., 2008). The mean annual air temperature at Grytviken station on South Georgia in 2014 was +2.4 °C (Met READER, 2015).

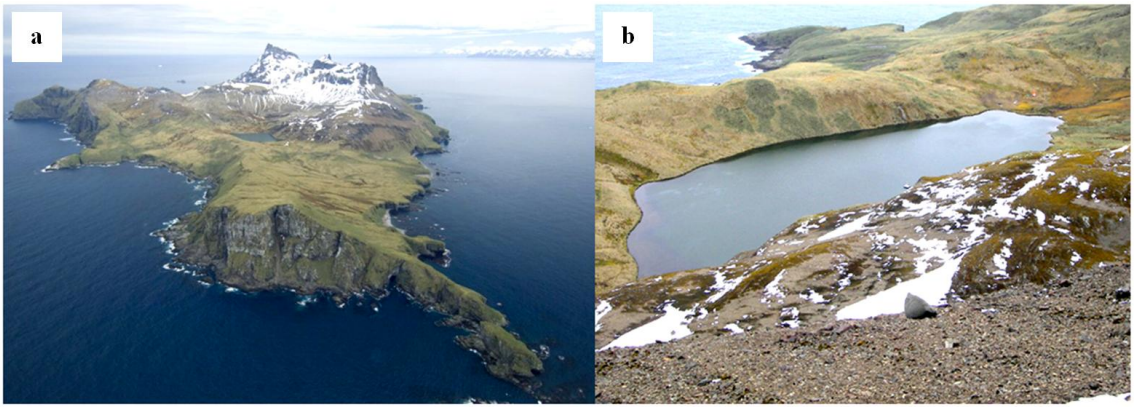

Figure 3.10: a) Arial photograph of Annenkov Island showing the position of Fan Lake and b) Fan Lake. Images from Strother *et al*. (2015).

Fan Lake (Fig. 3.10) is found on Annenkov Island to the south of South Georgia. The lake is located at 54°29'0"S, 37°5'0"W with an outflow at the eastern end, a maximum depth of 18 m and a spot summer surface water temperature of 4.6 °C measured in December 2005 (Hodgson, 2009; Pearson *et al*., 2011). The catchment of the lake consists of a series of vegetated, thinly veneered ridges (British Antarctic Survey, 2006). At the eastern end, inter-ridge hollows are filled by peat bogs and to the western end bedrock is covered with a thin (0.5 m) veneer of gravel overlain by peat deposits up to 1 m thick in some areas (British Antarctic Survey, 2006).

3.1.3.2. Marion Island

Marion Island (Fig. 3.11) is the larger of two islands which make up the Prince Edward Islands (Prinsloo *et al*., 2010). Marion Island is located at 46°54'S, 37°45'E roughly half way between South Africa and Antarctica (McDougall *et al*., 2001; Smith, 2002; Rouault *et al*., 2005; Prinsloo *et al*., 2010; Hall *et al*., 2011). Marion Island has an area of about 290 km^2 (Smith, 2002; Hall *et al*., 2011) and 72 km of coastline (Rouault *et al*., 2005). It is a volcanic island (Rouault *et al*., 2005) with a maximum elevation of 1231 m a.m.s.l. (Hall *et al*., 2011). The island is generally ice-free having recently lost its small permanent ice cap covering the island due to regional warming.

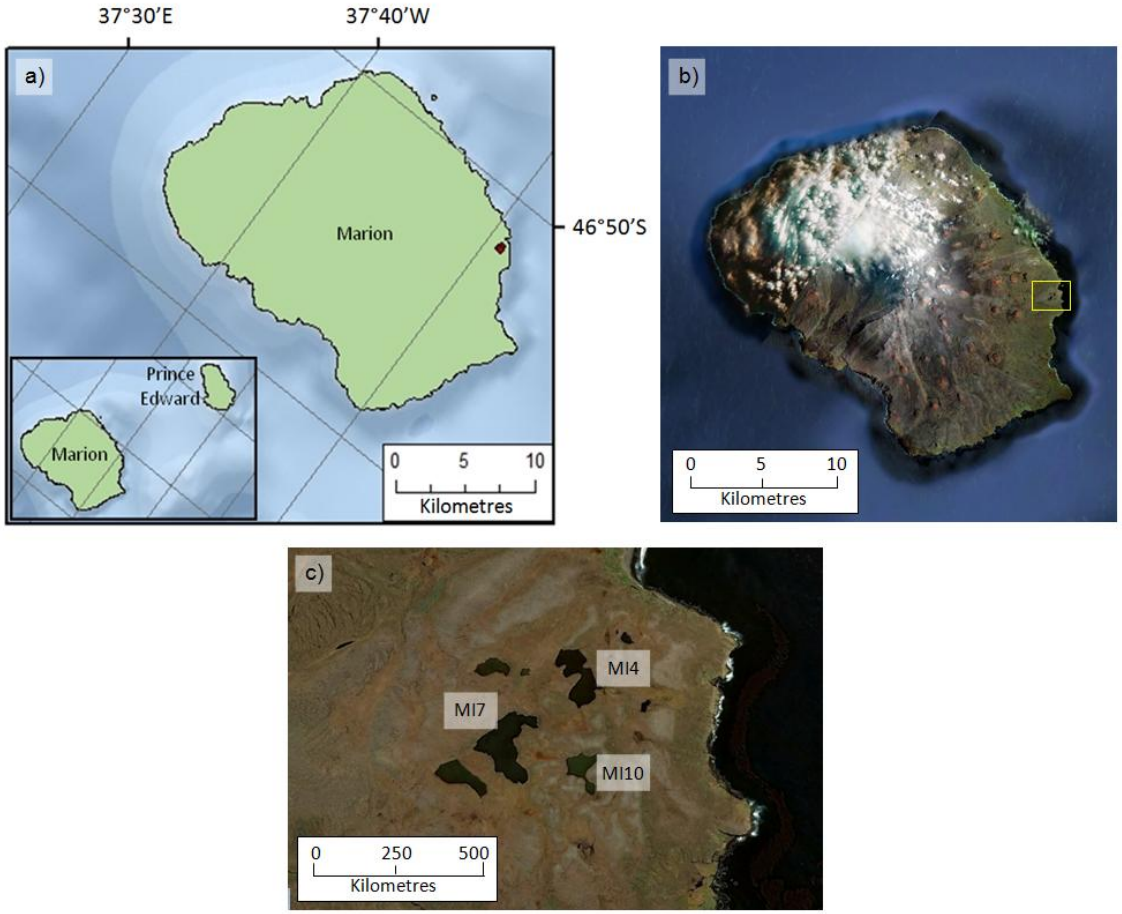

Figure 3.11: a) Map of Marion Island with an insert of the location of both Marion and Prince Edward Island. The location of the three lakes studied on Marion Island (MI4, MI7 and MI10) is indicated in red. b) Satellite image of Marion Island, the yellow box shows the location of the lakes studied. c) Satellite image of the three Marion Island lakes studied, the image shows the more vegetated catchment of the lakes compared to other environments within the dataset. Satellite images edited from Google Earth images.

Geologically Marion Island is a youthful, 500,000 year old, basaltic shield volcano (McDougall *et al*., 2001; Prinsloo *et al*., 2010) positioned in an inter-plate fracture zone, between the African and Antarctic plates (Prinsloo *et al*., 2010). As a result the geology of Marion Island is typical of oceanic volcanoes similar to those found in the Hawaiian archipelago (Prinsloo *et al*., 2010). Also, due to its position the island underwent extensive volcanism as well as glaciation during both the Quaternary and the Holocene (Hall *et al*., 2011). Nevertheless the most recent, and only volcanic eruption in recorded history occurred in 1980 A.D. (McDougall *et al*., 2001).

The climate of Marion Island is predominantly oceanic and thermally stable with a variation of only 3.6°C between the mean temperatures of the coldest and warmest months (Smith, 2002) and a mean annual air temperature of 5.0 °C. Marion Island has

undergone climatic changes in recent years and since the beginning of the 1970s, annual mean surface air temperature on the island has increased by 1.2 °C and annual precipitation has decreased to an average annual total of 700 mm in the 1990s 25% lower than the 1960s (Smith, 2002; Rouault *et al*., 2005).

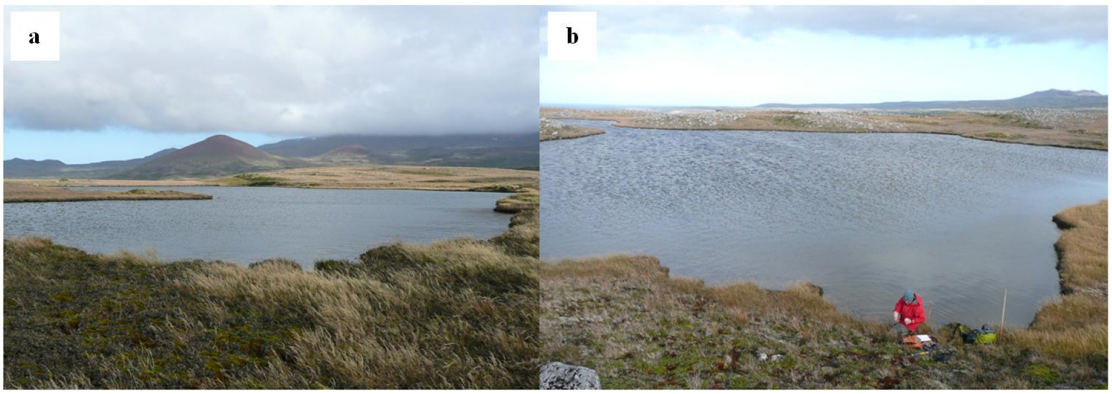

Figure 3.12: Photographs of two Marion Island lakes; a) MI4 and b) MI7. Photographs taken by Wim Van Nieuwenhuyze.

There are more than fifty lakes on Marion Island (Fig. 3.12) mostly consisting of small ponds. Even the larger lakes are still relatively shallow: one of the larger lakes MI4 has a maximum measured depth of 1.0 m and a spot surface water temperature of 7.4 °C measured in April 2011 (Verleyen and Van Nieuwenhuyze, 2011). MI7 (Fig. 3.12) another of the larger lakes on Marion Island had a spot surface water temperature of 7.8 °C when measured in April 2011 (Verleyen and Van Nieuwenhuyze, 2011).

3.1.3.3. Campbell Island

Campbell Island (Fig. 3.13) is located at 52°53’S, 159°10’E, 600 km south of the New Zealand mainland and 700 km to the east-northeast of Macquarie Island (Bestic *et al*., 2005; Marchant *et al*., 2011; Wanntorp *et al*., 2011; Scott and Kirkpatrick, 2013). Campbell Island is, 113 km^2 (McGlone *et al*., 2010) and surrounded by a number of rocks and islets including Dent Island, Folly Island, Isle de Jeanette Marie and Jacquemart Island (Department of Conservation, 2013). The lakes on the island include AB1, FR2, HO2, and NE2 which have water temperatures of 21.3 °C, 8.4 °C, 13.6 °C and 19.6 °C respectively (Saunders *et al.*, 2015). The location of these lakes can be seen in Fig. 3.13 and more information regarding the characteristics of these lakes can be seen in Table 3.1.

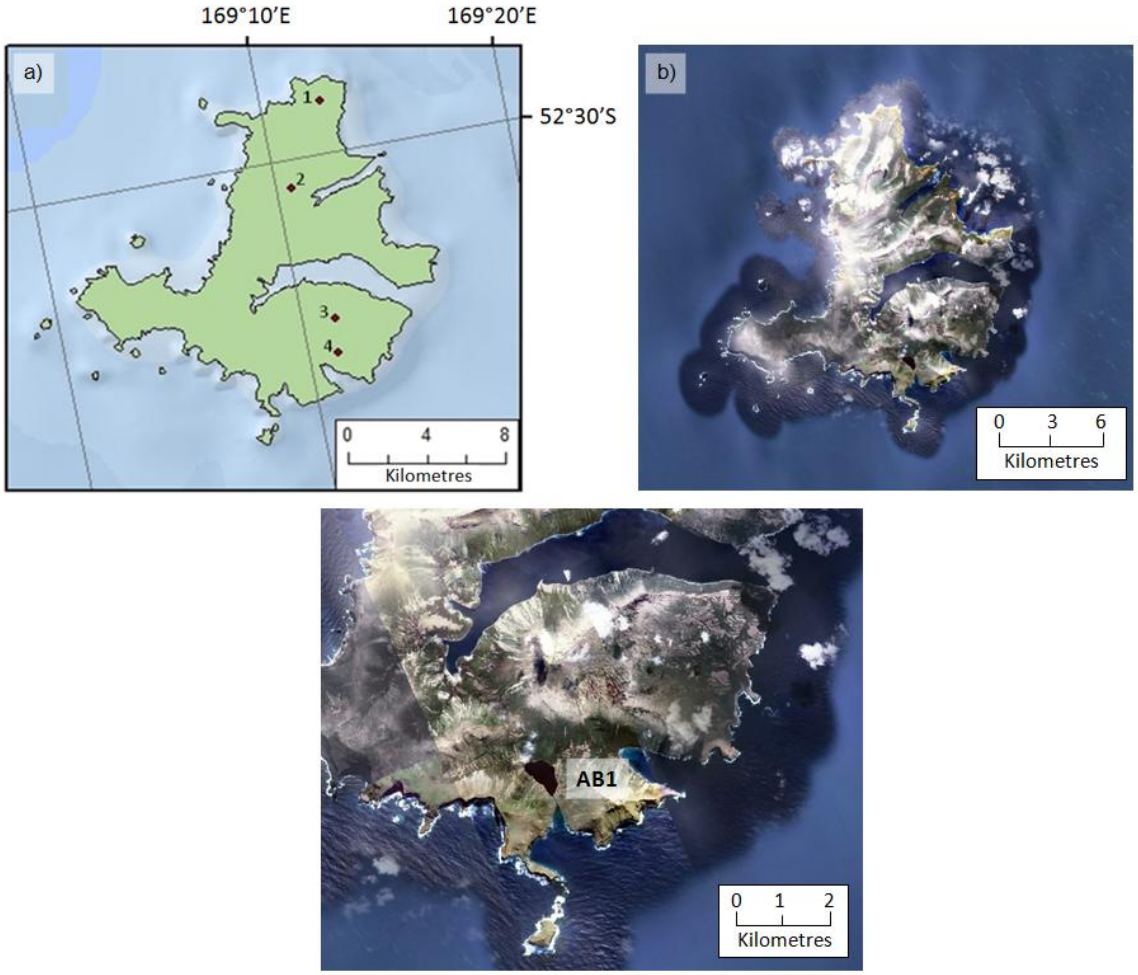

Figure 3.13: a) Map of Campbell Island showing the location of the lakes studied; 1) FR2, 2) NE2, 3) HO2 and 4) AB1. b) Satellite image of Campbell Island. c) Satellite image of AB1 and its catchment on Campbell Island. Satellite images edited from Google Earth images.

The climate of Campbell Island is influenced heavily by the westerly to north-westerly winds leaving it cool, wet and windy (Bestic *et al*., 2005; Saunders *et al*., 2009; McGlone *et al*., 2010; Department of Conservation, 2013). The mean annual temperature at sea level is 6.8 °C (Bestic *et al*., 2005; McGlone *et al*., 2010) and there are small annual and daily variations in temperature although the temperature rarely rises above 12 °C (Department of Conservation, 2013). Campbell Island has an average of 1400 mm of rain and at least 250 rain days a year (Bestic *et al*., 2005) and it rains on average 325 days of the year (Department of Conservation, 2013). The winds on the island are dominated by a persistent, strong westerly airflow (McGlone *et al*., 2010) with gusts over 96 km per hour on at least 100 days each year (Department of Conservation, 2013). Geologically Campbell Island is a remnant of a Miocene shield volcano (Wanntorp *et al*., 2011). It has a steep, rugged topography with the highest elevation of the 569 m a.m.s.l. at Mount Honey (Department of Conservation, 2013).

3.2. Site Selection

3.2.1. Calibration Site Selection

Thirty two lakes were selected from Antarctic, the sub-Antarctic Islands and Southern Chile for use in the GDGT-temperature calibration dataset. Lakes were selected from previously collected material to give a great enough range in mean summer air temperature (MSAT; December to February), -2.2 to 10.3 °C, to allow the development of a GDGT-temperature calibration. In ideal circumstances lakes would be selected to minimise variation in other environmental characteristics such as pH, conductivity and depth. Unfortunately, an adequate sample size could not be achieved when keeping these parameters broadly similar. Consequently the calibration lakes also covered a range of pH (4.5 to 9.8), conductivity (0.01 to 7.38 $mScm^{-1}$) and water depths (0.5 to 55 m). The average pH, conductivity and water depth for the dataset was 7.22, 0.49 (mS/cm) and 8.3 m respectively and standard deviation 1.3, 1.3 and 11.6 respectively. Table 3.1 contains summary data of some of the environmental characteristics of the lakes studied in this research summarised by region. See Appendix A for environmental data for each individual lake.

Region	Number of Lakes	Latitude		Longitude		Altitude (m)		Water Depth (m)		MAAT (°C)		MSAT (°C)		Conductivity (mS/cm)		pH	
		Min	Max	Min	Max	Min	Max	Min	Max	Min	Max	Min	Max	Min	Max	Min	Max
Alexander Island	2	S 70.85	S 71.78	W 68.25	W 68.33	98.0	126.0	5.6	55.0	-5.1	-4.9	0.1	0.3	0.058	0.158	6.67	7.97
Campbell Island	4	S 52.51	S 52.59	E 169.15	E 169.19	268.0	379.0	0.9	1.2	3.8	4.8	6.0	7.0	0.117	0.287	4.46	5.07
Fildes Peninsula	5	S 62.20	S 62.23	W 58.96	W 58.98	14.5	34.5	5.3	7.0	-2.5	-2.4	1.0	1.1	0.013	0.177	7.53	8.07
Larsemann Hills	4	S 69.38	S 69.41	E 76.05	E 76.40	5.0	65.0	3.8	38.0	-11.8	-11.2	-2.2	-1.6	0.261	7.380	6.30	7.10
Marguerite Bay	1	S 67.60	S 67.60	W 67.20	W 67.20	19.4	19.4	6.1	6.1	-4.5	-4.5	0.7	0.7	0.131	0.131	6.54	6.54
Marion Island	3	S 46.86	S 46.86	E 37.85	E 37.85	71.0	98.0	0.9	1.0	4.6	4.8	6.7	6.8	0.061	0.069	6.46	7.85
Potter Peninsula	2	S 62.24	S 62.25	E 58.66	E 58.67	21.0	35.0	2.2	5.6	-1.9	-1.8	1.0	1.1	0.050	0.050	6.17	6.40
South Georgia	1	S 54.50	S 54.50	W 37.05	W 37.05	94.0	94.0	18.0	18.0	1.6	1.6	4.4	4.4	0.038	0.038	8.07	8.07
Southern Chile	2	S 51.30	S 53.60	W 70.95	W 72.67	3.0	50.0	4.4	17.0	5.8	6.1	10.0	10.3	0.246	0.301	8.64	8.81
Syowa Oasis	4	S 69.03	S 69.47	E 39.51	E 39.61	-10.0	5.0	2.2	6.0	-10.7	-10.6	-2.0	-1.9	0.273	0.668	7.64	8.95
Trinity Peninsula	4	S 63.55	S 63.61	W 57.34	W 57.41	2.5	134	0.5	24.0	-5.9	-5.1	-0.4	-0.4	0.035	0.470	7.37	9.80

Table 3.1: Summary table detailing the characteristics of the lakes studied by region.

3.2.2. Core Site Selection

Two lake cores were selected for a downcore reconstruction of mid-late Holocene climates as part of this research. These lakes were Fan Lake located on Annenkov Island, South Georgia and Yanou Lake on King George Island, South Shetland Islands. Factors considered when selecting the core site included; (1) their position in relation to one another and the PFZ, (2) data already available from the lakes from previous research, (3) appropriateness of the archive avoiding issues such as external influences on the lake from either the local fauna or anthropogenic impacts and (4) the nature of the GDGT composition in the surface sample used in the GDGT-temperature calibration.

One of the aims of this research, aside from reconstructing palaeoclimates, was to compare records across the PFZ thus enhancing the current understanding of changes in the strength and / or position of the PFZ in relation to climatic change. The location of Fan Lake (54°29’0”S, 37°5’0”W) and Yanou Lake (62°13’15”S, 58°57’35”W) are either side of the current position but within the influence of the PFZ (Fig. 3.8). Therefore, records from Fan Lake and Yanou Lake not only allow a comparison across the PFZ but their close proximity to the PFZ mean changes in its strength and / or position may be identifiable in the records.

Considering the other factors outlined above, Fan Lake was chosen as there is a wealth of previously supporting data for the core including pigment and diatom data (Van Nieuwenhuyze *et al*., in prep), pollen data (Strother *et al*., 2015), ITRAX scans, carbon and nitrogen isotope data (Roberts, pers. comm.) enabling a thorough examination of the GDGT-temperature record with other proxies of environmental change. ITRAX scan and carbon and nitrogen isotope data also allow changes in the core sedimentology to be considered. The slightly faster sediment accumulation rate in Fan Lake, compared to other Antarctic and sub-Antarctic lakes such as Yanou Lake, means the resolution of c. 100 years from a 4 cm sampling strategy, can be achieved throughout the record. Moreover, Lead-210 (^{210}Pb) dating had previously been done on the top 11 cm of the Fan Lake core. Therefore, a more detailed study of the last 100 years would be possible in Fan Lake. Finally, in addition to the strong GDGT abundances seen in the surface sample from the calibration dataset, two core samples at 1.5 and 16 cm depth had previously run as a pilot study by Emma Pearson at Newcastle University and also contained GDGTs suggesting GDGTs would be present throughout the core.

Yanou Lake was chosen as the site currently south of the PFZ from a selection of South Shetland Island and Beak Island lakes. Yanou Lake was selected as, although ^{210}Pb was not possible, the current age-depth model at Yanou is more-well constrained in comparison to some of the other lakes on King George Island i.e., Belén Lake (Roberts, pers. comm.). Although Yanou Lake has previously being inundated with marine waters the terrestrial units in Yanou Lake cover the last c. 6000 years (Watcham *et al*., 2011) thus mid-late Holocene temperatures could be reconstructed. In addition, like Fan Lake, previously collected supporting data including ITRAX scans, ICP-MS and total carbon data (Roberts, pers. comm.) and diatom data (Watcham *et al*., 2011) where avaliable. No pigment data is currently available so that will be incorporated into this study. Finally, although no previous extractions of GDGTs in the core material have been undertaken on Yanou Lake, the surface samples had a strong presence of GDGTs.

These two lakes are the focus of Chapter 7 and 8 where the Antarctic and sub-Antarctic GDGT-temperature calibration developed in Chapter 6 is applied to the core material.

3.3. Conclusions

This chapter has introduced the different regions of Antarctica and the sub-Antarctic Islands where the 32 lakes used within the surface calibration dataset and the two cores, Fan Lake and Yanou Lake, are from. The lakes used within the surface dataset come from a range of environments from the sub-Antarctic Islands which are relatively warm but wet and windy due to the influence of the SWW to East Antarctica which is much colder and drier. The lakes studied range from larger, deeper lakes such as Moutonnée Lake to much smaller and shallower lakes including the Marion Island lakes at c. 1, depth. In addition, the lakes range in both pH and conductivity (see Table 3.1).

The chapter concludes with a description of the site selection process for the surface dataset which focused on including a great temperature range, whilst trying to minimise the variance in other environmental conditions. Finally, the core selection process which was based on proximity to the PFZ, data already available, appropriateness of the archive and the nature of the GDGT composition in the surface sample.

Chapter 4: A Review of the Application of Glycerol Dialkyl Glycerol Tetraethers (GDGTs) and Pigments in Palaeolimnology

Summary

In this chapter previous work on the development of both GDGTs and pigments as proxies and their application is reviewed. Advances in liquid chromatography have been key to the development of both proxies. The chapter starts by introducing GDGTs and some of the early work developing GDGTs as a temperature proxy in marine environments. Their development as a proxy and application in soils and lakes is then discussed. Finally, the methodological development of GDGTs is reviewed. The chapter then follows with a focus on pigments and their use as an indicator of primary productivity and other environmental conditions, particularly in lacustrine environments. The different types of pigments are introduced and how these different types of pigments degrade is summarised. Finally, previous applications of pigments on sediment cores from Antarctic lakes are reviewed.

4.1. Glycerol Dialkyl Glycerol Tetraethers (GDGTs)

Few quantitative temperature proxies exist for the continental environment hampering palaeoclimate studies in these environments. Recent analytical advances in the use of liquid chromatography coupled to a mass spectrometer (LC-MS) and their ability to rapidly screen for the presence of tetraethers has resulted in a marked increase in the use of Archaeal membrane lipids, such as glycerol dialkyl glycerol tetraethers (GDGTs) (Fig. 4.2), as biomarkers in the sedimentary record (Hopmans *et al*., 2000; Huguet *et al*., 2010a).

Research in this field has led to the development of a sea surface temperature proxy using isoprenoid GDGTs (isoGDGTs) called TEX_{86}, first documented by Schouten *et al*. (2002). Subsequently, Powers *et al*. (2004) went on to find that GDGTs are not restricted to marine environments, but are also found in lakes thus unlocking their potential as a continental temperature proxy. Since then, finding GDGTs in terrestrial environments attention has focused on the potential of branched GDGTs (brGDGTs) as a palaeoenvironmental tool for continental climate reconstruction in soils (e.g., Weijers *et al*., 2007a; Peterse *et al*., 2009a; 2012) and lakes (e.g., Blaga *et al*., 2010; Pearson *et al*., 2011; Sun *et al*., 2011; Loomis *et al*., 2012; 2014a; Shanahan *et al*., 2013; Wu *et al*., 2013; Woltering *et al*., 2014). In addition, research into the origin and composition of

GDGTs has also been conducted in other continental archives such as peat (e.g., Sinninghe Damsté *et al*., 2000; Huguet *et al*., 2010b; Peterse *et al*., 2011; Weijers *et al*., 2011), rivers (e.g., Zhu *et al*., 2011; Zell *et al*., 2013; De Jonge *et al*., 2014) and speleothems (e.g., Yang *et al*., 2011; Blyth and Schouten, 2013; Blyth *et al*., 2014).

4.1.1. GDGT sources and structures

GDGTs are specific membrane lipids which were originally thought to be biosynthesized by Group 1 Crenarchaeota, a subgroup of Archaea (Schouten *et al*., 2002; Huguet *et al*., 2006). Archaea form one of the three domains of living organisms on Earth alongside Bacteria and Eucarya (Fig. 4.1). The composition of the cellular membrane is the distinguishable characteristic of Archaea from Bacteria and Eucarya (Huguet *et al*., 2006). Bacterial membranes are commonly formed by straight-chain fatty acids ester bound to glycerol, alternatively, Archaeal membranes contain lipids with isoprenoid alkyl chains bound by ether bonds (Huguet *et al*., 2006).

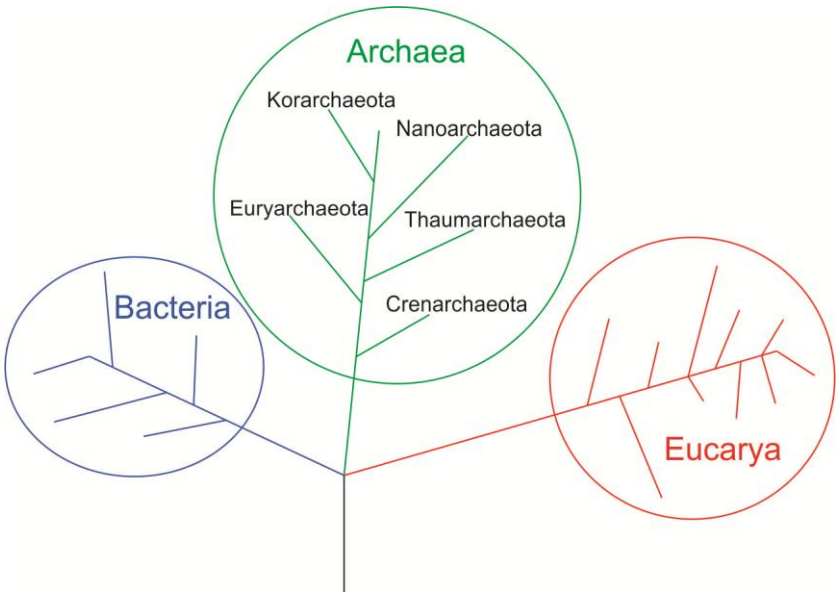

Figure 4.1: Phylogenetic tree representing the three domains of living organisms; Bacteria, Archaea and Eucarya and the five phyla of Archaea.

The kingdom of Archaea comprises of five phyla: Crenarchaeota, Euryarchaeota, Korarchaeota, Nanoarchaeota and Thaumarchaeota (Fig. 4.1) (Brochier-Armanet *et al*., 2008; Spang *et al*., 2010). Crenarchaeota were originally thought to be extremophiles which inhabit ecological niches characterised by extreme conditions i.e. high temperature, high salinity, high pH, or anoxic conditions (Schouten *et al*., 2002; Sinninghe Damsté *et al*., 2002; Powers *et al*., 2004; Huguet *et al*., 2006). However, research has indicated that carbon skeletons present in GDGTs are also present in non-

extreme environments suggesting they are derived from GDGTs of non-thermophilic Crenarchaeota (Schouten *et al*., 2000), in particular crenarchaeol which is thought to be an adaptation to relatively cold temperatures (Huguet *et al*., 2006). rRNA analysis of the GDGTs has also indicated that non-extremophilic Archaea are widespread and an abundant component of the marine planktonic community (Sinninghe Damsté *et al*., 2002). More recently, research by Brochier-Armanet *et al*. (2008) suggested that the mesophilic Archaea are without a doubt different from hyperthermophilic Crenarchaeota meaning the original affiliation of GDGTs to Crenarchaeota was incorrect. Brochier-Armanet *et al*. (2008) proposed a new Archaeal phylum named Thaumarchaeota. The new addition of Thaumarchaeota as a phylum of Archaea is also supported by further rRNA analysis by Spang *et al*. (2010).

In living cells GDGTs contain a polar head group and are known as intact GDGTs. Soon after death these polar head groups are cleaved off, leaving only the core GDGT compounds (Lipp *et al*., 2008; Pitcher *et al*., 2009; Huguet *et al*., 2010a). There are two main types of GDGTs, isoprenoid and branched (Fig. 4.2) identifiable by their molecular structure. Isoprenoid compounds are derived from Archaea and branched components from bacteria (Zink *et al*., 2010). Whilst isoGDGTs occur ubiquitously in open oceans and lakes (Bechtel *et al*., 2010) brGDGTs are ubiquitous compounds in peat (e.g., Sinninghe Damsté *et al*., 2000) and soil (e.g., Weijers *et al*., 2006a), and are found in some ocean margin sediments due to fluvial transport of terrestrial soil organic matter (e.g., Hopmans *et al*., 2004). Although brGDGTs were originally thought to be produced only in terrestrial environments more recent research has suggested that brGDGTs are also produced in freshwaters (Sinninghe Damsté *et al*., 2009; Tierney and Russell, 2009; Bechtel *et al*., 2010; Loomis *et al*., 2011; 2014b; Pearson *et al*., 2011; Wu *et al*., 2013; Naeher *et al*., 2014). Moreover, in their review, Schouten *et al*. (2013) state that GDGTs are amongst the most abundant and ubiquitously occurring lipids on Earth and an absence of them in present day environmental samples is unusual.

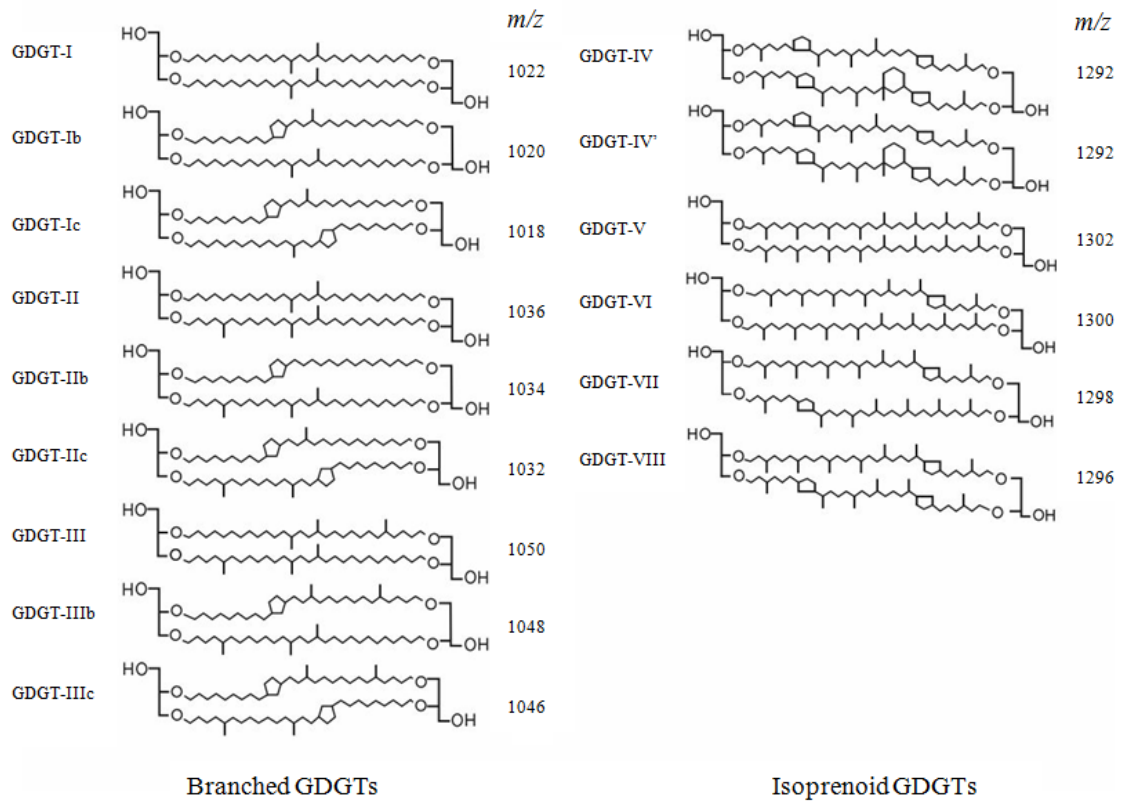

Figure 4.2: Chemical structures of GDGTs, branched compounds GDGT-I to GDGT-III (left) and isoprenoid compounds GDGT-IV to GDGT-VIII (right)

4.1.2. The GDGT-temperature relationship

Structural changes in the GDGT lipid cell membrane strongly depend on growth temperature (Schouten *et al*., 2002). This physical adaptation, which is similar to that of other thermophilic genetic relatives (Gliozzi *et al*., 1983; De Rosa *et al*., 1988; Uda *et al*., 2001), is due to the higher thermal transition points of cell membranes composed of GDGTs with cyclopentane rings (Gliozzi *et al*., 1983; Schouten *et al*., 2002). As a result the number of cyclopentane rings in the GDGT structure is considered to be a key factor in the adaptation to temperature change (Gliozzi *et al*., 1983; De Rosa *et al*., 1988; Uda *et al*., 2001; Schouten *et al*., 2002). These structural changes in GDGTs were first noted in marine environments by Schouten *et al*. (2002) and although much of the early work using GDGTs as temperature proxies was focused on ocean settings, recent studies (e.g., Powers *et al*., 2004; Blaga *et al*., 2009; Tierney *et al*., 2010a; Pearson *et al*., 2011; Loomis *et al*., 2012; Shanahan *et al*., 2013) have focused on their use in lakes finding similar relationships between GDGT composition and temperature in these environments.

4.1.3. GDGTs in marine environments

GDGTs are a well used temperature proxy in marine environments (e.g., Zachos *et al*., 2006; Shevenell *et al*., 2011; Kim *et al*., 2012; Turich *et al*., 2013) and have been found in sediments at least 112 million years old, thus allowing sea surface temperature (SST) reconstructions back to the middle Cretaceous (Schouten *et al*., 2002). The majority of work using GDGTs in the marine environment has involved the development and application of the TEX_{86} index (TetraEther indeX of tetraethers consisting of 86 carbon atoms). When Schouten *et al*. (2002) developed the proxy they stated that the establishment of a new organic geochemical temperature proxy allows a new way of deciphering past ocean water temperature. Although, several proxies for SST already existed, e.g., $\delta^{18}O$ and Mg/Ca of planktonic foraminifera and the $U^{K'}_{37}$ ratio using alkenones (e.g., Elderfield and Ganssen 2000; Farmer *et al*., 2008), limitations of the current methods include the carbonate concentration and oxygen isotopes within seawaters affecting foraminiferal studies (e.g., Spero *et al*., 1997; Schouten *et al*., 2002) and the diagenetic stability of alkenones (e.g., Hoefs *et al*., 1998; Schouten *et al*., 2002). Hence, Schouten *et al*. (2002) suggested that there is a real need for new SST proxies of which GDGTs could be the basis.

The TEX_{86} index (Eq. 4.1) is based on the linear relationship between the number of cyclopentane rings and SST. Schouten *et al*. (2002) analysed more than 40 surface sediments (0 – 2 cm) from 15 locations worldwide (Fig. 4.3) ranging in annual mean SST from 2 to 27 °C to determine the environmental controls on GDGT composition. They observed that in cold areas, such as Halley Bay, Antarctica, there was a predominance of GDGT-V and crenarchaeol whereas warmer samples, e.g. the Arabian Sea, were dominated by crenarchaeol and contained higher concentrations of GDGTs (VI-VIII).

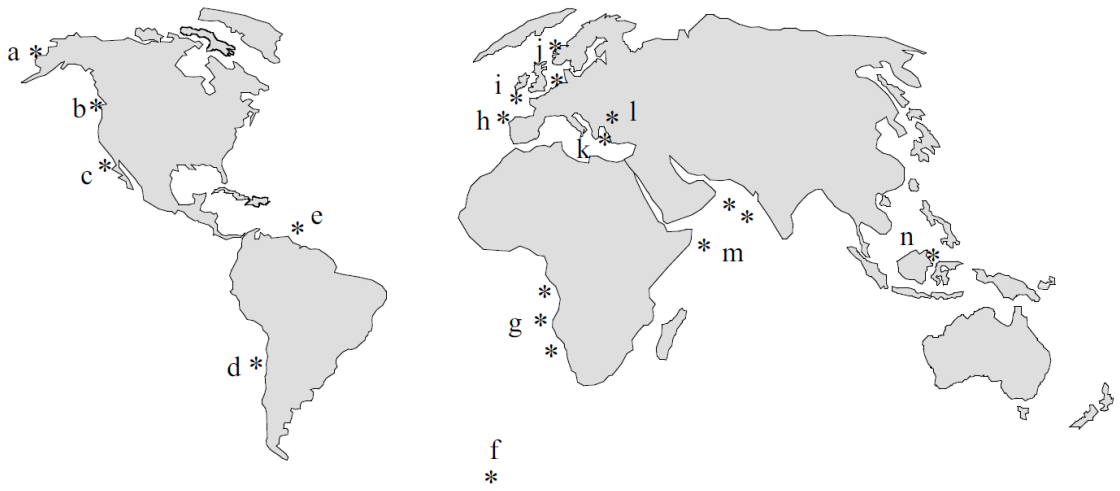

Figure 4.3: Location map of surface sediments analyzed by Schouten *et al*. (2002) and used in the development of the TEX_{86} index. a) Skan Bay, b) Saanich Inlet, c) Santa Monica Basin, d) Peru Margin, e) Cariaco Basin, f) Halley Bay Station, g) Angola Basin, h) Iberian Margin, i) Wadden Sea, j) Skagerrak and Drammensfjord, k) Aegean Sea, l) Black Sea, m) Arabian Sea and n) Kau Bay. Figure taken from Schouten *et al*. (2002).

To quantify the control of temperature on GDGT composition Schouten *et al*. (2002) compared several different ratios of GDGTs, using the weighted average number of cyclopentane rings, to the local annual mean SST. This led Schouten *et al*. (2002) to a best fit which they coined the TEX_{86} index defined as:

$$TEX_{86} = \frac{([VII]+[VIII]+[IV'])}{([VI]+[VII]+[VIII]+[IV'])} \quad \text{(Eq. 4.1)}$$

With the relationship between the TEX_{86} index and annual mean SST defined by Schouten *et al*. (2002) as:

$$TEX_{86} = 0.015T + 0.28 \ (r^2 = 0.92) \quad \text{(Eq.4.2)}$$

where T equals sea surface temperature (SST).

As with any other proxy the accuracy to which the TEX_{86} index can reconstruct temperature is paramount. For TEX_{86} Schouten *et al*. (2002) estimate the standard error in the temperature estimation as ± 2.0 °C. Nevertheless, Schouten *et al*. (2002) urge caution when using the TEX_{86} index to reconstruct temperatures as salinity also varied within the dataset and so temperature may not be the only environmental control on GDGT composition. This is of particular importance as other studies have also found that relative GDGT compositions in Archaea may be dependent on salinity (e.g., Tierney *et al*., 2010a; Pearson *et al*., 2011; Wu *et al*., 2013). One study in particular by

Wu *et al*. (2013) found a large switch in the composition of isoGDGTs in response to increased salinity. Therefore, it is important to assess the environmental controls on GDGT composition at any site prior to any palaeoenvironmental reconstruction. Nonetheless, since its development the TEX_{86} index has been applied worldwide on multiple cores covering a wide time range. In one study by Jenkyns *et al*. (2004) Arctic palaeotemperatures from Upper Cretaceous deposits were determined. Zachos *et al*. (2006) also used the proxy to estimate coastal SST during the Paleocene-Eocene Thermal Maximum and Shevenell *et al*. (2011) used TEX_{86} derived SST data to indicate the importance of regional summer duration as a driver of Antarctic seasonal sea-ice fluctuations.

Following the development of the Schouten *et al*. (2002) TEX_{86} index Kim *et al.* (2010) studied the isoGDGT composition in 116 core-top marine sediments from sub-polar and polar oceans. Incorporating these new core-top samples with the global dataset of 426 samples Kim *et al.* (2010) found different isoGDGTs to be significant within different temperature ranges, for example crenarchaeol regio-isomer (GDGT-IV' Fig. 4.2) was more significant in sub-tropical environments than sub-polar environments. Therefore, Kim *et al.* (2010) suggested two variations of the TEX_{86} index, TEX^{L}_{86} (Eq. 4.3 & 4.4) for low temperature regions (SST between -3 and 30 °C), which excludes the use of crenarchaeol regio-isomer and TEX^{H}_{86}, (Eq. 4.5 & 4.6) for high temperature regions where SST is greater than 30 °C.

$$TEX^{L}_{86} = \log \frac{([VII])}{([VI]+[VII]+[VIII])} \quad \text{(Eq. 4.3)}$$

$$SST = 67.5 \times TEX^{L}_{86} + 46.9 \ (r^2 = 0.86) \quad \text{(Eq. 4.4)}$$

$$TEX^{H}_{86} = \log \frac{([VII]+[VIII]+[IV'])}{([VI]+[VII]+[VIII]+[IV'])} \quad \text{(Eq. 4.5)}$$

$$SST = 68.4 \times TEX^{H}_{86} + 38.6 \ (r^2 = 0.87) \quad \text{(Eq. 4.6)}$$

Kim *et al.* (2010) first tested the applicability of TEX^{L}_{86} in core MD88-769 from the Southern Ocean. An average LGM temperature of 3 °C was reconstructed, comparable with estimated temperatures of 5 to 7 °C from diatom assemblage data (Kim *et al.* 2009). Kim *et al.* (2010) also applied TEX^{H}_{86} to Quaternary sediments from the Arabian Sea (10°47'N, 51°56'E) where reconstructed temperatures indicated a c. 2 °C increase between the LGM and present day SST. Such a temperature increase is consistant with

the MARGO project members (2009) temperature estimates for the Indian Ocean. Following this both calibrations have been applied on relevant material including core JPC-10 from the Antarctic Peninsula where Etourneau *et al.* (2013) successfully reconstructed SST using TEX^{L}_{86} from c. 9000 cal. yr. B.P. to present. Etourneau *et al.* (2013) found good correlation between the TEX^{L}_{86} reconstructed temperatures and the relative abundance of the cold and warm varieties of the diatom *Thalassiosira antarctica* from the same core.

More recently Tierney and Tingley (2014) have taken the regionalised approach to TEX_{86} of Kim *et al.* (2010) and developed BAYSPAR. BAYSPAR gives a regionally appropriate Bayesian regression model of TEX_{86} for application on core material. Tierney and Tingley (2014) showed BAYSPAR to produce reasonable results on both a Quaternary and Eocene time scale. Moreover, Linnert *et al.* (2014) found that in Shuqualak–Evans borehole, Mississippi, USA, the new BAYSPAR method gave similar results to TEX^{H}_{86} during the Late Cretaceous. Further application of BAYSPAR is required to determine whether a spatially restricted calibration using Bayesian modelling is more applicable than the global TEX_{86} index or TEX^{L}_{86} and TEX^{H}_{86}.

In addition to comparing different versions of the TEX_{86} index, research has also focused on the comparison of TEX_{86} derived SSTs with other SST reconstructions determined from different proxies, in particular, temperature reconstructions based on the $U^{K'}_{37}$ index. Turich *et al*. (2013) applied both the TEX_{86} and $U^{K'}_{37}$ indices in sinking particles from two shallow sediment traps at 275 m and 455 m in the Cariaco Basin, Venezuela. They found that temperatures derived from both proxies were cooler than measured mean summer SSTs. In the 275 m trap TEX_{86} derived temperatures were between 2 and 4 °C cooler than the measured SST during the late summer months (Turich *et al*., 2013). Turich *et al*. (2013) also found that TEX_{86} temperatures are overestimated by around 2 °C during periods of upwelling in November. In another study, Li *et al*. (2013) compare both proxies at ODP Site 1147 from the northern South China Sea over the past c. 356,000 cal. yr B.P. finding that both showed clear and similar glacial–interglacial patterns. $U^{K'}_{37}$ derived temperatures fluctuated between 22.3 and 28.3 °C with a glacial–interglacial difference of c. 4 to 5 °C while TEX_{86} temperatures varied between 20.3 and 25.4 °C with a glacial–interglacial difference of c. 4 °C (Li *et al*., 2013). Throughout the whole record TEX_{86} derived temperatures are lower than $U^{K'}_{37}$ derived temperatures and Li *et al*. (2013) suggest this could be as a result of $U^{K'}_{37}$ reflecting SST while TEX_{86} reconstructs sub-surface temperatures. Li *et*

al. (2013) were not the first to suggest this, other research in the Santa Barbara Basin, California (Huguet *et al*., 2007), Guinea Plateau Margin, tropical North Atlantic (Lopes dos Santos *et al*., 2010), South China Sea (Jia *et al*., 2012), Eastern Antarctic continental margin (Kim *et al*., 2012), Gulf of California (McClymont *et al*., 2012), and the Eastern Equatorial Pacific (Seki *et al*., 2012) all suggest that the TEX_{86} index reflects sub-surface rather than surface temperatures. This has allowed the TEX_{86} index to be used as an indicator of upwelling by Jia *et al*. (2012), Kim *et al*. (2012) and McClymont *et al*. (2012).

4.1.4. GDGTs in terrestrial environments

GDGTs have also been applied as a temperature proxy in terrestrial settings. BrGDGTs were first found in extracts of a Holocene Bargerveen peat from southeast Drenthe, the Netherlands by Sinninghe Damsté *et al*. (2000) who referred to them as unidentified non-isoGDGTs. Schouten *et al*. (2000) subsequently confirmed that these newly identified GDGTs were unlike any others as their carbon skeletons were not composed of isoprenoids but of branched skeletons. Hence these compounds were coined branched GDGTs. These brGDGTs contain 4–6 methyl groups attached to the *n*-alkyl chains and 0 to 2 cyclopentyl moieties in the alkyl chain (Weijers *et al*., 2007a) the exact producers of the brGDGTs are unknown. Weijers *et al*. (2006a; 2009) undertook 16S ribosomal RNA analysis to distinguish the producer of these brGDGTs in soils, finding that they are produced by bacteria but were unable to be more specific. More recently, Oppermann *et al*. (2010) identified heterotrophic organisms as a likely producer of branched GDGTs.

The analysis of terrestrial soils and peat by Hopmans *et al*. (2004) indicated that brGDGTs are the predominant GDGT compounds in these environments. The peat samples also contained crenarchaeol, although in one of the soil samples from Texel, the Netherlands, only the branched compounds were present, indicating that the organisms which biosynthesize GDGTs in soils only biosynthesize brGDGTs and not isoGDGTs (Hopmans *et al*., 2004). This revelation led Hopmans *et al*. (2004) to explore the use of branched compounds as a tracer of soil and peat organic matter, especially if found in coastal marine, open marine, and lacustrine sediments. From this finding Hopmans *et al*. (2004) developed the Branched and Isoprenoid Tetraether (BIT) index (Eq. 4.7).

The BIT index relies on the assumption that marine sediments are dominated by crenarchaeol, which makes up less than 1% of terrestrial GDGTs (Hopmans *et al*., 2004), and that branched compounds are only produced in terrestrial environments. Therefore, the index is based on the relative abundance of brGDGTs, representing terrestrial organic matter, and crenarchaeol, indicative of aquatic organic matter (Hopmans *et al*., 2004). Hopmans *et al*. (2004) define the BIT index as:

$$\mathrm{BIT} = \frac{[\mathrm{I}+\mathrm{II}+\mathrm{III}]}{[\mathrm{I}+\mathrm{II}+\mathrm{III}]+[\mathrm{IV}]} \qquad \text{(Eq. 4.7)}$$

Before application, the BIT index was first scrutinised by Hopmans *et al*. (2004) as well as Weijers *et al*. (2006b). To test the applicability Hopmans *et al*. (2004) applied the BIT index to core top sediments from the Angola Basin, eastern tropical Atlantic, near the mouth of the Congo River from which they found that at the outflow BIT values ranged from 0 in open marine surface sediments to 0.91 at the mouth of the river (Fig. 4.4). The results suggest that, as expected, higher BIT values are found near sources of terrestrial input where there is a greater abundance in branched compounds. Following this, Weijers *et al*. (2006b) completed a study analysing GDGT membrane lipid content in soil samples from across the global. They found that crenarchaeol is present in nearly all soils thus complicating not only the BIT index (Eq. 4.7) but also the TEX_{86} index (Eq. 4.1 & 4.2).

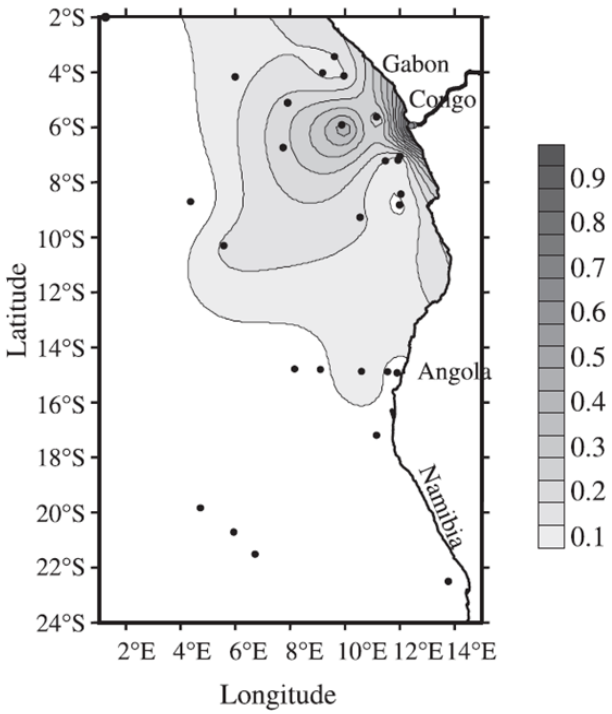

Figure 4.4: Map representing the 'drop off' in the BIT value with distance from the mouth of the Congo River. Figure taken from Hopmans *et al*. (2004).

Recently, however, research suggesting that brGDGTs may also be produced *in situ* in aquatic environments could complicate the use of BIT as an indicator of terrestrial input (Naeher *et al*., 2014; Shanahan *et al*., 2013; Loomis *et al*., 2014b; Peterse *et al*., 2014). For example, Wu *et al*. (2013) found that in Kusai Lake, on the Qinghai-Tibetan Plateau, the soil BIT values were lower than the BIT values in the near shore sediments therefore, some production of branched compounds within the lake is likely. Nevertheless, if these complicating factors are considered then the use of the BIT index to assess the terrestrial input could reduce the bias of the TEX_{86} index (Weijers *et al*., 2006b) or at least indicate locations where the use of the TEX_{86} index may not be applicable.

The controlling factors on the relative abundance of brGDGTs in soils were first investigated by Weijers *et al*. (2007a). As the producers of brGDGTs are unknown culture experiments are not possible therefore, Weijers *et al*. (2007a) analysed 134 soil samples from 90 globally distributed locations (Fig. 4.5). BrGDGTs were present in all samples analysed in differing abundances and with varying structure (Weijers *et al*., 2007a). Through principal component analysis (PCA) Weijers *et al*. (2007a) found relationships between the structural differences of the brGDGTs and pH and air temperature.

Figure 4.5: Map of the soil sample locations used by Weijers *et al*. (2007a) to evaluate the environmental controls on brGDGTs and develop the MBT/CBT index. Figure taken from Weijers *et al*. (2007a).

Weijers *et al*. (2007a) expressed the relationship between the number of cyclopentyl moieties and soil pH through the cyclisation ratio of branched tetraethers (CBT; Eq.4.8)

with an r^2 value of 0.70 when related to pH, however only 0.03 when related to temperature CBT is defined as:

$$\mathrm{CBT} = -\log\left(\frac{([\mathrm{Ib}]+[\mathrm{IIb}])}{([\mathrm{I}]+[\mathrm{II}])}\right) \quad \text{(Eq. 4.8)}$$

The relationship between the CBT index and pH is defined by Weijers *et al*. (2007a) as:

$$\mathrm{CBT} = 3.33 - 0.38 \times \mathrm{pH}\ (r^2 = 0.70) \quad \text{(Eq.4.9)}$$

Weijers *et al*. (2007a) also found the number of methyl branches to be positively correlated (r^2 = 0.62) to mean annual air temperature (MAAT) and to a lesser extent negatively correlated to pH (r^2 = 0.37) (Fig. 4.6).

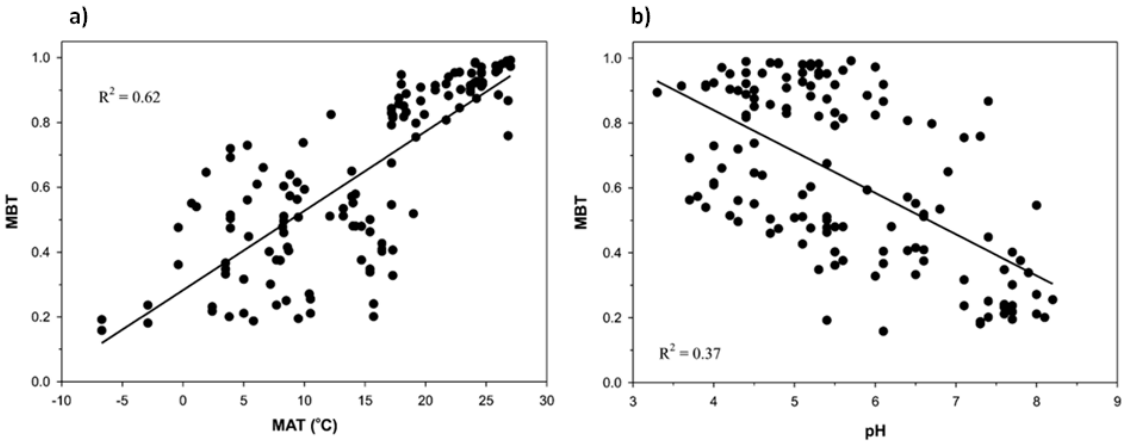

Figure 4.6: The relationship between MBT (eq. 3.6) and a) mean annual air temperature and b) soil pH in the 134 soil samples studied by Weijers *et al*. (2007a). Figure edited from Weijers *et al*. (2007a).

Weijers *et al*. (2007a) used these relationships to define the methylation index of branched tetraethers (MBT) as:

$$\mathrm{MBT} = \frac{[\mathrm{I}+\mathrm{Ib}+\mathrm{Ic}]}{[\mathrm{I}+\mathrm{Ib}+\mathrm{Ic}]+[\mathrm{II}+\mathrm{IIb}+\mathrm{IIc}]+[\mathrm{III}+\mathrm{IIIb}+\mathrm{IIIc}]} \quad \text{(Eq. 4.10)}$$

The relationship between the MBT index and MAAT is defined by Weijers *et al*. (2007a) as:

$$\mathrm{MBT} = 0.122 + 0.187 \times \mathrm{CBT} + 0.020 \times \mathrm{MAAT}\ (r^2 = 0.77) \quad \text{(Eq. 4.11)}$$

As MBT relates to MAAT as well as soil pH and CBT relates primarily to soil pH, Weijers *et al*. (2007a) were able to calculate MAAT by combining both MBT and CBT (Eq. 4.11) therefore making reconstructions of past MAAT from soil samples possible.

Since its development the MBT/CBT index has been used in many soil based temperature reconstructions (e.g., Peterse *et al*., 2009c; Niemann *et al*., 2012; Ajioka *et al*., 2014). In addition to its application in soil samples, Weijers *et al*. (2007b) applied the MBT and CBT indices in a marine sediment record located near the Congo River outflow to reconstruct MAAT over the past 25,000 years. The application of the MBT/CBT index allowed a comparison between MAAT and alkenone SST data obtained from the same core. Weijers *et al*. (2007b) found good correlation between the two records and other regional climate records. For example between the last glacial maximum and present the MBT/CBT reconstructed MAAT shows a temperature increase of c. 4 to 4.5 °C with regional temperature increases of c. 3.5 °C, 4 to 4.5 °C and 5.7 °C in TEX_{86}, pollen and speleothem records respectively.

Peterse *et al*. (2012) aimed to improve the accuracy of the MBT/CBT index for use in soils by adding 126 new soil samples to the Weijers *et al*. (2007a) dataset as well as previously reported data from 65 samples from China (Peterse *et al*., 2009b), the Amazon Fan (Bendle *et al*., 2010) and Svalbard (Peterse *et al*., 2009a) creating a total samples size of 278 globally distributed soils. Peterse *et al*. (2012) studied only the surface soils which are more directly influenced by MAAT and based on the relative abundance of the brGDGTs they recalibrated the MBT/CBT index. Firstly they exclude GDGT-IIIb and GDGT-IIIc from the MBT index:

$$\mathrm{MBT'} = \frac{(\mathrm{I+Ib+Ic})}{(\mathrm{I+Ib+Ic+II+IIb+IIc+III})} \qquad \text{(Eq. 4.12)}$$

This was done because GDGT-IIIb and GDGT-IIIc were frequently below the detection limit and where present comprised no more than 1% of the total brGDGTs on average. Peterse *et al*. (2012) then go on to recalibrate the MBT/CBT index using the new MBT':

$$\mathrm{MAAT} = 0.81 - 5.67 \times \mathrm{CBT} + 31.0 \times \mathrm{MBT'} \qquad \text{(Eq. 4.13)}$$

(r^2 = 0.59, RMSE = 5.0 °C)

Since its development the Peterse *et al*. (2012) MBT'/CBT index (Eq. 4.13) has been applied in several studies in both soil and lake sediments. Yang *et al*. (2013) compared reconstructed temperatures in soils from the Yangtze River catchment finding that both the MBT'/CBT and the Weijers *et al*. (2007a) MBT/CBT indices gave similar temperature reconstructions. Moreover, in Lake McKenzie, Australia Woltering *et al*. (2014) found that the MBT'/CBT index accurately represented both the trends and

magnitude of previous temperature reconstructions of the glacial to Holocene transition. Nevertheless, in Arctic Lakes Peterse *et al*. (2014) found that the reconstructed MAAT when using the MBT'/CBT (Eq. 4.13) was c. 8 °C higher than when applying the MBT/CBT (Eq. 4.11). Hence, Peterse *et al*. (2014) concluded that the MBT'/CBT over estimates temperatures at high latitudes and the original Weijers *et al*. (2007a) MBT/CBT is more appropriate in these environments. Therefore, the MBT'/CBT is unlikely to be suitable for reconstructing MAAT in Antarctic lake systems.

As well as using brGDGTs as an indicator of temperature in terrestrial environments, recent research by De Jonge *et al.* (2014b) has found a relationship between newly identified brGDGT isomers and pH. These unknown 5- and 6-methyl isomers of hexa- and penta-methylated brGDGTs (GDGT-IIa' and GDGT-IIIa') were first noted by De Jonge *et al.* (2013) in a Siberian peat. Following this De Jonge *et al.* (2014a) were able to sufficiently separate and quantify GDGT-IIIa', GDGT-IIIb' and GDGT-IIIc' and De Jonge *et al.* (2014b) separated and quantified GDGT-IIa', GDGT-IIb' and GDGT-IIc'. De Jonge *et al.* (2014b) went on to show that soil pH accounted for the greatest proportion a variation in the 6-methyl brGDGTs. Identifying and excluding these 6-methyl brGDGTs allowed De Jonge *et al.* (2014b) to improve MAAT and pH reconstructions when excluding the isomers from MBT' calculations.

4.1.5. GDGTs in lacustrine environments

Unlike marine environments, where long-chain alkenones can also be used to reconstruct SSTs using the $U^{K'}_{37}$ index, the occurrence of alkenones in lake sediments is highly sporadic therefore, they are unlikely to be a reliable proxy in lakes (Powers *et al*., 2004). Although some studies have looked at the composition and application of alkenones within a lacustrine environment (Pearson *et al*., 2008; Toney *et al*., 2010; 2011) they are not ubiquitously found in lakes. Pearson *et al*. (2008) found detectable concentrations of long-chain alkenones in only 14 of 54 Spanish lakes studied, Toney *et al*. (2010) found them in 13 of 55 US lakes and Toney *et al*. (2011) found them in 13 of the 19 Canadian lakes studied. Toney *et al*. (2010; 2011) studied the 26 lakes in which alkenones were found showing that they are most abundant in deep cold lakes were pH ranges between 8.4 and 9.9. Toney *et al*. (2011) found that there are only weak relationships between the alkenones and temperatures in Canada whereas in the US Toney *et al*. (2010) were able to develop a temperature calibration from water column filters in Lake George. Nevertheless, like isoprenoid GDGTs, alkenones seem to be

restricted to larger lakes thus a greater understanding of branched GDGTs within lakes is crucial. To enable the use of branched GDGTs as a temperature proxy in lacustrine environments, the environmental controls on their composition must first be understood.

Powers *et al*. (2004) studied four large lakes (Lake Superior, Lake Michigan, Lake Malawi and Issyk Kul) from different climatic regimes to analyse their GDGT content. Both brGDGTs and isoGDGTs were present and Powers *et al*. (2004) suggest that the branched compounds were transported into the lakes by erosion. In a later study Blaga *et al*. (2009) analysed 47 lakes from southern Italy to northern Scandinavia for GDGTs finding crenarchaeol to be present in almost all lakes, confirming that Thaumarchaeota are not only present in marine environments but also in lakes. It must be noted that this is only the case if the abundance of crenarchaeol in lakes is higher than that in catchment soils. The presence of GDGTs in lakes has now been studied around the globe, from regional studies of Zink *et al*. (2010) in New Zealand, Loomis *et al*. (2011; 2012) in Africa, Sun *et al*. (2011) in China and Nepal and Shanahan *et al*. (2013) in the Arctic to global studies spanning from Antarctica to Arctic Scandinavia (Pearson *et al*., 2011), indicating GDGTs are ubiquitous in lacustrine environments. On establishing that GDGTs are present in lacustrine environments their uses in lake sediments as a proxy must be assessed.

4.1.5.1. TEX_{86}

The TEX_{86} calibration was first applied to lake sediments by Powers *et al*. (2004) who hoped that its application would allow continental palaeoclimates to be reconstructed. Initial research, conducted in four large lakes, showed promise as the relationship between TEX_{86} and mean annual lake surface temperature (LST) was found to be similar to that between TEX_{86} and SST, except in Lake Michigan where GDGTs were close to the detection limit (Powers *et al*., 2004). These findings suggest that Thaumarchaeota in lacustrine environments behave in a similar manner to those in marine environments, although, more lakes need to be analysed to confirm this is the case. Powers *et al*. (2005) later developed a lake specific TEX_{86} index (Eq. 4.14) by adding an additional five large lakes to those studied by Powers *et al*. (2004). This improved the validity of TEX_{86} in lacustrine environments defining a specific relationship between TEX_{86} and LST:

$$TEX_{86} = 0.017LST + 0.25 \ (r^2 = 0.96) \qquad \text{(Eq. 4.14)}$$

The calibration and analytical error of this model was ± 2.0 °C and ± 1.0 °C respectively (Powers *et al*., 2005). When applied to Lake Malawi temperatures of c. 26 °C were reconstructed for the last 600 years which are consistent with the LST temperatures expected. In addition, a 3.5 °C cooling of the last glacial maximum was reconstructed (Powers *et al*., 2005) similar to the cooling seen in other palaeotemperature reconstructions (Chalie, 1995; Holmgren *et al*., 2003). Therefore, although initial research was based on just nine lakes, in large lakes the TEX_{86} index appears to accurately reconstruct past temperatures when isoGDGTs are present in a great enough abundance.

Nevertheless, since its development the success of the lacustrine TEX_{86} index has been varied, with some temperature reconstructions fitting well with measured or reconstructed temperatures and others under or over estimating temperatures. The lacustrine TEX_{86} calibration was used successfully by Tierney *et al*. (2010b) in Lake Tanganyika, East Africa, to reconstruct climate change over the last 60,000 years alongside other environmental proxies. Nevertheless, one problem with the application of TEX_{86} in lakes is its dependence on isoGDGTs as encountered by Blaga *et al*. (2009) who found that TEX_{86} could only be applied in 9 of 47 lakes studied as the others were dominated by brGDGTs. In the 9 lakes in which TEX_{86} reconstructions were possible however, Blaga *et al*. (2009) found a similar relationship between TEX_{86} and LST to Powers *et al*. (2005) (Fig. 4.7) suggesting that TEX_{86} may not be solely applicable to large lakes. On the other hand, in Lake Lugano, Switzerland, even though TEX_{86} reconstructs LST reasonably well the reconstructed temperatures were c. 3 to 4 °C lower than the estimated annual LSTs (Bechtel *et al*., 2010). Although Bechtel *et al*. (2010) point out that these values are within the calibration error, they are sizeable errors. Such errors would be particularly problematic when applying these calibrations to climatically sensitive sites such as the Antarctic Peninsula. This is perhaps the most serious disadvantage of this method.

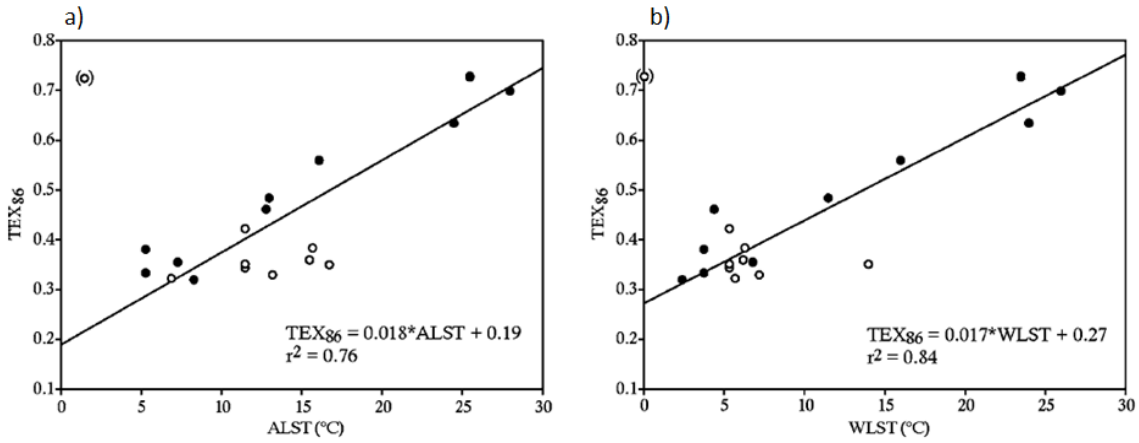

Figure 4.7: The relationship between TEX_{86} and a) mean annual lake surface temperature and b) mean winter lake surface temperature. The lakes studied include those from Blaga *et al*.'s (2009) European north–south transect (white dots) and Powers *et al*.'s (2005) large lakes (black dots). Figure taken from Blaga *et al*. (2009).

The overriding consensus of the research into the use of TEX_{86} in lakes is that in large lakes with little terrestrial input TEX_{86} may be applicable but in smaller lakes or those were there is a large terrestrial input TEX_{86} is unlikely to provide reliable temperature reconstructions. If brGDGTs are abundant, which is often the case in lakes as a result of either terrestrial input or *in situ* production, this can affect the performance of TEX_{86} as a palaeothermometer. Hence, Loomis *et al*. (2011) urge caution when applying the TEX_{86} index in lakes with high soil loading. Therefore, as in marine environments, the BIT value can be used to indicate the amount of terrestrial input into the lake hence the reliability of the TEX_{86} index (Blaga *et al*., 2009; Powers *et al*., 2010). Blaga *et al*. (2009) suggest a cut of value of BIT greater than 0.4 above which TEX_{86} should not be used.

4.1.5.2. MBT/CBT

The TEX_{86} index can be problematic in lake environments due to the relatively high proportions of brGDGTs. Consequently, some researchers have tried applying the brGDGT soil calibration and MBT/CBT proxy of Weijers *et al*. (2007a) to reconstruct lake pH and temperature (e.g., Sinninghe Damsté *et al*., 2009; Tierney and Russell, 2009; Naeher *et al*., 2014). Although the MBT/CBT proxy has been widely applied in peat bogs and soils (e.g., Weijers *et al*., 2007a; Peterse *et al*., 2009a; 2012; Sinninghe Damsté *et al*., 2000; Huguet *et al*., 2010b; Weijers *et al*., 2011), Tierney and Russell (2009) were one of the first to apply the proxy in lacustrine environments. Tierney and Russell (2009) found the application of MBT/CBT in lakes to be problematic. In Lake

Towuti, Central Indonesia, Tierney and Russell (2009) reconstructed a MAAT of 19 to 23 °C from lake sediments, slightly colder than the actual MAAT of 24 °C.

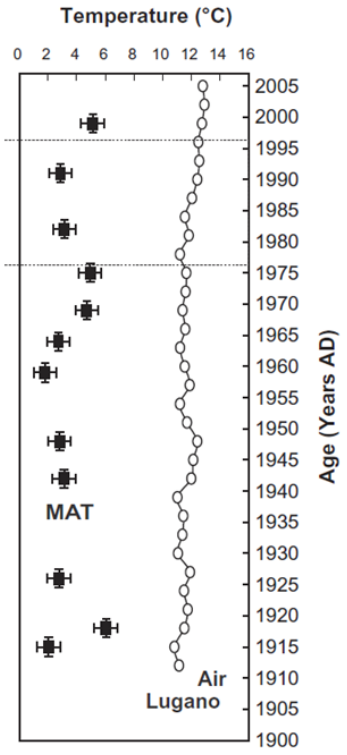

Figure 4.8: Comparison of MBT/CBT derived MAAT (black) with a three year moving average MAAT since 1900 AD in Lake Lugano, Switzerland. Figure taken from Bechtel *et al*. (2010).

An underestimation of MBT/CBT temperature reconstructions is echoed in several other studies including in Lake Lugano, Switzerland where temperatures were between 6 and 9 °C lower than actual MAAT (Bechtel *et al*., 2010; Fig. 4.8), in China and Nepal where reconstructed temperatures were on average c. 8.7 °C lower than MAAT (Sun *et al*., 2011), in East Africa temperatures were underestimated by almost 15 °C (Tierney *et al*., 2010b) and in Lake Rotsee, Switzerland, reconstructed temperatures were up to 15 °C below measured MAAT (Naeher *et al*., 2014; Fig. 4.10). Nevertheless, Bechtel *et al*. (2010) found that in Lake Brienz, Switzerland, although the reconstructed temperatures did fluctuate, they compared reasonably with measured air temperatures. Even so, in the majority of cases MBT/CBT appears to underestimate MAAT when using lake sediments suggesting that the MBT/CBT index may not be applicable in lakes. As a result Sun *et al*. (2011) define the following relationship between MBT/CBT and MAAT on a global scale when applied to lake sediments:

$$MAAT = 6.803 - 7.062 \times CBT + 37.090 \times MBT \quad \text{(Eq. 4.15)}$$

(r^2 = 0.62, RMSE = 5.24 °C)

Sun *et al*. (2011) also include an alternative calibration when the pH of the lake is less than 8.5:

$$MAAT = 3.949 - 5.593 \times CBT + 38.213 \times MBT \quad \text{(Eq. 4.16)}$$

(r^2 = 0.73, RMSE = 4.27 °C)

Applying the Sun *et al*. (2011) lacustrine MBT/CBT calibration for lakes with pH <8.5 (Eq. 4.16) Naeher *et al*. (2014) found that the calibrated temperatures varied between 6 and 13 °C and fit well with measured MAAT between 7 and 11 °C in Lake Rotsee, Switzerland. However, Wu *et al*. (2013) found that when applied in Kusai Lake, on the Qinghai-Tibetan Plateau, the MBT/CBT index overestimates MAAT by almost 20 °C with the calibrated temperatures more comparable with summer temperatures.

These global lacustrine calibrations show only limited applicability when used on a regional scale, particularly in a study by Loomis *et al*. (2012) who applied a variety of different calibrations to reconstruct lake temperatures with varying degrees of success. Even when applying the MBT/CBT calibration by Tierney *et al*. (2010a) for East Africa on lakes from East Africa Loomis *et al*. (2012) found substantial variability in the reconstructed MAAT. While trying to understand why neither Weijers *et al*.'s (2007a) original soil MBT/CBT calibration or the more recent lacustrine calibrations of Tierney *et al*. (2010a) and Sun *et al*. (2011) provide sound temperature reconstructions Loomis *et al*. (2012) speculate that brGDGTs are produced in lakes as well as soils. Tierney and Russell (2009) also considered this while studying lake, river and soil samples from the same catchment suggesting that *in situ* production could complicate the MBT/CBT proxy. This concern was also echoed by Bechtel *et al*. (2010). Therefore, establishing the source of GDGTs, in particular the branched compounds, is paramount to successfully implement them as reliable temperature indicators.

Several studies have tried to determine the origin of brGDGTs using different approaches (e.g., Sinninghe Damsté *et al*., 2009; Loomis *et al*., 2011; Naeher *et al*., 2014; Wu *et al*., 2013; Buckles *et al*., 2014). One approach has been to investigate the composition of brGDGTs in the catchment soils and lake surface sediments to determine any similarity or differences between these two environments. Assuming the brGDGTs are wholly soil derived it would be expected that both compositions would be identical. Taking this approach Loomis *et al*. (2011) found an offset between the composition of GDGTs in western Ugandan lake sediments and catchment soil samples,

indicating that either there is selective transport of some GDGT compounds, which is unlikely, or that brGDGTs are being produced *in situ* in lacustrine environments.

Other studies have focused on GDGT composition within the water column by either comparing brGDGT composition in suspended particulate matter in the water column with lake surface material and/or catchment soil samples (e.g., Naeher *et al*., 2014), or studying changes in composition throughout the water column (e.g., Sinninghe Damsté *et al*., 2009; Bechtel *et al*., 2010; Schouten *et al*., 2012; Naeher *et al*., 2014). Comparing water column brGDGT composition with that of soils or surface sediments in Lake Rotsee, Switzerland, Naeher *et al*. (2014) found that the composition of brGDGTs in the water column were more similar to those in lake sediments than the catchment soils. Therefore, Naeher *et al*. (2014) suggest that brGDGTs are produced *in situ* in either the water column or surface sediments. When investigating GDGT compositions within the water column Sinninghe Damsté *et al*. (2009) found that in Lake Challa, Tanzania, brGDGT concentrations were one to two orders of magnitude higher in deep waters than in the near lake surface waters, also reflected in the BIT values. They state that the high concentrations of brGDGTs in the bottom water cannot be caused by re-suspension of the sediment and thus these brGDGTs are either being produced *in situ* in the anoxic lower water column or transported by groundwater entering the lake at greater depth (Sinninghe Damsté *et al*., 2009).

Conversely, in another study Naeher *et al*. (2014) found that in the water column both brGDGT and isoGDGT concentration decreased with depth. Therefore, suggesting either that GDGT input is primarily from soils or GDGTs are produced in the upper part of the water column as previously indicated by Bechtel *et al*. (2010) in Lake Brienz, Switzerland and Schouten *et al*. (2012) in Lake Tanganyika , East Africa. Wu *et al*. (2013) take a different approach when determining the origin of the brGDGTs using C/N ratios and carbon isotopes to infer that lacustrine algae are the main sources of the organic matter within Kusai Lake, Qinghai-Tibetan Plateau, NW China. They also found that the BIT index in near shore sediments was higher than in catchment soils thus concluding that brGDGTs were produced within the lake (Wu *et al*., 2013). These results highlight the importance of understanding each lake system individually as both the input and environmental controls vary between lakes.

4.1.5.3. Lacustrine brGDGT calibrations

Three current lacustrine specific GDGT-temperature calibrations include a global calibration by Pearson *et al*. (2011) and two regional East African calibrations developed by Tierney *et al*. (2010a) and Loomis *et al*. (2012). To develop their calibration Pearson *et al*. (2011) used surface sediments (the top 0 – 2 cm) from 90 lakes across a north-south transect from the Scandinavian Arctic to Antarctica (Fig. 4.9) with a temperature gradient from c. 1 to 31 °C. Pearson *et al*. (2011) use redundancy analysis (RDA) and variance partitioning to examine the relationship between all fifteen isoprenoidal and branched GDGT compounds and temperature, pH, conductivity and water depth. They found that temperature accounts for a large and statistically independent fraction of variation in branched GDGT composition.

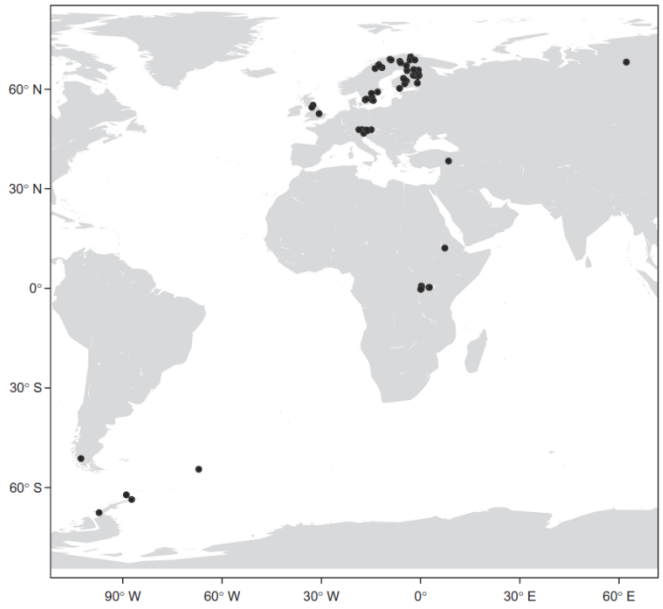

Figure 4.9: Map showing the location of the 90 lakes studied by Pearson *et al*. (2011) when developing their brGDGT-temperature calibration. Figure taken from Pearson *et al*. (2011).

Following thorough analysis of the brGDGT-temperature relationship Pearson *et al*. (2011) developed a branched GDGT-temperature regression model (Eq. 4.17) with high accuracy and precision (R^2 = 0.88, RMSE = 2.0 °C, RMSEP = 2.1 °C) which is not influenced by pH, conductivity or water depth. The Pearson *et al*. (2011) GDGT-temperature model was derived using best sub-sets regression and can be described using the following equation based on fractional abundances of the brGDGT compounds:

$$Temperature\ (°C) = 20.9 + [98.1 \times Ib] - [12.0\ \times II] - [20.5\ \times III] \qquad \text{(Eq. 4.17)}$$

The maximum standard error in temperature reconstructions using this model is ± 0.24 °C. Unlike many studies before Pearson *et al*. (2011) used summer air temperature data rather than mean annual LST or MAAT. Summer temperatures are used by Pearson *et al*. (2011) for two reasons; firstly, many of the lakes are only monitored during the summer, especially those which are ice covered for much of the year; secondly, annual temperatures are not a biologically relevant parameter for regions of great seasonal temperature fluctuations and/or lake with long periods of ice cover. Further research by Sun *et al*. (2011) and Wu *et al*. (2013) has indicated a bias in GDGT calibrated temperatures towards summer months when the lakes are most productive. Wu *et al*. (2013) found that when applying the Sun *et al*. (2011) MBT/CBT index in Kusai Lake MAAT is overestimated, reconstructed temperature 14.7 °C, compared to a measured MAAT of -4.5 °C. However, the measured summer temperature is 17 °C thus supporting a bias towards summer temperatures when the brGDGT producing bacteria are likely to be more abundant and active (Wu *et al*., 2013). This is a particular problem in the high latitudes where seasonal ice cover is also a factor alongside lake temperature fluctuations. Moreover, quantifying the absolute length of the period of ice cover on the lakes is difficult and is likely to have changed throughout even the recent past let alone over longer time scales (Shanahan *et al*., 2013).

Naeher *et al*. (2014) applied several GDGT-temperature calibrations to Lake Rotsee, Switzerland including the Weijers *et al*. (2007a), Pearson *et al*. (2011), Sun *et al*. (2011), Peterse *et al*. (2012) and Loomis *et al*. (2012) to reconstruct temperatures since 1860 AD (Fig. 4.10). They found that, as expected, the reconstructed summer temperatures when applying the Pearson *et al*. (2011) were higher than other GDGT-temperature reconstructions for the Weijers *et al*. (2007a), Sun *et al*. (2011), Peterse *et al*. (2012) and Loomis *et al*. (2012) calibrations which are calibrated to MAAT. Reconstructed temperatures when applying the Pearson *et al*. (2011) calibration, however, were between 9 – 19 °C consistent with temperatures observed in late spring / summer, the average temperature May to June is 12 – 18 °C (Fig. 4.10) and April to September 13 – 17 °C (Naeher *et al*., 2014). A slight bias towards spring temperatures rather than summer was observed by Naeher *et al*. (2014) suggesting that perhaps brGDGT productivity is highest during the spring in Lake Rotsee.

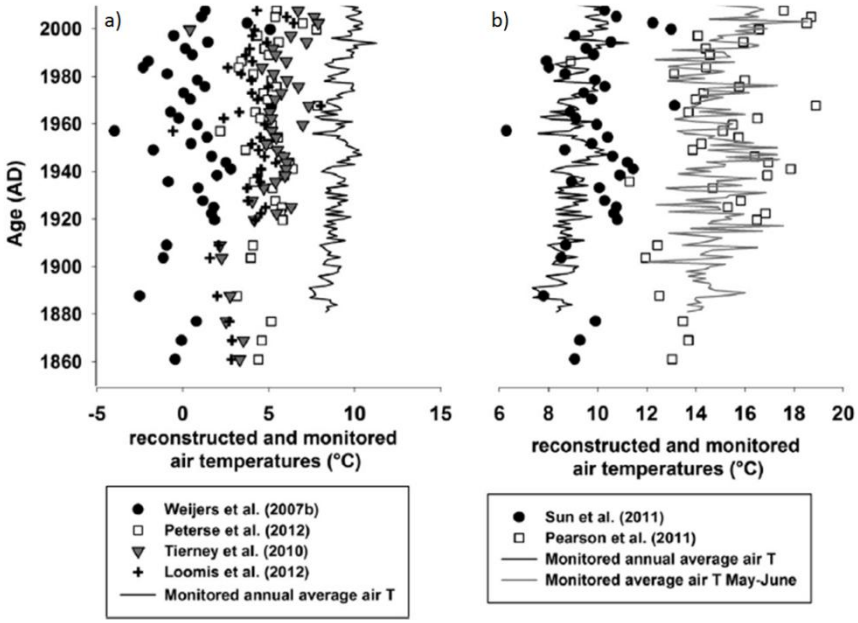

Figure 4.10: The application of GDGT-temperature calibrations downcore in Lake Rotsee, Switzerland (Naeher *et al*., 2014). a) Reconstructed MAAT using the Weijers *et al*. (2007a), Peterse *et al*. (2012), Tierney *et al*. (2010a) and Loomis *et al*. (2012) calibrations compared to monitored MAAT. b) Reconstructed MAAT using the Sun *et al*. (2011) and MSAT using the Pearson *et al*. (2011) calibrations compared to monitored MAAT and MSAT. Figure edited from Naeher *et al*. (2014).

When applying the Pearson *et al*. (2011) calibration to Lake Challa on the south-east slope of Mount Kilimanjaro Sinninghe Damsté *et al*. (2012) found a temperature difference between the Last Glacial Maximum (LGM) and the Holocene of between c. 4 to 5 °C. Such a temperature difference is in agreement with other African temperature records (e.g., Powers *et al*., 2005; Weijers *et al*., 2007b; Tierney *et al*., 2008). Finally, Loomis *et al*. (2012) also applied the Pearson *et al*. (2011) global brGDGT-temperature calibration on their regional African dataset. They found that when the calibration was applied to surface sediments from East African lakes the model errors increase, RMSEP = 5.1 °C, with the calibration showing a warm bias at 'colder' sites. Following this Loomis *et al*. (2012) developed a new regional lacustrine branched GDGT calibration for African lakes (Eq. 4.18) using the fractional abundance of the branched GDGT and stepwise forward selection (SFS):

$$\mathrm{MAAT} = 22.77 - [33.58 \times \mathrm{III}] - [12.88 \times \mathrm{II}] - [418.53 \times \mathrm{IIc}] + [86.43 \times \mathrm{Ib}] \quad \text{(Eq.4.18)}$$

To develop this regional calibration Loomis *et al*. (2012) added 70 new lakes to the 41 studied by Tierney *et al*. (2010a). The calibration has improved accuracy and error

prediction which is uniform across the dataset, r^2 = 0.94, RMSE = 1.9 °C and RMSEP = 2.1 °C (Loomis *et al*., 2012). The application of the SFS calibration (Eq. 4.18) downcore at Sacred Lake reconstructs a c. 6.3 °C warming between the last glacial maximum and mid-Holocene followed by a cooling of c. 1.2 °C (Loomis *et al*., 2012) giving an overall temperature differential of c. 5.1 °C between the LGM and present. A similar amplitude in warming has been recorded in the pollen based estimates from Sacred Lake indicating that the LGM was approximately 5.1 °C colder than present (van Zinderen Bakker and Coetzee, 1972). When applying the Loomis *et al*. (2012) calibration to lake sediments from Baffin Island, eastern Canadian Arctic, Shanahan *et al*. (2013) found that the calibrated temperatures were 10 to 20 °C warmer than MAAT and better represented summer temperatures. This may be reflecting a seasonality in brGDGT production, however, it must also be noted that the Loomis *et al*. (2012) calibration is a low latitude regional calibration so the errors may be due to the fact Shanahan *et al*. (2013) are applying this calibration at a high latitude site.

Although Loomis *et al*. (2012) have found previous calibrations give less accurate palaeotemperature reconstructions at Sacred Lake compared to their new calibration, it must now be applied elsewhere in the region as to date there has been limited application. Nevertheless, Loomis *et al*. (2012) do suggest that regional calibrations could be more accurate at reconstructing temperatures using brGDGTs and suggest that lakes may require regional calibrations rather than a global calibration. Aside from the study by Pearson *et al*. (2011), most studies examining brGDGTs in lacustrine environments have been carried out at a local or regional scale and Pearson *et al*. (2011) is the only one, to date, to have examined GDGTs in Antarctic lakes. The focus on developing a regional calibration for Antarctic lake sediments in this study will not only provide a regional model but will also allow the examination of the environmental controls on Antarctic GDGTs.

4.1.6. GDGT Methodological Development

Without the advances in the use of liquid chromatography with a mass spectrometer (LC-MS) enabling the rapid analysis of Archaeal membrane lipids (Hopmans *et al*., 2000) the use of GDGTs as a temperature biomarker would not have been possible. Hopmans *et al*. (2000) were able to develop a method combining normal phase high performance liquid chromatography (HPLC) with positive ion atmospheric pressure chemical ionization mass spectrometry (APCI-MS) to analyse intact GDGTs in

Archaeal cell material and sediments. Before the GDGTs can be analysed using LC-MS they must be extracted from the sediments. There are a number of different extraction methods available, see Appendix B.

4.1.6.1. Extraction Procedure

Although there are some standard procedures as part of the GDGT extraction process, for instance freeze-drying and homogenising samples prior to extraction, the extraction method itself is varied. Appendix B shows the methodological development in the extraction process over a 12 year period between 2000 and 2014. Of the 23 studies, 5 use an ultrasonic technique, 3 use the soxhlet technique with one using both this and accelerated solvent extraction (ASE), 14 other studies also use ASE to extract lipids and 2 use the microwave-aided extraction (MAE) technique. Earlier studies tend to use the ultrasonic or soxhlet method but, following the development of the ASE and MAE techniques, the majority of studies use the ASE method. Often the method chosen can depend on the type and amount of sediment to be extracted, as well as the amount of time and funding available.

A study by Kornilova and Rosell-Melé (2003) goes some way to analysing the pros and cons of three of the extraction methods; ultrasonic, ASE and MAE. Kornilova and Rosell-Melé (2003) focus on developing the use of MAE and how this method could combat some of the issues with ultrasonic and ASE methods. The main limitation of the ultrasonic method is that, although it is relatively inexpensive, the method is both time and labour intensive due to required repetition of extractions. The ASE method tackles the issue of the time required to run extractions through providing a faster alternative, however the drawback with this method is that the system required is expensive. Further concern regarding the use of ASE for the extraction of GDGTs has been raised by Huguet *et al*. (2010a) who found inconsistent yields, thus stating that further assessment and improving of the ASE extraction method is necessary before using this technique in proxy studies.

The use of MAE to extract GDGTs provides several advantages over ultrasonic and ASE techniques. In comparison with the ultrasonic and soxhlet techniques a smaller quantity of solvent is used, the extraction time is shorter and more importantly there is a reported high recovery, whilst compared to ASE, MAE is a cheaper option which allows simultaneous extractions (Kornilova and Rosell-Melé, 2003). Huguet *et al*. (2010a) also briefly studied the use of MAE in a comparison study of different

extraction methods finding good yields in water column particles however, they did not test the techniques using sediment samples. Overall there is yet to be a recommended or standard extraction method for the extraction of GDGTs from sediments with different research groups in the field seeming to have preferences towards different techniques often dependant of previous set-ups used and funding available.

4.1.6.2. Analysis

Although gas chromatography (GC) is the most commonly used separation technique for analysis within the field of organic geochemistry, GDGTs are insufficiently volatile for analysis using this method (Schouten *et al*., 2013). Nevertheless, GDGTs are detectable through the use of LC-MS developed by Hopmans *et al*. (2004). Unlike with the extraction procedure, there is little debate regarding the analysis of the GDGT compounds with studies by Schouten *et al*. (2002), Powers *et al*. (2004; 2005), Weijers *et al*. (2007a), Tierney and Russell (2009), Pearson *et al*. (2011), Shanahan *et al*. (2013), Naeher *et al*. (2014), Woltering *et al*. (2014) and many more using LC-MS set ups to analyse GDGTs. Nevertheless, Sutton and Rowland (2012) have been working on the development of a method in which high weight molecular hydrocarbons, including GDGTs, can be analysed using a high temperature GC with time-of-flight mass spectrometry. This development could unlock the use of GC for analysing GDGTs, however, further research into this method is still required.

The majority of GDGT analysis and temperature indices focuses on relative and/or fractional abundances of different GDGT compounds. However, there has been some research into the use of external and internal standards allowing the quantification of the different compounds. Finding a suitable internal standard which does not occur naturally in samples and does not co-elute with other GDGT compounds but is chemically similar has proved problematic and currently the only option is the synthesised C_{46} GDGT. Huguet *et al*. (2006) tested this synthesised C_{46} GDGT by adding C_{46} GDGT in hexane:isopropanol (99:1) into the total extracts. They found that C_{46} GDGT eluted in the same fraction as the GDGTs meaning it could be possible to use C_{46} as an internal standard. Through careful analysis of this C_{46} GDGT, alongside external standard curves using a GDGT-V standard, similar average GDGT concentrations are obtained for both methods (Huguet *et al*., 2006). Since this study many others have used C_{46} GDGT as an internal standard for the quantification of the different GDGT compounds (e.g., Tierney and Russell, 2009; Peterse *et al*., 2009a;

2014; Bechtel *et al*., 2010; Tierney *et al*., 2010a; 2012; Loomis *et al*., 2011; 2012; Niemann *et al*., 2012; Naeher *et al*., 2014; Wu *et al*., 2013; De Jonge *et al*., 2014). Quantification of the GDGTs is not paramount to use the current calibrations and develop new calibrations as long as repeatability within the samples is assessed and achieved.

4.2. Pigments

Within freshwater environments a great diversity of pigments are produced by aquatic algae, bacteria and higher plants (Hodgson *et al*., 1997). Pigments are sometimes the only fossil remains of non-siliceous algae and bacteria (Hodgson *et al*., 1997) surviving long after all morphological structures have disappeared (Leavitt and Hodgson, 2001). As a result, pigments are a valuable tool in palaeolimnology. They can be used as indicators of algal and bacterial community composition, food-web interactions, changes in the physical structure of lakes, mass flux within lakes, past UV radiation environments and scales of lake variation as well as anthropogenic impacts including eutrophication, acidification, fisheries management, land- use practices and climate change (Leavitt and Hodgson, 2001).

The use of pigments as a biomarker depends on accurate isolation and identification of the compounds (Hodgson *et al*., 1997; Leavitt and Hodgson, 2001). As a result, the advance in the use of fossil pigments as a proxy of environmental conditions has been greatly enhanced through the use of High Performance Liquid Chromatography (HPLC) to separate the pigments (Hodgson *et al*., 1997). There are, however, some considerations to be made when studying pigments in the sediment record, not least the issue of preservation as pigments are known to be sensitive to light, heat, oxygen, acids and alkalis (Wright and Jeffery 2006). Even so, pigments are often successfully used as a biomarker of the relative abundance and productivity of individual algal classes (Buchaca and Catalan, 2007). Where preservation is considered and accounted for correctly, pigments are one of the best techniques to map and monitor phytoplankton populations (Wright and Jeffery, 2006), and can yield information about changes in community composition and trophic status throughout the depositional history of the lake (Squier *et al*., 2002). In addition, pigment derivatives themselves can be used as indicators of the presence of grazers or oxidation within the water column in the palaeodepositional environment (Squier *et al*., 2002).

4.2.1. Pigment types

There are two main groups of pigments found in lacustrine environments; chlorophylls and carotenoids, the most common of which are outlined in Table 4.1, together with their origin. Chlorophylls are found in all photosynthetic phytoplankton and many are preserved, if not in their original form, then as derivatives (Wright and Jeffery, 2006). Chlorophylls are magnesium coordination complexes of four pyrrole units cyclically arranged with a fifth isocyclic ring (McGowan, 2007). The structure of chlorophyll *a* can be seen in Figure 4.11.They include chlorophylls *a*, *b* and *c* derived from algae and a range of bacteriochlorophylls (Bchls) derived from photosynthetic bacteria (McGowan, 2007).

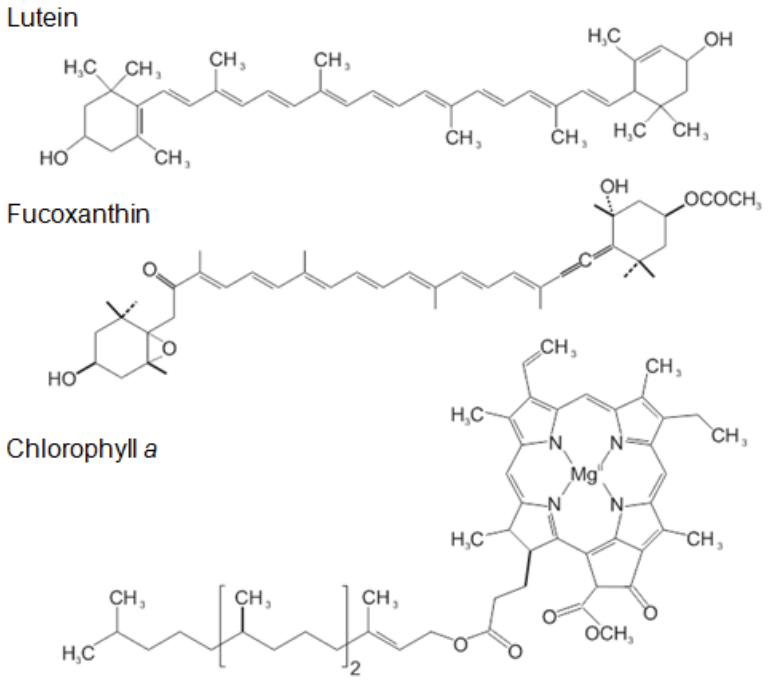

Figure 4.11: Example chemical structures of three key pigments found in lacustrine environments.

Carotenoids are the other large group of algal pigments of which there are over 600 different types occurring naturally (Wright and Jeffery, 2006). They are characterised by a long aliphatic polyene chain composed of eight isoprene (C_5H_8) units (McGowan, 2007). There are two main types of carotenoid; carotenes and xanthophylls (McGowan, 2007). Structurally carotenes are made up of carbon and hydrogen atoms only (e.g. β-carotene) whereas the xanthophylls also include at least one oxygen atom (e.g. fucoxanthin) (McGowan, 2007). Figure 4.11 shows the structure of some of the key lacustrine carotenoids. Many of these carotenoids are involved in photoprotection

notably diadinoxanthin and diatoxanthin in chromophytes and violaxanthin, antheraxanthin and zeaxanthin in green algae (Wright and Jeffery, 2006). Appendix C contains a detailed list of chlorophylls and carotenoids often found in lake sediments and their interpretation.

Pigment	Origin
Chlorophyll *a*	Plantae and all photosynthetic algae (Leavitt, 1993; Leavitt and Hodgson, 2001; Hodgson *et al*., 2003; 2005; Verleyen *et al*., 2004; Mikomägi and Punning, 2007).
Chlorophyll *b*	Plantae, chrysophytes (golden algae), Chlorophyta (green algae), pyrrophyta, and Euglenophyta (Leavitt, 1993; Leavitt and Hodgson, 2001; Hodgson *et al*., 2003; 2005; 2006a; Verleyen *et al*., 2004; Waters *et al*., 2010).
Fucoxanthin	Siliceous algae, Bacillariophyta (Diatoms), Chrysophytes, some Dinophyta (dinoflagellates), Haptophytes and Raphidophytes (Leavitt, 1993, Hodgson *et al*., 1997; Leavitt *et al*., 1999; Leavitt and Hodgson, 2001; Hodgson *et al*., 2003; 2005; Verleyen *et al*., 2004; Reuss and Conley, 2005; Buchaca and Catalan, 2007; Waters *et al*., 2010; Huguet *et al*., 2011; Sterken *et al*., 2012).
Zeaxanthin	Cyanobacteria and Chlorophyta (Leavitt, 1993; Leavitt and Hodgson, 2001; Verleyen *et al*., 2004; Hodgson *et al*., 2005; 2006a; Buchaca and Catalan, 2007; Mikomägi and Punning, 2007; Matsumoto *et al*., 2010; Waters *et al*., 2010).
Lutein	Chlorophyta, Euglenophyta, Tracheophytes and Plantae (Leavitt, 1993; Leavitt and Hodgson, 2001; Verleyen *et al*., 2004; Hodgson *et al*., 2003; 2005; Buchaca and Catalan, 2007; Mikomägi and Punning, 2007; Waters *et al*., 2010).
Echinenone	Cyanobacteria and Zooplankton (Cladocera) (Leavitt, 1993; Leavitt and Hodgson, 2001; Verleyen *et al*., 2004; Hodgson *et al*., 2005; 2006a; Buchaca and Catalan, 2007; Mikomägi and Punning, 2007; Waters *et al*., 2010).
β, β-carotene	Plantae; some phototrophic bacteria; Chlorophyta and Cyanobacteria (Leavitt, 1993; Leavitt and Hodgson, 2001; Verleyen *et al*., 2004; Hodgson *et al*., 2005; Buchaca and Catalan, 2007; Mikomägi and Punning, 2007; Sterken *et al*., 2012).

Table 4.1: Pigments commonly found in lacustrine sediments and their origin. More details of these and other lacustrine pigments can be found in Appendix C.

Chlorophylls and carotenoids alike are both particularly labile molecules (Wright and Jeffery, 2006) yet, they are often well preserved in lake sediments (Lami *et al*., 2009). Both chlorophylls and carotenoids are susceptible to oxidatived degradation. For chlorophylls, this produces a number of coloured degradation products whereas, for carotenoids, the saturation of their double bond produces colourless compounds mostly undetectable by spectroscopic techniques (McGowan, 2007). Nevertheless, carotenoids, especially carotenes, e.g. β-carotene, are often more stable than chlorophylls (McGowan, 2007).

Table 4.2 shows some of the chlorophyll derivatives often found in the fossil pigment record and the structural changes they have undergone through degradation. For example the loss of the central magnesium ring creates pheophytins whereas the loss of the phytol chain forms chlorophyllides (McGowan, 2007). Due to the colourless nature of the carotenoid derivatives they are harder to detect, however early stages of carotenoid degradation can be seen through the presence of coloured cis-isomers (McGowan, 2007). Although many of these derivatives are naturally occurring, they can also be artefacts of extraction and analytical techniques, and these techniques must be optimised to reduce such artefacts being produced (Wright and Jeffery, 2006).

Derivative	**Structural change**
Pheophytins	lost the Mg atom
Chlorophyllides	lost the phytol chain
Pheophorbides	lost both the Mg and phytol
Pyro-derivatives	lost C-13^2 carbomethoxy group
Epimers	spontaneous rearrangement
Allomers	spontaneous oxidisation

Table 4.2: Chlorophyll derivatives and their structural change (Wright and Jeffery, 2006).

4.2.2. Pigments as Proxies

Leavitt (1993) conducted one of the early studies using fossil pigments and identified a quantitative link with algal production. Despite degradation issues Leavitt (1993) found that fossil and algal abundance remain correlated through time assuming a constant basin morphometry, light penetration, stratification or deepwater oxygen content. Hodgson *et al*. (2005) backed this up, stating that in some lakes changes in pigment abundances reflect changes in relative productivity rather than preservation. As a result, pigment assemblages are now frequently used as an indicator of relative productivity in lake and marine environments. For example, β, β-carotene and chlorophyll *a* which are present in all green algae are reliable markers of changes in relative production (Hodgson *et al*., 2003) and can be applied in most lakes from highly productive to oligotrophic environments (Buchaca and Catalan, 2007).

There is a great diversity of pigments found in lake waters as well as being preserved as fossil pigments in lake sediments. The main sources of lacustrine pigments are planktonic and benthic algal communities, phototrophic bacterial populations and aquatic higher plants, or macrophytes (Leavitt and Hodgson, 2001). Specific pigments or pigment groups can be used to reconstruct more specific environmental changes such as water depth (e.g., Cantonati *et al*., 2014), allochthonous organic matter input (e.g.,

Buchaca and Catalan, 2007) lake acidification (e.g., Leavitt *et al*., 1999) and climatic changes (e.g., Reuss *et al*., 2010; Sterken *et al*., 2012). Pigments can also be used as indicators of cyanobacteria associated with eutrophication (e.g., Mikomägi and Punning, 2007; Catalan *et al*., 2009), see Appendix B for details. In addition, both total carotenoid and total chlorophyll derivative concentrations in lake sediments have been shown to be highly correlated to within lake primary productivity (e.g., Adams *et al*., 1978; Guilizzoni *et al*., 1982; 1983; Leavitt, 1993; Leavitt and Hodgson, 2001). Water depth has also been reconstructed through variations in light penetration inferred from benthic to planktonic pigment composition, specifically the molar ratio between two marker pigments; alloxanthin (planktonic signal) and diatoxanthin (benthic signal) (Buchaca and Catalan, 2007). This ratio is positively correlated with lake depth (Buchaca and Catalan, 2007). Mikomägi and Punning (2007) also found a strong relationship between water depth and the abundance of carotenes and xanthophylls in lakes. Another pigment, okenone is a marker pigment for photosynthetic bacteria which Buchaca and Catalan (2007) tentatively suggest may be a marker of allochthonous organic matter, due to its high abundance in lakes with forested catchments. Finally, in western Canada, Vinebrooke *et al*. (1998) found that fucoxanthin was replaced by lutein- zeaxanthin and diatoxanthin as salinity increased. Changes in pigment composition therefore, have the potential to allow the reconstruction of specific environmental changes in many lakes.

4.2.3. Degradation

In lake environments most pigment degradation occurs before burial, in the water column and surface sediment layer (Hodgson *et al*., 1997, Leavitt and Hodgson, 2001). In the water column degradation is particularly rapid and extensive with more than 95% of compounds having a half-life of days (Leavitt and Hodgson, 2001). Mikomägi and Punning (2007) also found that more than 90% of pigments were degraded to colourless compounds before permanent burial with degradation continuing in the surface sediment layers. Once in the sediment, pigment degradation tends to be less rapid and is dependent on the amount of light reaching the bed of the lake as well as the abundance of burrowing invertebrates (Leavitt and Hodgson, 2001). Nevertheless, this does vary depending on the individual pigments and the characteristics of the lake (Leavitt and Hodgson, 2001). As most pigment degradation takes place in the water column, the degree of degradation can relate to the time taken for the pigments to reach the bed of the lake. Therefore, the amount of degradation can indicate the distance between

pigment source and the deposition zone (Buchaca and Catalan, 2007) and potentially the sedimentation history (Mikomägi and Punning, 2007).

If degradation can be accounted for, fossil carotenoids, chlorophylls and their derivatives can be used as a valuable palaeolimnological indicator of algal and bacterial responses to changes in lake ecology (Hodgson *et al*., 1997). For example, Leavitt *et al*. (1999) used pigments as an indicator of lake acidification. In Lake 302 south basin, north-western Ontario, the concentration of fucoxanthin, un-degraded chlorophyll *b* and lutein-zeaxanthin increased between two and four fold immediately upon acidification, thus can be used as an indicator of acidification in the sediment record. On the other hand, alloxanthin concentration remained fairly constant while, diatoxanthin reduced by 50%.

In another study, Mikomägi and Punning (2007) used fossil pigment concentrations as an indicator of eutrophication in Lake Kuradijärv, Estonia, using zeaxanthin and myxoxanthophyll as a marker of cyanobacteria. They also found that the concentrations of pheophytin *b*, pheophytin *a*, lutein, alloxanthin, zeaxanthin changed in response to lake eutrophication. Further details regarding the environmental interpretation of specific pigments in lakes can be found in Appendix C.

4.2.4. Pigment studies in Antarctic lakes

In an early study, Vincent *et al*. (1993) assessed the distribution of pigments in Antarctic lakes, ponds and streams focusing particularly on microbial mats. They were able to identify myxoxanthophyll, canthaxanthin, echinenone, fl-carotene, myxoI-2'-O-methyl-methylpentoside as the dominant pigments in Antarctic mats. Vincent *et al*. (1993) also found that the concentration of chlorophylls not only varied between differing mat communities, with the highest concentrations found in hypersaline pond mats, but also within individual mats, with chlorophyll concentrations often higher in the bottom half of the mat.

Following the early pigment research of Vincent *et al*. (1993) there have been many more studies assessing the distribution of pigments in Antarctic lakes with particular focus on the Larsemann Hills region of East Antarctica. At Kirisjes Pond, in the Larsemann Hills, Squier *et al*. (2002) were able to use pigments to reconstruct the presence of oxygenic primary producers, in particular, chlorophyll *b* derivatives, which they attributed to inputs from green algae (chlorophyta) since higher plants are absent

from the region. Similarly, Hodgson *et al*. (2005) used the presence of purple photosynthetic bacterial pigments, as indicators of oxygen depletion consistent with perennial ice cover during the LGM in Lake Reid. In another study, Verleyen *et al*., (2004) reconstructed changes in sea-ice conditions in the region over the past 6000 years through the relative abundance of diatoxanthin (stratified, open-water conditions) and dinoxanthin (increased sea-ice duration) in coastal Pup Lagoon. Also in the Larsemann Hills Verleyen *et al*. (2005) developed a proxy for lake water depth and were able to reconstruct late Holocene water depths inferred from changes in ultraviolet radiation penetration based on the relative abundance of scytonemin and its derivatives, alongside diatom abundances.

Three other studies using pigments in Antarctic lakes include Matsumoto *et al*. (2010) at Lake Skallen Oike near the Syowa Station and Sterken *et al*. (2012) and Fernandez-Carazo *et al*. (2013) on Beak Island, to the northeast of the Antarctic Peninsula. Matsumoto *et al*. (2010) used fossil pigments as indicators of primary production, green algae, diatoms and cyanobacteria and other algal conditions. When combined with other palaeolimnological techniques they were able to infer periods of coastal marine and freshwater conditions. On Beak Island, Sterken *et al*. (2012) used fossil pigments, alongside sedimentological proxies and diatoms, to reconstruct a deglaciation history and changes in sea ice and climate. From the fossil pigment record they were able to identify five pigment zones in which total pigment concentrations varied, as well as the abundance of individual pigments. Sterken *et al*. (2012) were also able to identify the timing of lake isolation and changes in ice cover from the fossil pigment record together with proxy indicators. Finally, Fernandez-Carazo *et al*. (2013) used fossil pigments, alongside fossil 16S rRNA genes, to identify changes in cyanobacterial community throughout the Holocene in response to climate change.

In Antarctic lake systems, cyanobacteria are not only the most abundant photosynthetic organisms, but they also play an important role in the ecosystem function (Fernandez-Carazo *et al*., 2013). Fernandez-Carazo *et al*. (2013) suggest that reconstructing the relative abundance of filamentous cyanobacteria, which typically form benthic microbial mats in shallow lakes, can provide an indication of the amount of light reaching the lake bed and in turn changes in lake depth. Conversely, diatoms dominate primary production in deeper lakes where low light conditions prevail (Fernandez-Carazo *et al*., 2013). These changes in cyanobacteria, diatoms and other ecological niches give a clear indication of lake productivity and perhaps climate-induced

environmental change. As a consequence, fossil pigments have been and can be used to reconstruct such changes in Antarctic lake environments.

4.3. Conclusions

GDGTs were first found in ocean sediments and soil, since then their presence has been noted in lakes and many other environments. GDGTs are thought to be ubiquitous in these environments; in fact it would be unusual not to find GDGTs in a present day environmental sample. Following their isolation, the relationship between GDGTs and temperature in oceans and soils led to the development of the TEX_{86} and MBT/CBT temperature indices respectively. These indices have been well applied in their respective environments allowing successful GDGT-temperature reconstructions. The application of TEX_{86} and MBT/CBT in lake environments has been met with varying degrees of success therefore, GDGT-temperature calibrations specific to lacustrine environments have been developed. Currently, there are several lacustrine GDGT-temperature calibrations including global and regional models though, to date none of them have incorporated samples from sites where MSAT is less than 1.5 °C.

Pigments have previously been used as an indicator of primary productivity, as well as other environmental conditions such as the presence of cyanobacteria or diatoms, in both marine and lacustrine settings. There are two different types of pigments, chlorophylls, which are found in all photosynthetic phytoplankton, and carotenoids, of which there are two main types; carotenes and xanthophylls. One of the issues with the use of pigments as a proxy is that they are particularly liable to degradation however, where their derivatives can be found they can also used as an environmental indicator. Despite pigments being liable to degradation, several previous Antarctic lake studies have successfully reconstructed environmental conditions through pigment analysis.

Chapter 5: Materials and Methods

Summary

In this chapter the different methods used as part of this research are described from the collection of the lake surface sediments and cores used to the statistical analysis applied. A detailed methodology of the GDGT extraction is outlined in Section 5.2 including the procedure for assessing sample quality control. Details of the pigment extraction can be found in Section 5.3 with an assessment of the environmental controls on pigment composition in Antarctic lakes also undertaken. Section 5.4 contains the loss on ignition method used for Yanou Lake. Finally, the strategy for the collection of environmental data for all of the lakes studied and the statistical analysis undertaken on the surface material and sediment cores are detailed in Sections 5.5 and 5.6 respectively. The methodologies of previous analysis undertaken on the two cores are outlined in Appendix D for completeness.

5.1. Collection and Storage

All surface samples used in this study were collected as part of other research projects during previous field campaigns to Antarctica. During field campaigns short cores were collected using a UWITEC surface gravity corer fitted with either a hydraulic core catcher for soft sediments or a steel orange-peel core catcher for consolidated sediment (British Antarctic Survey, 2006; 2008). All samples were bagged in whirlpak/ziplock bags in the field. Livingston, UWITEC Percussion or Russian corers were used for extracting deeper sediments. Long cores were collected with several overlapping drives alternatively through two adjacent holes c. 1 m apart with an overlap of c. 20 cm. The majority of the lakes were cored using a small inflatable boat on fixed lines during ice-free conditions, i.e. Belén, Long, Fan and Viewpoint Lakes, while others were cored when the lakes were ice covered through a hole in the ice made using a Jiffy drill, i.e. Ardley, Gaoshan and Yanou Lakes (British Antarctic Survey, 2006; 2008). Cores were collected from the deepest point of the lakes, frozen in the field and shipped back to the UK and stored frozen at either -80 °C or -20 °C. Specific details for the collection of Fan and Yanou sediment cores can be found in Chapters 7 and 8 respectively.

5.2. GDGTs

5.2.1. Sample preparation and extraction

Sample preparation and extraction was done at Newcastle University using microwave assisted solvent extraction (MAE) and followed the methods of Pearson *et al*. (2011) outlined below.

Samples were freeze-dried and homogenised using a pestle and mortar before extraction. Any samples containing a large amount of gravel were dried sieved at 500 μm. Samples weighing 0.1 to 4.6 g were extracted using a MARS 5 microwave (Fig. 5.1) assisted solvent extraction (MAE) system. Each sample was transferred into a microwave vessel with a stirring magnet and 15 ml of HPLC grade dichloromethane (DCM):methanol (3:1) was added before the vessel was capped and placed in the microwave. The extraction programme ramped up to 70 °C in 3 mins and was held at 70 °C for 5 mins. Following extraction, the samples were transferred into test tubes and centrifuged at 2500 rpm for 3 mins before the supernatant, containing the lipids, was decanted into a round bottomed flask. Samples were dried using a rotovap, transferred to test tubes and dried under a nitrogen stream. The total lipid extract was then saponified for 1 hr at 70 °C in 1 ml of 6% potassium hydroxide (KOH):methanol and left overnight. The neutral fraction (containing the GDGTs) was then extracted with HPLC grade hexane (3 x 3 ml or until the hexane was clear), centrifuging each time before decanting. Following the hexane extractions, DCM extracted ultrapure water was added to the hexane extracts. The extracts were then shaken and centrifuged and any traces of KOH removed via pipetting off the water fraction. Once dried the neutral extracts were stored at -20 ˚C.

Figure 5.1: The MARS 5 microwave at Newcastle University used for extracting total lipids as part of the GDGT extraction procedure.

Before GDGT analysis the neutral extracts were filtered through a 0.2 µm Whatman PTF filter using 0.5 ml hexane:isopropanol (99:1) before being dried under a nitrogen stream. Samples were then diluted in hexane:isopropanol (99:1) prior to analysis on the LCMS.

5.2.2. GDGT analysis and peak identification

GDGT analysis and identification was carried out at Newcastle University using an Acquity Xevo TQ-S (triple quadrupole with step wave; Waters Ltd). LC-MS set up with an atmospheric pressure chemical ionisation (APCI) source (Ion saber II) operated in positive ion mode. Analytical separation was achieved using a Grace Prevail Cyano HPLC column (3 µm, 150 x 2.1 mm i.d.) fitted with an in line filter (Waters Acquity UPLC in-line filter, 0.2 µm) at 40 °C using a binary solvent gradient where eluent A was hexane and eluent B was propanol, with a flow rate of 0.2 ml per minute. The gradient profile is indicated in Table 5.1. The LC-MS settings were: Source offset 50 V, capillary 1.5 KV, Desolvation temperature 200 °C, cone voltage 30 V, Desolvation gas (N_2). Detection was achieved using selected ion monitoring (SIM) of targeted $[M+H]^+$ ions (dwell time 50 ms). The target ions are indicated in Figure 4.2. Peak identification and integration was carried out using MassLynx software (version 4.1). The statistical analysis used to interpret the GDGT data from the surface material and core samples is outlined in Sections 5.6.1 and 5.6.2 respectively.

Time (min)	Flow rate (ml/min)	Eluent A (%)	Eluent B (%)
0	0.2	99	1
5	0.2	99	1
50	0.2	98.2	1.8
55	0.2	90	10
65	0.2	90	10
66	0.2	99	1
80	0.2	99	1

Table 5.1: Gradient profile used for GDGT separation.

5.2.3 Sample Quality Control

Extraction and analytical repeats were run during the GDGT analysis. As the Antarctic samples were small, duplicate extractions were not possible so a standard sample form Esthwaite in the Lake District was used as a replicate sample. GDGTs were extracted and analysed from three UK sites and Lake Esthwaite was chosen for the sample quality control testing as it contained all the GDGTs compounds. The Esthwaite material was extracted and analysed for GDGTs six times to test the reproducibility of the extraction process. Figure 5.2 shows the percentage abundance of the three most abundant brGDGTs, GDGT-I, GDGT-II and GDGT-III. There was good reproducibility between the six samples with GDGT-I ranging between 22.3 and 23.5%, GDGT-II between 37.9 and 38.9% and GDGT-III between 29.1 and 30.2%. In addition, the BIT values ranged between 0.995 and 0.996 further indicating replication of the results.

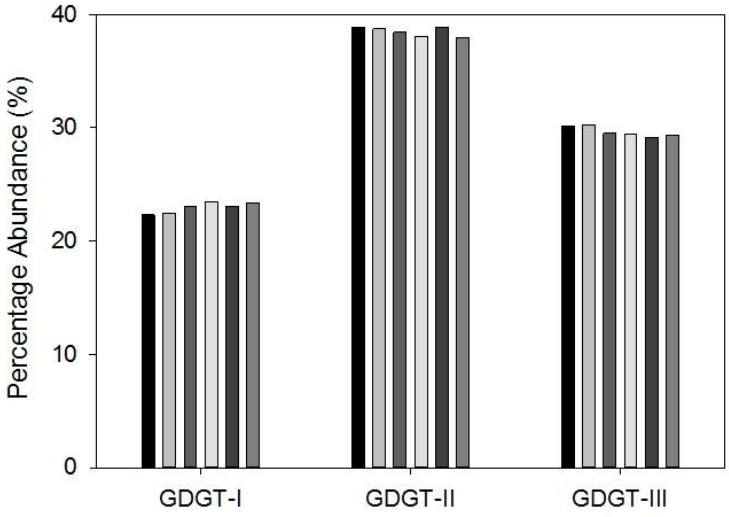

Figure 5.2: Percentage abundance of GDGT-I, GDGT-II and GDGT-II in six replicate samples from Lake Esthwaite.

Several samples were also run repeatedly on the LCMS to check for reproducibility of the analytical procedure. Notably one sample from Marion Island was run seven times and several other samples were run two to three times. In each case all samples run were integrated and good repeatability of the results was seen. For example, the Marion Island sample run seven times, showed good reproducibility with GDGT-I ranging between 16.1 and 16.5%, GDGT-II between 43.9 and 44.2% and GDGT-III between 35.0 and 35.3%. For fair comparison between these samples and other samples that were only run once the first sample run was used for statistical analysis

A blank was also run in each extraction batch, allowing checks for contamination within each batch.

5.3. Pigments

5.3.1. Sample preparation and extraction

Pigment sample preparation and extraction was undertaken at the British Antarctic Survey. The methods were based on those of Zapata *et al*. (2000) with minor modifications. All pigment preparation was done in an ice tray, under subdued light and vials were purged with N_2 gas to minimise the degradation of the pigments. Pigments were extracted from c. 2 cm^3 of wet sediment. First, the wet sediment was homogenised using a pestle and mortar then it was transferred into a pre-weighed sample tube. Any excess water was pipetted off before adding 5 ml of HPLC grade methanol. Oxygen is known to cause degradation of pigments so samples were purged with nitrogen before being stored over night at -20 °C.

Samples were then centrifuged at 2000 rpm for 3 minutes and the supernatant pipetted into an extract tube and dried using a rotary evaporator. The extraction process was repeated until the supernatant was clear. After each extraction, the supernatant was pipetted into the same extract tube as before. Once the extracted pigments samples were dried the test tubes were purged with nitrogen and stored at -20 °C. Prior to analysis, the extracts were dissolved in 0.5 ml methanol, 0.1 ml milliQ water, filtered through a 0.2 µm Whatman PTFE filter and transferred into a sample vial.

Finally, the extracted sediment was dried using a rotary evaporator, weighed, and the dry weight of the sediment calculated and recorded. Each dry sediment sample was then analysed for loss on ignition see Section 5.4.

5.3.2. Pigment analysis, identification and quantification

Pigment analysis, identification and quantification was carried out at the British Antarctic Survey within 48 hours of extraction. HPLC (high performance liquid chromatography) analysis followed the method of Zapata *et al*. (2000) using a Dionex HPLC with a diode array detector (DAD). Analytical separation was achieved using a Waters Symmetry C8 column (150 x 4.6 mm, 3.5 pm particle size, 100 A pore size) at 25 °C as the stationary phase. Two mobile phases were used, eluent A was methanol:acetonitrile:aqueous pyridine solution (0.25 M pyridine) (50:25:25) and eluent B was methanol:acetonitrile:acetone (20:60:20). The pyridine solution was prepared by adding 10 ml of acetic acid and 20 ml of pyridine to 900 ml of milliQ water and mixed using a magnetic stirrer. A pH of 5.0 was then achieved by adding acetic acid a drop at a time. Finally, the solution was made up to 1000 ml with additional milliQ water. The flow rate of the mobile phase was 1.0 ml per minute with the gradient profile indicated in Table 5.2. Pigment detection was achieved at 435, 470 and 665 nm for all chlorophylls and carotenoids, with spectra from 300 – 700 nm being collected continuously. Peaks were identified and integrated using Chromeleon software.

Time (min)	Flow rate (ml/min)	Eluent A (%)	Eluent B (%)
0	1.0	100	0
22	1.0	60	40
28	1.0	5	95
38	1.0	5	95
40	1.0	100	0

Table 5.2: Gradient profile of eluent A and eluent B used to isolate individual pigments via HPLC.

During pigment analysis analytical β-carotene and Chlorophyll standards were run repeatedly to check for machine drift during the analysis. Several samples were run twice on the HPLC to check for repeatability. The standards also allowed the concentration of the individual pigments using the following formula:

$$\text{Concentration} = ((\text{Peak Area} / \text{Standard Constant}) \times \text{Dilution Factor}) / \text{LOI}$$

Finally, the sediment core pigment concentrations were calculated as a flux by multiplying the concentration by dry sediment accumulation rate. This accounts for changes in pigment concentration as a result of changes in sediment accumulation rate.

5.3.3. Environmental controls on pigments composition in Antarctic lakes

Previous research (e.g., Squier *et al*., 2002; Verleyen *et al*., 2004; 2005; Hodgson *et al*., 2005; Matsumoto *et al*., 2010; Sterken *et al*., 2012; Fernandez-Carazo *et al*., 2013) has utilised pigments as indicators of primary production, oxygen depletion, lake water depth, deglaciation history, changes in sea ice and other algal conditions in lakes (see Chapter 4). Prior to downcore application, the controls on pigment composition in the Antarctic and sub-Antarctic lakes surface dataset was assessed. This assessment was based on the previous interpretations of chlorophylls and carotenoids found in lake sediments (Appendix C).

The presence and / or dominance of specific pigments or pigment groups enabled inferences about certain environmental conditions. Table 5.3 shows some of the inferences which can be made, a more detailed list can be found in Appendix C.

Pigment / Pigment Groups	**Interpretation**
Chlorophyll a	Relative algal production
Fucoxanthin, Chlorophyll c2, Pheophorbide *a* Diadinoxanthin and Diatoxanthin	Benthic diatoms
Chlorophyll a Zeaxanthin, Myxoxanthin, Echinenone, Nostoxanthin and Canthaxanthin	Cyanobacteria / cyanobacterial mats
Lutein, Zeaxanthin, Chlorophyll b and Antheraxanthin,	Green algae
Okenone	Purple sulphur bacteria
Astaxanthin	Zooplankton

Table 5.3: Pigments and pigment groups and their interpretation in previous Antarctic lake research. The pigments in italics are abundant in the majority of the Antarctic and sub-Antarctic surface dataset from this study. Interpretations taken from Squier *et al*. (2002); Verleyen *et al*. (2004; 2005); Hodgson *et al.* (2005); Matsumoto *et al*. (2010); Sterken *et al*. (2012) and Fernandez-Carazo *et al*. (2013).

Field reports (e.g., British Antarctic Survey, 2006; 2008) identify the lakes studied in which cyanobacterial mats are present including Pup Lagoon and Mago Ike, East Antarctica, Beak 2, Antarctic Peninsula, Ardley and Yanou Lakes, South Shetland Islands and many more. The total concentration of all pigments previously associated with cyanobacterial mats, and their derivatives, were summed giving an interpretation, from the pigment data, as to which lakes record the presence of cyanobacterial mats. Figure 5.3 shows all the lakes in which cyanobacterial associated pigments were found within the surface samples (top 0 – 2 cm) and in black are the lakes where cyanobacterial mats have been recorded previously. The results show that where

cyanobacterial mats were known to be present cyanobacterial pigments were in their highest concentrations, therefore, suggesting that the pigments were accurately representing known environments.

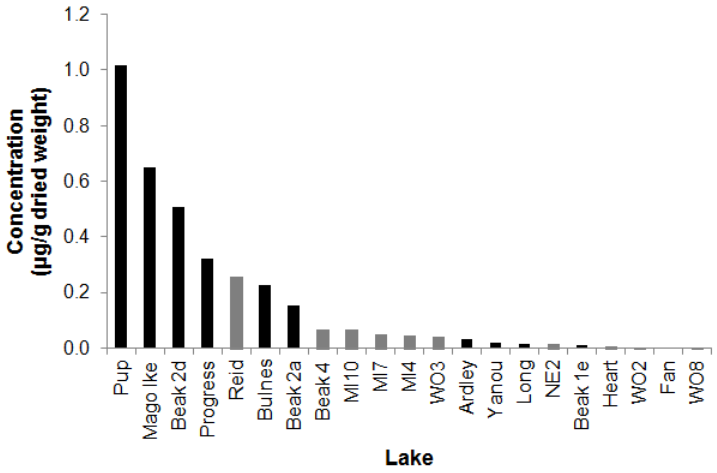

Figure 5.3: Concentration of cyanobacteria pigments in the surface material from Antarctic and sub-Antarctic lakes. The graph represents only the lakes in which the cyanobacteria pigments were successfully identified. The black columns represent lakes where field reports or previous research has indicated a presence of cyanobacterial mats while the grey columns have no record of cyanobacterial mats.

Taking a different approach, all the identifiable pigments found in Fan Lake were plotted (Fig. 5.4). Previous research by Van Nieuwenhuyze *et al*. (in prep) used diatoms in Fan Lake as part of their multiproxy approach to reconstruct palaeoenvironments therefore, it is known that diatoms are present in Fan Lake. Indicator pigments of diatom presence include; Fucoxanthin, Chlorophyll *c*2, Pheophorbide *a*, Diadinoxanthin and Diatoxanthin (Table 5.3). Although Chlorophyll *c*2 and Diadinoxanthin were not identified in Fan Lake, Fucoxanthin and Pheophorbide *a* where found in relatively high abundance and Diatoxanthin was also present (Fig. 5.4). This suggests that the pigment data from Fan Lake has successfully recorded the presence of diatoms within the lake.

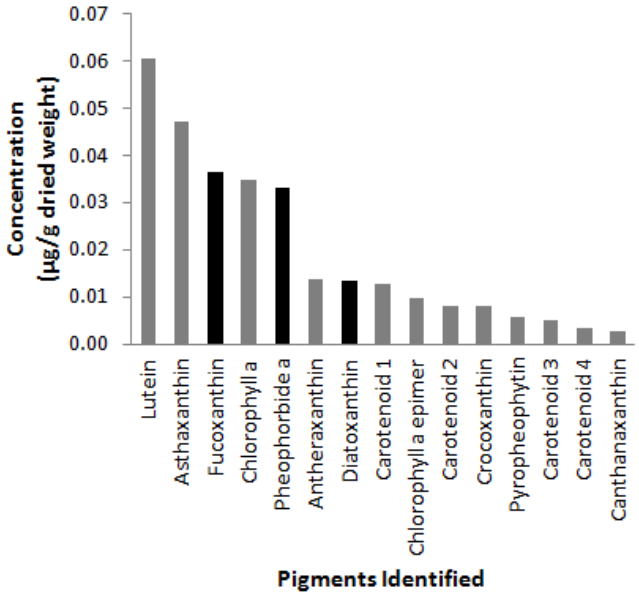

Figure 5.4: Concentration of all identified pigments in Fan Lake, South Georgia. The black columns are pigments previously used to interpret the presence of diatoms while the grey columns are pigments which represent other environmental parameters.

Pigment analysis of surface material from the Antarctic and sub-Antarctic lakes has shown that pigments were accurately recording known characteristics of the lakes. Therefore, not only has a greater understanding of pigments in Antarctic and sub-Antarctic lakes being achieved but also from this knowledge of the present composition of pigments in Antarctic lakes a more robust reconstruction of the past can be achieved.

5.4. Loss on Ignition

Loss on ignition (LOI) was undertaken on the Yanou Lake core at 2 cm intervals to correspond with the pigment sampling strategy. One dry porcelain crucible per sample was weighed and the dried sediment sample used for pigment extraction added to the crucible. The dry weight of each sample was recorded. Crucibles were heated to 550 °C in a furnace then held at 550 °C for 2 hours to estimate changes in organic carbon. Once cooled samples were re-weighed and the LOI calculated as a percentage of the original pre-combustion dry weight using the following equation:

$$LOI_{550} = ((DW_{150} - DW_{550}) / DW_{150}) \times 100$$

where DW_{150} (in grams) is the pre-combustion weight and DW_{550} (in grams) the post-combustion weight.

5.5. Environmental Data

Environmental data was gathered from a range of sources including unpublished field reports from BAS and other collaborators, research stations and previously published research at the sites, this data can be found in Appendix A. Water chemistry data collected included pH, conductivity, salinity and dissolved oxygen, again gathered from field reports and past research papers (e.g., Hodgson *et al*., 2001; 2005; 2006a; Kaup and Burgess. 2002; Verleyen *et al*., 2003; Sabbe *et al*., 2004; Bentley *et al*., 2005; Roberts *et al*., 2008; 2009; 2011; Pearson *et al*., 2011; Watcham *et al*., 2011; Sterken *et al*., 2012). Due to their location, Antarctic lakes are rarely monitored year round therefore environmental data is often based on spot data taken at the time of sediment collection.

Air temperatures were used as a surrogate for lake water temperature based on their strong relationship (Edinger *et al*., 1968; Webb and Nobilis, 1997; Livingstone and Dokulil, 2001). Following Pearson *et al*. (2011), austral summer rather than annual air temperature data was used for two main reasons: first, Antarctic lakes are rarely monitored all year round, and lake water temperature data is largely restricted to the austral summer and/or when lakes were cored or otherwise investigated; second, many lakes remain ice-covered for much of the year and annual temperature is not a biologically relevant parameter in regions where large seasonal temperature fluctuations or long periods of ice cover exist. Finally, summer is the peak growing season when GDGTs and pigments are produced. Shanahan *et al*. (2013) confirmed a seasonal bias in brGDGT production which increased in Arctic lakes during the summer when temperatures are warmest and when the lakes are ice free. Loomis *et al*. (2014b) also found that GDGT-derived temperatures reflected seasonal changes in lake water column temperature.

Air temperature data was taken from the nearest meteorological station to each individual lake. Mean summer air temperatures were determined from mean December, January and February air temperatures. Mean annual air temperatures were also collated for each station. Temperatures were lapse rate corrected for the altitudinal differential between the research station and each individual lake. Corrections were done by firstly calculating the difference between the elevation of the meteorological station and the lake. The elevation difference was then multiplied by the lapse rate giving a temperature offset. This temperature difference was added or subtracted, as needed, to the air

temperature data from the meteorological station giving an estimate of air temperature at the lake. Regionally specific lapse rates were taken from previous research in the region (e.g., Braun *et al*., 2004; Magand *et al*., 2004)

5.6. Statistical Analysis

All statistical analyses were performed in R software for statistical computing and graphics (R Core Team, 2014) using several packages; vegan (Oksanen *et al*., 2013), leaps (Lumley, 2009) and rioja (Juggins, 2014).

5.6.1. Analysis of Surface Samples

Redundancy analysis (RDA) allowed the examination of the relationship between the branched GDGT abundances in lake surface sediments and environmental parameters; for further details see Chapter 6, Section 6.2.4. RDA is a form of constrained principal components analysis which provides an ordination in which variation of GDGT composition is directly related to lake physical-chemical characteristics including pH, conductivity, lake depth and temperature (Pearson *et al*., 2011). Prior to analytical analysis, the normality of the data was assessed, lake depth and lake water conductivity were all right skewed distributions. Conductivity was therefore $\log_{10}$ transformed and depth was square-root transformed.

To develop the GDGT-temperature calibration, all nine branched GDGT compounds were analysed with respect to mean summer air temperatures. Best subsets regression was applied to select an optimal set of branched GDGT compounds and develop the Antarctic and sub-Antarctic GDGT-temperature calibration using linear regression (Chapter 6, Section 6.2.4)

5.6.2. Analysis of Core Samples

The relative abundance of the branched GDGTs was calculated for each sample in both the Fan Lake and Yanou Lake cores. The Antarctic and sub-Antarctic GDGT-temperature calibration developed in Chapter 6 was applied to reconstruct GDGT-temperatures in each core.

Constrained CONISS cluster analysis with Hellinger standardisation was run on the relative abundance of the branched GDGTs known to relate to temperature. Constrained CONISS cluster analysis creates clusters or zones by hierarchical agglomeration of

stratigraphically-adjacent samples (Grimm, 1987; Bennett, 1996). Broken stick analysis was undertaken to test the statistical significance of the clusters.

Constrained CONISS cluster analysis, with broken-stick analysis, was also run on the main ITRAX-Mo tube measurable elements (Ca, Ti, Mn, Fe, Rb, Sr, Zr, and REE) and incoherent (inc.) and coherent (coh.) scattering parameters, which collectively always make up >95% of total cps (Roberts, pers. comm.). Principal Components Analysis (PCA) was undertaken on both Mo- and Cr-tube data individually to quantify the main trends in the datasets.

Finally, cross correlation analysis was run for the GDGT-derived temperature reconstructions and other proxy and instrumental records to assess the relationship between the different records. Prior to cross correlation, the datasets were re-sampled using piecewise linear interpolation at either a 50, 100 or 200 year scale depending on the resolution of the original dataset. The higher resolution datasets were always reduced in resolution to match the dataset with the lowest resolution. Re-sampling was done using Analyseries software.

5.7. Conclusions

Surface sediments (top 0 – 2 cm) from Antarctic, sub-Antarctic and Chilean lakes, as well as long cores from Fan Lake and Yanou Lake, were successfully retrieved during previous field campaigns. GDGTs and pigments were extracted from these sediments alongside multiple other analytical techniques.

The extraction of GDGTs from the surface samples, along with the application of the statistical techniques outlined in Section 5.6, will allow the potential development of a GDGT-temperature calibration model (see Chapter 6). GDGT-temperature reconstructions can then be made in Fan Lake and Yanou Lake in Chapters 7 and 8 respectively. Confidence in the extraction and analytical techniques for GDGT analysis can be taken from good replication of results from samples extracted and / or run on the LC-MS multiple times.

The isolation of pigments within the surface dataset allowed the assessment of the current interpretations of the abundance of individual pigments or pigment groups in Antarctic sediments. A high concentration of cyanobacterial pigments in lakes known to have cyanobacterial mats and pigments indicative of diatoms found in Fan Lake, where

diatoms have previously been found, gives confidence in any downcore interpretations made in Chapters 7 and 8.

A combination of the GDGT-temperature reconstruction downcore with indicators of primary productivity i.e. pigments, diatoms and TOC will allow a detailed palaeoenvironmental reconstruction of the mid-late Holocene in Fan Lake and Yanou Lake. Finally, the previous sedimentological data will enable changes in not only the lake sedimentology, but also terrestrial inputs through meltwater inputs, to be assessed in relation to temperature changes throughout the records.

Chapter 6: Development of a Regional Glycerol Dialkyl Glycerol Tetraether (GDGT) Temperature Calibration for Antarctic and Sub-Antarctic Lakes

This chapter has been prepared as a journal article with the following authors. Approximate author contributions are indicated as a percentage.

Louise C. Foster [a,b*] (60%)
Major additional contribution:
Emma J. Pearson[b], Steve Juggins[b] & Stephen J. Roberts[a] (30% combined)
Minor additional contribution:
Dominic A. Hodgson[a], Krystyna M. Saunders[c] & Elie Verleyen[d] (10% combined)

[a]British Antarctic Survey, Natural Environment Research Council, High Cross, Madingley Road, Cambridge, CB3 0ET**,** UK
[b]School of Geography, Politics and Sociology, Newcastle University, Newcastle-upon-Tyne, NE1 7RU, UK
[c]Institute of Geography and the Oeschger Centre for Climate Change Research, University of Bern, 3012, Bern, Switzerland
[d]Ghent University, Protistology and Aquatic Ecology, Krijgslaan 281 S8, 9000 Gent, Belgium
*Author for correspondence

Keywords: palaeoclimate, temperature reconstruction, GDGTs, Southern Hemisphere, palaeolimnology, Antarctic

Abstract

A regional network of quantitative reconstructions of past climate variability is required to test climate models. In recent studies, temperature calibration models based on the relative abundances of sedimentary glycerol dialkyl glycerol tetraethers (GDGTs) have enabled past temperature reconstructions in both marine and terrestrial environments. Nevertheless, to date these methods have not been widely applied in high latitude environments due to poor performance of the GDGT-temperature calibrations at lower temperatures. To address this we studied 32 lakes from Antarctica, the sub-Antarctic Islands and Southern Chile to: 1) quantify their GDGT composition and investigate the environmental controls on GDGT composition; and 2) develop a GDGT-temperature calibration model for inferring past temperatures from Antarctic and sub-Antarctic lakes. GDGTs were found in all 32 lakes studied and in 31 lakes branched GDGTs (brGDGTs) were the dominant compounds. Statistical analyses of brGDGT composition in relation to temperature, pH, conductivity and water depth showed that the composition of brGDGTs is strongly correlated with mean summer air temperature (MSAT). This enabled the development of the first regional brGDGT-temperature calibration for use in Antarctic and sub-Antarctic lakes using four brGDGT compounds (GDGT-Ib, GDGT-II, GDGT-III and GDGT-IIIb). A key discovery was that GDGT-IIIb is of particular importance in cold lacustrine environments. The addition of this compound significantly improved the model's performance from $r^2 = 0.67$, RMSEP-LOO = 2.23 °C, RMSEP-H = 2.37 °C for the re-calibrated global GDGT-temperature calibration to our Antarctic dataset to $r^2 = 0.83$, RMSEP-LOO = 1.68 °C, RMSEP-H = 1.65 °C for our new Antarctic calibration. This shows that Antarctic and sub-Antarctic, and possibly all high latitude, palaeotemperature reconstructions should be based on a regional GDGT-temperature calibration where specific compounds can be identified and included to improve the model performance. Finally, downcore temperature reconstructions using the new Antarctic brGDGT-temperature calibration were tested in sub-Antarctic Fan Lake from South Georgia providing a proof of concept for the new calibration in the Southern Hemisphere.

6.1. Introduction

Previous studies of past climates in high-latitude regions have used a range of biological proxies including changes in the accumulation rates and species composition of pollen, diatoms, pigments and chironomids to give indirect qualitative or quantitative

inferences about past environmental changes (e.g., Anderson *et al.,* 2001; Hodgson *et al.,* 2005*;* 2006a; Rolland *et al.,* 2009; Strother *et al*., 2015; Verleyen *et al.,* 2003; Watcham *et al.,* 2011). Many of these proxies respond to a range of environmental controls, including pH, salinity or atmospheric circulation, all of which can influence their ability to accurately quantify past changes in temperature (Shanahan *et al.,* 2013). Moreover, in the harsh Antarctic environment, palaeoclimate techniques are restricted due to the biological proxies being limited or absent, so there is a real need for a robust method to quantify temperature. This is particularly important in Antarctic lakes where quantitative temperature reconstructions using biogeochemical proxies in lake sediment cores will enable a substantial improvement in our understanding of past atmospheric temperature without the complicating factors of changing ocean currents (which limit the application of marine-based palaeothermometry) and high altitudes (which affect most ice core reconstructions).

One such approach is the application of glycerol dialkyl glycerol tetraethers (GDGTs) as a temperature proxy. Several studies have focussed on using changing relative abundances of GDGTs in ocean sediments (e.g., Schouten *et al*., 2002; Kim *et al*., 2010; Tierney and Tingley 2014), soils (e.g., Weijers *et al*., 2007a; Peterse *et al*., 2012) and lake sediments (e.g., Powers *et al*., 2005; Tierney *et al*., 2010a; Pearson *et al.,* 2011; Loomis *et al.,* 2012) for quantitatively reconstructing past temperature. GDGTs are cell membrane lipids found in archaea and bacteria and their structure strongly depends on growth temperature (Schouten *et al.,* 2002; 2013; Weijers *et al.,* 2006b). More specifically, the number of cyclopentane rings in the GDGT structure is a key factor in the adaptation to temperature change (Gliozzi *et al.,* 1983; Uda *et al.,* 2001; Schouten *et al.,* 2002; 2013). To date GDGTs have only been studied in seven Antarctic and sub-Antarctic lakes (as part of the Pearson *et al*. (2011) global calibration model). In these few sites the GDGT-temperature relationship does not appear to be as strong as the global relationship, suggesting a need to expand upon and further investigate the environmental controls on GDGT composition in Antarctic lakes.

6.1.1. GDGTs in lacustrine environments

Powers *et al.* (2004; 2005) first investigated the use of GDGTs in lacustrine environments, developing a lacustrine variation of the marine TEX_{86} index and demonstrated its potential as a temperature proxy in large lakes. However, its dependence on isoprenoid GDGTs (isoGDGTs), which are frequently in low abundance

in lakes, means TEX_{86} is often not applicable in lacustrine systems where the Branched Isoprenoid Tetraether (BIT) index is high (e.g., Blaga *et al.*, 2009). This BIT index was developed by Hopmans *et al.* (2004) as a proxy of terrestrial material input into marine environments which are dominated by isoGDGTs. As the BIT index is a ratio of branched GDGTs (brGDGTs) to isoGDGTs it is often used to identify lakes with a high proportion of brGDGTs and thus where the TEX_{86} index will be unreliable e.g. BIT > 0.5 (Hopmans *et al.*, 2004; Weijers *et al.*, 2006b; Blaga *et al.*, 2009). This interpretation must be approached with caution as Weijers *et al.* (2007a), Tierney *et al.* (2010a) and Pearson *et al.* (2011) all found that the BIT value was predominantly related to low Crenarchaeol concentration rather than a high abundance of brGDGTs.

Alternatively, the soil MBT/CBT index, developed by Weijers *et al*. (2007a) uses brGDGTs which often dominate the GDGT composition in lacustrine environments. Although several studies have applied this MBT/CBT soil index in lakes (e.g., Sinninghe Damsté *et al*., 2009; Tierney *et al*., 2010a; Sun *et al*., 2011; Loomis *et al*., 2012; Naeher *et al*., 2014), it can underestimate measured temperatures by up to 15˚C.

The limitations of TEX_{86} and MBT/CBT indices has led to the development of GDGT-temperature calibrations specific to lacustrine environments, including a global brGDGT-temperature regression model by Pearson *et al.* (2011) and regional models for East Africa by Tierney *et al.* (2010a) and Loomis *et al.* (2012). Pearson *et al.* (2011) used the fractional abundances of brGDGTs to develop a global calibration using 85 lakes from the Scandinavian Arctic to Antarctica and applied best subsets regression to select a model with optimal predictive properties for mean summer air temperature (MSAT) (Eq. 6.1).

MSAT = 20.9 + (98.1 x GDGT-Ib) – (12.0 x GDGT-II) – (20.5 x GDGT-III) (Eq. 6.1)

This global calibration has a high accuracy and precision (r^2 = 0.88, RMSE = 2.0 ˚C, RMSEP = 2.1 ˚C) and is not significantly influenced by pH, conductivity or water depth. Naeher *et al.* (2014) applied the model to Lake Rotsee, Switzerland and found good correlation between reconstructed and measured temperatures.

Loomis *et al*. (2012) developed a regional East African brGDGT-temperature calibration (Eq. 6.2) adding 70 lakes to the 41 studied by Tierney *et al*. (2010a), and adding one additional brGDGT compound (GDGT-IIc) to those used by Pearson *et al*. (2011).

$$MAAT = 22.77 - (35.58 \times GDGT\text{-}III) - (12.88 \times GDGT\text{-}II) - (418.53 \times GDGT\text{-}IIc) + (86.43 \times GDGT\text{-}Ib) \quad \text{(Eq. 6.2)}$$

Although GDGT-IIc does not have a significant relationship with temperature in the global dataset of Pearson *et al*. (2011), it does improve model performance in the East African regional model. Loomis *et al*. (2012) concluded that regional calibrations had better predictive capability compared with global calibrations. This improvement can only be achieved where temperature gradients are sufficiently large. In the East Africa dataset this is achieved by sampling lakes along an altitudinal gradient.

Sinninghe Damsté *et al*. (2012) applied both the Tierney *et al*. (2010a) and the Pearson *et al*. (2011) brGDGT-temperature calibrations in Lake Challa, equatorial Africa, finding that the temperature difference between the Last Glacial Maximum and the Holocene for both calibrations was consistent with previous temperature reconstructions by Powers *et al*. (2005), Weijers *et al*. (2007b) and Tierney *et al*. (2008). More recently, Woltering *et al*. (2014) applied ten different GDGT-temperature calibrations, including both soil and lake calibrations, to a core from Lake McKenzie, Australia. They showed that although all calibrations indicated significantly lower temperatures during the last glacial period, the choice of calibration affected both the trend and absolute values of the reconstructed temperatures thus correct calibration selection is crucial (Woltering *et al*., 2014).

Equation (6.1) provides the best fit calibration with minimum prediction error across a wide range of temperatures for the global dataset (Pearson *et al*. 2011), but the model included only six sites with MSAT below 5 °C and none below 1.5 °C. As a consequence, it performs relatively poorly at low temperatures and overestimated MSAT in this part of the gradient (e.g. Pearson *et al*., 2011).

To address this limitation we studied 32 lakes from Antarctica, the sub-Antarctic Islands and Southern Chile, adding 26 new lakes to the high latitude Southern Hemisphere lakes studied by Pearson *et al*. (2011). Combining the two datasets we had a total of 37 samples including five replicate samples from sites analysed as part of this study and also previously by Pearson *et al*. (2011). The aims of the study were to: 1) quantify the GDGT composition of lake surface sediments and investigate the environmental controls on GDGT composition; 2) develop a brGDGT-temperature calibration for inferring past temperatures from Antarctic and sub-Antarctic lakes using redundancy

analysis, variance partitioning and regression analysis and 3) test the calibration on a representative sediment core from the sub-Antarctic.

6.2. Materials and Methods

6.2.1. Study locations

Surface sediments (top 0 – 2 cm) from 32 lakes from Antarctica, the sub-Antarctic Islands and Southern Chile (Fig. 6.1) were collected using a UWITEC surface gravity corer during several field campaigns in the Southern Hemisphere spring-summer season. Sites spanned a range of mean annual air temperature (MAAT) from -11.8 to 6.1 °C and MSAT (December to February) from -2.2 to 10.3 °C. The sites also covered a range of pH (4.5 to 9.8), conductivity (0.01 to 7.38 $mScm^{-1}$) and water depths (0.5 to 55 m). A summary of the temperature and limnological data for lakes in each region is listed in Table 6.1 and outline for each individual lake in Appendix A.

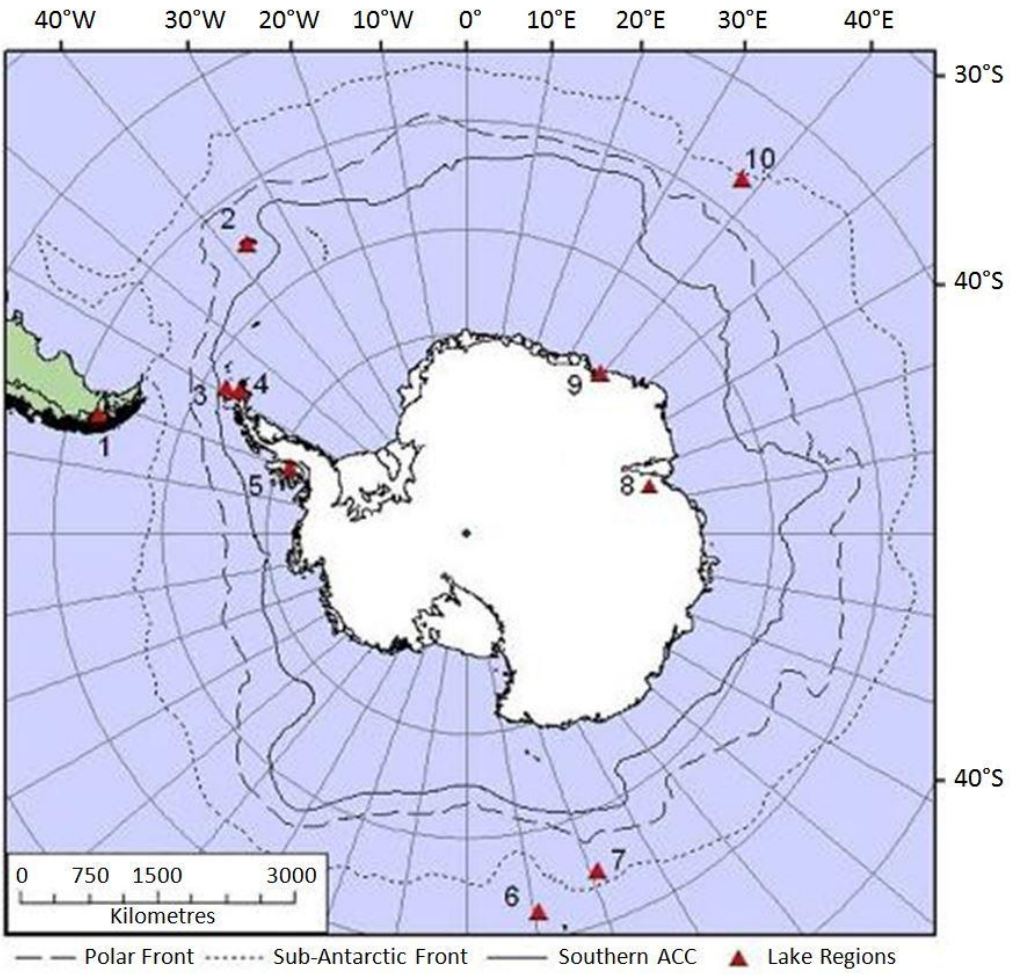

Figure 6.1: Map of the locations of the lake surface sediments, 1) Southern Chile, 2) Annenkov Island, South Georgia, 3) South Shetland Islands, 4) Trinity Peninsula, 5) Alexander Island, 6) Campbell Island, 7) Macquarie Island, 8) Larsemann Hills, 9) Syowa Oasis and 10) Marion Island.

Region	No. of Lakes	Latitude		Longitude		Altitude (m)		Water Depth (m)		MAAT (°C)		MSAT (°C)		Conductivity (mS/cm)		pH		Source
		Min	Max	Min	Max	Min	Max	Min	Max	Min	Max	Min	Max	Min	Max	Min	Max	
Alexander Island	2	S 70.85	S 71.78	W 68.25	W 68.33	98.0	126.0	5.6	55.0	-5.1	-4.9	0.1	0.3	0.058	0.158	6.67	7.97	British Antarctic Survey (2002)
Cannonball		S 71.78		W 68.25		98.0		5.6		-4.9		0.3		0.058		6.67		Roberts *et al.* (2008)
Moutonnée		S 70.85		W 68.33		126.0		55.0		-5.1		0.1		0.158		7.97		Roberts *et al.* (2009)
Campbell Island	4	S 52.51	S 52.59	E 169.15	E 169.19	268.0	379.0	0.9	1.2	3.8	4.8	6.0	7.0	0.117	0.287	4.46	5.07	
AB1		S 52.59		E 169.19		268.0		0.9		4.8		7.0		0.117		4.46		Saunders (Pers. Comm.) Department of Conservation (2013)
FR2		S 52.41		E 169.15		300.0		1.2		4.5		6.7		0.283		4.68		
HO2		S 52.57		E 169.19		379.0		0.9		3.8		6.0		0.266		5.03		
NE2		S 52.51		E 169.18		377.0		1.0		3.8		6.0		0.287		5.07		
Fildes Peninsula	5	S 62.21	S 62.23	W 58.94	W 58.98	14.5	34.5	5.3	7.0	-2.5	-2.4	1.0	1.1	0.013	0.177	7.53	8.07	
Ardley		S 62.21		W 58.94		18.0		6.1		-2.4		1.1		0.013		7.71		British Antarctic Survey (2008) Watcham *et al.* (2011)
Belén		S 62.23		W 58.98		19.9		7.0		-2.4		1.1		0.081		7.72		
Gaoshan		S 62.22		W 58.97		34.5		7.0		-2.5		1.0		0.074		8.07		
Long		S 62.21		W 58.97		15.0		5.6		-2.4		1.1		0.177		8.05		
Yanou		S 62.22		W 58.96		14.5		5.3		-2.4		1.1		0.094		7.53		
Larsemann Hills	4	S 69.38	S 69.41	E 76.05	E 76.40	5.0	65.0	3.8	38.0	-11.8	-11.2	-2.2	-1.6	0.261	7.380	6.30	7.10	
Heart		S 69.40		E 76.38		5.0		4.5		-11.2		-1.6		1.649		6.30		Hodgson *et al.* (2001; 2003; 2005; 2006a) Verleyen *et al.* (2003) Sabbe *et al.* (2004)
Progress		S 69.38		E 76.40		65.0		38.0		-11.8		-2.2		0.261		6.70		
Pup Lagoon		S 69.41		E 76.05		5.0		4.6		-11.2		-1.6		0.985		6.40		
Reid		S 69.39		E 76.38		30.0		3.8		-11.5		-1.9		7.380		7.10		
Marguerite Bay	1	S 67.60	S 67.60	W 67.20	W 67.20	19.4	19.4	6.1	6.1	-4.5	-4.5	0.7	0.7	0.131	0.131	6.54	6.54	British Antarctic Survey (2003)
Narrows		S 67.60		W 67.20		19.4		6.1		-4.5		0.7		0.131		6.54		Bentley *et al.* (2005)
Marion Island	3	S 46.86	S 46.86	E 37.85	E 37.85	71.0	98.0	0.9	1.0	4.6	4.8	6.7	6.8	0.061	0.069	6.46	7.85	
MI10		S 46.86		E 37.85		95.0		0.9		4.6		6.7		0.064		6.46		Verleyen and Van Nieuwenhuyze (2011)
MI4		S 46.86		E 37.85		71.0		1.0		4.8		6.8		0.061		7.85		
MI7		S 46.86		E 37.85		98.0		1.0		4.6		6.8		0.069		6.71		
Potter Peninsula	2	S 62.24	S 62.25	E 58.66	E 58.68	21.0	35.0	2.2	5.6	-1.9	-1.8	1.0	1.1	0.050	0.050	6.17	6.40	
GPS15		S 62.24		E 58.68		21.0		2.2		-1.8		1.1		0.050		6.40		Pearson (Pers. Comm.) Roberts (Pers. Comm.)
Matias		S 62.25		E 58.66		35.0		5.6		-1.9		1.0		0.050		6.17		

South Georgia	1	S 54.50	S 54.50	W 37.05	W 37.05	94.0	94.0	18.0	18.0	1.6	1.6	4.4	4.4	0.038	0.038	8.07	8.07	British Antarctic Survey (2008)
Fan		S 54.50		W 37.05		94.0		18.0		1.6		4.4		0.038		8.07		Hodgson (2009) Pearson *et al.* (2011)
Southern Chile	2	S 51.30	S 53.60	W 70.95	W 72.68	3.0	50.0	4.4	17.0	5.8	6.1	10.0	10.3	0.246	0.301	8.64	8.81	
Lago Bulnes		S 53.60		W 70.95		3.0		17.0		6.1		10.3		0.301		8.64		British Antarctic Survey (2008)
Laguna Pato		S 51.30		W 72.68		50.0		4.4		5.8		10.0		0.246		8.81		Pearson *et al.* (2011)
Syowa Oasis	4	S 69.03	S 69.47	E 39.51	E 39.61	-10.0	5.0	2.2	6.0	-10.7	-10.6	-2.0	-1.9	0.273	0.668	7.64	8.95	
Mago Ike		S 69.47		E 39.61		5.0		5.8		-10.7		-2.0		0.484		8.95		British Antarctic Survey (2007)
West Ongul 2		S 69.03		E 39.57		0.1		2.2		-10.7		-2.0		0.451		7.78		Kimura *et al.* (2010)
Higashi-ure Ike (WO6)		S 69.03		E 39.52		-10.0		5.0		-10.6		-1.9		0.668		7.64		
Nishi Ike (WO8)		S 69.03		E 39.51		-4.0		6.0		-10.6		-1.9		0.273		7.76		
Trinity Peninsula	4	S 63.55	S 63.61	W 57.34	W 57.41	2.5	134.0	0.5	24.0	-5.9	-5.1	-0.4	0.4	0.035	0.470	7.37	9.80	
Beak 1		S 63.61		W 57.34		11.0		24.0		-5.2		0.3		0.172		7.37		British Antarctic Survey (2006)
Beak 2		S 63.61		W 57.35		2.5		4.0		-5.1		0.4		0.188		8.60		Roberts *et al.* (2011)
Beak 4		S 63.61		W 57.37		6.0		0.5		-5.2		0.3		0.470		9.80		Sterken *et al.* (2011)
Viewpoint 7		S 63.55		W 57.41		134.0		15.0		-5.9		-0.4		0.035		8.15		

Table 6.1: Lake temperature and environmental characteristics summarised by region and for each individual lake.

A previously published sediment core from sub-Antarctic Fan Lake (54°29'0"S, 37°5'0"W), on Annenkov Island, South Georgia was used to test the Antarctic and sub-Antarctic brGDGT-temperature calibration. Fan Lake (Fig. 6.1) is 18 m deep and had a surface water temperature of 4.6 °C in December 2005 (Pearson *et al*., 2011; Strother *et al*., 2015; Van Nieuwenhuyze *et al*., in prep). The Bayesian age-depth model for the core was based on ^{210}Pb dating of the top 11 cm of the core and 32 radiocarbon dates (see Strother *et al*., 2015 and Appendix D for details).

6.2.2. GDGT extraction and analysis

GDGTs were extracted from 0.1 – 2.9 g of freeze dried and homogenised sediment. The samples were microwave extracted using DCM:Methanol (3:1, v:v). The total extracts were saponified and GDGTs isolated using hexane extractions following Pearson *et al.* (2011). The GDGT extracts were filtered through a 0.2 µm Whatman PTFE filter prior to analysis using an Acquity Xevo TQ-S (triple quadrupole with step wave; Waters Ltd). LC-MS set up with an atmospheric pressure chemical ionisation (APCI) source (Ion saber II) operated in positive ion mode. Analytical separation was achieved using a Grace Prevail Cyano HPLC column (3 µm, 150 x 2.1 mm i.d.) fitted with an in line filter (Waters Acquity UPLC in-line filter, 0.2 µm) at 40 °C using a binary solvent gradient where eluent A was hexane and eluent B was propanol. The flow rate of the mobile phase was 0.2 ml per minute with a gradient profile of 99% A 1% B (0 – 50 min); 98.2% A 1.8% B (50 – 55 min); 90% A 10% B (55 – 65 min) and finally 99% A 1% B (66 – 80 min). The LC-MS settings were: Source offset 50 V, capillary 1.5 KV, Desolvation temperature 200 °C, cone voltage 30 V, Desolvation gas (N_2). All sediment analysis was done at Newcastle University using HPLC grade solvents purchased from Fisher (Loughborough, UK).

Detection was achieved using selected ion monitoring (SIM) of targeted $[M+H]^+$ ions (dwell time 50 ms). The target ions are indicated in Figure 4.2. Peak identification and integration was carried out using MassLynx software (version 4.1).

6.2.3. Environmental data

Environmental data was collected from a range of sources including unpublished field reports from the British Antarctic Survey and other collaborators, research stations and previously published research. The water pH and conductivity data was taken from field reports and past research papers (Hodgson *et al.*, 2001; 2005; 2006a; Kaup and Burgess,

2002; Verleyen *et al.*, 2003; 2012; Sabbe *et al.*, 2004; Bentley *et al.*, 2005; Roberts *et al.*, 2008; 2009; Pearson *et al*., 2011; Watcham *et al.*, 2011; Sterken *et al.*, 2012).

Air temperatures were used as a surrogate for lake water temperature based on their strong relationship with the latter (Edinger *et al*., 1968; Webb and Nobilis, 1997; Livingstone and Dokulil, 2001). Following Pearson *et al*. (2011), we used MSAT rather than MAAT for two reasons. First, Antarctic lakes are rarely monitored all year round, and lake water temperature data are largely restricted to the austral summer and/or when lakes were cored or otherwise investigated. Second, many lakes remain ice-covered for much of the year and annual temperatures are not a biologically relevant parameter in regions where large seasonal temperature fluctuations or long periods of ice cover exist. Shanahan *et al*. (2013) confirmed a seasonal pattern in brGDGT production in Arctic lakes where production increased during the summer when temperatures were warmest and lakes were ice free. For each lake air temperature data was taken from the nearest research station and MSAT calculated by taking an average of the December, January and February mean air temperatures. Finally temperatures were lapse rate corrected (see Chapter 5 for details).

6.2.4. Statistical analysis

Previous lacustrine studies have shown a strong correlation between brGDGTs and temperature (e.g., Tierney *et al.*, 2010a; Pearson *et al.*, 2011; Sun *et al.*, 2011; Loomis *et al.*, 2012; Shanahan *et al.*, 2013), therefore we focused on the brGDGT compounds only, and individual brGDGTs were normalised to a percentage of the total brGDGTs prior to all numerical analysis.

The relationship between brGDGT composition and environmental conditions was explored using redundancy analysis (RDA) (see Pearson *et al*. 2011). RDA is a form of constrained principal components analysis in which variations in GDGT composition are directly related to lake physical-chemical characteristics. The relative strength and statistical independence of each environmental variable was assessed using a series of RDAs and partial RDAs to partition the variation in brGDGT composition into the (a) total, and (b) unique, or independent, effect of each variable (Borcard *et al*., 1992) and the statistical significance of each component of variation assessed using a Monte-Carlo permutation test.

To develop the brGDGT-temperature calibration for our Antarctic dataset we used best subsets regression to select an optimal set of brGDGT compounds yielding the minimum prediction error. Errors estimated from the original regression model suffer from resubstitution bias, and will generally underestimate true prediction error when the model is applied to new data outside of the calibration set. Some method of cross-validation, such as leave-one-out (LOO), is therefore usually employed to provide a more accurate estimate of model performance (e.g. Pearson *et al*., 2011). However, LOO fails to account for the effects of spatial autocorrelation and pseudoreplication that may exist in spatially structured calibration data, and consequently yields an over-optimistic estimate of prediction error (Telford and Birks, 2005). We therefore use Mantel correlograms (Borcard *et al*., 2011) and multivariate variograms (Dray *et al*., 2006) to identify the extent of spatial dependency in the brGDGT and associated temperature data, and then cross-validate our model using a so-called *h*-block procedure. This involves obtaining a prediction for calibration sample where that sample, and its neighbours with a distance of '*h*', are omitted from the calibration set (Burman *et al*., 1994). To facilitate comparison with earlier work we summarise model performance using four measures, the squared correlation between observed and predicted MSAT for the calibration set (r^2), the root mean squared error for the calibration set (RMSE), and the RMSE estimated by LOO and *h*-block cross-validation (RMSEP-LOO and RMSEP-H, respectively).

Lake depth and lake water conductivity had right skewed distributions and were either square-root (depth) or $\log_{10}$ (conductivity) transformed prior to all numerical analysis. R software for statistical computing and graphics (R Core Team (2014) with the packages vegan (Oksanen *et al*., 2013), leaps (Lumley, 2009), and rioja (Juggins, 2014)) was used for all numerical analysis.

6.3. Results

6.3.1. Environmental controls on brGDGT composition

GDGTs were found in all 32 lakes although only 11 lakes had a full suite of isoGDGTs (Fig. 6.2). BrGDGTs were the dominant compounds in 31 lakes. In Moutonnée Lake isoGDGTs were anomalously abundant, likely due to its hydraulic connection to the seawater in George VI Sound (Smith *et al.*, 2007; Roberts *et al.*, 2008; 2009). This site was therefore excluded from further analysis leaving 36 samples, including replicates, from 31 lakes. The BIT index values of the 31 remaining lakes ranged from 0.71 to 1.0

with the majority (88.9%) having a BIT > 0.95 (Fig. 6.2). The BIT value showed a stronger correlation with Crenarchaeol abundance (r = -0.999, $p < 0.001$) than brGDGT abundance (r = 0.40, $p = 0.018$).

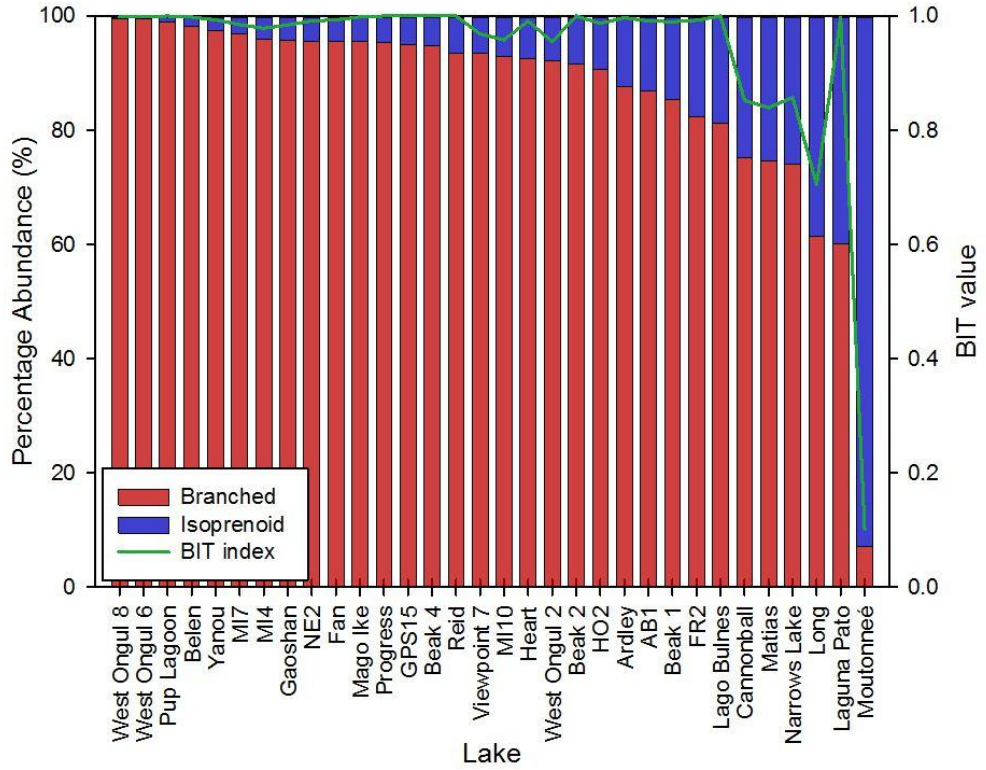

Figure 6.2: Bar chart of the relative distribution of the branched and isoprenoid GDGTs in the lake surface sediments. The line represents the BIT index.

RDAs and associated permutation test using individual environmental variables as explanatory variables showed that only MSAT, pH and lake depth explained significant portions of variation in brGDGT composition. Other environmental variables were therefore excluded from further analysis. The first and second components of the RDA (Fig. 6.3.a & b) summarise the relationship between the nine branched GDGT compounds with the three significant environmental variables and accounting for 33.8% and 5.1% of the variance in brGDGT composition respectively. Component 1 reflects a gradient from higher pH and depth and lower temperatures on the left, to lakes with higher pH, greater depth and higher temperatures to the right of the ordination diagram (Fig. 6.3.a). GDGT-I, GDGT-II and GDGT-III all have weak but significant correlations with depth (r = -0.37, -0.33 and 0.40 respectively, $p \leq 0.05$). Significant relationships were also found between GDGT-I, GDGT-Ib, GDGT-Ic and GDGT-III and pH (r = -0.40, -0.36, -0.55, 0.37, $p \leq 0.05$).

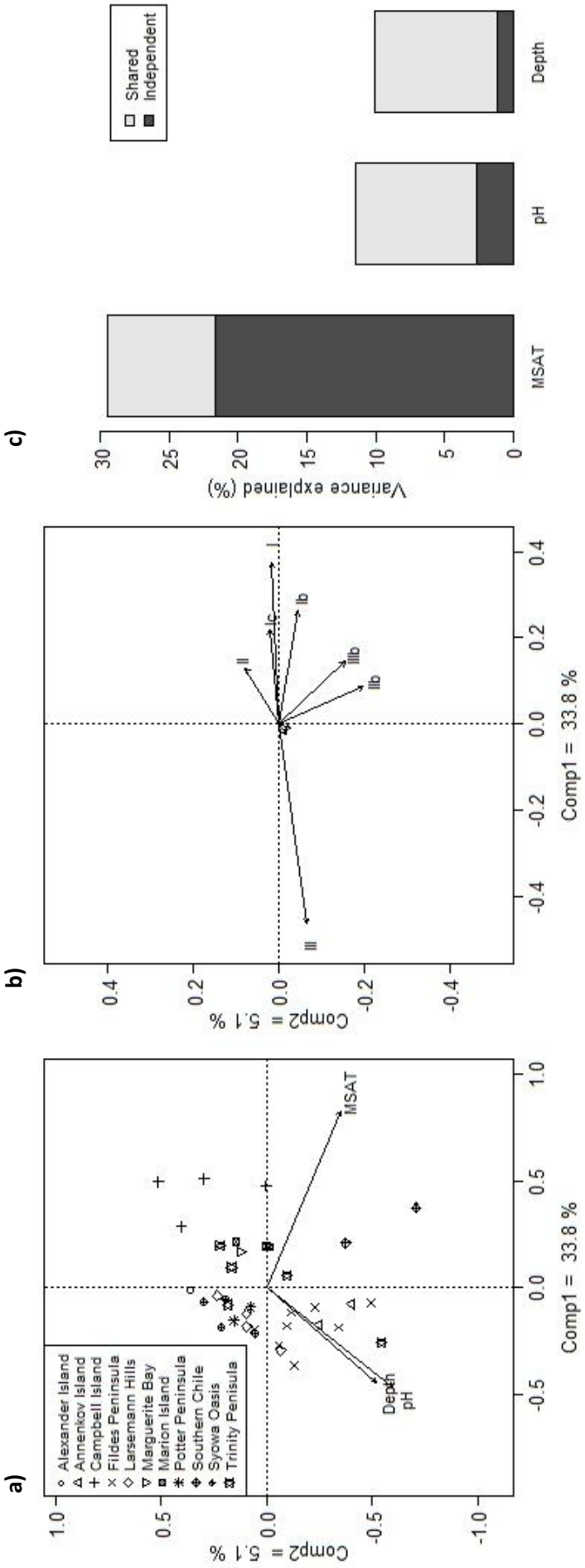

Figure 6.3: Plots showing the results of the redundancy analysis (RDA) and variance partitioning. a) ordination plot showing the relationships between sites and branched GDGT composition and b) their relationship with the environmental variables. c) Bar chart showing the percentage variance in GDGT composition explained by MSAT, pH, and depth.

Temperature has a strong and significant positive correlation with GDGT-I, GDGT-Ib, GDGT-Ic and GDGT-IIIb (r = 0.63, 0.66, 0.45 and 0.76 respectively) and a negative correlation with GDGT-III (r = -0.57; all $p < 0.005$) (Fig. 6.3.b). Component 2 is negatively correlated to pH and depth and reflects a small amount of residual variation (5.1%) due to these variables independent of MSAT.

Variance partitioning (Fig. 6.3.c) indicated that MSAT accounts for the largest fraction of variance in brGDGT composition (29.5%) and that the effect of MSAT was largely independent of other variables, with only 7.8% shared with pH and water depth. pH and depth account for 11.4% and 10.1% of variance respectively but only have a small independent effect on brGDGT composition (2.6% and 1.2% respectively; Fig. 6.3.c).

6.3.2. Development of a new brGDGT-temperature calibration for Antarctic and Sub-Antarctic Lakes

To address the limitations of existing GDGT-temperature calibrations in cold environments, we developed a regional calibration for Antarctic and the sub-Antarctic lakes. Initially, this was based on multiple regression using the set of compounds included in the Pearson *et al.* (2011) global calibration, but re-calibrated using our expanded surface sample Antarctic GDGT dataset (Fig. 6.4.a). Results of the Mantel correlograms and multivariate variograms (not shown) both indicate spatial dependency in the GDGT data at distances up to 500 km. We therefore use this distance as the cut-off value for *h*-block cross-validation.

MSAT = 32.5 + (85.4 x GDGT-Ib) – (43.1 x GDGT-II) – (32.1 x GDGT-III) (Eq. 6.3)

(r^2 = 0.67, RMSE = 2.00 °C, RMSEP-LOO = 2.23 °C, RMSEP-H = 2.37 °C, n = 36)

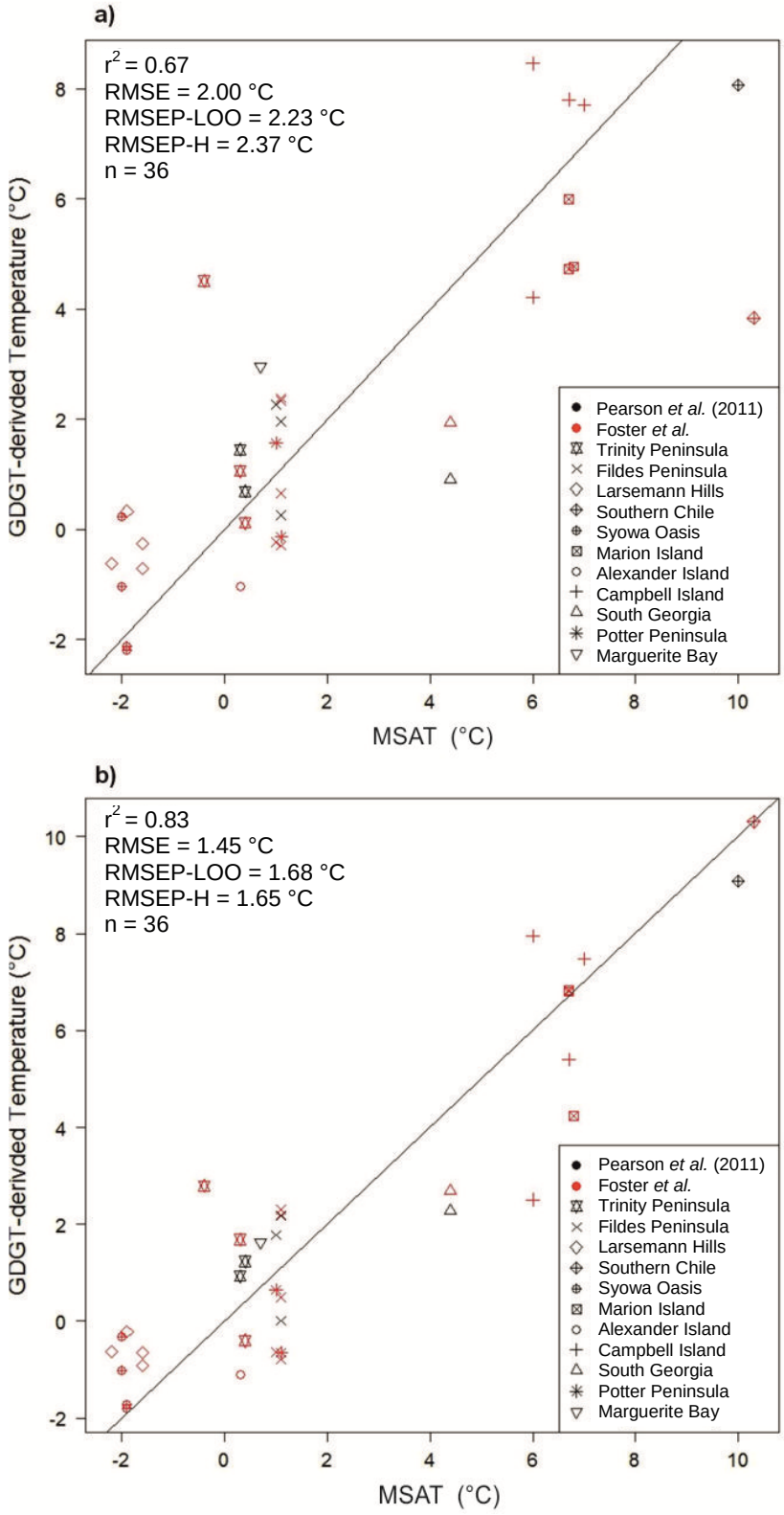

Figure 6.4: Relationships between measured temperature and GDGT-calibrated temperature for a regression models based on (a) the compounds used in the Pearson *et al.* (2011) (Eq. 6.3) and (b) new best subsets regression model for Antarctica (Eq. 6.4). Symbols indicate the location of the surface sediments.

We then developed a regression model using best subsets regression (Fig. 6.4.b) to select a set of compounds with optimal predictive properties. This model included GDGT-IIIb as an additional predictor:

$$MSAT = 18.7 + (80.3 \times GDGT\text{-}Ib) - (25.3 \times GDGT\text{-}II) - (19.4 \times GDGT\text{-}III) + (369.9 \times GDGT\text{-}IIIb) \quad \text{(Eq. 6.4)}$$

($r^2 = 0.83$, RMSE = 1.45 °C, RMSEP-LOO = 1.68 °C, RMSEP-H = 1.65 °C, n = 36)

Compared to the Antarctic dataset brGDGT-temperature calibration using the same compounds as Pearson *et al.* (2011) (Eq. 6.3; Fig. 6.4.a), the new calibration (Eq. 6.4; Fig. 6.4.b) has an increased $r^2 = 0.83$ and substantially lower RMSE under both LOO (1.68 °C) and *h*-block (1.65 °C) cross-validation (Table 6.2). Additionally, the replicate samples from the same lake, as analysed as part of this study and previously by Pearson *et al.* (2011), plot close to one another when applying the Antarctic and sub-Antarctic calibration (Eq. 6.4; Fig. 6.4.b) showing good reproducibility in the method. Finally, the residuals of the Antarctic and sub-Antarctic GDGT-temperature calibration were not significantly correlated with pH (r = 0.18, $p = 0.29$), depth (r = 0.14, $p = 0.42$) or conductivity (r = 0.28, $p = 0.10$).

	Calibration Equation		r^2	*p* value	RMSE (°C)	RMSEP-LOO (°C)	RMSEP-H (°C)
Pearson *et al.* (2011)	MSAT =	20.9 + (98.1 x GDGT-Ib) – (12.0 x GDGT-II) – (20.5 x GDGT-III)	0.54	< 0.001	2.32	N/A	N/A
Antarctic calibration based on Pearson *et al.* (2011) compounds	MSAT =	32.5 + (85.4 x GDGT-Ib) – (43.1 x GDGT-II) – (32.1 x GDGT-III)	0.67	< 0.001	2.00	2.23	2.37
New Antarctic Calibration	MSAT =	18.7 + (80.3 x GDGT-Ib) – (25.3 x GDGT-II) – (19.4 x GDGT-III) + (369.9 x GDGT-IIIb)	0.83	< 0.001	1.45	1.68	1.65

Table 6.2: Equation and model statistics including r^2, *p*, RMSE and RMSEP for the application of: the global brGDGT-temperature calibration (Pearson *et al*., 2011), an Antarctic brGDGT-temperature calibration based on the same three compounds used in the global calibration and our new Antarctic brGDGT-temperature calibration which also includes GDGT-IIIb.

6.3.4. Application of the brGDGT-temperature calibration

In the 4000 year Fan Lake record the reconstructed temperatures were between 2.2 and 13.7 °C (Antarctic and sub-Antarctic calibration) and 5.7 and 8.7 °C (global

calibration). The warmest temperatures were reconstructed at c. 3400 cal. yr B.P. when applying the Antarctic and sub-Antarctic calibration and for the global calibration at c. 3700 cal. yr B.P. (Fig. 6.5). Reconstructed core top temperatures were 2.2 and 6.6 °C respectively compared to a measured MSAT of 4.4 °C.

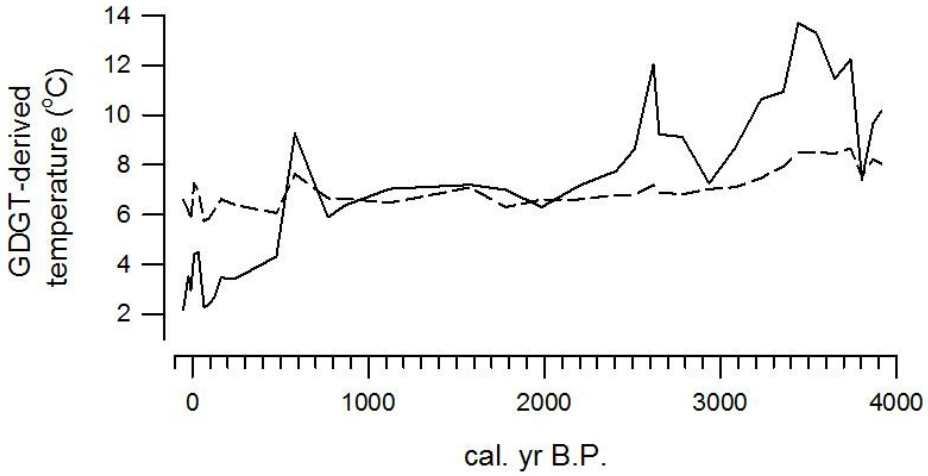

Figure 6.5: A downcore comparison of the Pearson *et al*. (2011) global GDGT-temperature calibration (dashed) and the new Antarctic and sub-Antarctic GDGT-temperature calibration (solid) at Fan Lake, South Georgia.

6.4. Discussion

6.4.1. Environmental controls on GDGT composition in Antarctic and sub-Antarctic lakes

All of the lakes studied apart from Moutonnée Lake had a dominance of brGDGTs and BIT values comparable with those found in other lakes (e.g., Pearson *et al.*, 2011; Sun *et al.*, 2011; Shanahan *et al.*, 2013) and soils (e.g., Hopmans *et al.*, 2004; Weijers *et al.*, 2007a). The main finding when analysing the environmental controls on brGDGT composition in Antarctic and sub-Antarctic lakes was that although pH, conductivity and depth show significant but weak correlations with some brGDGT compounds the relationship between brGDGT composition and temperature is more significant. Moreover, RDA and variance partitioning showed that the main independent environmental control on brGDGT composition in our data set was temperature.

Previous research by Weijers *et al.* (2007a), Tierney *et al.* (2010a) and Pearson *et al.* (2011) suggested that BIT value was predominantly related to low Crenarchaeol abundance rather than a high abundance of brGDGTs. We found this to be the case also in the Antarctic and sub-Antarctic dataset. These results support the conclusions of

Weijers *et al.* (2007a), Tierney *et al.* (2010a) and Pearson *et al.* (2011) that high BIT values predominantly reflect low Crenarchaeol concentrations rather than a high abundance of brGDGTs.

Weijers *et al*. (2007a) also indicated that the cyclisation of GDGTs related to pH as well as temperature while Tierney *et al*. (2010a) found that GDGT-Ic and GDGT-IIc were correlated with water depth. Nevertheless, Pearson *et al*. (2011) and Loomis *et al*. (2012) include cyclic GDGTs in their temperature calibrations as they found no relationship between them and pH or water depth, and these cyclic compounds are a significant component of their brGDGT-temperature calibrations. Pearson *et al*. (2011) assessed the relationship between GDGT-Ib and pH in their dataset in more detail. Although they found a significant correlation between GDGT-Ib and pH ($r = 0.29$, $p = 0.008$), the residuals of the brGDGT-temperature calibration were not significantly correlated with pH thus they concluded that their model was not confounded by lake-water pH.

In the Antarctic dataset, GDGT-Ib showed a weak correlation with pH ($r = -0.30$, $p = 0.080$), weaker than for GDGT-I or GDGT-Ic ($r = -0.33$, $p = 0.046$ and $r = -0.46$, $p = 0.005$). Pearson *et al.* (2011) also found a relationship between pH and GDGT-Ib in their global GDGT-temperature calibration ($r = 0.29$, $p = 0.008$). GDGT-IIIb showed no significant relationship with pH ($r = 0.16$, $p = 0.355$), conductivity or water depth. Similarly to Pearson *et al*. (2011), we found that although GDGT-Ib showed a weak correlation with pH, the residuals of the new Antarctic and sub-Antarctic GDGT-temperature calibration model presented in the following section were not significantly correlated to pH ($r = 0.18$, $p = 0.286$). In addition, the residuals were not significantly correlated to conductivity or water depth, therefore, the calibration is not confounded by pH, conductivity or water depth.

Similar relationships between brGDGT compounds and temperature in this research have been identified in previous studies. GDGT-I and GDGT-Ic dominated in warmer environments (Pearson *et al*., 2011; Loomis *et al*., 2012 Woltering *et al*., 2014), whereas in colder environments, such as the Arctic (Shanahan *et al*., 2013; Peterse *et al*., 2014) and the high mountains of the Tibetan Plateau (Günther *et al*., 2014), GDGT-II and GDGT-III dominated over GDGT-I. As expected, in the Antarctic and sub-Antarctic dataset GDGT-III or GDGT-II dominated in every sample.

6.4.2. Application of the global brGDGT-temperature calibration to the Antarctic dataset

As our dataset is an extension of the original Antarctic, sub-Antarctic and Chilean dataset from Pearson *et al*. (2011) we applied the global brGDGT-temperature calibration to the Antarctic dataset to evaluate its performance (Table 6.2). Previous applications of the global brGDGT-temperature calibration produced reconstructed temperatures that were comparable with either summer lake or air temperatures in Minnesota and Iowa, USA (Schoon *et al.,* 2013), Switzerland (Naeher *et al.,* 2014) and the Canadian and Siberian Arctic (Peterse *et al.,* 2014). When applying the Pearson *et al.* (2011) global brGDGT-temperature calibration to our Antarctic dataset we saw a reduction in the r^2 value to 0.54 however, the model errors were similar to those of the original global dataset (RMSE = 2.3 °C; Table 6.2). Nevertheless, the model showed a warm bias with a slight overestimation of temperatures at all sites apart from our warmest site (Lago Bulnes, Chile at 53 °S latitude).

6.4.3. Assessment of the new Antarctic and sub-Antarctic lakes brGDGT-temperature calibration model

We based our initial Antarctic and sub-Antarctic brGDGT-temperature calibration on the fractional abundances of the same three brGDGTs, GDGT-III, GDGT-II and GDGT-Ib, used in the Pearson *et al.* (2011) global brGDGT-temperature calibration (Eq. 6.3; Fig. 6.4.a). Applying this new calibration to the expanded Antarctic dataset reduced the r^2 of the original global calibration from 0.88 to 0.67, but the prediction error of RMSEP-LOO = 2.23 °C, RMSEP-H = 2.93 °C remained comparable to that of the Pearson *et al.* (2011) calibration (Table 6.2). There were some notable outliers in the model, for example, the MSAT at Viewpoint on the Trinity Peninsula was -0.4 °C, but the GDGT-derived temperature was 4.5 °C. Conversely, the GDGT-derived temperature at Lago Bulnes of 3.8 °C underestimated the observational data by 6.5 °C (Fig. 6.4.a).

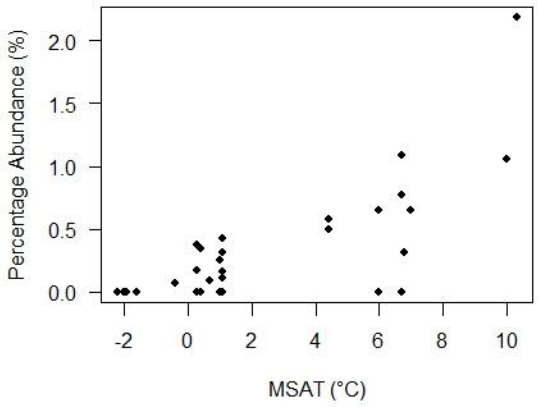

Figure 6.6: Relationship between GDGT-IIIb abundance and MSAT in the Antarctic and sub-Antarctic lakes dataset.

Our new Antarctic and sub-Antarctic brGDGT-temperature calibration (Eq. 6.4; Fig. 6.4.b) exhibited a higher r^2 value of 0.83 and lower overall model errors (RMSE = 1.45 °C, RMSEP-LOO = 1.68 °C and RMSEP-H = 1.73 °C) than the re-calibration of the expanded Antarctic dataset (Eq. 6.3). Most importantly, the addition of GDGT-IIIb significantly improved the model and reduced the errors of many of the outliers in the previous calibration (Fig. 6.4.a), most likely because of the strong positive and statistically significant relationship between GDGT-IIIb and temperature ($r = 0.74$, $p < 0.001$; Fig. 6.6). Furthermore, GDGT-IIIb accounted for an additional and significant fraction of variance in temperature and was a significant term within the regression model. As a result, the overestimation at Viewpoint has been reduced by 1.8 °C and the 6.5 °C underestimation of temperature at Lago Bulnes was eliminated. Therefore, our new calibration equation incorporating GDGT-IIIb is more reliable for reconstructing palaeotemperature from brGDGTs in Antarctic and sub-Antarctic lake sediments.

Significantly, this is the first time that GDGT-IIIb has been used in calibration models despite its presence in lake sediments in previous analyses in East Africa (Loomis *et al*., 2012) and in the Arctic (Shanahan *et al*., 2013), with maximum abundances of 2.1% in both regions. In our dataset the maximum abundance was similarly low (2.2%). Further investigation showed that below 1 °C the maximum abundance of GDGT-IIIb was 0.4% and below -0.5 °C GDGT-IIIb was below the detection limit. The limited abundance of GDGT-IIIb below c. 1 °C was largely responsible for the increased performance of our regional calibration.

The addition of GDGT-IIIb suggests that, although on a global scale GDGT-Ib, GDGT-II and GDGT-III have a significant relationship with temperature, incorporating

additional compounds on a regional scale can significantly improve model performance. Our new Antarctic and sub-Antarctic brGDGT-temperature calibration may also be applicable in other cold environments, for example the Arctic or high altitudes. To assess the applicability of our calibration to other cold environments further research is needed to determine whether this key relationship between GDGT-IIIb and temperature in Antarctic lakes is significant in all cold environments or if this relationship is regionally-specific to Antarctica.

6.4.4. Downcore application of the global and new Antarctic and sub-Antarctic brGDGT-temperature calibrations

We applied both the global Pearson *et al*. (2011) and our new Antarctic and sub-Antarctic brGDGT-temperature calibration to a sediment core from Fan Lake, Annenkov Island, South Georgia to evaluate the use of both calibrations as a palaeothermometer (Fig. 6.5). The Fan Lake sediment core was dated to c. 7700 cal. yr B.P. through ^{210}Pb and radiocarbon dating (see Strother *et al*., 2015). Here we focused on a 4000 year record as previous research at Fan Lake by Van Nieuwenhuyze *et al*. (in prep) showed that prior to c. 4300 cal. yr B.P. the lake was heavily influenced by a deglaciating catchment.

The Antarctic and sub-Antarctic GDGT-temperature reconstruction for Fan Lake (Fig. 6.5) showed the warmest conditions between c. 3800 – 3300 cal. yr B.P. with additional peaks in temperature at c. 2600 and 600 cal. yr B.P. The former was consistent with the mid-Holocene warm period when drier/warmer conditions prevailed on South Georgia (e.g., Van der Putten *et al*., 2009; Strother *et al*., 2015). Furthermore, the peak in temperature at c. 600 cal. yr B.P. may correlate with warmer conditions reconstructed by Strother *et al*. (2015) in the Fan Lake pollen record between c. 900 and 700 cal. yr B.P. The peaks in temperature during these known warm events c. 600 cal. yr B.P. and, more so, the mid-Holocene warm period were more prominent when applying our new GDGT-temperature calibration suggesting this calibration performs better than the global calibration in Fan Lake. This further emphasises the importance of GDGT-IIIb in Antarctic environments not only in the surface dataset but also when applying our new Antarctic and sub-Antarctic GDGT-temperature calibration downcore.

A more detailed reconstruction and interpretation of the GDGT-derived temperatures from Fan Lake will follow in Chapter 7.

6.5. Conclusions

We found that GDGTs were present in all 32 Antarctic, sub-Antarctic and Southern Chilean lakes and that brGDGTs were dominant in 31 of the lakes studied.

Statistical tests showed that the primary environmental control on the composition of brGDGTs in Antarctic lakes was temperature. This finding was consistent with prior GDGT analysis in lakes (e.g., Tierney *et al.*, 2010a; Pearson *et al.*, 2011; Sun *et al.*, 2011; Loomis *et al.*, 2012; Shanahan *et al.*, 2013). Furthermore, this highlights the value of brGDGTs as a temperature proxy in cold environments.

The relationship between GDGT-IIIb and temperature in Antarctica is of particular importance, being near absent in lakes with a temperature lower than 1 ˚C, and absent below -0.5˚C. In addition, GDGT-IIIb was not significantly correlated to any of the other environmental variables.

The incorporation of GDGT-IIIb into our brGDGT-temperature calibration, together with GDGT-Ib, GDGT-II, and GDGT-III resulted in improved accuracy and precision (r^2 = 0.83, RMSE = 1.45 °C, RMSEP-LOO = 1.68 °C, RMSEP-H = 1.73 °C, n = 36) when compared to the application of the Pearson *et al*. (2011) global calibration to our Antarctic dataset (Eq. 6.3) based on the same three compounds (r^2 = 0.67, RMSE = 2.00 °C, RMSEP-LOO = 2.23 °C, RMSEP-H = 2.93 °C, n = 36). Our new Antarctic brGDGT-temperature calibration (Eq. 6.4) was not confounded by water pH, conductivity or depth. GDGT-IIIb may also be important in other cold environments, for example the Arctic or high altitudes, meaning our new Antarctic calibration may be applicable in these environments.

The application of our regional lacustrine Antarctic and sub-Antarctic brGDGT-temperature calibration to sediment cores will enable us to substantially improve our understanding of past temperature in the region. A pilot study of a 4000 year record from Fan Lake, South Georgia based on our Antarctic and sub-Antarctic brGDGT-temperature calibration correlated well with some key warm phases identified in previous research. The forthcoming extension of this record and additional records will explore these correlations in more detail and enable us to improve and expand our knowledge of palaeoclimates in the Southern Hemisphere.

Chapter 7: A Mid to Late Holocene GDGT-Temperature Reconstruction for Fan Lake, South Georgia

This chapter has been prepared as a journal article with the following authors. Approximate author contributions are indicated as a percentage.

Louise C. Foster [a,b*] (70%)
Major additional contribution:
Stephen J. Roberts[a], Emma J. Pearson[b] & Wim Van Nieuwenhuyze[c] (20% combined)
Minor additional contribution:
Elie Verleyen[c], Dominic A. Hodgson[a] & Steve Juggins[b] (10% combined)

[a]British Antarctic Survey, Natural Environment Research Council, High Cross, Madingley Road, Cambridge, CB3 0ET**,** UK
[b]School of Geography, Politics and Sociology, Newcastle University, Newcastle-upon-Tyne, NE1 7RU, UK
[c]Ghent University, Protistology and Aquatic Ecology, Krijgslaan 281 S8, 9000 Gent, Belgium

Summary
In this chapter the Antarctic and sub-Antarctic GDGT-temperature calibration developed in Chapter 6 is applied to Fan Lake from Annenkov Island, South Georgia. The GDGT-derived temperature record for Fan Lake reconstructed variations in temperatures since c. 4300 cal. yr B.P. including the mid-Holocene warm period (c. 4500 – 2600 cal. yr B.P.), some of which have been identified in other records from South Georgia and the Antarctic Peninsula. Cross correlation between the Fan Lake GDGT-derived temperature record and other Antarctic and Southern Hemisphere temperature reconstructions is used to identify any leads and lags between the records with particular focus on the mid-Holocene warm period and the last 1000 years. The Fan Lake GDGT-temperature record is also compared with other records from Fan Lake including pollen, pigment and diatom records giving a well evidenced palaeoenvironmental reconstruction which can be used to determine the influence of the PFZ on South Georgia during the mid-late Holocene. Finally, within-lake and external processes which could be influencing the GDGT-temperature record, in particular at the start of the mid-Holocene warm period, are discussed.

7.1. Introduction

Previous research into palaeoenvironments on South Georgia has focused on the qualitative reconstruction of climates using either lake sediment cores (e.g., Rosqvist *et al*. 1999; Rosqvist and Schuber, 2003; Strother *et al*., 2015) or peat cores (e.g., Clapperton *et al*., 1989; Van der Putten *et al*., 2009), thus there is a real need to quantify palaeotemperatures. The application of the Antarctic and sub-Antarctic GDGT-temperature calibration developed in Chapter 6 on an existing dated sediment core from Fan Lake, Annenkov Island will allow the first quantitative reconstruction of terrestrial temperatures on South Georgia during the mid-late Holocene.

South Georgia's position within the Southern Ocean means it is of particular interest to palaeoclimatologists, thus is one of the most studied sub-Antarctic Islands (Van der Putten *et al*., 2009). Not only does South Georgia's location make it an ideal place to reconstruct terrestrial palaeoenvironments within an oceanic setting it also allows for the climatic connections between temperate and polar environments in the Southern Hemisphere to be assessed (Clapperton *et al*., 1989; Birnie, 1990; Rosqvist and Schuber, 2003; Van der Putten *et al*,. 2009). For example, the climate of South Georgia can reflect that of the Antarctic Peninsula i.e. during the mid-Holocene warm period (Strother *et al*., 2015) but also at times is more closely related to the climatic trends of southern South America, i.e. during the Medieval Climate Anomaly (MCA) and Little Ice Age (LIA) (Van Nieuwenhuyze *et al*., in prep).

The location of South Georgia is also fundamental to the mechanisms which are thought to control its climate. South Georgia is positioned directly within the influence of both the Polar Frontal Zone (PFZ) and the South Westerly Winds (SWW), therefore, changes in the position of the PFZ and SWW play a key role in climatic change on the island (Rosqvist and Schuber, 2003; Strother *et al*., 2015). Van Nieuwenhuyze *et al*. (in prep) suggested that a shift in the position of the PFZ, to south of South Georgia causing a climatic barrier between South Georgia and Antarctica, could play a key role in the close relationship between South Georgian and southern South American climates over the last 2000 years.

7.1.1. Previous mid-late Holocene palaeoenvironmental reconstructions on South Georgia

Palaeoclimatic reconstructions for South Georgia have shown evidence of warm periods, for example the mid-Holocene warm period (e.g., Rosqvist and Schuber, 2003; Van der Putten *et al*., 2004; Strother *et al*., 2015) and MCA (e.g., Clapperton *et al*., 1989; Strother *et al*., 2015; Van Nieuwenhuyze *et al*., in prep) interspersed with colder conditions after the mid-Holocene warm period from c. 2500 cal. yr B.P. (e.g., Birnie, 1990; Rosqvist and Schuber, 2003; Van der Putten *et al*., 2009; Strother *et al*., 2015) and during the LIA (Van Nieuwenhuyze *et al*., in prep).

One of the first palaeoenvironmental reconstructions from South Georgia by Clapperton *et al*. (1989) utilised plant macrofossil, pollen and inorganic sediment records from three peat cores in the Cumberland Bay area to the northeast of the island (Fig. 7.1). Clapperton *et al*. (1989) found evidence of drier, and possibly warmer, conditions between c. 6770 and 5500, 4700 and 2600 and 1000 and 750 cal. yr B.P. interspersed with colder conditions. They, however, do urge caution regarding the limited radiocarbon dating of both their peat and lake cores, therefore, any discrepancies between their records and those from elsewhere could be as a result of dating errors. Nevertheless, the warmer conditions suggested by Clapperton *et al*. (1989) between c. 4700 and 2600 cal. yr B.P. have also been evidenced at Tønsberg Peninsula and Kanin Point, at Stromness Bay c. 17 km northwest of Cumberland Bay (Fig. 7.1), between c. 4500 and 2600 cal. yr B.P. and c. 4400 and 3400 cal. yr B.P. respectively (Van der Putten *et al*. 2004; 2009). On the south of the island Strother *et al*. (2015) also recorded the mid-Holocene warm period between c. 3800 and 2800 cal. yr B.P. in palynological and sedimentological data from Fan Lake, Annenkov Island (Fig. 7.1).

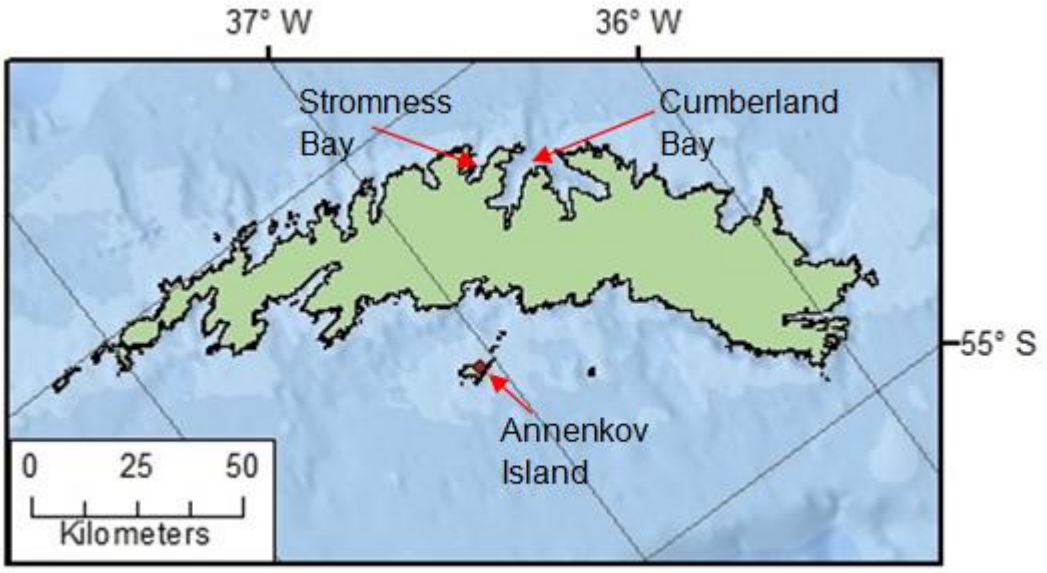

Figure 7.1: Map of South Georgia highlighting the three focus regions of previous palaeoenvironmental reconstructions; Cumberland Bay, Stromness Bay and Annenkov Island.

Following the mid-Holocene warm period the general consensus regarding the climates of South Georgia is of a period of colder conditions. Evidence of these colder climates commencing at c. 2700 cal. yr B.P. has been seen in lake records from Maiviken, Cumberland Bay (Birnie, 1990), the Tønsberg Peninsula (Van der Putten *et al*., 2004) and Fan Lake (Strother *et al*., 2015). Moreover, a period of glacial advance, thus cooler climates, was reconstructed in Block Lake, also in Stromness Bay, by Rosqvist and Schuber (2003) but starting slightly later at c. 2400 cal. yr B.P. Cooling seen on South Georgia after the mid-Holocene warm period was not confined to South Georgia and was also evident in records from the Antarctic Peninsula (Bentley *et al*., 2009) and East Antarctica (Kulbe *et al*., 2001) after c. 2500 cal. yr B.P. The termination of these cooler conditions on South Georgia occurred at c. 1600 cal. yr B.P. (Rosqvist and Schuber, 2003; Strother *et al*., 2015).

High resolution records of South Georgian palaeoclimates during the late-Holocene (c. 1000 cal. yr B.P. to present) are of particular interest as globally this period is well studied, therefore, allowing us to identify if South Georgia is in phase with Antarctic and / or hemispheric climate trends. Strother *et al*.'s (2015) palynological and sedimentological evidence from Fan Lake indicated a period of warmer conditions at c. 710 cal. yr B.P. which they interpret as the MCA. Warmer conditions were also reconstructed in Moraine Fjord and Hamberg Lakes by Clapperton *et al*. (1989) between c. 1000 and 750 cal. yr B.P, however, this warm period was not evident in some South Georgian records. Birnie (1990) and Rosqvist and Schuber (2003) did not

see evidence of the MCA, both reconstructing generally colder conditions over the last 1000 years with warming confined to post 1940 AD. Higher resolution records, such as the Fan Lake record, with well defined age-depth models may be required to see smaller scale changes including the MCA and LIA over the last 1000 years.

A mid-late Holocene quantitative GDGT-temperature record for Fan Lake will not only allow the reconstruction of temperature changes associated with periods of environmental change on South Georgia, but the high resolution nature of the record will also allow a detailed reconstruction of the late-Holocene. Van Nieuwenhuyze *et al*. (in prep) have suggested that the climates on South Georgia have become decoupled with Antarctica over the last 2000 years and represent more widespread hemispheric trends. The presence or absence of the MCA and LIA in the Fan Lake GDGT-temperature record will help determine if late-Holocene South Georgian climates were in phase with larger scale hemispheric climates during this period.

The aims of this chapter are to: 1) quantitatively reconstruct mid-late Holocene temperatures in Fan Lake, South Georgia; 2) compare the temperature reconstructions with previously published records from Fan Lake including elemental data from ITRAX scanning, diatom, pollen and pigment records and 3) compare the Fan Lake temperature record with previously published qualitative palaeoclimate reconstructions of South Georgia throughout the mid-late Holocene and determine any leads or lags between these records. A comparison of the new GDGT-temperature record with diatom and pigment records from Van Nieuwenhuyze *et al*. (in prep) will allow the relationship between temperature and primary productivity to be assessed. In addition, the Strother *et al*. (2015) pollen record, which contains zones of long distance pollen from southern South America, also allows temperature and the strength of the SWW to be compared. Finally, elemental data from the ITRAX scans, in particular titanium, gives an indication of ongoing catchment processes at Fan Lake during the mid-late Holocene (Roberts pers. comm.).

7.2. Study Area

South Georgia (Fig. 7.2.a & b) is a sub-Antarctic island in the north-eastern Scotia Sea situated c. 1500 km north of the northern tip of the Antarctic Peninsula and c. 1300 km east of the Falkland Islands (Van der Putten *et al*., 2004; Roberts *et al*., 2010) between 54 and 55°S, and 36 to 38°W (Bentley *et al*., 2007). The island is heavily glaciated on the southwest coast with ice-free peninsulas found to the northeast (Gordon *et al*.,

2008). The current average annual position of the PFZ is to the north of South Georgia which lays 5°N of the average limit of winter sea ice (Rosqvist and Schuber, 2003; Bentley *et al*., 2007).

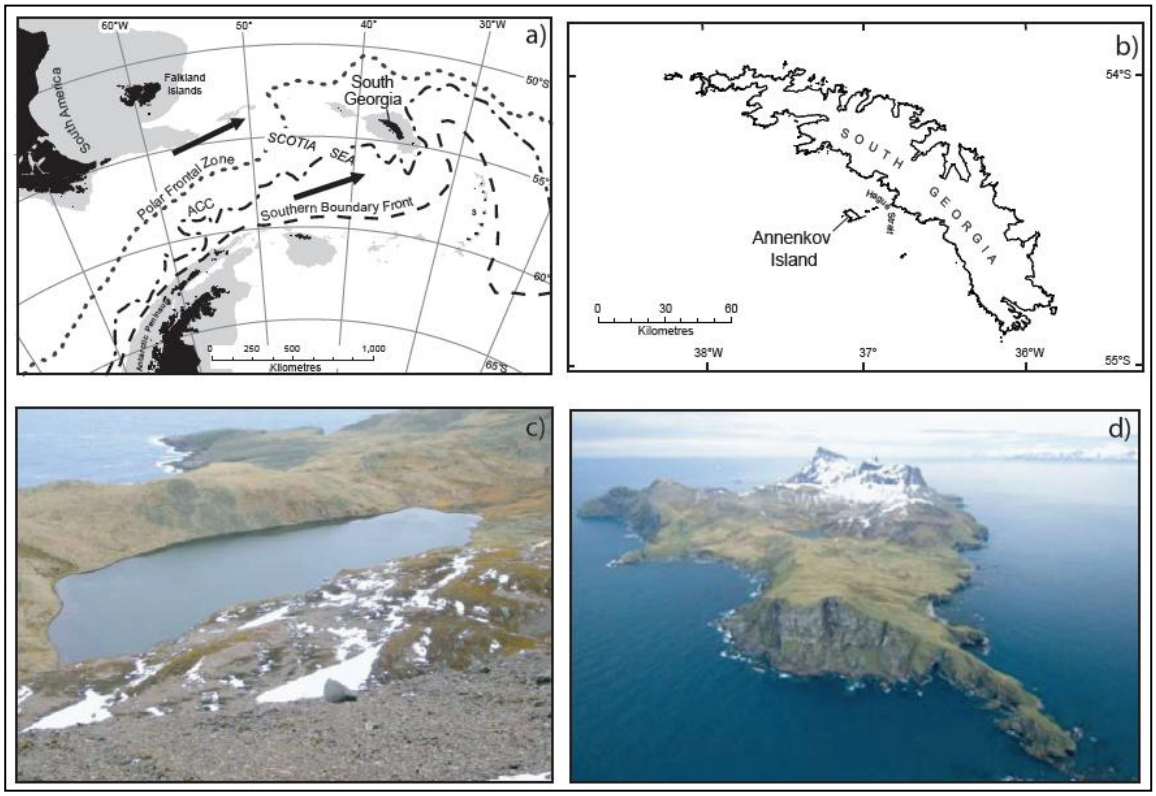

Figure 7.2: The location maps and photographs of Fan Lake, Annenkov Island, South Georgia. a) Map showing the location of South Georgia with respect to the Antarctic Peninsula, Chile and the Polar Frontal Zone. b) Map of South Georgia highlighting the location of Annenkov Island. c) Photograph of Fan Lake. d) Aerial photograph of Annenkov Island with Fan Lake located in the centre of the Island. Figure edited from Strother *et al*. (2015).

South Georgia is c. 170 km long and ranges from between c. 2 and 40 km in width (Van der Putten *et al*., 2004; Bentley *et al*., 2007). The island is dominated by a mountain chain comprising the Salvesen and Allardyce Ranges which rise to 2960 m a.m.s.l. (Rosqvist and Schuber, 2003; Bentley *et al*., 2007; Gordon *et al*., 2008). These mountains provide a barrier to the prevailing SWW (Gordon *et al*., 2008) consequently the climates, and glacial extent, on either side of the range is different.

The modern climate of South Georgia is predominantly influenced by the position of the PFZ and the SWW (Fig. 7.2.a) (Rosqvist and Schuber, 2003). As a consequence, the climate is cool, moist and windy with a strong maritime influence (Bentley *et al*., 2007; Gordon *et al*., 2008). The mean annual air temperature at Grytviken station on South

Georgia in 2014 was +2.4 °C (Met READER, 2015) and the mean annual precipitation at sea level is c. 1400 mm (Bentley *et al*., 2007).

Fan Lake (54°29'0"S, 37°5'0"W; Fig. 7.2.c) is located on Annenkov Island (54°29'– 55°00'S, 35°30'– 38°30'W; Fig. 7.2.d), c. 15 km southwest from South Georgia (Strother *et al*., 2015). In December 2005 Fan Lake had a depth of 18 m and surface water temperature of 4.6 °C (British Antarctic Survey, 2006; Hodgson, 2009; Pearson *et al*., 2011; Strother *et al*., 2015). The lake is found at c. 90 m above sea level with a length of c. 430 m and width c. 200 m (Strother *et al*., 2015). An outflow is present at the eastern end of the lake and a small inflow is located to the western end through peat land (Strother *et al*., 2015). Within the catchment of Fan Lake there are several vegetated, thinly veneered ridges (British Antarctic Survey, 2006).

7.3. Materials and Methods

7.3.1. Core Collection and Sampling

Fan Lake was cored in December 2005 from the deepest part of the lake. The composite core analysed in this study is c. 5.8 m long at which point rock was reached (British Antarctic Survey, 2006; Strother *et al*., 2015). An additional short surface core of 18 cm was also extracted (Strother *et al*., 2015). Cores were taken using a UWITEC gravity corer for the upper sediments and a UWITEC piston corer for the deeper sediments (Strother *et al*., 2015; Van Nieuwenhuyze *et al*., in prep). The 5.8 m core is composed of four overlapping and correlated c. 2 m long core sections (FAN 2A, 2B, 1C, 2C). Cores and subsamples were kept frozen at -20 °C during transport and storage. Cores were sub-sampled inside a Class II fume-hood into air-tight Whirlpak/ziplock bags at 1 cm intervals.

7.3.2. Lithology and Sedimentology

Sedimentological logging of the 5.8 m core was undertaken on a defrosted half-core inside a Class II fume-hood using Munsell colour charts[1] prior to sub-sampling (Appendix D). Micro-XRF (μ-XRF) geochemical core scanning was also undertaken on the 5.8 m core using the ITRAX core scanner at the Aberystwyth University[1] (Appendix D). During analysis cores were stored at 4 °C and re-frozen to -20 °C once analysis was complete. Grain size analysis was completed for Fan Lake at 1 cm intervals[1]. Total organic carbon (TOC), total nitrogen (TN) and bulk organic carbon isotopic ratios

[1] Analysis undertaken by Stephen Roberts (British Antarctic Survey); data are used here with permission

($\delta^{13}C_{org}$) were calculated at 2 cm intervals between 0 and 280 cm and 4 cm intervals between 280 and 580 cm core depth[2] (see Appendix D for details).

7.3.3. GDGT, diatom and pigment extractions

GDGTs were extracted from 82 samples at 1 cm intervals between 0 and 20 cm[3], 8 cm intervals between 20 and 360 cm and 16 cm intervals between 360 and 550 cm core depth. GDGTs were extracted from 0.3 – 4.6 g of freeze dried and homogenised sediments at Newcastle University following the methods outlined in Chapter 5. Detection was achieved using selected ion monitoring (SIM) of targeted $[M+H]^+$ ions (dwell time 50 ms). The target ions are indicated in Figure 4.2. Peak identification and integration was carried out using MassLynx software (version 4.1).

Diatoms were extracted from 47 samples at a maximum sampling interval of 16 cm[4]. Organic matter was removed from weighed, oven dried (at 60 °C) samples using hydrogen peroxide (H_2O_2) (Van Nieuwenhuyze *et al*., in prep). The Battarbee and Kneen (1982) microsphere addition method was used by Van Nieuwenhuyze *et al*. (in prep) to determine the absolute number of diatom valves and stomatocysts per gram of dried sediment. Identification was achieved at 10x100x magnification (Van Nieuwenhuyze *et al*., in prep).

Pigments were extracted from 40 samples at an average sampling interval of 16 cm[4]. Pigments were extracted following the Leavitt and Hodgson (2001) method. Acetone was added to freeze-dried samples and the samples sonicated and filtered at 0.20 μm (Van Nieuwenhuyze *et al*., in prep). HPLC (high performance liquid chromatography) analysis allowed the isolation and quantification of the pigments. Analytical separation was achieved using a reversed phase Spherisorb ODS2 column (4.6 mm diameter, 5 pm particle size) (Van Nieuwenhuyze *et al*., in prep). Three mobile phases were used, eluent A was methanol:0.5 M ammonium acetate (80:20), eluent B was acetonitrile: milliQ water (90:10) and eluent C was ethyl acetate (Van Nieuwenhuyze *et al*., in prep).

[2] Analysis undertaken by Melanie Leng (British Geological Survey); data are used here with permission
[3] Analysis undertaken by both Louise Foster and Emma Pearson (Newcastle University)
[4] Analysis undertaken by Wim Van Nieuwenhuyze (Ghent University); data are used here with permission

7.3.4. Chronological analysis and age model

Existing chronological data was made available (Roberts pers. comm.). Lead-210 (^{210}Pb) and Caesium-137 (^{137}Cs) dating was undertaken on the upper 11 cm of the surface core using dried and homogenised samples. The method is outlined in Appendix D and Strother *et al*. (2015).

In addition, 32 samples from the 5.8 m core were radiocarbon dated via Accelerator Mass Spectrometry (AMS). These included 21 moss samples, one bone fragment, three bulk sediment samples and seven bulk organic sediment samples. Radiocarbon ages were calibrated in OXCAL (version 4.2; Bronk-Ramsey, 2009) using the SHCal13 Southern Hemisphere calibration curve (Hogg *et al*., 2013). Post-bomb samples were corrected using $^{13}C/^{12}C$ isotopic ratios and calibrated using the SHCal13 SH Zone 1 – 2 Bomb curve in CALIBomb (Hua *et al*., 2013; Reimer and Reimer, 2004) see Appendix D.

Radiocarbon and ^{210}Pb were used to generate a master age-depth model[1] (Strother *et al*., 2015; Fig. 7.3) in BACON v.2.2 (Bayesian) age-depth modelling software in R v3.1 (Blaauw, 2010; Blaauw and Christen, 2011; Roberts pers. comm.). The BACON age-depth model allowed ages to be interpolated from the best-fit age. The age-depth model estimated a core age of 7700 cal. yr B.P. Outside of the ^{210}Pb data ages were rounded to 10 years or 50 years after c. 3000 years to give a fair reflection of the 95% confidence interval (Roberts pers. comm.).

7.3.5. Statistical Analysis

The relative abundance of the brGDGTs was calculated throughout the core and the Antarctic and sub-Antarctic GDGT-temperature calibration (Chapter 6) applied to reconstruct summer temperatures. A temperature anomaly record was also calculated for the Fan Lake GDGT-temperature record to enable a comparison with other temperature anomaly records. The temperature anomalies were calculated from a mean post 1960 AD temperature.

Constrained CONISS cluster analysis was undertaken in R v3.1 (R Core Team, 2014) on the relative abundance of the brGDGTs known to relate to temperature thus used in the Antarctic and sub-Antarctic GDGT-temperature calibration. Broken stick analysis was done to test that all zones identified were statistically significant.

Finally cross correlations between the Fan Lake GDGT-derived temperature record and other proxy and instrumental records for the region were run in R v3.1 to determine any leads and lags between these records (R Core Team, 2014). Prior to cross correlation the datasets were re-sampled on either a 10, 50 or 100 year scale depending on the resolution of the original dataset. The re-sampling strategy meant that the higher resolution records were re-sampled to match that of the record with the lowest resolution (see Chapter 5 for details). Re-sampling was done using Analyseries software.

7.4. Results

7.4.1. Chronology and Sedimentology

The sedimentology of Fan Lake was defined by the lithofacies zones as described by Strother *et al*. (2015). These zones were characterised by a general upwards fining of sediments from a basal unit of clast supported diamicton and sandy matrix with sporadic supported clasts (Zone 1, 587 – 500 cm) to a dominance of laminated organic lake mud in zones 7 and 8 from 258 to 0 cm (see Fig. 7.3 for summary).

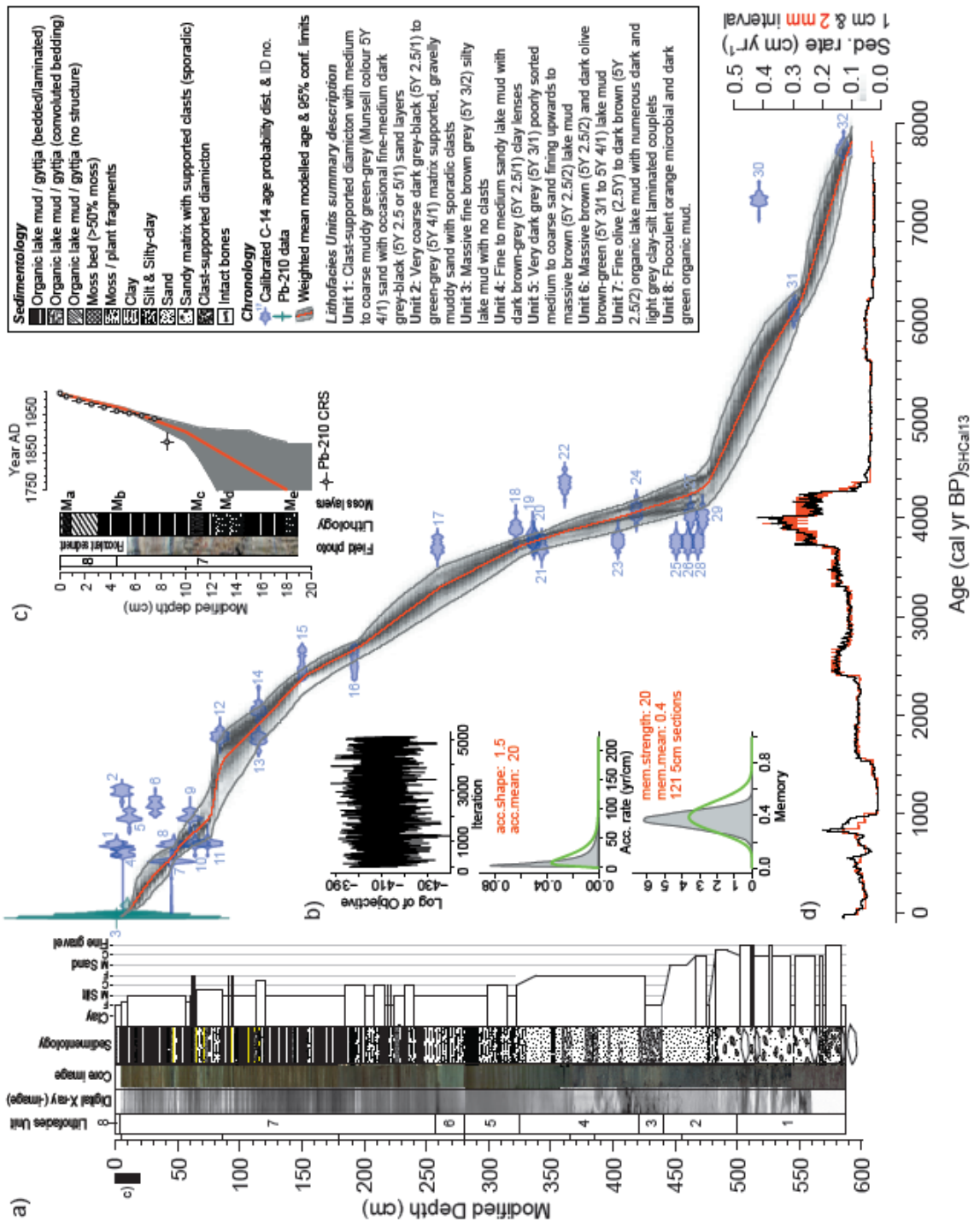

Figure 7.3: Age Depth Model for Fan Lake: a) Age depth model for the whole core with lithological units, x-ray and core images, sedimentology logs and a grain size summary. The red line on the age-depth model represents the median best-fit; b) Set up parameters for the BACON age–depth model; c) Age depth model for the top 20 cm of the core which were ^{210}Pb dated and d) Fan Lake sediment accumulation rate at 1 cm (black) and 2 mm (red) intervals. Figure taken from Strother *et al.* (2015).

7.4.2. Glycerol Dialkyl Glycerol Tetraethers (GDGTs)

In Fan Lake the nine brGDGT compounds were present in varying proportions downcore (Fig. 7.4). Throughout the core brGDGTs were more abundant than isoprenoid GDGTs, brGDGTs had an abundance of between 91 and 97% of all GDGTs. GDGT-III had the highest relative abundance ranging between 47 and 60% of the total brGDGT abundance alternatively GDGT-IIIc had the lowest relative abundance with a maximum abundance of 3% (Fig. 7.4).

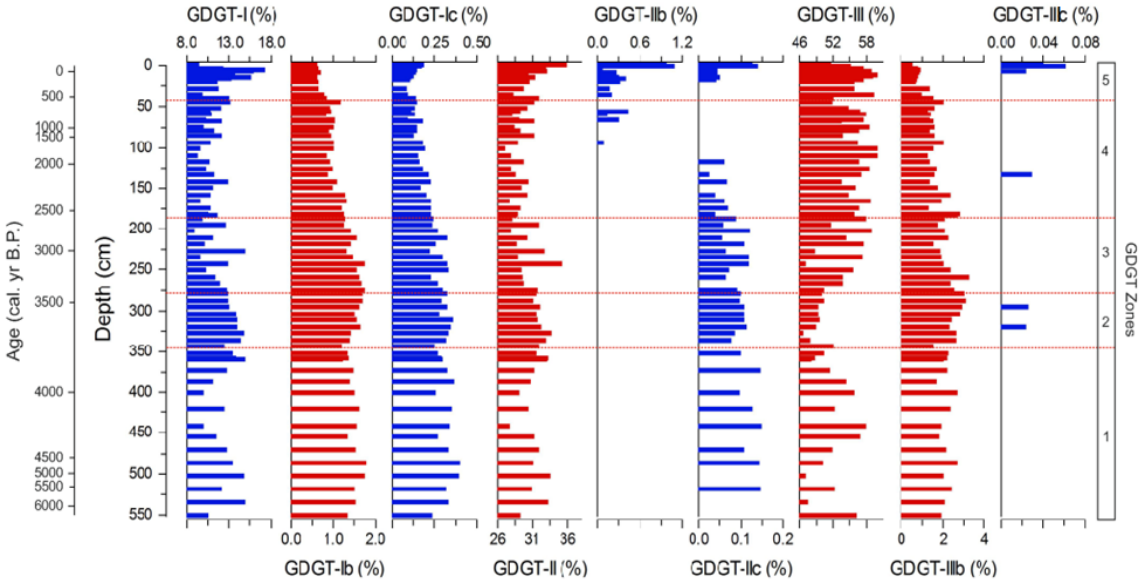

Figure 7.4: Relative abundance of the nine branched GDGTs downcore in the Fan Lake sediment core. The red GDGT compounds are those used in the Antarctic and sub-Antarctic GDGT-temperature calibration developed in Chapter 6. The dashed red lines indicate the significant brGDGT zones identified through CONISS cluster analysis.

The GDGT-derived summer temperatures ranged from c. 1.5 °C ± 1.45 °C at 1.5 cm core depth (c. 1994 AD) to c. 14.2 °C ± 1.45 °C at 260 cm depth (c. 3300 cal. yr B.P.) with a mean summer temperature throughout the core of c. 7.9 °C. Constrained CONISS cluster analysis on the brGDGTs indicated five significant GDGT zones (Fig. 7.4 & 7.5).

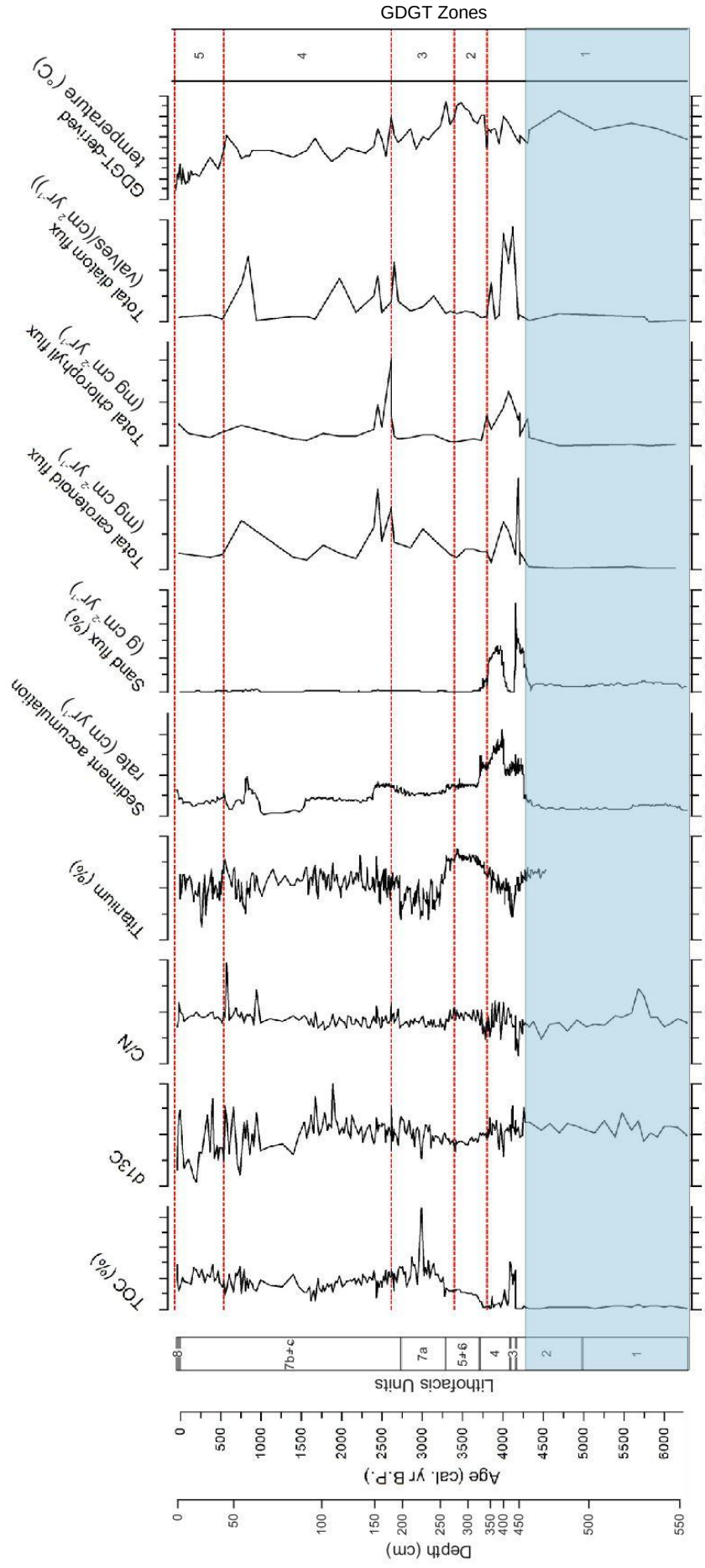

Figure 7.5: Downcore data for Fan Lake including, TOC, $\delta^{13}C$, C/N ratios, Titanium (%), sediment accumulation rate, sand flux and GDGT-derived summer temperatures and total diatom, carotenoid and chlorophyll flux[4]. The plot also shows the lithofacies units from Strother *et al.* (2015) and the GDGT zones. The blue area at the base of the core represents the part of the core known to be influenced by a deglaciating catchment.

7.4.3. Zone 1: 587 – 345 cm (c. 7700 – 3800 cal. yr B.P.)

This zone included the section of the core, between 587 and 469 cm, known to be affected by a deglaciating catchment meaning palaeoclimates cannot be reconstructed (Roberts pers. comm.). Nevertheless, when looking at the section of this zone not affected by the deglaciating catchment, 469 to 345 cm core depth, the GDGT-temperature record showed higher than average temperatures with an average temperature of c. 9.6 °C (Fig. 7.5). A general warming trend was seen in the temperature record between 469 and 345 cm core depth.

Sediment accumulation rate throughout Zone 1 was relatively stable until 464 cm when it increased from 0.12 to 0.20 cm y^{-1} before it stabilised at c. 0.2 cm y^{-1} (Fig. 7.5). At 404 cm depth the sediment accumulation rate peaked at 0.37 cm y^{-1} before it decreased again. These two periods of increased sediment accumulation correspond with the only peak in sand flux in the core between 468 and 440 cm and 404 and 349 cm (Fig. 7.5). Carbon isotope data[2] showed relatively stable C/N ratios (average c. 9) and $\delta^{13}C$ (average c. -26%) between 470 and 345 cm and TOC peaked to 4.6% between 440 and 425 cm (Fig. 7.5).

The peak in sediment accumulation rate and sand flux also coincides with the greatest total diatom flux[4] in the core to 1.9 x 10^{11} valves per cm^2 yr^{-1} at 434 cm. Total carotenoid and total chlorophyll flux[4] also peaked at 1.4 x 10^{-3} mg per cm^2 yr^{-1} and 0.04 mg per cm^2 yr^{-1} respectively between c. 440 and 360 cm core depth (Fig. 7.5).

7.4.4. Zone 2: 345 – 276 cm (c. 3800 – 3410 cal. yr B.P.)

The GDGT-derived summer temperatures in Zone 2 had the highest average temperature seen in the record at c. 12.0 °C ± 1.45 °C, 4.1 °C warmer than the core average. Temperatures in Zone 2 varied between 7.4 °C ± 1.45 °C at 345 cm and 14.0 °C ± 1.45 °C at 289 cm (Fig. 7.5). The GDGT-temperature record showed a general warming trend throughout the zone.

Sediment accumulation rate at 345 cm was 0.23 cm y^{-1} and it remained stable at c. 0.2 cm y^{-1} until it dropped to 0.15 cm y^{-1} at 320 cm (Fig.7.5). All other sedimentological data and primary productivity proxies were relatively stable during this period (Fig. 7.5). Total diatom, carotenoid and chlorophyll fluxes[4] reduced from their Zone 1 maxima and were stable throughout Zone 2, sand flux also reduced fully. Finally, the

C/N ratios were stable throughout Zone 2 while $\delta^{13}C$ values decreased slightly and TOC values increased a little[2] (Fig. 7.5).

7.4.5. Zone 3: 276 – 183 cm (c. 3410 – 2620 cal. yr B.P.)

The GDGT-derived summer temperatures in Zone 3 showed a general reduction in temperature but the average temperature was still relatively high at c. 10.1 °C (Fig. 7.5). Zone 3 contained the highest recorded GDGT-temperature in the core of 14.2 °C ± 1.45 °C at 260 cm. Sediment accumulation rate was stable throughout Zone 3 with an average of c. 0.12 cm y^{-1}. Zone 3 also contained the highest peak in TOC of 9.8% at 226 cm and a greater fluctuation in $\delta^{13}C$ than in Zone 2 between -27.0 and -24.9% (Fig. 7.5). C/N ratios were stable at around 9.2.

Total chlorophyll flux was stable in Zone 3 but total diatom flux and total carotenoid flux[4] both showed small peaks to 5.2 x 10^{10} valves per cm^2 yr^{-1} at 244 cm and 1.2 x 10^{-3} mg per cm^2 yr^{-1} at 228 cm respectively (Fig. 7.5). Total diatom flux[4] peaked again to 1.2 x 10^{11} valves per cm^2 yr^{-1} at 188 cm.

7.4.6. Zone 4: 183 – 42 cm (c. 2620 – 540 cal. yr B.P.)

The GDGT-derived summer temperature record for Zone 4 showed a slight cooling trend punctuated with three warm peaks to 10.3, 8.9 and 9.3 °C ± 1.45 °C at 159, 95 and 45 cm respectively (Fig. 7.5). The average temperature for Zone 4 of c. 7.5 °C was comparable with the core average temperature of c. 7.9 °C.

Sediment accumulation rate dropped by c. 0.1 cm yr^{-1} twice in Zone 4, at 150 and 85 cm (Fig. 7.5). Sediment accumulation then increased from 73 cm to a peak of 0.20 cm y^{-1} at 64 cm before it decreased again. C/N ratios[2] were relatively stable throughout Zone 4 at c. 9.3 with two peaks to 12.1 and 14.7 at 73 and 45 cm respectively (Fig. 7.5). The $\delta^{13}C$ record peaked to -24.0% at 113 cm and to -24.6% at 95 cm before it dropped off at 81 cm. $\delta^{13}C$ was then stable at an average of -26.2% until 67 cm following which larger fluctuations were seen in the rest of the zone between -27.8 and -24.6% (Fig. 7.5).

Total diatom flux[4] data also showed three peaks in Zone 4 to 9.0 x 10^{10}, 8.4 x 10^{10} and 1.3 x 10^{11} valves per cm^2 yr^{-1} at 159, 119 and 65 cm respectively (Fig. 7.5). Total carotenoid flux[4] peaked to 2.3 x 10^{-3} mg per cm^2 yr^{-1} at 159 cm and additionally to 1.8 x 10^{-3} mg per cm^2 yr^{-1} at 183 and 1.4 x 10^{-3} mg per cm^2 yr^{-1} at 57 cm. Total chlorophyll

flux[4] peaked to 0.06 mg per cm^2 yr^{-1} at 183 cm with another smaller peak to 0.03 mg per cm^2 yr^{-1} at 159 cm (Fig. 7.5).

7.4.7. Zone 5: 42 – 0 cm (c. 540 cal. yr B.P. to present)

The GDGT-derived summer temperatures in Zone 5 were the coldest of the whole core with an average of c. 3.6 °C, 4.3 °C below the average temperature for the record (Fig. 7.5). The lowest temperature in the record of 1.5 °C ± 1.45 °C was found at 1.5 cm core depth (Fig. 7.5). Reconstructed summer temperatures showed a general decrease from 7.0 °C ± 1.45 °C at 42 cm to 2.2 °C ± 1.45 °C at 0.5 cm. This was punctuated with two peaks in temperature of 4.2 °C ± 1.45 °C at 16 cm and 5.1 °C ± 1.45 °C at 6 cm.

The sediment accumulation rate decreased slightly to 0.05 cm yr^{-1} at 16 cm at which point it increased to 0.13 cm yr^{-1} at the top of the core (Fig. 7.5). C/N ratio was stable with one small peak at 6 cm (Fig. 7.5). TOC and $\delta^{13}C$ both showed greater fluctuations in Zone 5, with $\delta^{13}C$ fluctuating between -27.8 and -24.6%[2] (Fig. 7.5). Total diatom flux and total carotenoid flux[4] were both low and stable with average values of c. 9.6 x 10^9 valves per cm^2 yr^{-1} and c. 4.2 x 10^{-4} mg per cm^2 yr^{-1} respectively (Fig. 7.5). The total chlorophyll flux[4] was also low, average c. 9.7 x 10^{-3} mg per cm^2 yr^{-1}, however it did increase slightly at the top of the core above 13 cm to 1.5 x 10^{-2} mg per cm^2 yr^{-1}.

7.4.8. Comparison of the Fan Lake GDGT-derived temperatures with previously published records

7.4.8.1. James Ross Island and EPICA Dome C ice core records.

A comparison of temperature anomaly records from the James Ross Island (JRI) ice core (Mulvaney *et al*., 2012) and the EPICA Dome C ice core (Stenni *et al*., 2010) with the Fan Lake GDGT-derived summer temperature anomaly data suggested periods of good correlation between the records alongside periods of disparity (Fig. 7.6). All three records showed evidence of a 'warm' period at the beginning of the record before c. 3000 cal. yr B.P. The highest temperature anomaly in the Fan Lake record (Fig. 7.6.c) was between c. 3200 and 3800 cal. yr B.P. In the JRI the highest temperature anomaly was similarly at c. 3200 cal. yr B.P. At EPICA Dome C it was later at c. 2800 cal. yr B.P. but the temperature anomaly was also high at c. 3700 cal. yr B.P (Fig. 7.6.a & b). Nevertheless, the warming trend seen in both JRI (Fig. 7.6.a) and EPICA Dome C (Fig. 7.6.b) after c. 600 cal. yr B.P. and 500 cal. yr B.P., respectively, was not evident in Fan

Lake where the temperature anomaly record showed a general cooling trend post c. 600 cal. yr B.P. (Fig 7.6.c).

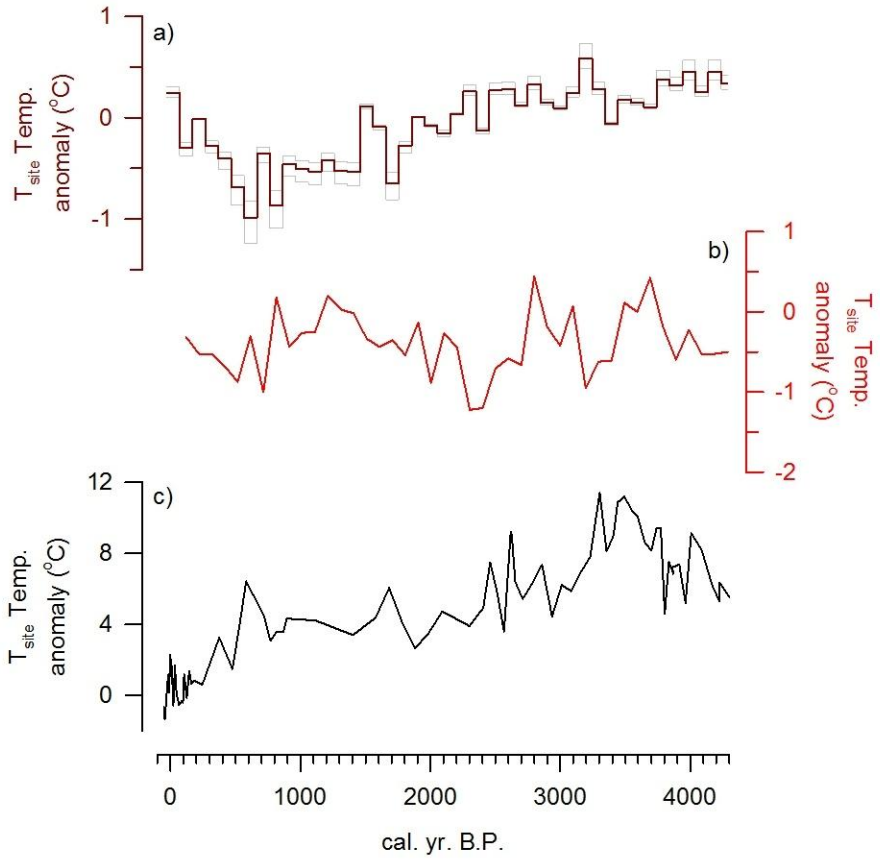

Figure 7.6: A comparison between temperature anomaly data from: a) the James Ross Island ice core (Mulvaney *et al*., 2012); b) the EPICA Dome C ice core (Stenni *et al*., 2010); and c) the GDGT-derived summer temperature record from Fan Lake.

The Fan Lake and JRI temperature anomaly data both recorded decreasing and relatively low temperatures between c. 2900 and 800 cal. yr B.P. (Fig. 7.6.a & c). In Fan Lake these temperatures are still greater than the post 1960 AD average, whereas, at JRI there was a negative temperature anomaly. Alternatively, the EPICA Dome C anomaly data showed conditions only marginally colder than the peak temperatures at c. 2800 cal. yr B.P and c. 3700 cal. yr B.P during this period (Fig. 7.6.b). Finally, both the JRI and Fan Lake temperature anomaly records indicated a temperature decrease followed by a peak in temperature at c. 1700 – 1500 cal. yr B.P. and c. 1900 – 1600 cal. yr B.P. respectively (Fig. 7.6.a & c), though this was not evident in the EPICA Dome C record (Fig. 7.6.b).

Cross correlation of 100 year time series temperature anomaly data from Fan Lake, JRI and EPICA Dome C records since c. 4300 cal. yr B.P. were run to identify any leads or

lags between the datasets (Fig. 7.7.a & b). The positive lag between the Fan Lake and JRI temperature anomaly records indicated in red in Figure 7.7.a shows that Fan Lake lags JRI by between 300 and 500 years. This was a significant lag with an r value of c. 0.6. Alternatively, cross correlation between the EPICA Dome C and Fan Lake temperature anomaly data showed a less dominant pattern although there is a significant but weak (r = 0.4) 200 year lag where Fan Lake lags EPICA Dome C.

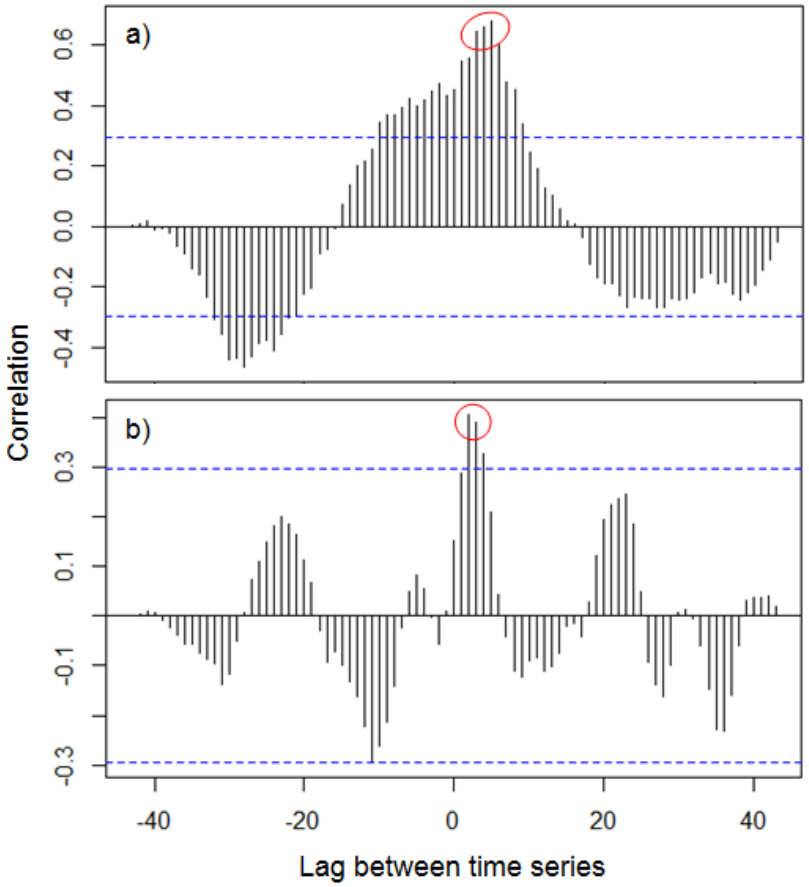

Figure 7.7: Graphical results of cross correlation on 100 year time series temperature anomaly data for a) Fan Lake and JRI (Mulvaney *et al*., 2012) and b) Fan Lake and EPICA Dome C (Stenni *et al*., 2010). Results outside of the blue dashed line are statistically significant at the 95% level. The red circles on a) and b) indicate the most significant lags between the records.

7.4.8.2. Southern Hemisphere proxy records

The fraction of ensemble members for the proxy records across the Southern Hemisphere from Neukom *et al*. (2014) show periods of extreme warm (red) and cold (blue) during the last 1000 years (Fig. 7.8.b). The two most prominent warm periods in the record are between c. 1200 and 1350 AD and post c. 1960 AD (Fig. 7.8.b). The former was represented in the Fan Lake GDGT-derived summer temperature record which indicated a temperature peak between c. 1250 and 1400 AD (Fig. 7.8.a). The post

1960 AD warming of the Neukom *et al*. (2014) Southern Hemisphere proxy records was not evident in the Fan Lake GDGT-derived summer temperature record (Fig. 7.8.a). Post 1960 AD, Fan Lake showed a decreasing temperature trend from 5.1 °C to 2.2 °C (Fig. 7.8.a).

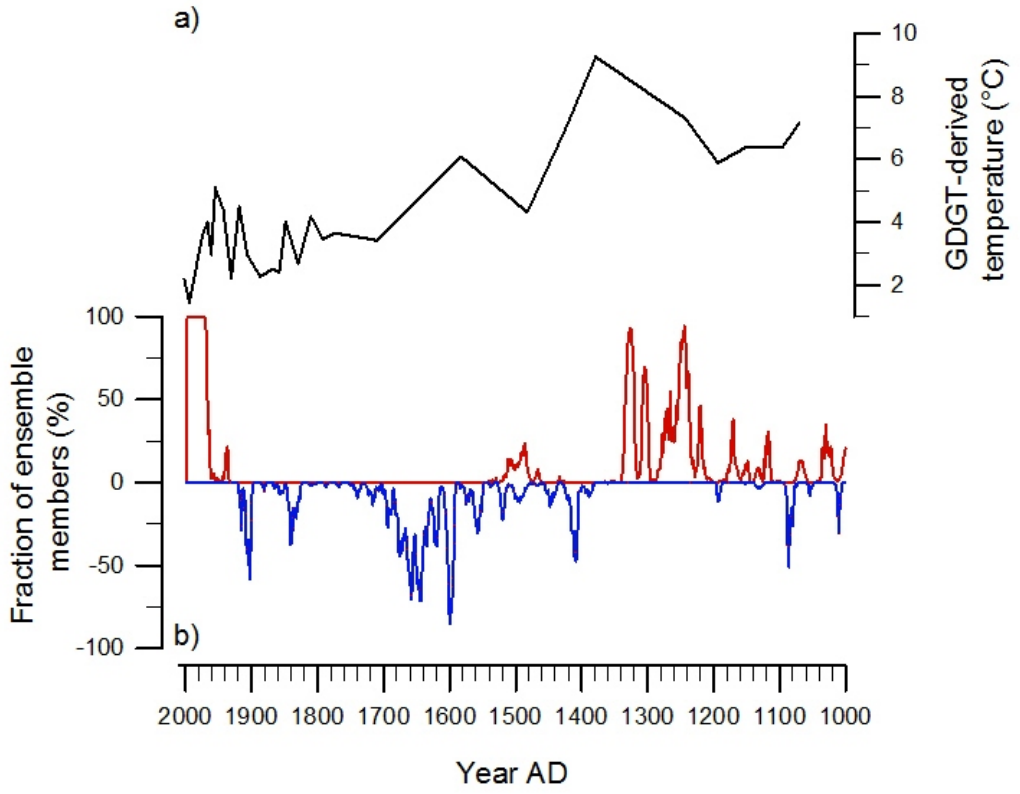

Figure 7.8: A 1000 year comparison between; a) the GDGT-derived summer temperature record from Fan Lake; and b) the fraction of ensemble members for the proxy records across the Southern Hemisphere from Neukom *et al*. (2014), the red line indicates extreme warm events and the blue line extreme cold events.

The Neukom *et al*. (2014) Southern Hemisphere proxy data evidenced colder conditions between c. 1350 and 1920 AD and a pronounced cold event around c. 1580 to 1700 AD. During these colder conditions some of the Southern Hemisphere proxy records show one warm event at c. 1500 AD while others indicated extreme cold conditions. The Fan Lake GDGT-temperature record also reconstructed declining temperatures post c. 1400 AD with a warming around 1600 AD and smaller temperature fluctuations post 1800 AD. During this period there appears to be a disparity between the Fan Lake record and the other Southern Hemisphere proxy data. For example, the Fan Lake record showed small peaks in temperature at c. 1840 AD and c. 1920 AD with colder conditions between c. 1860 and 1900 AD, however, the Southern Hemisphere proxy data showed two cold extremes at c. 1840 and 1910 AD.

7.4.8.3. Instrumental data from Grytviken station, South Georgia

A comparison of the instrumental mean summer air temperature record from Grytviken on South Georgia showed a disparity between the records post c. 1960 AD (Fig. 7.9). While measured summer temperatures showed an increasing trend since c. 1930 AD between 1960 and 1990 AD the GDGT-derived summer temperature data reconstructed a decreasing temperature trend (Fig. 7.9). Nevertheless, the most recent Fan Lake GDGT-temperature does indicate an increase in temperature post 1994 AD, however, this increase in temperature must not be over analysed as it is based on only one sample.

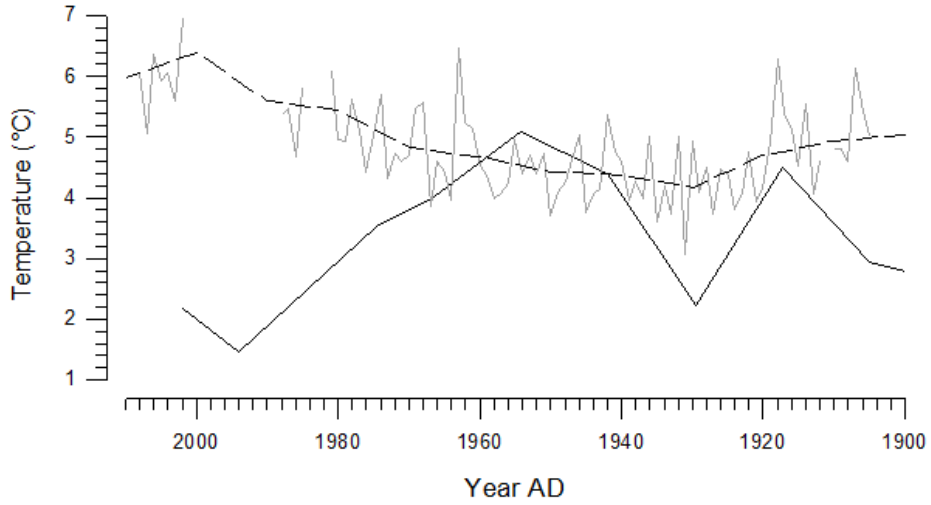

Figure 7.9: A 100 year comparison between the GDGT-derived summer temperature records from Fan Lake (black), the measured mean summer air temperature data from Grytviken station (grey) and a 10 year mean of the mean summer air temperature data from Grytviken (dashed).

Cross correlation of the Fan Lake GDGT-derived summer temperature and Grytviken measured summer temperature records indicated that there were no significant lags between the two records (Fig. 7.10). The greatest correlation between the two records, and the only significant correlation, was identified with no lags and was negative in nature ($r = -0.7$). A higher resolution record may be required to assess leads and lags on this scale.

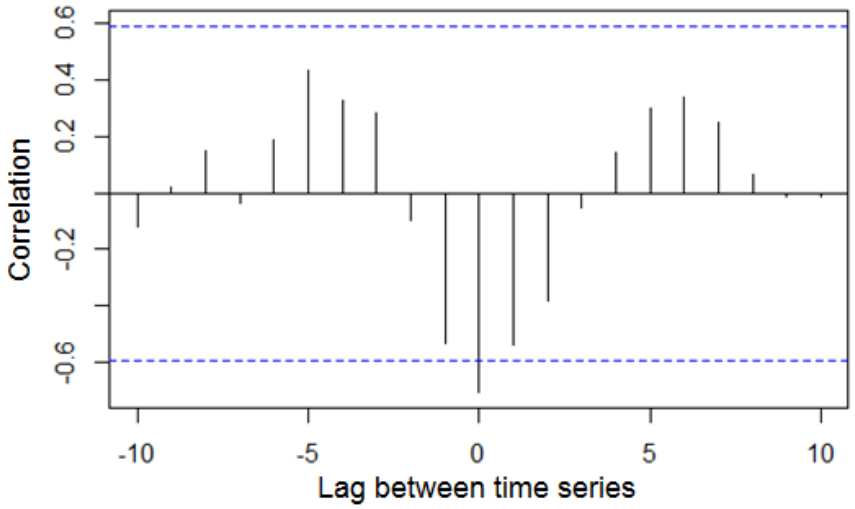

Figure 7.10: Graphical results of cross correlation between the Fan Lake GDGT-derived temperature and the Grytviken measured air temperatures. Results outside of the blue dashed line are statistically significant at the 95% level.

7.5. Discussion

7.5.1. Early Holocene (c. 7700 – 4300 cal. yr B.P.)

The sediment core from Fan Lake dates to c. 7700 cal. yr B.P. however, palaeoclimate reconstructions in the record focused on the period post c. 4300 cal. yr B.P. Previous research by Van Nieuwenhuyze *et al*. (in prep) has shown that prior to c. 4300 cal. yr B.P. Fan Lake was heavily influenced by the deglaciation of the catchment visible through the presence of poorly sorted sediments such as clast-supported diamicton indicative of increased meltwater input. By c. 4300 cal. yr B.P. the glaciers in the catchment had retreated to, or close to, their present day positions and were no longer influencing the lake (Van Nieuwenhuyze *et al*., in prep).

7.5.2. Mid-Holocene (c. 4300 – 2600 cal. yr B.P.)

The Fan Lake GDGT-derived summer temperature record for the mid-Holocene was characterised by a period of climatic warming from c. 4300 to 3800 cal. yr B.P. after which temperatures remained high with an average of c. 12.4 °C before they decreased again after c. 3200 cal. yr B.P. (Fig. 7.5). Temperatures peaked once more at the end of the mid-Holocene to 12.0 °C ± 1.45 °C at c. 2620 cal. yr B.P. The warm period between c. 3800 and 3200 cal. yr B.P. included the highest recorded temperature in Fan Lake of 14.2 °C ± 1.45 °C at c. 3300 cal. yr B.P. (Fig. 7.5). TOC also peaked to its highest value of 9.8% at c. 3000 cal. yr B.P. further suggesting warmer conditions.

Van Nieuwenhuyze *et al*. (in prep) interpreted the whole of the mid-Holocene as a period of high primary production as indicated in the diatom, carotenoid and chlorophyll flux data in the Fan Lake core between c. 4300 and 2500 cal. yr B.P. (Fig. 7.5). They went on to link these conditions to the mid-Holocene warm period, also recorded on the Antarctic Peninsula between c. 4500 and 2600 cal. yr B.P. (Bentley *et al*., 2009). This mid-Holocene warm period was not seen in some previous records from South Georgia (e.g., Clapperton *et al*., 1989). This could be as a result of Clapperton *et al*.'s (1989) research being conducted on the northern side of the island as there is known to be a strong orographic effect between the north and south of the island.

The highest peaks in diatom, carotenoid and chlorophyll flux data are seen in the Fan Lake record between c. 4200 and 3800 cal. yr B.P. suggesting warmer conditions in the lake yet the highest temperatures in the record were not seen until later between c. 3800 and 3200 cal. yr B.P. (Fig. 7.5). This suggests that although there was a peak in primary productivity at the start of the mid-Holocene warm period the lake temperatures did not reach their peak until later at c. 3800 cal. yr B.P. One hypothesis for this delay in the GDGT-temperature record is that meltwater inputs into the lake prevented within lake temperature increasing with air temperatures.

Although the Antarctic and sub-Antarctic GDGT-temperature calibration (Chapter 6) was calibrated to air temperatures these were used as a surrogate for lake water temperature. One reason for this was that on a global scale there is a tight coupling between the two and also long-term lake temperature data was not available. However, as the brGDGTs are now known to be produced within lakes (e.g., Loomis *et al*., 2011; 2014b; Wu *et al*., 2013; Naeher *et al*., 2014) they are likely to actually be representing the lake water temperature and it is only as a result of this tight coupling between air and lake temperature that there is a relationship between branched GDGT composition and MSAT. Therefore, when lake water and air temperatures become decoupled the GDGT-temperature record will more likely represent the lake temperatures. In Lake Challa Sinninghe Damsté *et al*. (2012) also saw a GDGT-derived temperature change greater than expected from other records nearby. They found that reconstructed temperatures were colder than expected during the last glacial maximum and attributed this to a reduction in annual precipitation. This reduction meant the lakes water budget was dominated by colder subsurface flow thus reducing its temperature (Sinninghe Damsté *et al*., 2012). Therefore, meltwater inputs into lakes are known to affect the

chemical and physical conditions on lake waters (Wu and Zhu, 2008) meaning they could have an influence on the within-lake temperatures in the Fan Lake record.

Evidence of meltwater inputs into Fan Lake at c. 4300 cal. yr B.P. were seen in the sediment accumulation rate and sand flux records which both peaked to their maximum values between c. 4300 and 3800 cal. yr B.P. Therefore, although air temperatures increased and glacial retreat records indicate warming conditions the meltwater input into Fan Lake appears to have prevented the lake from warming until c. 3800 cal. yr B.P. Moreover, this particular meltwater input reduced the temperatures in Fan Lake seen through an inverse relationship between sand flux and GDGT-derived temperature between c. 4300 and 3800 cal. yr B.P. As the sand flux decreased, thus the volume of meltwater input decreased, at c. 3800 the GDGT-derived temperatures increased. This is consistent with Van Nieuwenhuyze *et al.*'s (in prep) theory that by c. 3500 cal. yr B.P. Fan Lake had established an ice covered/ice free winter/summer regime similar to present and glacial meltwater was no longer influencing the lake temperature.

Combining the Strother *et al*. (2015) pollen data and diatom, pigment and other primary productivity indicators Van Nieuwenhuyze *et al*. (in prep) postulated a warm period indicated in the Fan record from c. 4300 to 2500 cal. yr B.P. Although the GDGT-temperatures suggest that the lake itself did not reach its peak warmth until c. 3800 cal. yr B.P., the evidence of increased meltwater availability at the culmination of the Fan Lake catchment deglaciation from c. 4300 cal. yr B.P. could be associated with increased air temperatures. This meltwater input held back the warming of Fan Lake until the end of the catchment deglaciation.

Finally, the GDGT-derived summer temperatures for the height of the mid-Holocene warm period of 14 °C are higher than anticipated. There are several reasons why this might be the case. Firstly, 14 °C is outside of the Antarctic and sub-Antarctic calibration boundaries, where the highest temperature was 10 °C, therefore during the mid-Holocene temperatures are being extrapolated thus increasing the errors. However, once the meltwater input had ceased at 3800 cal. yr B.P., and there was no longer a cold water input into the lake, temperatures are likely to have increased. Over a persistent period without input into the lake cooling the lake temperature could potentially increase more rapidly when compared to air temperatures. Moreover, if all inputs into Fan Lake dried up, the lake volume would likely have decrease due to evaporation. Björck *et al*. (1996) observed this in meltwater fed lakes on James Ross Island. They

found that during periods of glacier absence large lakes became small, enclosed, brackish, water bodies (Björck *et al*., 1996), which could also amplify any temperature increase within the lake.

Moreover, as air temperature increased during the mid-Holocene the ice-free season of the lake also increased. Quayle *et al*. (2002) found that a 0.5 °C increase in MSAT at Signy Island between 1980 and 1993 AD led to a significant increase in ice free lake conditions of 63 days. They state that longer periods of ice free lake conditions allowed both the water and lake sediments to absorb more solar energy, creating a positive forcing effect. Once the lake became ice covered during the winter heat within the lake is retained. This causes the lake water warming to be amplified in comparison to increases in air temperature (Quayle *et al*., 2002). A combination of these physical factors had the potential to drive the lake water temperatures to be higher than air temperature during the mid-Holocene warm period thus producing higher than expected GDGT-derived temperatures.

7.5.3. Mid-Late Holocene (c. 2600 – 1000 cal. yr B.P.)

The mid-late Holocene was characterised by relatively cool conditions in comparison with the mid-Holocene warm period but there were still brief periods of increased productivity and temperature in Fan Lake. The Fan Lake GDGT-derived summer temperature record for the mid-late Holocene is represented by a period of relatively stable and cool conditions with two peaks in temperature to 10.3 °C ± 1.45 °C and 8.9 °C ± 1.45 °C at c. 2460 and 1680 cal. yr B.P. respectively (Fig. 7.5). At c. 2460 cal. yr B.P. primary production proxies including diatom, carotenoid and chlorophyll fluxes all peaked too and the $\delta^{13}C$ record peaked at 1680 cal. yr B.P. supporting the warmer GDGT-temperature reconstruction (Fig. 7.5). Diatom flux also peaked at c. 1980 cal. yr B.P. suggesting increased productivity in the lake 300 years prior to the increased lake temperature at c. 1680 cal. yr B.P.

Evidence of colder conditions between c. 2600 and 1000 cal. yr B.P. have previously been described on South Georgia by Rosqvist and Schuber (2003). They reconstructed a period of glacial advance between c. 2400 and 1600 cal. yr B.P. In addition, wetter and possibly colder conditions were reconstructed at Stromness Bay at Tønsberg Peninsula (Van der Putten *et al*., 2004), Kanin Point (Van der Putten *et al*., 2009) and in the Sink Hole sequence (Van der Putten *et al*., 2012) post c. 2200 cal. yr B.P. In Fan Lake itself, Strother *et al*. (2015) reconstructed a decline in pollen flux from c. 2750 to 1670 cal. yr

B.P. which they interpreted as a period of climatic deterioration to a generally cooler-wetter climate. The Antarctic Peninsula (Bentley *et al*, 2009; Sterken *et al*., 2012) and East Antarctic (Verleyen *et al*., 2011) also experienced colder conditions after c. 2000 cal. yr B.P. This cooling was also evident in the JRI ice core (Mulvaney *et al*., 2012) where temperature decreased from c. 2200 to 600 cal. yr B.P. (Fig .7.6.a) but not at EPICA Dome C where temperatures increased after c. 2300 cal. yr B.P. (Fig. 7.6.b). This suggests that assuming no major disparities between the age depth models of the different records the Fan Lake record correlates well with most other records from South Georgia and the Antarctic Peninsula during the mid-late Holocene, with some potential lags discussed in Section 7.5.6, but records from East Antarctica show different climatic trends.

During the mid-late Holocene previous studies by Clapperton *et al*. (1989) and Van Nieuwenhuyze *et al*. (in prep) hypothesised a de-coupling of South Georgian climates with the rest of Antarctica. As a result, South Georgia exhibited climates more closely correlated with global climatic trends. Although the Fan Lake GDGT-temperature record is decoupled with the EPICA Dome C ice core record after c. 2300 (Fig. 7.6.b & c), the 1.2 to 1 ka period of rapid climate change described by Mayewski *et al*. (2004) in their globally distributed palaeoclimate records was not apparent in the Fan Lake temperature reconstruction.

7.5.4. Late-Holocene (1000 cal. yr B.P. – present)

The Fan Lake GDGT-derived summer temperature record for the late-Holocene was the most detailed section of the core due to higher resolution sampling therefore, the late-Holocene showed the most variability throughout the record. At c. 1000 cal. yr B.P. temperatures were 7.0 °C ± 1.45 °C and stayed relatively stable until c. 700 cal. yr B.P. when temperature increased to a peak of 9.3 °C ± 1.45 °C at 580 cal. yr B.P. (Fig. 7.5). Other indicators of this warm period in Fan Lake data were seen through a peak in C/N ratio at c. 580 cal. yr B.P. (Fig. 7.5). In addition, before the GDGT-derived summer temperature increased there was a peak in both diatom flux and sediment accumulation rate at c. 840 cal. yr B.P. and carotenoid flux at c. 770 cal. yr B.P. (Fig. 7.5). The increased sediment accumulation rate to 0.20 cm yr^{-1} at c. 840 cal. yr B.P. may be evidence of a meltwater input due to glacial retreat perhaps forcing a small lag in the GDGT-temperature record again. Increased diatom and carotenoid flux suggest increased productivity possibly linked to warmer climates between c. 1000 and 500 cal.

yr B.P. After this warmer period, temperatures generally decreased to a temperature of 2.2 °C ± 1.45 °C at the top of the core.

Van Nieuwenhuyze *et al*. (in prep) also noted high primary production flux values in the Fan Lake record between c. 1000 and 500 cal. yr B.P. which peaked between 1000 and 750 cal. yr B.P. and Strother *et al.*'s (2015) pollen record also showed an increase in *Acaena*, possibly indicative of warmer conditions, coinciding with high pollen fluxes between c. 900 and 700 cal. yr B.P. A synthesis of all of these proxies is indicative of warmer conditions between c. 1000 and 500 cal. yr B.P. Such relatively warm climate on South Georgia was also documented by Clapperton *et al*. (1989) in the glacial extent record from c. 900 cal. yr B.P. but they suggested this warm period terminated earlier than indicated in the Fan Lake records around c. 650 cal. yr B.P. Nevertheless, the differential in the termination between Fan Lake and Clapperton *et al.*'s (1989) record is within the 95% range of the age model uncertainties of the Fan Lake core at 500 cal. yr B.P. of ± 150 years.

On a global scale this warm period correlates with Neukom *et al.*'s (2014) extreme warming events seen in temperature proxy ensemble data from the Northern Hemisphere c. 950 to 850 cal. yr B.P. earlier than the Southern Hemisphere (Pacific Ocean) warm period c. 750 to 600 cal. yr B.P. Perhaps more significantly the timing of this warm period c. 1000 – 500 cal. yr B.P. in Fan Lake correlates with the northern hemisphere MCA between c. 1100 and 700 cal. yr B.P. (Diaz *et al*., 2011). The MCA was initially thought to be restricted to the Northern Hemisphere however, more recently it has been noted in Southern Hemisphere records also (Neukom *et al*., 2010; 2014; Bird *et al*., 2011; Ledru *et al*., 2013). The presence of the MCA in the Fan Lake record may be an indicator that at this time South Georgian climates were influenced by global climate trends (Van Nieuwenhuyze *et al*., in prep)

The LIA, has also previously been noted in Antarctica by Bertler *et al*. (2011), on the Antarctic Peninsula by Bentley *et al*. (2009) and in East Antarctica by Verleyen *et al*. (2011). Some evidence of the LIA may be seen in the GDGT-temperature record and pigment, diatom and TOC fluxes (Fig. 7.5) which showed a potential deterioration in climatic conditions between c. 300 and 100 cal. yr B.P. Nevertheless, two small warmer punctuations in the generally declining temperature record at c. 370 and 160 cal. yr B.P. are evident in the GDGT-derived summer temperature record. These were not visible in the diatom, carotenoid and chlorophyll fluxes which were all low throughout (Fig. 7.5).

This could indicate that there was limited primary productivity hence, colder conditions at this time however, due to a lower sampling resolution of the carotenoid and chlorophyll records (4 cm, c. 150 years) it could be that these short lived warmer periods have simply been missed in these records.

The potential presence of the MCA and LIA are further evidence that climate on South Georgia during the late-Holocene may have been influenced by some global or even Northern Hemisphere climates (Verleyen *et al*., 2011) therefore, supporting the hypothesis of Clapperton *et al*. (1989) and Van Nieuwenhuyze *et al*. (in prep). Moreover, evidence for changes in the strength and or the position of the PFZ were visible in the Strother *et al*. (2015) pollen record which showed a minor increase in long distance pollen such as *Ephedra* and *Nothofagus* from sub-Antarctic South America after c. 2430 cal. yr B.P. with small peaks seen at c. 2210 to 1670 cal. yr B.P. and c. 570 to 95 cal. yr B.P. They interpreted this as a strengthening or change in position of the SWW which could correlate to the potential de-coupling of South Georgia and Antarctic climates.

7.5.5. The last 100 years at Fan Lake – A comparison with instrumental records from Grytviken Station

Lead-210 dating on the first 11 cm of the Fan Lake core allowed a tighter age depth model for the last 100 years where the 95% range of the age depth model varied between 1 and 47 years. This enabled a comparison between the Fan Lake GDGT-derived summer temperature record and a 100 year instrumental record from Grytviken Station on South Georgia, alongside other palaeotemperature reconstructions of recent climate through glacier extent (e.g., Clapperton *et al*., 1989; Gordon *et al*., 2008; Cook *et al*., 2010). The instrumental record from Grytviken indicated colder summer temperatures between 1920 and 1940 AD with warming post 1960 AD (Fig. 7.9). In addition, Cook *et al*. (2010) showed that since 1950 AD 97% of glaciers on South Georgia had retreated, although, there was a brief period of advance at c. 1970 AD during which many glaciers were close to their LIA extent noted by Gordon *et al*. (1992; 2008).

The Fan Lake GDGT-temperature record suggested a potential increase in summer temperature at the very top of the core around 1990 AD, though more samples would be needed to validate this increase (Fig. 7.8.a & 7.9). Cold periods seen in the record at c. 1930 and 1960 AD may correlate to the c. 1920 and 1970 AD periods of glacial advance

the latter is within the 95% dating uncertainty of the Fan Lake age depth model of ± 13 years. There was limited evidence of the recent rapid warming seen in the instrumental record post c. 1950 AD in the Fan Lake GDGT-temperature record with warming only reconstructed post 1990 AD (Fig. 7.9). Nevertheless, on JRI Abram *et al*. (2014) suggest that although instrumental temperature records from JRI show an increase in temperature during the last few decades this increase was not unprecedented in terms of the last 1000 years. More significantly, the increase in melt intensity over the last few decades on JRI was unprecedented (Abram *et al*., 2014). If the same climatic patterns hold true on South Georgia, meltwater inputs into Fan Lake could be prohibiting the lake temperatures warming, as seen at the beginning of the mid-Holocene warm period. Therefore, an increase in meltwater inputs into Fan Lake could explain the lack of warming seen in the GDGT-temperature record post c. 1950 AD. Such meltwater inputs could result in a lag between increases in air temperatures on South Georgia and Fan Lake GDGT-derived temperature (see Section 7.5.6 for further discussion).

7.5.6. Lags in GDGT-derived temperature record

Lags between the Fan Lake GDGT-derived summer temperature record and the JRI and EPICA Dome C temperature reconstructions from the mid-Holocene warm period to present were determined through cross correlation (Section 7.4.8). The most statistically significant lag was found between the JRI ice core and Fan Lake temperature anomaly datasets between c. 4300 cal. yr B.P. and present. The cross correlation indicated that Fan Lake lags JRI by c. 300 to 500 years (Fig. 7.7). Dating uncertainties in the Fan Lake core during the mid-Holocene (c. 4300 to 2600 cal. yr B.P.) have an average of ± c. 150 years meaning that, although the lower end of the lag could be an artefact of dating uncertainties, a lag of 500 years is greater than these uncertainties. As discussed in Section 7.5.2, as air temperatures increased at the beginning of the mid-Holocene warm period glacial retreat caused by increased air temperatures could lead to an input of meltwater into Fan Lake. This has the potential to create a lag in the GDGT-temperature record compared to air temperature records such as the JRI ice core temperature reconstruction. The evidence of glacial meltwater input into Fan Lake suggests that meltwater is the most likely source of lag in the Fan Lake GDGT-temperature record.

The most recent warming seen in many records from the Antarctic Peninsula and in the Grytviken Station measured summer air temperatures on South Georgia was not indicated in the Fan Lake GDGT-derived summer temperature record. The absence of

this warming could be due to a lag in the GDGT-temperature record therefore, cross correlation was also run between the Grytviken temperature data and Fan Lake GDGT-temperature reconstruction. Nevertheless, this cross correlation suggested there was no significant lags between the records (Fig. 7.10) with the only significant correlation of r = -0.7 found between the two records when no lags are present.

Further comparison, however, with records of previous glacial extent suggested a potential c. 30 year lag in the GDGT-temperature record. For example, in the Fan Lake GDGT-temperature record the LIA culminated at c. 1900 AD whereas, previous studies have stated that on South Georgia the LIA ended between 1850 and 1870 AD (Hayward, 1983; Clapperton *et al*., 1989; Roberts *et al*., 2010) at which time the GDGT-derived temperatures were still low. This lag would mean the c. 1930, 1960 and 1990 AD cold periods at Fan Lake may correlate to periods of glacial advance at c. 1910, 1930 and 1970 AD (Hayward, 1983; Gordon *et al*., 1992; 2008). Nevertheless, the dating uncertainties within this section of the core have a 95% range of between 6 years at c. 1970 AD and 115 years at c. 1870 AD outside of the ^{210}Pb dated section of core, meaning the lag could be an artefact of dating uncertainties.

Nevertheless, if this lag is not an artefact of dating uncertainties it has the potential to provide some explanation as to why the warming on South Georgia post 1960 AD was not yet represented in the Fan Lake GDGT-temperature record. This warming was also not evident in the pollen record at Fan Lake (Strother *et al*., 2015) and Van Nieuwenhuyze *et al*. (in prep) saw no significant changes in pigment composition at this time. Nevertheless, post 100 cal. yr B.P. Nieuwenhuyze *et al*. (in prep) did suggest there was an increase in primary productivity in Fan Lake which could be indicative of warmer conditions, however, they noted that this increase was less pronounced in Fan than their other site at Lake POH1 perhaps due to Fan's larger size.

7.6. Conclusions

GDGT-derived summer temperature reconstructions in Fan Lake, South Georgia, have reconstructed varied temperatures since c. 4300 cal. yr B.P. prior to which palaeoclimates cannot be reconstructed due to a deglaciating catchment influencing the lake.

The GDGT-temperature record showed lake temperatures did not increase at the start of the mid-Holocene warm period (c. 4500 cal. yr B.P.). This could be due to the cooling

effect of a meltwater input into the lake evident in the sedimentological record until c. 3800 cal. yr B.P. After the meltwater input concluded, the GDGT-temperature reconstruction showed increased summer temperatures to the record maximum of 14.2 °C ± 1.45 °C at c. 3300 cal. yr B.P.

When evaluating all of the records from Fan Lake including the GDGT, diatom, pigment and sedimentological data the timing of the mid-Holocene warm period is closely correlated with other research from Fan Lake, elsewhere on South Georgia and the Antarctic Peninsula. However, a lag of c. 300 to 500 years was visable when comparing just the GDGT-temperature record from Fan Lake with the JRI ice core temperature reconstructions.

After the mid-Holocene warm period colder conditions were reconstructed in Fan Lake between c. 2400 and 1000 cal. yr B.P. The timing of these colder conditions also correlates with other studies indicating cold conditions on South Georgia and the Antarctic Peninsula, however, the East Antarctic EPICA Dome C ice core showed increase temperatures post c. 2300 cal. yr B.P. The GDGT-derived temperature record also showed evidence of the MCA and LIA at South Georgia. This supports the hypothesis that South Georgian climates over the last 2000 years have been in phase with global or even Northern Hemisphere climates.

Comparisons between instrumental temperature records and the GDGT-derived temperatures for the last 100 years indicated that the warming seen in the Grytviken Station measured temperature data is not apparent in the GDGT-derived temperatures. It is possible that the water temperature is lagging the air temperature due to meltwater inputs, however, the current resolution of data was not sufficient to identify any statistically significant lags.

Chapter 8: A Holocene GDGT-Temperature Reconstruction for Yanou Lake, King George Island, South Shetland Islands

Summary

In this chapter the Antarctic and sub-Antarctic GDGT-temperature calibration developed in Chapter 6 is applied to Yanou Lake, South Shetland Islands (SSI). This temperature record from Yanou Lake is the first terrestrial quantitative temperature record from the SSI. Comparing the GDGT-temperature reconstruction with other records from Yanou Lake such as pigments, diatoms, total organic carbon etc. gives a more rounded palaeoenvironmental reconstruction of temperature, primary productivity and other environmental factors. Previous palaeoenvironmental reconstructions from elsewhere on the SSI and the Antarctic Peninsula are compared with the Yanou Lake record. Differences between the records are considered, specifically leads and lags between the records, and mechanisms affecting the Yanou Lake temperature record such as tephra deposits, local storm intensity and precipitation are discussed. The mid-Holocene warm period was recorded later at Yanou Lake than previously in Fan Lake (Chapter 7), theories for this difference e.g. stormier conditions at the SSI are considered. Differences are also noted between Yanou Lake and records from James Ross Island confirming previous suggestions of different climate regimes on the western and eastern sides of the Antarctic Peninsula.

8.1. Introduction

Intense recent warming on the Antarctic Peninsula has accounted for more than 50% of the total Antarctic surface melt intensity between 2000 and 2009 (Trusel *et al*., 2012; Abram *et al*., 2014). An understanding of current and past climatic change on the Antarctic Peninsula is therefore crucial. On the Antarctic Peninsula changes in climate have been attributed to several factors including solar insolation (Bentley *et al*., 2009) and changes in the position of the Polar Frontal Zone (PFZ), South Westerly Wind (SWW) belt and Southern Annular Mode (SAM) (Rosqvist and Schuber, 2003; Abram *et al*., 2014; Strother *et al*., 2015). During the mid-late Holocene, temperature proxy and instrumental records from the Antarctic Peninsula have broadly shown evidence of three periods of warming; 1) the mid-Holocene warm period (c. 4500 to 2800 cal. yr B.P.); 2) Medieval Climate Anomaly (MCA; c. 1200 to 600 cal. yr B.P.) and 3) recent rapid warming over the last 100 years (Bentley *et al*., 2009). Colder conditions are also

evidenced in some records during the Little Ice Age (LIA) between 500 – 100 cal. yr B.P. (e.g., Shevenell *et al*., 1996; 2011).

On James Ross Island (JRI), to the northeast of the Antarctic Peninsula, the mid-Holocene warm period has been noted in isotope records between c. 5000 and 3000 cal. yr B.P. when conditions were slightly warmer than present (Mulvaney *et al*., 2012). Björck *et al*. (1996) also suggested more humid / warmer conditions prevailed at Keyhole Lake on JRI from c. 4200 cal. yr B.P. Following these warm mid-Holocene conditions Mulvaney *et al*. (2012) showed evidence of cooling after c. 2500 cal. yr B.P. More recently, over the last 600 years, JRI has been dominated by warming conditions particularly during the last 100 years as temperatures have increased by 1.56 ± 0.42 °C (Mulvaney *et al*., 2012).

Located at the northern tip of the western Antarctic Peninsula, but south of the Antarctic Convergence, the South Shetland Islands (SSI) are sensitive to changes in the SAM, PFZ and SWW and are thus ideally located for documenting the nature and timing of climatic fluctuations in Antarctica (Hall, 2010). Changes in the strength and / or position of the SWW, bringing warm air masses to the western Antarctic Peninsula, have been attributed to climatic differences seen when comparing west and east Antarctic Peninsula records (Turner *et al*., 2005a; Bentley *et al*., 2009). Cross-peninsula differences have been noted by Turner *et al*. (2005a) during the warming of the last 50 years and also during the early Holocene climate optimum (Bentley *et al*., 2009). These cross-peninsula disparities may be seen when comparing Holocene records from JRI, to the east, and SSI to the west of the Antarctic Peninsula.

Björck *et al*. (1991; 1993) qualitatively analysed palaeoenvironmental change in lake sediment cores from Livingstone Island. In Midge Lake, Björck *et al*. (1991) saw a peak in sediment accumulation, pollen concentration and changes in diatom assemblage between c. 3200 and 2700 cal. yr B.P. They interpreted this as a period of milder, more humid maritime climates consistent with the mid-Holocene warm period seen in other archives from the northern Antarctic Peninsula between c. 4500 to 2800 cal. yr B.P. (e.g., Björck *et al*., 1996; Shevenell *et al*., 1996; Bentley *et al*., 2009). Other research at Lake Åsa from Byers Peninsula, Livingston Island (Björck *et al*., 1993) and in Maxwell Bay (Yoon *et al*., 2000) showed evidence of a climatic optimum at c. 3000 and 2700 cal. yr B.P. respectively.

After the mid-Holocene climate optimum, a period of climatic deterioration was evident in the SSI lacustrine records when conditions became colder with long periods of ice cover (Björck *et al*., 1991; 1993). In Midge Lake cooling was interrupted by a brief warm period at c. 2000 cal. yr B.P. before colder, drier conditions prevailed again between c. 1500 and 500 cal. yr B.P. (Björck *et al*., 1991). Similar colder, more arid conditions were also evident on JRI (Björck *et al*., 1996; Mulvaney *et al*., 2012) and a period of glacial advance was evident on South Georgia between c. 2400 and 1600 cal. yr B.P. (Rosqvist and Schuber, 2003). In addition, isotope records from Vostok and Komsomolskaya ice cores showed a shift to colder conditions after c. 2500 cal. yr B.P. (Bentley *et al*., 2009). The synthesis of these records suggests that climatic deterioration at c. 2500 cal. yr B.P. was widespread in Antarctica.

Palaeoclimatic research on the late-Holocene in the SSI is sparse although Björck *et al*. (1991; 1993) suggested that since c. 500 cal. yr B.P. conditions gradually warmed to a milder climate in core top samples. On a hemispheric scale, Neukom *et al*.'s (2014) proxy ensemble records indicated warming throughout the Southern Hemisphere post 1900 AD as also seen in Chilean (e.g., Kaiser *et al*., 2005; Sepúlveda *et al*., 2009) and Australian (e.g., Collins, 2000; Hughes, 2003) records. In addition, a period of recent warming after 1940 AD was evident in both temperature and melt intensity records from JRI (Abram *et al*., 2014). On the other hand, meteorological records from Bellingshausen station on the Fildes Peninsula suggest temperatures have been relatively stable since 1970 AD with mean summer air temperatures c. 1 °C and mean annual air temperatures c. -3 °C (Met READER, 2015).

All previous research on the SSI has relied on qualitative palaeoclimate reconstructions based on species changes or glacial extent. The aims of this chapter are to: 1) improve the current understanding of mid to late Holocene climatic change on the SSI by applying the Antarctic and sub-Antarctic GDGT-temperature calibration to a sediment core from Yanou Lake on King George Island; 2) quantitatively reconstruct mid to late Holocene temperatures on the SSI, thus providing the first quantitative temperature reconstruction from a terrestrial record on the Antarctic Peninsula where previous temperature reconstructions have focused on marine sediment cores (e.g., Shevenell *et al*., 2011) or ice cores (e.g., Mulvaney *et al*., 2012); 3) compare the GDGT-temperature record from Yanou Lake with other records from the lake including pigments, diatom and total organic carbon; 4) compare the Yanou Lake quantitative temperature reconstruction with other palaeoenvironmental archives from the SSI and Antarctic

Peninsula and determine any leads and lags between the records; 5) consider mechanisms driving changes in the palaeoenvironment and differences between records.

8.2. Study Area

The SSI (Fig. 8.1) are a 500 km long island arc in the maritime sub-Antarctic located between 61 and 63°S, and 54 to 62°W, c. 160 km across the Bransfield Strait from the Antarctic Peninsula (Fretwell *et al*., 2010; Watcham *et al*., 2011). They include King George Island, Livingston Island and multiple smaller islands. The islands have a sub-polar marine climate regime and are the warmest location in the Antarctic Peninsula region (Heroy *et al*., 2008). The mean annual air temperature at Bellingshausen station on Fildes Peninsula, King George Island, South Shetland Islands in 2014 was -2.3 °C (Met READER, 2015).

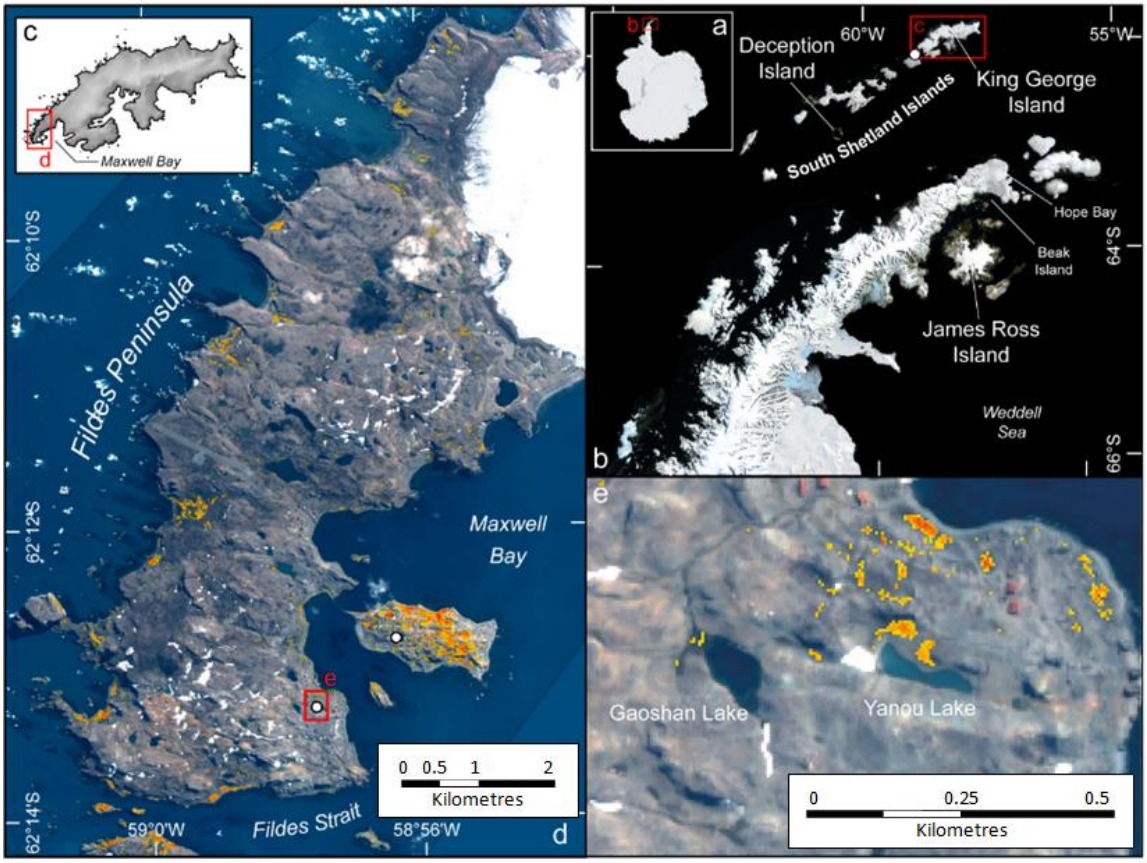

Figure 8.1: Map showing the location of Yanou Lake on Fildes Peninsula, King George Island, South Shetland Islands adapted from Monien *et al*. (in prep): a) Map of Antarctic highlighting the location of the Antarctic Peninsula; b) Northern Antarctic Peninsula; c) King George Island; d) Fildes Peninsula on King George Island and e) the location of Gaoshan Lake and Yanou Lake on the Fildes Peninsula. The yellow-orange-red highlighted areas on map d) and e) show an increasing density of terrestrial vegetation (primarily moss banks).

Currently, the Islands are covered by extensive ice caps and permanent snowfields with some ice-free areas, the largest of which is the Fildes Peninsula measuring 38 km^2 (Fretwell *et al*., 2010; Watcham *et al*., 2011). At these ice-free locations vegetation such as mosses and lichens occur on the wet valley floors, drained slopes, dry soils and on rock surfaces (Björck *et al*., 1993).

Yanou Lake (62°13'15"S, 58°57'35"W ; Fig. 8.1), one of numerous lakes on the South Shetland Islands, is located at 62°13'15"S and 58°57'35"W on the Fildes Peninsula, King George Island. Situated 500 m from the sea at 14.5 m a.m.s.l (Watcham *et al*., 2011), Yanou Lake has a maximum water depth of 5.3 m and had a surface water temperature of 3.1 °C when the site was cored in November 2006. The lake has an inflow from Gaoshan Lake located at 34.5 m a.m.s.l 400 m west of Yanou (Fig. 8.1.e). The catchment has patches of yellow-green moss, predominantly to the north of Yanou Lake (Fig. 8.1.e). Cyanobacterial mats are also present on the southwest shore (British Antarctic Survey, 2008).

8.3. Materials and Methods

8.3.1. Core Collection and Sampling

Yanou Lake was cored in November 2006 from the deepest part of the lake at 5.3 m water depth. The composite core analysed in this study is c. 3.2 m long at which point the bedrock was reached (Watcham *et al*., 2011). The core was obtained using a UWITEC cable-operated piston corer and is composed of three overlapping and correlated c. 2 m long core sections (YAN 8A, 9B, 8B). All cores and subsamples were kept frozen during transport and stored at -20 °C. Cores were split in the laboratory, and a half-core was defrosted, logged inside a Class II fume-hood using Munsell colour charts[1] and sub-sampled to air-tight Whirlpak/ziplock bags at 1 cm intervals.

8.3.2. Lithology and Sedimentology

The sediment core was x-rayed and micro-XRF (μ-XRF) scanned[1] (see Appendix D for details). Cores were stored at 4 °C during analysis and re-frozen and stored at -20 °C on return to the British Antarctic Survey. Grain size analysis was also completed for Yanou Lake at 2 cm intervals[1] (Appendix D). Finally, total organic carbon (TOC) was

[1] Analysis undertaken by Stephen Roberts (British Antarctic Survey); data are used here with permission

calculated at 1 cm intervals between 0 and 40 cm and 2 cm intervals between 190 and 210 cm core depth[2] (Appendix D).

8.3.3. GDGT and Pigment Extractions

The GDGT sub-sampling strategy focused on the terrestrial deposits in the top half of the core after the isolation of the lake basin. The Watcham *et al*. (2011) diatom record indicates that above c. 208 cm depth the core is dominated by freshwater, fresh-brackish and brackish fresh conditions suggesting the lake became isolated from the sea at c. 6050 cal. yr B.P. GDGTs were extracted from 41 samples taken at 1 cm intervals in the top 20 cm of the core and at 2 cm intervals between 20 and 38 cm and 188 and 210 cm core depth. No samples were extracted between 38 and 188 cm as this is a unit of reworked volcanic ash (see Section 8.4.1). GDGTs were extracted from 0.2 – 4.3 g of freeze dried and homogenised sediments at Newcastle University following the methods outlined in Chapter 5.

Pigment preparation was undertaken at the British Antarctic Survey at 2 cm intervals between 0 and 38 cm and 188 and 210 cm core depth. Pigments were extracted from 30 samples of c. 2 cm^3 of sediment with dry weights ranging between 0.2 and 3.4 g. Pigment concentrations were standardised to LOI and calculated as a flux as outline in Chapter 5.

8.3.4. Chronological analysis and age model

Fifteen samples from the Yanou Lake core were taken for Accelerator Mass Spectrometry (AMS) radiocarbon dating (Watcham *et al*., 2011), including eleven terrestrial and four marine samples[3]. Within the terrestrial samples, eight were taken from moss layers. Terrestrial moss samples are preferable when dating as they are not complicated by any lake reservoir effects (Björck and Wohlfarth, 2001). Radiocarbon ages were calibrated in OXCAL (version 4.2; Bronk-Ramsey, 2009) using the SHCal13 and Marine13 Southern Hemisphere calibration curves for terrestrial and marine dates respectively (Hogg *et al*., 2013; Reimer *et al*., 2013). A local marine reservoir correction of 1064 ± 10 years (DR ¼ 664 years) was applied to marine dates, calculated from the ages of modern water samples reported from Maxwell Bay (Milliken *et al*., 2009).

[2] Analysis undertaken by Melanie Leng (British Geological Survey); data are used here with permission
[3] Analysis undertaken by Patrick Monien (Bremen University); data are used here with permission

Radiocarbon dates were used to generate a master age-depth model[1] (Fig. 8.2) in BACON v.2.2 (Bayesian) age-depth modelling software in R v3.1 (Blaauw, 2010; Blaauw and Christen, 2011; Roberts pers. comm.). Large ash layers (> 1 cm thick) were excluded, similarly to Björck *et al*. (1993), as they were most likely deposited over a short time during a period of high deposition. The BACON age-depth model allowed ages to be interpolated from the best-fit age. Zero ages for surface and living moss layers were achieved when applying the age-depth model providing confidence in the accuracy of the model. The age-depth model estimated a core age of 11000 cal. yr B.P.

8.3.5. Statistical Analysis

The relative abundance of brGDGTs was calculated for the Yanou core and the Antarctic and sub-Antarctic GDGT-temperature calibration (Chapter 6) applied to reconstruct summer temperatures. CONISS Cluster analysis was undertaken on the relative abundance of the four brGDGTs used in the Antarctic and sub-Antarctic GDGT-temperature calibration (Chapter 6). Broken stick analysis was used to identify statistically significant zones.

Cross correlations between the Yanou Lake GDGT-derived temperature record and other proxy and instrumental records for the region were run in R v3.1. (R Core Team, 2014). Prior to cross correlation datasets were re-sampled at 200 year intervals using Analyseries software.

8.4. Results

8.4.1. Sedimentology

The Yanou Lake core was composed of marine and lake sediments and tephra layers as described by Watcham *et al*. (2011) from diatom assemblage and sedimentological data. The basal unit (Unit 1; 355 – 259 cm) consisted of light grey to dark grey clast supported diamicton (Fig. 8.2). Unit 2 (295 – 210 cm) was composed of dark brown silty clays mixed with tephra beds and tephra rich deposits (Fig. 8.2). The unit coarsens upwards from clays to fine sands (Fig. 8.2). These two basal units were of marine origin as indicated by Watcham *et al*. (2011) who reported a dominance of marine diatoms until around 216 – 208 cm depth. Unit 3 (210 – 190 cm) contained laminated organics with moss fragments and moss beds (Fig. 8.2). This unit coincided with the lake basin isolation identified by Watcham *et al*. (2011) at c. 208 cm (c. 6050 cal. yr B.P.). Unit 4 (190 – 43 cm) was comprised of a large unit of often laminated, reworked volcanic ash

and minerogenic sediment (Fig. 8.2). These deposits were generally dark grey clay sized particles with a coarser sand deposit between 140 and 122 cm (Fig. 8.2). Finally, unit 5 (43 – 0 cm) consisted of fine grained laminated organic muds containing moss beds (Fig. 8.2).

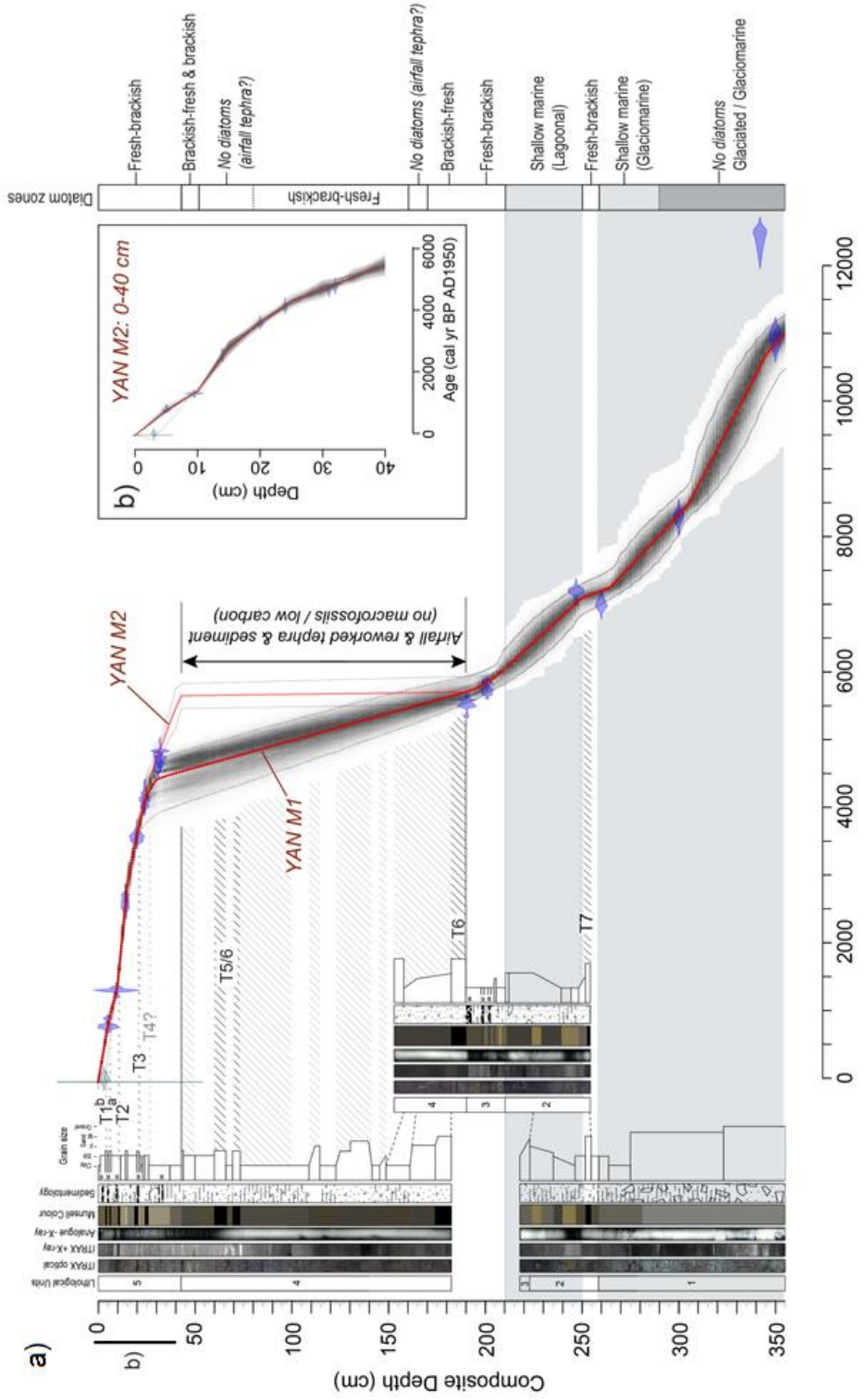

Figure 8.2: Age-depth model for Yanou Lake[1&3]: a) Age-depth model for whole core; b) Age-depth model for the top 40 cm of the core. The logs to the left of the age depth model include: lithological units; ITRAX optical; ITRAX & X-ray; Analogy X-ray; Munsell Colour; Sedimentology and Grain size.

8.4.2. Glycerol Dialkyl Glycerol Tetraethers (GDGTs)

In Yanou Lake, all nine brGDGT compounds, previously identified in Fan Lake (Chapter 7), were present in varying proportions throughout the core (Fig. 8.3). GDGT-IIIc, was only detected in one sample at 3 cm core depth and had the lowest relative abundance of all brGDGT compounds at 0.3% (Fig. 8.3). In contrast, GDGT-III had the highest relative abundance ranging between 49 and 70% of the total brGDGT abundance (Fig. 8.3).

The GDGT-derived summer temperatures reconstructed using the Antarctic and sub-Antarctic GDGT-temperature calibration ranged from -0.73 °C ± 1.45 °C at 204 cm core depth (c. 5900 cal. yr B.P.) to 13.84 °C ± 1.45 °C at 17 cm depth (c. 3100 cal. yr B.P.) with a mean temperature throughout the core of 2.88 °C. The Branched Isoprenoid Tetraether (BIT) index, a ratio of brGDGTs to isoGDGTs is often used to identify lakes with a high proportion of brGDGTs, was high throughout the core ranging from 0.79 to 1.00. The lowest BIT value was found at the base of the core at 210 cm.

Constrained cluster analysis of the brGDGTs indicated three statistically significant brGDGT zones (Fig. 8.3 & 8.4). The brGDGT zones represented three well defined areas in the brGDGT composition and brGDGT temperature record. Zone 1 from 210 to 19 cm (c. 6050 – 3450 cal. yr B.P.) was cold but relatively stable, Zone 2 from 19 – 8 cm (c. 3450 – 1100 cal. yr B.P.) represented a period of warm conditions and Zone 3 from 8 – 0 cm (c. 1100 cal. yr B.P. to present) saw a reduction in temperatures to -0.15 °C (Fig. 8.4).

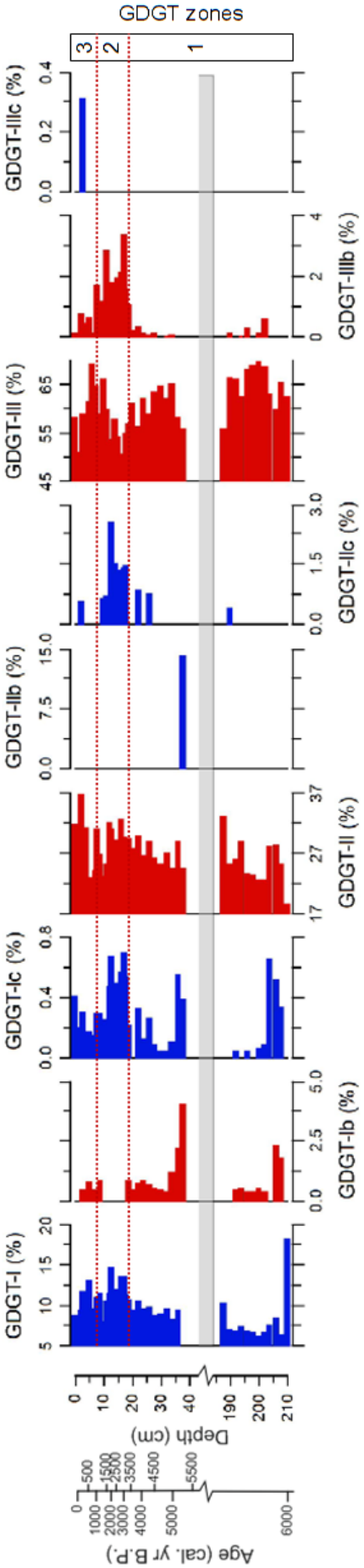

Figure 8.3: Relative abundance of the nine branched GDGTs downcore in the Yanou Lake sediment core. The red GDGT compounds are those used in the Antarctic and sub-Antarctic GDGT-temperature calibration developed in Chapter 6.

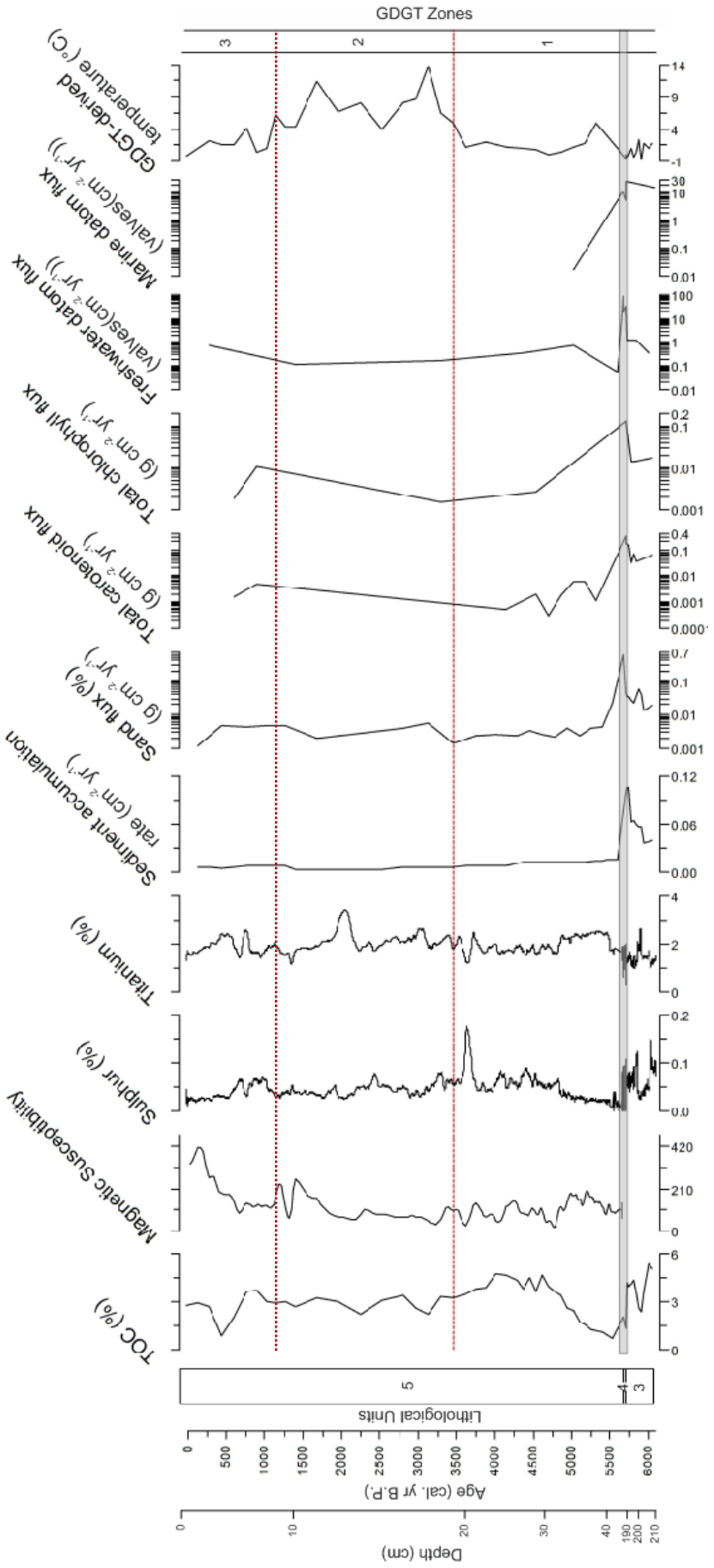

Figure 8.4: Downcore data for Yanou Lake including; magnetic susceptibility; sulphur content and titanium content[1]; TOC, sediment accumulation; sand flux and freshwater and marine diatom flux data from Watcham *et al.* (2011) and total carotenoid and chlorophyll flux and GDGT-derived summer temperatures reconstructed using the Antarctic and sub-Antarctic brGDGT-temperature calibration (Chapter 6). The red dashed line indicates the brGDGT zones. The grey band at c. 5500 cal. yr B.P. represents the reworked volcanic ash and minerogenic sediment within the core.

8.4.3. GDGT Zone 1: 210 – 19 cm (c. 6050 – 3450 cal. yr B.P.)

The GDGT-derived summer temperatures in Zone 1 were relatively low with the lowest average temperature of the core at c. 0.9 °C, 2.0 °C below the core average temperature of c. 2.9 °C (Fig. 8.4). Zone 1 also recorded the lowest temperature in the record of -0.73 °C ± 1.45 °C at 204 cm core depth. Temperature was relatively stable in Zone 1 with a small peak at 38 cm to 4.86 °C ± 1.45 °C, otherwise temperatures were c. 0 – 2 °C (Fig. 8.4).

Sediment accumulation rate, sand flux, carotenoid, chlorophyll and diatom fluxes all peaked to their core maximum in Zone 1 (Fig. 8.4). Sediment accumulation peaked to 0.11 cm yr^{-1} at 194 cm core depth. Zone 1 recorded both the highest and lowest TOC values for the whole core (data from Watcham *et al*., 2011). At the bottom of the zone TOC was at a core maximum of 5.4% at 208 cm depth (Fig. 8.4). It then showed a decreasing trend and reached the core minimum of 0.7% at 41 cm core depth in the volcanic ash and minerogenic sediments. Above 41 cm TOC gradually increased reaching another peak of 4.7% at 23 cm core depth (Fig. 8.4; data from Watcham *et al*., 2011). Magnetic susceptibility showed some variation throughout Zone 1 ranging between 18 and 200 (Fig. 8.4). Both sulphur, an indicator of productivity (Roberts pers. comm.), and titanium, an indicator of meltwater input and / or tephra deposits (Roberts pers. comm.), showed increased variability at the base prior to the unit of reworked volcanic ash. Above this unit sulphur and titanium were relatively stable until sulphur peaked to 0.18% (of scatter-normalised cps data) at c. 20.5 cm and titanium dropped to 1.21% (of scatter-normalised cps data) at c. 20.3 cm (Fig. 8.4).

Freshwater and marine diatom flux both peaked to 30.63 and 9.69 g cm^{-2} yr^{-1} at 90 and 184 cm core depth, respectively (Fig. 8.4; data from Watcham *et al*., 2011). Sand flux peaked to 0.57 g cm^{-2} yr^{-1} at 99 cm depth but dropped to 0.02 g cm^{-2} yr^{-1} by 41 cm and remained low throughout the rest of Zone 1 (Fig. 8.4; data from Watcham *et al*., 2011). Total carotenoid and chlorophyll flux peaked to 0.32 and 0.14 g cm^{-2} yr^{-1} at 188 and 190 cm depth respectively (Fig. 8.4). The most dominant pigments were lutein, unknown carotenoid A, diatoxanthin, crocoxanthin, alloxanthin, zeaxanthin, chlorophyll *a*, and chlorophyll *b*. After a core maximum the carotenoid and chlorophyll flux both dropped rapidly and remained stable and low throughout the rest of the zone.

8.4.4. GDGT Zone 2: 19 – 8 cm (c. 3450 – 1100 cal. yr B.P.)

The GDGT-derived summer temperature increased rapidly at the bottom of Zone 2 to a core peak of 13.84 °C ± 1.45 °C at 17 cm depth (Fig. 8.4) after which temperatures decreased to a Zone 2 minimum at 14 cm (3.93 °C ± 1.45 °C) before increasing again. There was a second peak in summer temperature of 11.34 °C ± 1.45 °C at 11 cm depth then temperatures decreased rapidly to 4.34 °C ± 1.45 °C at 9 cm (Fig. 8.5). Although temperatures in Zone 2 have a high average of c. 7.4 °C, c. 4.5 °C above the core average, Zone 2 included the greatest temperature fluctuations, nevertheless, temperatures were always higher than 1 °C above the core average.

Sediment accumulation rate and sand flux were comparatively stable and low throughout Zone 2, around an average of 0.005 cm yr^{-1} and 0.003 g cm^{-2} yr^{-1} respectively (Fig. 8.5; data from Watcham *et al*., 2011). TOC was relatively stable in Zone 2 varying between 2.2% at 17 cm and 3.4% at 15 cm (Fig. 8.5; data from Watcham *et al*., 2011). Magnetic susceptibility was relatively stable in Zone 2 until 12.6 cm above which it increased from 54 to 230 at 8.4 cm (Fig. 8.5). Sulphur was also relatively stable with minor peaks to 0.08% (of scatter-normalised cps data) at c. 18.1 and 13.7 cm (Fig. 8.5). Titanium showed some minor peaks in Zone 2 but more notably peaked to its highest value throughout the core of 3.42% (of scatter-normalised cps data) at 12.3 cm (Fig.8.5).

No marine diatoms were recorded in Zone 2 and freshwater diatoms were present in low concentrations with a maximum of 0.06 g cm^{-2} yr^{-1} at 18 cm (Fig. 8.5; data from Watcham *et al*., 2011). Finally, total chlorophyll flux was low in Zone 2 and no carotenoids were detected (Fig. 8.5). Zone 2 contained a very small peak in total chlorophyll flux at 18 cm core depth to 0.001 g cm^{-2} yr^{-1} (Fig. 8.5) consisting of chlorophyll *a* only.

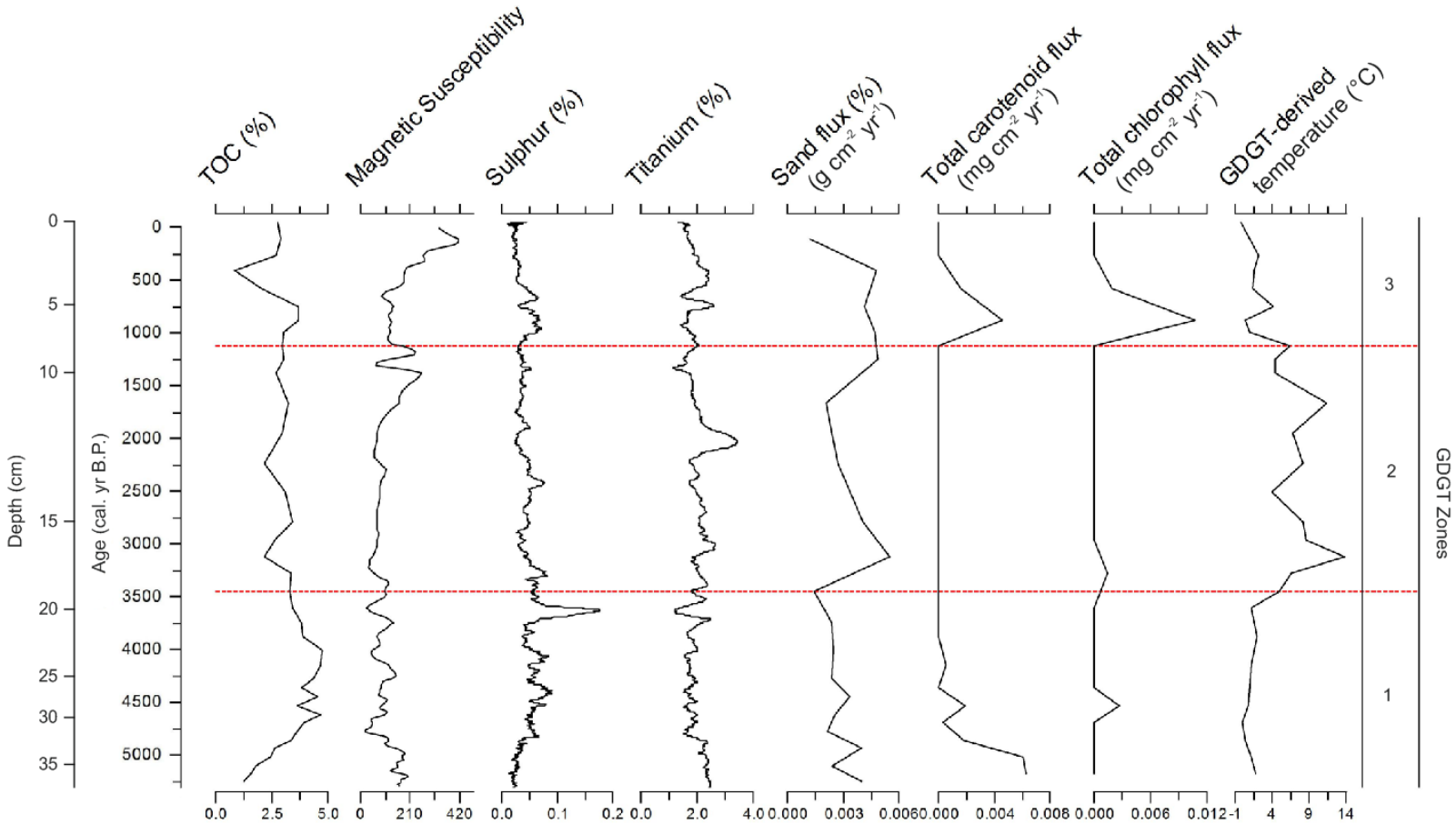

Figure 8.5: Downcore data for Yanou Lake for the last c. 5300 cal. yr B.P. including; magnetic susceptibility; sulphur content and titanium content[1]; TOC and sand flux from Watcham *et al*. (2011) and total carotenoid and chlorophyll flux and GDGT-derived summer temperatures reconstructed using the Antarctic and sub-Antarctic brGDGT-temperature calibration (Chapter 6). The red dashed lines on the plot indicate the branched GDGT zones.

8.4.5. GDGT Zone 3: 8 – 0 cm (c. 1100 cal. yr B.P. to present)

The GDGT-derived summer temperatures in Zone 3 showed a cooling trend from a zone maximum of 6.35 °C ± 1.45 °C at 8 cm core depth to a minimum of -0.15 °C ± 1.45 °C at 0 cm. Low temperatures of 0.97 and 0.47 °C ± 1.45 °C were also recorded at 7 and 6 cm depth respectively (Fig. 8.5). The average GDGT-derived temperature for Zone 3 was c. 2.1 °C, c. 0.8 °C below the core average.

The sediment accumulation rate in Zone 3 was relatively stable around 0.007 cm yr^{-1} (Fig. 8.5). Sand flux was also stable at c. 0.005 g cm^{-2} yr^{-1} until 1 cm depth when it dropped to 0.001 g cm^{-2} yr^{-1} (Fig. 8.5). At the bottom of Zone 3 TOC was 2.96% and remained around 3% until it decreased to 0.85% at 3 cm core depth. At 2 cm TOC increased to 2.72% and remained around an average of 2.8% throughout the rest of the zone (Fig. 8.5; data from Watcham *et al*., 2011). Magnetic susceptibility was stable in Zone 3 until 4.4 cm after which it increased rapidly from 91 to a core maximum of 418 at 1.0 cm before decreasing again at the top of the core (Fig. 8.5). Sulphur was also relatively stable at c. 0.06% (of scatter-normalised cps data) between 7.0 cm and 4.3 cm with one drop to 0.03% (of scatter-normalised cps data) at c. 5 cm. Sulphur dropped to 0.04% (of scatter-normalised cps data) at 4.0 cm after which it remained around an average of 0.03% (of scatter-normalised cps data) (Fig. 8.5). Titanium was more varied in Zone 3. Two peaks were recorded, one brief peak to 2.6% (of scatter-normalised cps data) at 5.0 cm and one more sustained increase to an average of 2.2% (of scatter-normalised cps data) between 3.9 and 2.1 cm. Titanium then showed a decreasing trend to a value of 1.5% (of scatter-normalised cps data) at 0 cm (Fig. 8.5).

Freshwater diatoms peaked to 0.31 g cm^{-2} yr^{-1} in Zone 3 while marine diatoms were not detected (Fig. 8.5; data from Watcham *et al*., 2011). Both total carotenoid and chlorophyll flux showed a small peak between 6 and 4 cm depth to 0.005 and 0.002 g cm^{-2} yr^{-1} respectively (Fig. 8.5). The most dominant pigments were unknown carotenoid A, lutein, diatoxanthin, alloxanthin, chlorophyll *c*1, pheophorbide *a* and chlorophyll *b.*

8.4.6. Comparison of the Yanou Lake GDGT-derived temperatures with previously published records

A comparison of temperature anomaly records from the JRI ice core (Mulvaney *et al*., 2012) and the EPICA Dome C ice core (Stenni *et al*., 2010) with the Yanou Lake GDGT-derived summer temperature data showed periods of good correlation alongside

periods of differing trends (Fig. 8.6). For example, the Yanou Lake GDGT-temperature reconstruction and JRI temperature record suggest a warming during the mid-Holocene c. 3600 to 3000 cal. yr B.P. however, the warming in EPICA Dome C during the mid-Holocene peaks twice, once prior to the Yanou and JRI at c. 3700 cal. yr B.P. and once after at c. 2800 cal. yr B.P. (Fig. 8.6). Moreover, the warming seen in the JRI and EPICA Dome C records post c. 500 cal. yr B.P. were not represented in Yanou Lake (Fig. 8.6). Some of these differences between the records might be due to leads and lags between the reconstructions which cross correlation may be able to identify.

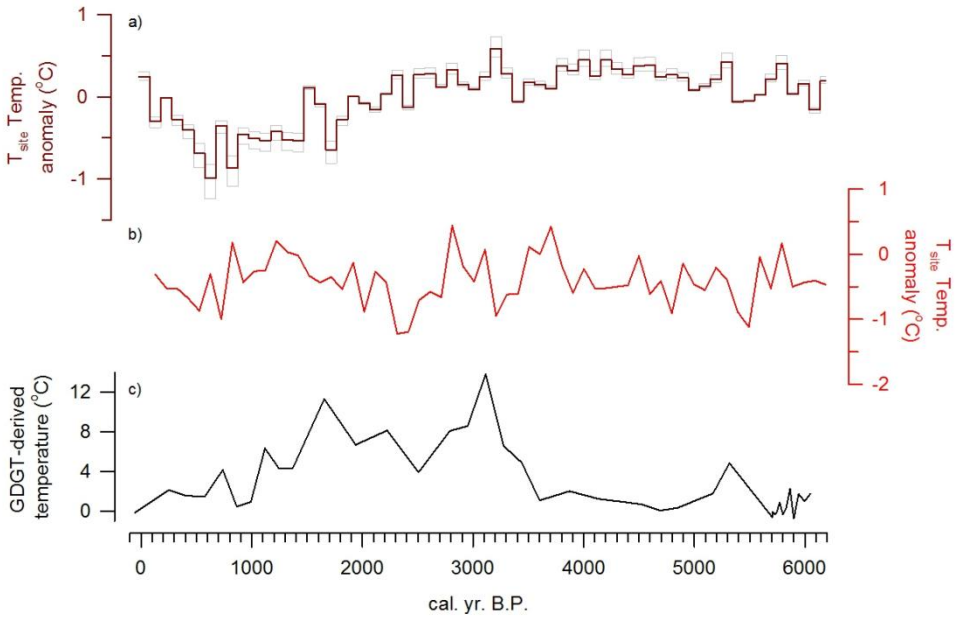

Figure 8.6: A comparison between temperature anomaly data from: a) the JRI ice core (Mulvaney *et al*., 2012); b) the EPICA Dome C ice core (Stenni *et al*., 2010); and c) the GDGT-derived summer temperature record from Yanou Lake.

Initial cross correlation of the summer temperature record from Yanou Lake and the temperature anomaly record from JRI from the mid-Holocene warm period (c. 4600 cal. yr B.P.) to present indicated a potential lag between the records of c. 1000 years in which the Yanou Lake temperature record lags that of the JRI ice core. A lag of this scale was outside the 95% error range of the ^{14}C age-depth model, thus not related to dating inaccuracies. Closer investigation suggested that post c. 800 cal. yr B.P. the Yanou Lake and JRI records were decoupled perhaps driving the suggested 1000 year lag.

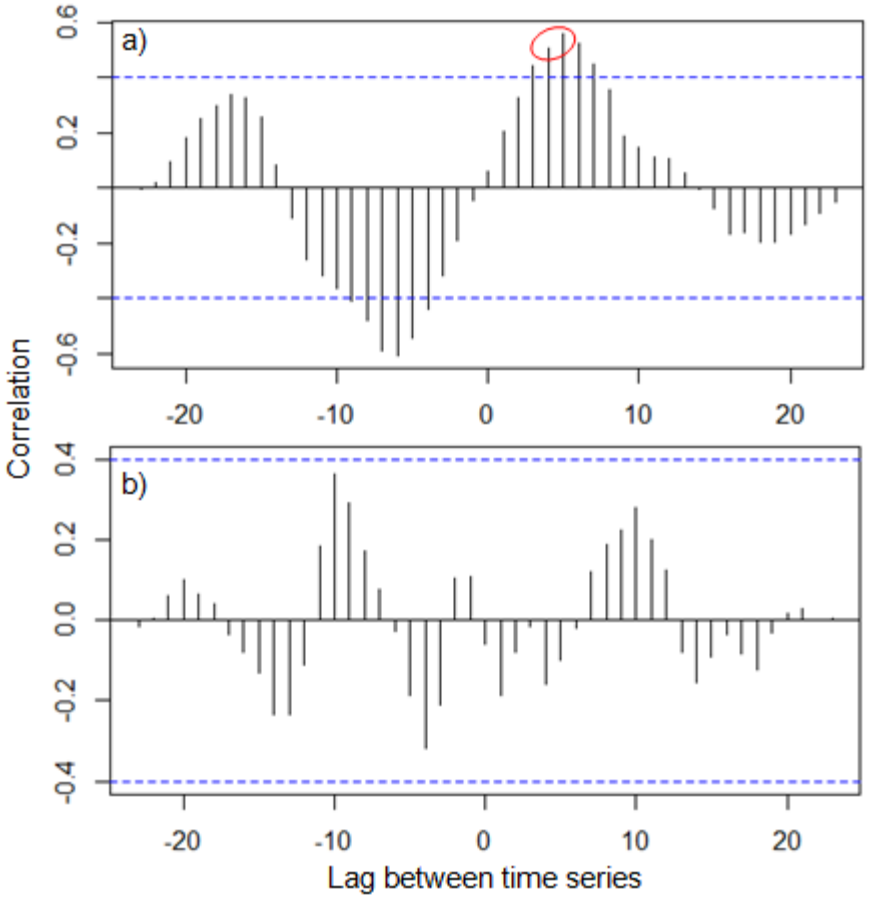

Figure 8.7: Graphical results of cross correlation on 200 year time series temperature anomaly data for a) Yanou Lake and JRI (Mulvaney *et al*., 2012) and b) Yanou Lake and EPICA Dome C (Stenni *et al*., 2010) since c. 4600 cal. yr B.P. Results outside of the blue dashed line are statistically significant at the 95% level. The red circles on a) indicates the most significant lag between the records.

A more specific examination of the mid-Holocene warm period showed warming in the Yanou Lake GDGT-derived summer temperature record between c. 3300 and 2700 cal. yr B.P. which peaked to the record maximum at c. 3100 cal. yr B.P. (Fig. 8.6) consistent with the highest temperature anomaly in the JRI record at c. 3150 cal. yr B.P. EPICA Dome C however, recorded a drop in temperature at c. 3200 cal. yr B.P. with temperatures peaking at c. 3700 and 2800 cal. yr B.P. (Fig. 8.6.b). Although a visual comparison between the Yanou Lake and JRI temperature records suggested that the two are in good correlation between c. 3800 and 2600 cal. yr B.P. there was not a statistically significant relationship between the two during this time ($r = 0.22$, $p = 0.633$). Nevertheless, cross correlation (Fig. 8.8) showed no evidence of a statistically significant lag between the two records but this could be in part due to the limited number of samples available during this period.

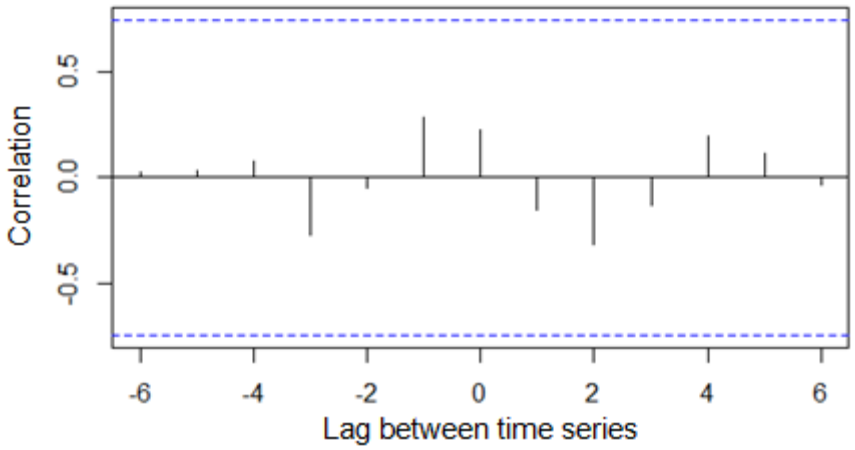

Figure 8.8: Graphical results of cross correlation on 200 year time series temperature anomaly data for Yanou Lake and JRI (Mulvaney *et al*., 2012) between c. 3800 and 2600 cal. yr B.P. encompassing the mid-Holocene warm period. Results outside of the blue dashed line are statistically significant at the 95% level.

The Yanou Lake and JRI temperature records both indicated decreasing temperatures between c. 3000 and 800 cal. yr B.P. with a peak at c. 1650 and 1500 cal. yr B.P. respectively (Fig. 8.6.a & c). As a result, post c. 3000 cal. yr B.P. Yanou Lake and JRI had a significant positive correlation (r = 0.51, p = 0.04) despite the opposing post c. 800 cal. yr B.P. trends. Alternatively, the EPICA Dome C record showed an increased temperature trend from c. 2400 to 800 cal. yr B.P. (Fig. 8.6.b) with a negative but not statistically significant relationship found between Yanou Lake and EPICA Dome C during this period (r = -0.22, p = 0.568). Post c. 500 cal. yr B.P. JRI and EPICA Dome C both indicated a period of warming, in the JRI record, this was the most pronounced warming throughout the record (Fig. 8.6a & b). Warming was not evident in Yanou Lake which recorded some of its lowest temperatures after c. 500 cal. yr B.P. (Fig. 8.6.c).

8.5. Discussion

8.5.1. Early-mid Holocene (c. 6050 – 3400 cal. yr B.P.)

The early-mid Holocene in Yanou Lake was characterised by relatively low temperatures with the coldest summer temperature throughout the record of -0.73 °C ± 1.45 °C reconstructed at c. 5900 cal. yr B.P. (Fig. 8.4). Average temperatures between c. 6050 and 3400 cal. yr B.P. were c. 0.9 °C, 2.0 °C below the core average of c. 2.9 °C. These colder temperatures between c. 6050 and 3400 cal. yr B.P. correspond with colder climates reconstructed in the Antarctic Peninsula region at Livingstone Island (c.

5000 – 4000 cal. yr B.P.; Björck *et al*., 1991; 1993), JRI (c. 5000 – 4200 cal. yr B.P.; Björck *et al*., 1996) and Lallemand Fjord (c. 6700 – 4900 cal. yr B.P.; Shevenell *et al*., 1996). Moreover, they were consistent with Yoon *et al*.'s (2000) marine records from nearby Maxwell Bay which showed low diatom abundances, depleted TOC and enriched $\delta^{18}O$ indicative of a period of advanced glacier margins with extensive ice cover between c. 6200 and 4000 cal. yr B.P. Milliken *et al*. (2009) also used TOC alongside carbon and nitrogen percentage data to infer colder conditions and seasonal ice cover in Maxwell Bay after c. 5900 cal. yr B.P.

Although the GDGT-derived summer temperatures were low during the early-mid Holocene, all of the traditional primary productivity indicators (TOC, diatoms and pigments) peaked at c. 5800 cal. yr B.P. Brackish diatoms in the record suggested a transition from marine to lacustrine conditions as the lake basin became isolated from the sea (Watcham *et al*., 2011). In this study, the lowest BIT index of 0.79 was recorded at c. 6050 cal. yr B.P. potentially indicating a greater marine influence. During the transition, there was a period of primary productivity maxima seen in both the total carotenoid and chlorophyll flux and diatom flux between c. 5800 and 5700 cal. yr B.P. (Fig. 8.4). In addition, freshwater and marine diatom flux both peaked at c. 5700 cal. yr B.P. and TOC peaked at c. 6000 cal. yr B.P. (Fig. 8.4). Peaks in organic carbon content, pigment and diatom fluxes indicated high primary productivity possibly as a result of continued availability of the marine nutrient pool. Similar trends were previously noted by Sterken *et al*. (2012) who found organic content, C/N ratios and diatom concentrations all peaked during lake isolation in Beak 1 on Beak Island in the Prince Gustav Channel. Hodgson *et al*. (2013) also saw a similar peak in *Branchinecta gaini* eggs as well as some diatom taxa including *Navicula veneta, Planothidium quadripunctatam* and *Pinnularia microstrauron* in Narrows Lake, Pourquoi-pas Island during and straight after the transition from marine to lacustrine conditions.

In Yanou Lake, a unit of volcanic ash and minerogenic sediment interrupted the primary productivity peak at c. 5700 cal. yr B.P. when sediment accumulation rate peaked and TOC dropped to a minimum of 0.74% at c. 5500 cal. yr B.P. (Fig. 8.4). Similar volcanic ash units have also been identified in other lakes from the SSI including Midge Lake (Björck *et al*., 1991), Lake Åsa (Björck *et al*., 1993) and Ardley Lake (Roberts pers. comm.). Following the minima, TOC increased steadily from 0.74% to a peak of 4.64% at c. 4600 cal. yr B.P. similar to TOC values prior to the tephra deposit. GDGT-derived temperatures did not increase with TOC, thus the increase in TOC could reflect the

recovery of Yanou Lake ecosystem post the tephra deposit. After c. 4600 cal. yr B.P. TOC remained stable at c. 4%. GDGT-derived temperatures also remained relatively cold and stable throughout this period at an average of c. 1.2 °C consistent with the colder conditions seen at Livingstone Island between c. 5000 and 4000 cal. yr B.P. (Björck *et al.*, 1991; 1993).

8.5.2. Mid-Holocene (c. 3400 – 2700 cal. yr B.P.)

The mid-Holocene was characterised by rapid warming from 5.39 °C ± 1.45 °C at c. 3500 cal. yr B.P. which culminated with the highest summer temperatures in the record of 13.84 °C ± 1.45 °C at c. 3100 cal. yr B.P. (Fig. 8.5). Primary productivity also increased slightly with a small peak in total chlorophyll to 1.48 g cm^{-2} yr^{-1} at c. 3300 cal. yr B.P. (Fig. 8.5). Nevertheless, this was not reflected in the carotenoid record. The small increase in chlorophyll and absence of carotenoids during this warm period does not represent the increase in productivity that could be expected with such a warming as seen in the GDGT-temperature record. This suggests that perhaps in this part of the core pigments may not be accurately reflecting productivity and there could be a degradation issue. From the peak at c. 3100 cal. yr B.P. the temperature decreased until c. 2700 cal. yr B.P. but still remained comparatively high at c. 8 °C (Fig. 8.5).

At the peak of the mid-Holocene warm period temperatures in Yanou Lake were significantly higher than the rest of the record which averaged 2.88 °C. During periods of sustained warming on the SSIs lake levels at Yanou Lake are likely to have reduced due to increased evaporation. Moreover, as the warm period continued a reduction in meltwater input could have increased temperatures in Yanou Lake further. The bathymetry of Yanou Lake (British Antarctic Survey, 2008) showed that if lake levels fell by more than 1.5 m, when compared to the November 2006 levels, not only could the lake be significantly smaller but it may also have split into three shallow pools (Fig. 8.9). With lake volume significantly reduced, temperature increases could become not only more rapid but also greater in amplitude. Contemporary seasonal reductions seen on Signy Island (Ellis-Evans pers. comm.) would suggest that a reduction in lake level of this extent is not unattainable during a period of sustained warm conditions. On Signy Island, to the north of the Antarctic Peninsula, lake levels reduce as both air and lake temperatures increase during the summer months (December to February) (Ellis-Evans pers. comm.). Therefore, if there was a significant reduction in lake level and / or

a reduction in the amount of cold water input into Yanou Lake during the mid-Holocene warm period lake temperatures of c. 14 °C could be feasible.

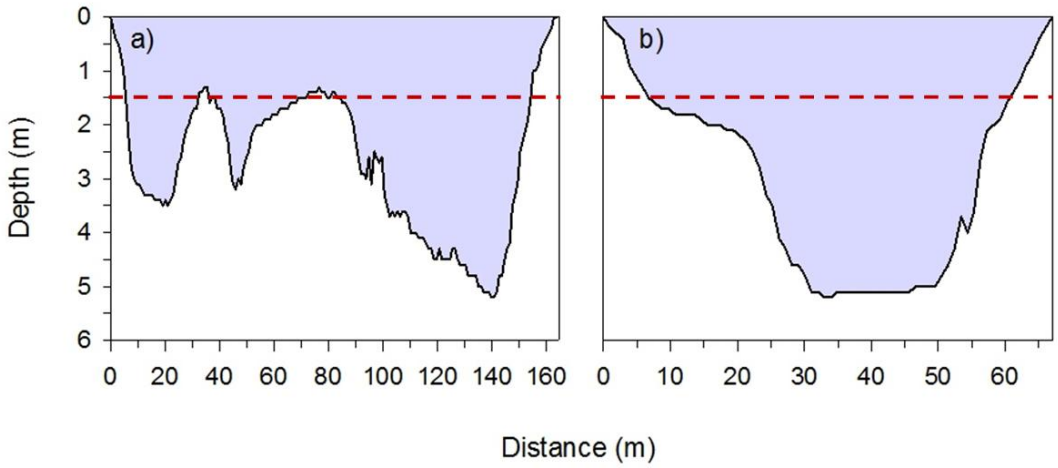

Figure 8.9: Bathymetric profiles of Yanou Lake: a) East to West Transect; b) North to South Transect. Unpublished field report data (British Antarctic Survey, 2008). Red dashed line represents a drop in lake level by 1.5 m.

A reduction in lake level could also explain why, as outlined above, the pigments concentrations are low during warmer conditions of the mid-Holocene warm period in the Yanou Lake record. Pigments are highly susceptible to degradation by light, oxygen and heat (Leavitt and Hodgson, 2001; Chapter 4, Section 4.2.3) therefore, an increase of and / or exposure to these conditions could cause a decrease in pigment concentration or a disparity between increased productivity and pigment concentrations. During the mid-Holocene warm period pigment degradation could have increased not only as a result of increased water temperatures but also a reduction in lake level thus more light penetration at the lake bed. PAR light penetration data collected in November 2006 indicated light penetration of c. 10% at the bed of the lake (British Antarctic Survey, 2008). Moreover, the November 2006 data shows that a reduction in lake level of c. 1.5 m might increase PAR light penetration to c. 15% (British Antarctic Survey, 2008). As most pigment degradation occurs before burial either in the water column or surface sediment layer (Hodgson *et al*., 1997, Leavitt and Hodgson, 2001) the slow sediment accumulation rate in Yanou Lake during the mid-late Holocene coupled with increased ice free conditions would increase the period during which degradation could occur. Although chlorophyll degradation produces coloured degradation products carotenoid derivatives are colourless meaning they are often undetected (McGowan, 2007). This could explain the absence of carotenoids and near absence of chlorophylls between c. 3800 and 1100 cal. yr B.P. (Fig. 8.5).

The timing of the mid-Holocene warm period between c. 3400 and 2700 cal. yr B.P. is consistent with previous records from the SSI. Björck *et al*. (1991) saw peaks in sediment accumulation, pollen and changes in diatom assemblage between c. 3200 and 2700 cal. yr B.P. in Midge Lake, Livingstone Island while Björck *et al*. (1993) reconstructed a climatic optimum at c. 3000 cal. yr B.P. in Lake Åsa from Byers Peninsula, Livingston Island. In Maxwell Bay Yoon *et al*. (2000) attributed increased TOC, diatom abundance and decreased C/N ratio to deglaciation at the margin between c. 4000 and 2700 cal. yr B.P. however, deeper into the bay itself Milliken *et al*. (2009) suggested sea surface temperatures were decreasing and sea ice increased between c. 5900 and 2600 cal. yr B.P. Differences between the two records in Maxwell Bay could be due to the deeper Milliken *et al*. (2009) record providing an oceanic record influenced more heavily by changes in ocean circulation while the more landward location of the Yoon *et al*. (2000) record was more controlled by deglaciation along the SSI coastline.

Elsewhere on the Antarctic Peninsula the mid-Holocene warm period started earlier at c. 4500 cal. yr B.P. and continued until c. 2600 cal. yr B.P. (Bentley *et al*., 2009). These timings were consistent with warmer conditions on JRI between c. 4200 and 3000 cal. yr B.P. (Björck *et al*., 1996) and open marine conditions in Lallemand Fjord between c. 4700 and 2700 cal. yr B.P. (Shevenell *et al*., 1996). Also, in Marguerite Bay Hodgson *et al*. (2013) saw evidence of the mid-Holocene warm period in Col Lake 1, Horseshoe Island from c. 6200 cal. yr B.P. The warm period terminated with a decline in organic carbon at c. 2050 cal. yr B.P. in Col Lake 1. This encompasses the timing of the mid-Holocene warm period elsewhere but, beginning earlier and terminating later in Col Lake 1 than other records.

Although, terminating around the same time as the GDGT-temperature record for Yanou Lake the commencement of the mid-Holocene warm period in other records from the region predates the Yanou Lake record and those of Björck *et al*. (1991; 1993) also from the SSI. Similar timings of the mid-Holocene warm period between all three records from the SSI suggests that, rather than dating uncertainties being the cause of the delay in the mid-Holocene warm period at Yanou Lake, the mid-Holocene warm period started later on the SSI than elsewhere. Unlike in Fan Lake, South Georgia where meltwater input appeared to be prohibiting the mid-Holocene temperature increase within the lake (see Chapter 7) the sand flux record for Yanou Lake throughout the mid-Holocene was stable around a value of c. 0.003 g cm^{-2} yr^{-1} suggesting that meltwater

input is unlikely to be influencing the GDGT-temperature record. Further ITRAX analysis also showed no evidence of major terrestrial influx into the lake (Roberts, pers. comm.). Nevertheless, there was a peak in sulphur in the core at c. 3600 cal. yr B.P. and increased TOC between c. 4500 and 3600 cal. yr B.P. at an average of c. 4.1% (Fig. 8.5) both of which could indicate that productivity increased at the beginning of the mid-Holocene warm period prior to temperature increases.

Tephra deposits seen in Yanou Lake were also evident in the other SSI lakes studied by Björck *et al*. (1991; 1993). These deposits could impact the lake ecosystem and therefore, during a period of recovery after tephra deposition palaeoenvironmental reconstructions may be affected. However, as discussed in Section 8.5.1 TOC in Yanou Lake had recovered by c. 4600 cal. yr B.P. indicating the lake had recovered from the 5700 cal. yr B.P. unit of reworked ash. Thus ruling out the possibility that the volcanic eruption, that was the source of the c. 5700 cal. yr B.P. tephra deposit, affected regional climates in the long-term or was the cause of any delay in the mid-Holocene warm period. Nevertheless, the affect of the reworked ash would have influenced the lake environment until the TOC began to increase at c. 5000 cal. yr B.P.

Another possible cause of the delayed onset of the mid-Holocene warm period on the SSI is that increased snow cover during low sea ice periods could be dampening the start of the warming. Global climate models investigating the relationship between sea ice and precipitation indicate that during periods of reduced sea ice precipitation is significantly increased in coastal locations (Weatherly, 2004; Deconto *et al*., 2007). Although Milliken *et al*. (2009) suggest that sea ice began to increase in Maxwell Bay from c. 5900 cal. yr B.P., their T/I ratio, which they used as a proxy for sea ice, increased most rapidly after c. 3000 cal. yr B.P. peaking at c. 2600 cal. yr B.P. Moreover, Watcham *et al*.'s (2011) diatom record from Ardley and Belén Lakes, on Ardley and King George Islands respectively, showed an increase in sea-spray associated diatoms between c. 5900 and 4750 cal. yr B.P. indicating potentially limited sea ice cover and stormier conditions. An increase in storm intensity and precipitation, particularly in the form of snow, could have had a significant effect on the climate of the SSI. Not only could increased precipitation directly influence lake temperatures as it enters the lake, the increase in runoff and gradual meltwater input as air temperatures increased and snow patches melted might explain some of the delay of the mid-Holocene warm period on the SSI.

Cross correlation between the Yanou Lake GDGT-derived summer temperature record and the JRI ice core temperature reconstruction (Mulvaney *et al*., 2012) suggests that, even though the delay of the mid-Holocene warm period was beyond the 95% error range of the age-depth model of ± 150 years, the delay was not statistically significant, as there was no lag evident between the two records (Fig. 8.7). Moreover, the lack of correlation between the Yanou Lake temperatures and the Stenni *et al*. (2010) temperature reconstruction from EPICA Dome C, r = -0.16 (Fig. 8.7), suggests that, although the Yanou Lake record was relatively consistent with other SSI records, aspects of the climates of the East Antarctic and the SSI appear to be indicating different climatic trends.

8.5.3. Mid-Late Holocene (c. 2700 – 1200 cal. yr B.P.)

After the mid-Holocene warm period the GDGT-derived summer temperature record for Yanou Lake decreased in temperature from 8.11 °C ± 1.45 °C at c. 2700 cal. yr B.P. to 4.34 °C ± 1.45 °C at c. 1200 cal. yr B.P. punctuated by a peak to 11.34 °C ± 1.45 °C at 1650 cal. yr B.P. following which temperature decreased again to 4.34 °C ± 1.45 °C at 1250 cal. yr B.P. (Fig. 8.5). Björck *et al*. (1991; 1993) reconstructed a similar period of climatic deterioration on Livingstone Island after c. 2500 cal. yr B.P. The Antarctic Peninsula (Bentley *et al*, 2009; Sterken *et al*., 2012) and the East Antarctic (Verleyen *et al*., 2011) also experienced climatic deterioration after c. 2000 cal. yr B.P. In addition, colder conditions were evident in the JRI ice core (Mulvaney *et al*., 2012) with a cooling trend between c. 2200 and 600 cal. yr B.P. (Fig. 8.6.a) but not at EPICA Dome C where temperatures increased after c. 2300 cal. yr B.P. (Fig. 8.6.b). Further north on South Georgia, GDGT-derived summer temperature reconstructions indicated that conditions were relatively cool between c. 2600 and 1000 cal. yr B.P. with an average temperature of c. 7.3 °C, compared to the peak temperature of the mid-Holocene at Fan Lake of 14.23 °C ± 1.45 °C (see Chapter 7). Colder conditions were also evidenced on South Georgia by Rosqvist and Schuber (2003) who reconstructed glacial advance between 2400 and 1600 cal. yr B.P. Therefore, suggesting that the climatic deterioration at c. 2700 cal. yr B.P. was widespread not only at the northern tip of the Antarctic Peninsula and sub-Antarctic Islands but also in some areas of the East Antarctic coastline (Bentley *et al*, 2009; Verleyen *et al*., 2011; Mulvaney *et al*., 2012; Sterken *et al*., 2012).

The Yanou Lake record showed a peak in summer temperature at c. 1660 cal. yr B.P. when temperatures reached 11.34 °C ± 1.45 °C (Fig. 8.5). Björck *et al*. (1991) also found evidence in their LOI and pollen record from Midge Lake of a short warmer period at c. 2000 cal. yr B.P. and Mulvaney *et al*.'s (2012) JRI ice core record indicated a temperature peak at c. 1450 cal. yr B.P. both of which are within the 95% error range of the Yanou Lake age-depth model. The cause of this peak in summer temperature at the SSI may be a result of a reduction in precipitation as reconstructed by Björck *et al*. (1993) through the relative percentage abundance of aerophilic, eu-terrestrial, and bryophytic diatoms and periphytic diatoms between c. 2500 and 2000 cal. yr B.P in their record for Lake Åsa. Björck *et al*. (1993) interpreted this reduction in allochthonous or erosional variables as a reduction in precipitation on Livingstone Island. As discussed in Section 8.5.2, a decrease in precipitation and associated reduction in lake level can cause a significant increase in lake temperature, especially where precipitation was the main or only cold water lake input. These factors may be the cause of the rapid temperature increase seen in the Yanou Lake record from 3.93 to 11.34 °C between c. 2500 and 1700 cal. yr B.P. Further evidence for warmer conditions around 1700 cal. yr B.P. were also seen in Björck *et al*. (1991) Midge Lake record where pollen concentration remained high until c. 1500 cal. yr B.P. followed by a large reduction. Björck *et al*. (1991) interpreted this as a worsening of climatic conditions at c. 1500 cal. yr B.P. consistent with a reduction in temperature of c. 7 °C between c. 1650 and 1350 cal. yr B.P. in Yanou Lake.

8.5.4. Late-Holocene (1200 cal. yr B.P. – present)

During the late-Holocene temperatures at Yanou Lake were low, around 1 °C, with a general cooling trend in GDGT-derived summer temperatures from 6.35 °C ± 1.45 °C at c. 1100 cal. yr B.P. to -0.15 °C ± 1.45 °C at the surface (Fig. 8.4). A peak in temperature to 4.18 °C ± 1.45 °C at c. 740 cal. yr B.P., consistent with the timing of Medieval Climate Anomaly (MCA) c. 1100 – 700 cal. yr B.P. (Neukom *et al*., 2010; 2014; Bird *et al*., 2011; Diaz *et al*., 2011; Ledru *et al*., 2013) punctuated the cooling trend. At the same time total carotenoid and chlorophyll fluxes showed small peaks between c. 870 and 580 cal. yr B.P. (Fig. 8.4) suggesting a potential increase in primary productivity as temperatures increased. TOC also showed a minor increase to 3.7 % between c. 870 and 740 cal. yr B.P. further indicating an increase in within lake productivity.

Although the MCA has been noted on South Georgia (e.g., Clapperton *et al*., 1989; Van Nieuwenhuyze *et al*., in prep; Chapter 7) and elsewhere in the Southern Hemisphere, in particular in southern South America (Moy *et al*., 2008; Neukom *et al*., 2010), Argentina (Kastner *et al*., 2010) and further north in the Peruvian Andes (Bird *et al*., 2011), previous climatic reconstructions on the SSI by Björck *et al*. (1991) reconstructed cold, drier conditions between c. 1500 and 500 cal. yr B.P. with no indication of the MCA. However, in Maxwell Bay Hass *et al*. (2010) showed evidence of warmer 'summer-type' conditions during the MCA in their marine sediment record. Therefore, combining the evidence from Yanou Lake and Maxwell Bay it appears that warmer conditions may have prevailed at the SSI during the MCA and perhaps higher resolution sampling was required at Midge Lake to see this smaller scale climatic event.

Following the 'warmer' MCA conditions in the Yanou Lake GDGT-temperature record showed a c. 3 °C reduction in summer temperature at c. 570 cal. yr B.P. (Fig. 8.5) consistent with the timing of the Little Ice Age (LIA) previously noted on the Antarctic Peninsula by Bentley *et al*. (2009) and on South Georgia (Nieuwenhuyze *et al*., in prep; Chapter 7). A reduction in TOC to 0.85%, the lowest value in the record, other than in the reworked ash and minerogenic unit, could be an indicator of reduced productivity in Yanou Lake at this time perhaps linked to the colder conditions of LIA (Fig. 8.5). Furthermore, the chlorophyll and carotenoid flux was reduced after c. 570 cal. yr B.P. suggesting a potential reduction in primary productivity during the LIA (Fig. 8.5).

Similarly to the MCA, the LIA was not seen in previous palaeoclimate reconstructions on the SSI by Björck *et al*. (1991; 1993) who suggested temperatures had increased from c. 500 cal. yr B.P. to present but Hass *et al.* (2010) saw some evidence of the LIA in Maxwell Bay. Once again the absence of the LIA, like the MCA, could be an issue of sample resolution or it may be that palaeoenvironments on either or both King George Island and Livingstone Island reflect a localised signal. It might be assumed that King George Island is reflecting more regional climatic trends. Interestingly, the LIA was not evident in the JRI ice core record either. In fact, the JRI and Yanou Lake temperature records appear to become decoupled at c. 600 cal. yr B.P. as JRI temperatures increased (Fig. 8.6.a). The decoupling was most notable after c. 200 cal. yr B.P. when the JRI temperature record continued to increase but the Yanou Lake GDGT-derived summer temperature record showed decreased temperatures (Fig. 8.6.a & c).

Other records from the Southern Hemisphere including palaeo-reconstructions, meteorological data and climate models, have also shown evidence of warming post 1900 AD in Chile (Kaiser *et al*., 2005; Sepúlveda *et al*., 2009) and Australia (Collins, 2000; Hughes, 2003) as well as the Southern Hemisphere ensemble proxy data (Neukom *et al*., 2014). Nevertheless, like the Yanou Lake record, the Fan Lake record (Chapter 7) also showed no evidence of recent warming. In Fan Lake this was attributed to meltwater inputs into Fan Lake which could be prohibiting lake warming (Chapter 7, Section 7.5.5) however, there was no clear evidence in the sand flux record from Yanou Lake of meltwater input.

One possible explanation for the lack of recent warming in Yanou Lake, and perhaps Fan Lake, is that the GDGT-temperature reconstructions are a summer temperature record and they are being compared with annual temperature trends. Although, summer temperatures at Bellingshausen, King George Island, have shown a small increase since 1969 AD, when records began, Turner *et al*. (2005a) showed that there was a bias to winter warming which would not be represented in the GDGT-temperature record but, would cause a warming trend in annual temperature records such as those from ice cores (see Chapter 9 for further discussion). Finally, another complication is that due to the slow sedimentation rate only one sample at Yanou Lake represents the recent warming, post 1950 AD. Therefore, the analysis of other nearby lakes with faster sedimentation rates may be more applicable for the reconstruction of these recent changes.

8.6. Conclusions

GDGT compounds present in Yanou Lake, King George Island were used to reconstruct temperatures since the lake became isolated from the sea at c. 6050 cal. yr B.P.

On isolation, primary productivity within the lake was at its peak, but this was not driven by increased temperatures as the GDGT-derived summer temperature record showed relatively low temperatures between c. 6050 and 3400 cal. yr B.P. The peak in primary production appears to have been a result of continued availability of the marine nutrient pool, previously noted in lakes on Beak Island and Pourquoi-pas Island.

The mid-Holocene warm period was recorded in Yanou Lake between c. 3400 and 2700 cal. yr B.P. during which time summer temperatures reached a core maximum of 13.8 °C ± 1.45 °C. The timing of the mid-Holocene warm period was consistent with previous records from Midge Lake and Lake Åsa on the SSI, but commenced later than

other records from the Antarctic Peninsula at Lallemand Fjord and JRI and Fan Lake on South Georgia where the mid-Holocene warm period began at c. 4500 cal. yr B.P. Stormier conditions on the SSI, thus increased snow cover, due to open water conditions in Maxwell Bay at the onset of the Antarctic Peninsula mid-Holocene warm period could have dampened the start of the mid-Holocene warm period on the SSI.

After the mid-Holocene warm period, colder conditions were reconstructed in Yanou Lake between c. 2700 and 1200 cal. yr B.P. consistent with other records from Midge Lake and Lake Åsa on the SSI and Beak Island and JRI on the Antarctic Peninsula. These cooler conditions were punctuated by a brief warm period at c. 1660 cal. yr B.P. in Yanou Lake which coincides with a reduction in precipitation at the SSI. Such a reduction in precipitation could have led to a reduction in cold-water input into Yanou Lake and lower lake levels thus increasing lake temperature.

The late-Holocene was characterised by cold summer temperatures with a peak in temperature and primary productivity between c. 870 and 740 cal. yr B.P. possibly consistent with the MCA (c. 1100 – 700 cal. yr B.P). After the MCA both summer temperature and primary productivity dropped at c. 570 cal. yr B.P. during the LIA (c. 500 – 100 cal. yr B.P). The LIA was not evident in the JRI or EPICA Dome C records which both show warming post 500 cal. yr B.P. at which time they became decoupled with the Yanou Lake temperature record.

Chapter 9: The Wider Implications of the Fan and Yanou Lake GDGT-temperature Reconstructions

Summary

In Chapters 7 and 8 the Antarctic and sub-Antarctic GDGT-temperature calibration developed in Chapter 6 was applied to Fan Lake, South Georgia and Yanou Lake, South Shetland Islands (SSI) respectively. In this chapter the GDGT-derived summer temperature record from these two sites is compared and the similarities, differences, leads and lags between the two records discussed. One of the main differences between the two records is the timing of the mid-Holocene warm period, which appears much later in Yanou Lake than in Fan Lake. The GDGT-temperature records from Fan and Yanou Lakes are then compared with other temperature reconstructions from elsewhere in Antarctica and Chile and again similarities, differences, leads and lags between the records are considered. One noticeable difference is the absence of the recent rapid warming in both the Fan Lake and Yanou Lake temperature records that is seen in other Antarctic Peninsula and Chilean reconstructions and instrumental records. The wider synthesis of the GDGT-temperature records and previously published temperature records allows changes the position and / or strength of the PFZ and SWW during the mid-late Holocene to be considered. Finally, a disparity between primary productivity proxies, such as diatom and pigment fluxes and total organic carbon (TOC), and temperature in Fan Lake and Yanou Lake suggests that within lake productivity is more closely related to ice cover and nutrient availability than temperature.

9.1. Introduction

During the mid-late Holocene two prominent warm phases, the mid-Holocene warm period and recent rapid warming, have been noted in lake sediment cores (e.g., Björck *et al*., 1991; 1993; Jones *et al*., 2000; Rosqvist and Schuber, 2003; Van der Putten *et al*., 2004; 2009), marine sediment cores (e.g., Milliken *et al*., 2009, Shevenell *et al*., 1996; 2011) and ice cores (e.g., Mulvaney *et al*., 2012; Masson-Delmotte *et al*., 2011) from Antarctica. Although, in ice and marine cores temperatures have been reconstructed quantitatively using stable isotopes (e.g., Mulvaney *et al*., 2012) or the TEX_{86} index (Shevenell *et al*., 2011) respectively, to date temperature reconstructions in lake cores are qualitative. The development of the lacustrine Antarctic and sub-Antarctic GDGT-temperature calibration (Chapter 6) allowed the first quantitative lacustrine temperature

reconstructions on South Georgia and the SSI (Chapter 7 and 8). The Fan Lake and Yanou Lake GDGT-temperature records both indicated evidence of varying temperatures throughout the mid-late Holocene with substantial warming during the mid-Holocene warm period (c. 4500 to 2600 cal. yr B.P.).

A comparison between the Fan Lake and Yanou Lake GDGT-temperature records and other records from Antarctica and Chile allows these two records to be put into perspective. In addition, similarities and differences between the records may help determine some of the mechanisms of climate variability. Bentley *et al*. (2009) previously suggested several mechanisms for Holocene palaeoenvironmental changes at the Antarctic Peninsula including changes in solar forcing, the Antarctic Circumpolar Current (ACC), South Westerly Winds (SWW), sea-ice interactions and El Niño Southern Oscillation (ENSO).

The ACC flows clockwise around Antarctica passing along the western side of the Antarctic Peninsula, thus changes in the ACC, and consequent changes in the upwelling of warm deep waters, plays a key role on the regions climate (Smith *et al*., 1999; Smith and Klinck, 2002). The ACC and SWW are interconnected through the steep temperature gradient in sea surface temperatures (SST) created by the ACC. The temperature gradient plays a key role in the position of the SWW while changes in the strength of the SWW can drive changes in ACC (Bentley *et al*., 2009). A strong annual correlation between sea ice extent and winter air temperature also causes a strong positive feedback at the western Antarctic Peninsula with the potential to amplify warming events in the region (Vaughan *et al*., 2001; Bentley *et al*., 2009). Nonetheless, understanding the specific causes of climatic change is complex as many of these mechanisms are interlinked, that is a poleward intensification of the SWW could strengthen the ACC which in turn affects upwelling and therefore changes in sea-ice extent.

Comparing records from South Georgia, the SSI and elsewhere in Antarctica and southern South America will help determine firstly, if temperature changes seen on the Antarctic Peninsula are confined to the region or are more widely distributed and secondly, potential mechanisms for these climatic changes. For example, Bentley *et al*. (2009) suggested a synchronisation between records from the Antarctic Peninsula and Southern America could indicate a poleward shift in the position of the SWW. To enable such a comparison the Fan and Yanou Lake records will be compared with SST

records from Chile (Sepúlveda *et al*., 2009; Caniupán *et al*., 2014) and Palmer Deep on the Antarctic Peninsula (Shevenell *et al*., 2011; Etourneau *et al*., 2013) and air temperature reconstructions from ice cores on James Ross Island (JRI), East Antarctic Peninsula (Mulvaney *et al*., 2012) and East Antarctica (Vimeux *et al*., 2002; Stenni *et al*., 2010). These records span an area from 44 to 78 °S and 74 °W to 123 °E (Fig. 9.1).

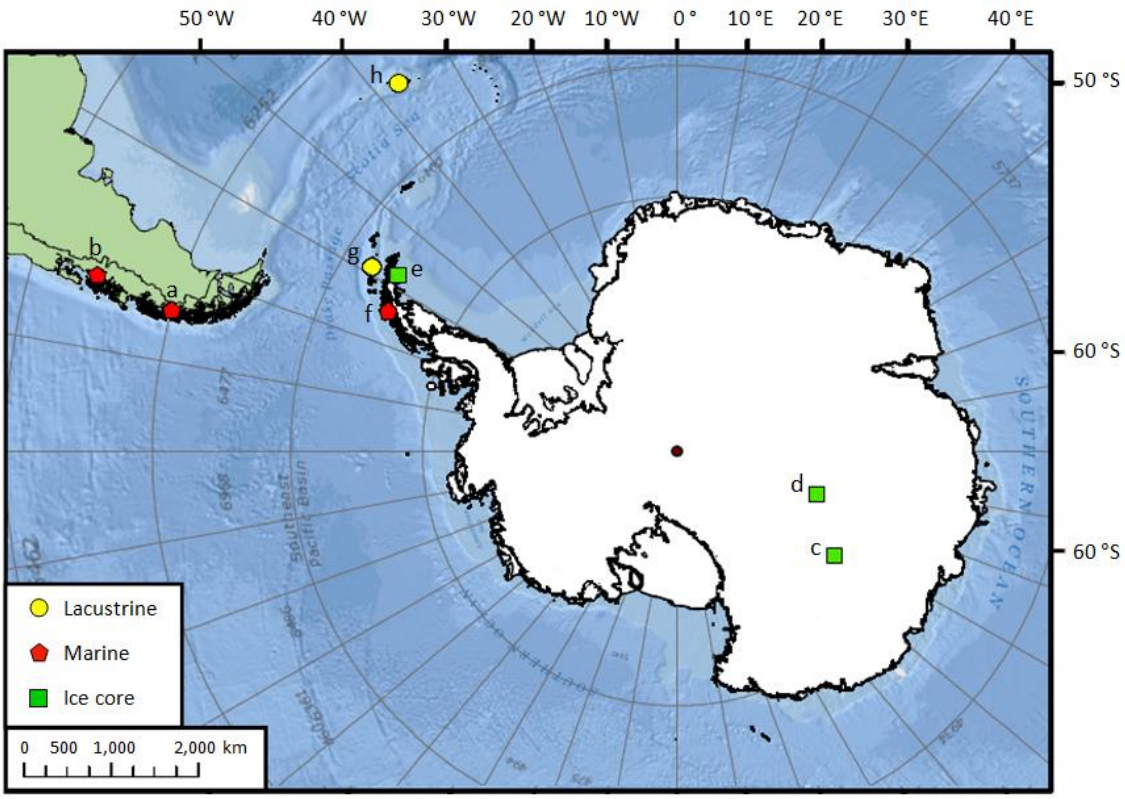

Figure 9.1: Map of Antarctica and southern South America showing the location of lacustrine, marine and ice core temperature reconstructions for comparison: a) Canal Wide; b) Jacaf Fjord; c) EPICA Dome C; d) Vostok; e) James Ross Island; f) Palmer Deep; g) South Shetland Islands and h) South Georgia.

9.2. Results

9.2.1. Comparison of Fan Lake and Yanou Lake

GDGT-derived summer temperatures from c. 6200 cal. yr B.P. to present determined for Fan Lake and Yanou Lake in Chapter 7 and 8 were compared (Fig. 9.2). As discussed in Chapter 7 prior to c. 4300 cal. yr B.P. Fan Lake was heavily influenced by a deglaciating catchment, therefore, no comparisons between Fan and Yanou Lakes were made prior to c. 4300 cal. yr B.P. Both records peak to their highest summer temperatures (c. 14 °C) during the mid-Holocene warm period, although Fan Lake reaches its maximum 400 years before Yanou Lake at c. 3500 and 3100 cal. yr B.P.

respectively (Fig. 9.2). Another difference between the records was that temperatures in Yanou Lake increased more rapidly at the beginning of the mid-Holocene warm period from 6.6 °C at c. 3300 c. cal. yr B.P. to 13.8 °C at c. 3100 cal. yr B.P. Alternatively, in Fan Lake summer temperatures were high from c. 3800 cal. yr B.P., with an average temperature of c.12.4 °C between c. 3800 and 3350 cal. yr B.P., prior to two peaks in temperature of c. 14 °C at c. 3500 and 3300 cal. yr B.P. (Fig. 9.2).

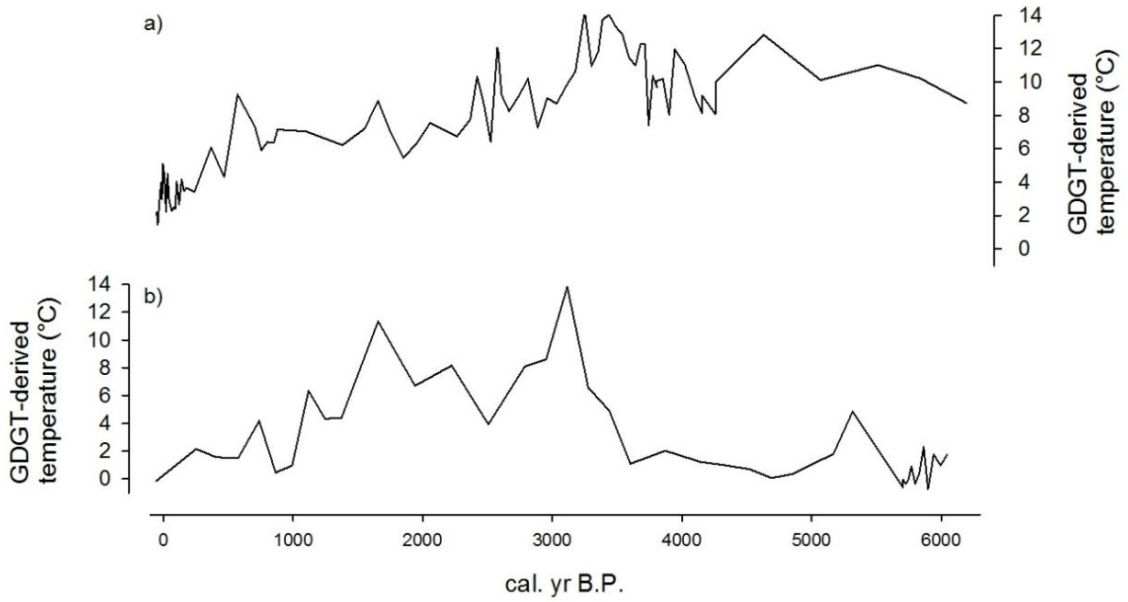

Figure 9.2: Temperature reconstructions using the Antarctic and sub-Antarctic GDGT-temperature calibration for a) Fan Lake, Annenkov Island, South Georgia and b) Yanou Lake, King George Island, South Shetland Islands.

Although, Pearson's correlation coefficient suggests that Fan Lake and Yanou Lake were correlated over the last 2000 years, r = 0.55, p = 0.078, correlations between c. 4300 and 2600 cal. yr B.P. of r = -0.32, p = 0.400 suggested they differed during the mid-Holocene. For further comparison both records were re-sampled at a 200 year resolution and cross correlated in R (see Chapter 5 for methodological details). Cross correlation between the Fan Lake and Yanou Lake temperature records indicated a statistically significant lag in which Yanou Lake lags Fan Lake by up to 800 years between c. 4300 cal. yr B.P. and present (Fig. 9.3). A more specific examination of the mid-Holocene warm period indicated a significant lag of 400 years between Yanou Lake and Fan Lake, again with Yanou Lake lagging Fan Lake, between c. 4300 and 2600 cal. yr B.P. (Fig. 9.3). No statistically significant lags between Yanou Lake and Fan Lake were seen through cross correlation during the period from c. 2000 cal. yr B.P. to present.

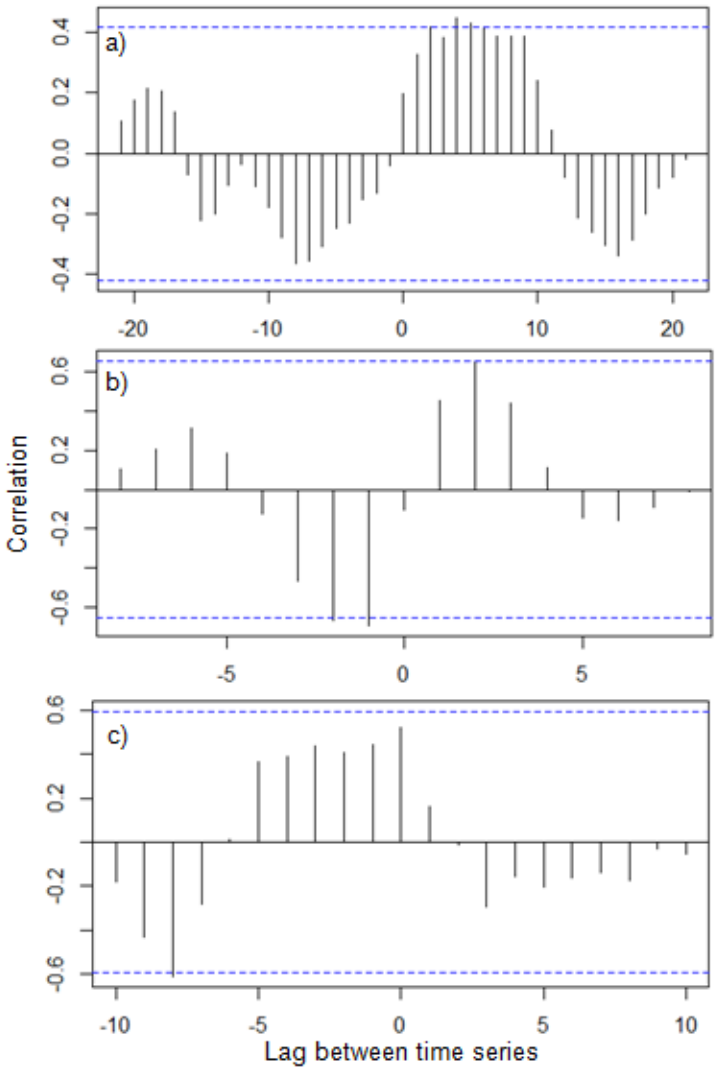

Figure 9.3: Graphical results of cross correlation on 200 year time series temperature anomaly data for Yanou Lake and Fan Lake over different time periods. a) c. 4300 cal. yr B.P. to present, b) c. 4300 to 2600 cal. yr B.P. (mid-Holocene warm period) and c) c. 2000 cal. yr B.P. to present. Results outside of the blue dashed line are statistically significant at the 95% level.

9.2.2. Wider comparison with previously published temperature records from Antarctica and Chile

The Fan Lake and Yanou Lake GDGT-derived summer temperature records were compared with previously published temperature records including SST records from Chile (Sepúlveda *et al*., 2009; Caniupán *et al*., 2014) and the Antarctic Peninsula (Shevenell *et al*., 2011; Etourneau *et al*., 2013) and ice core temperature reconstructions from East Antarctica (Vimeux *et al*., 2002; Stenni *et al*., 2010) and the Antarctic Peninsula (Mulvaney *et al*., 2012) (Fig. 9.4). All the records were correlated with one another using Pearson's correlation coefficient during three periods; 1) c. 4300 cal. yr B.P. to present (Table 9.1); 2) c. 4300 to 2600 cal. yr B.P. (Table 9.2) and 3) c. 2000 cal. yr B.P. to present (Table 9.3). In addition, cross correlation was run between the

records, with particular focus on those where Pearson's correlation coefficient indicated weak or no correlation, to determine any leads or lags between these temperature reconstructions.

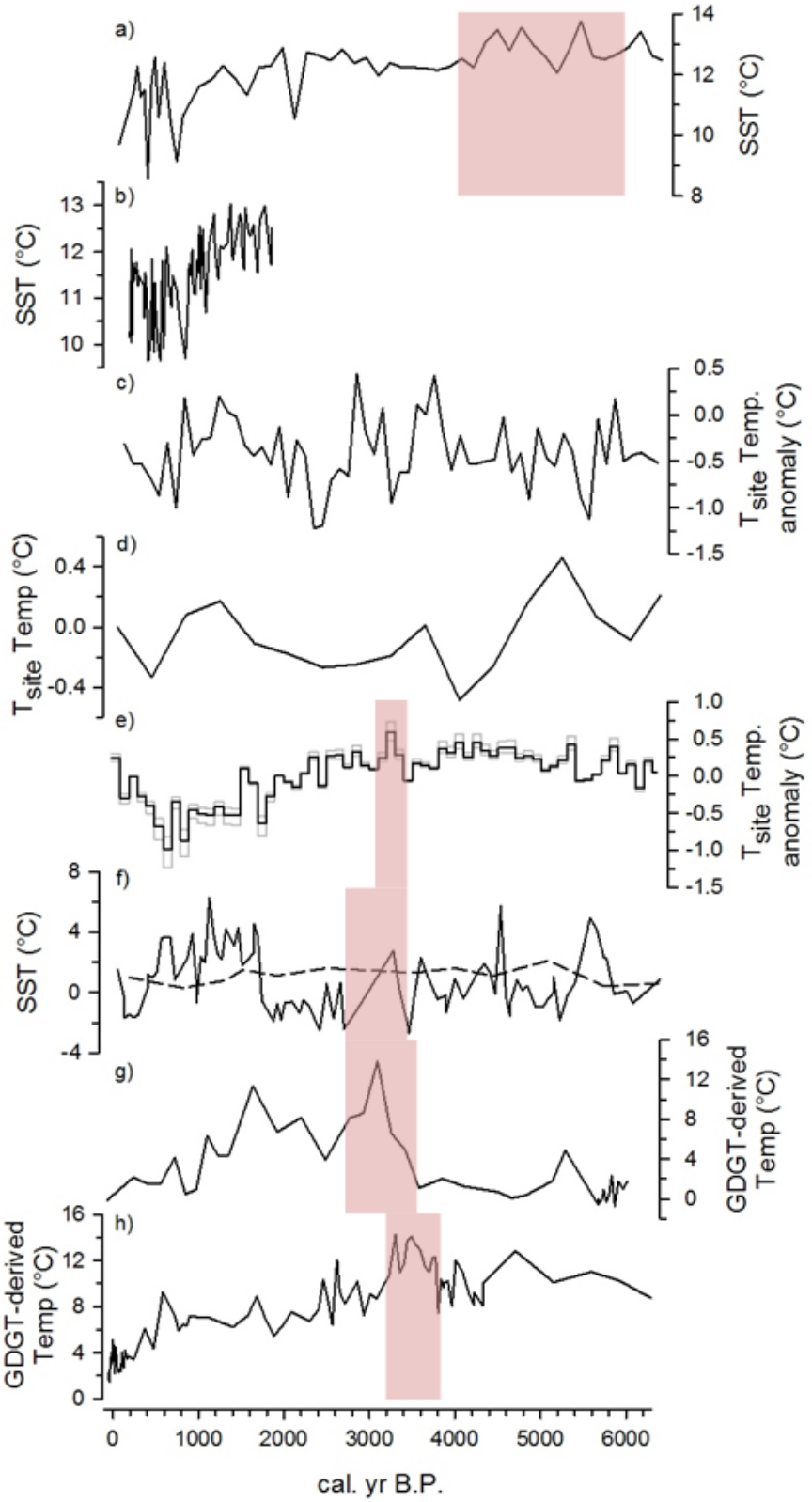

Figure 9.4: Comparison of Antarctic and Chilean Holocene temperature reconstructions: a) Canal Wide (Caniupán *et al*., 2014); b) Jacaf Fjord (Sepúlveda *et al*., 2009); c) EPICA Dome C (Stenni *et al*., 2010); d) Vostok (Vimeux *et al*., 2002); e) JRI (Mulvaney *et al*., 2012); f) Palmer Deep (Shevenell *et al*., 2011; solid and Etourneau *et al*., 2013; dashed); g) Yanou Lake and h) Fan Lake. The red boxes indicate the timing of the mid-Holocene "warming" in appropriate records, as seen in either the temperature reconstructions or other proxy records.

Since c. 4300 cal. yr B.P. Fan Lake has had a statistically significant positive correlation with JRI, r = 0.45, *p* = 0.002 and also with the Canal Wide SST record, r = 0.52, *p* = 0.013 (Table 9.1). Yanou Lake was most closely correlated with the Canal Wide record from Chile, r = 0.39, *p* = 0.077. Cross correlation, on re-sampled data (Chapter 5), indicated that, as well as lagging Fan Lake, Yanou Lake also lagged JRI by c. 1000 years (Fig. 9.5.a) but showed no lag with the Canal Wide record (Fig. 9.5.b). Many other records either showed a negative correlation, such as Palmer Deep and JRI r = -0.43, or indicated no relationship i.e. EPICA Dome C, which was not correlated with Yanou, JRI or Canal Wide (Table 9.1).

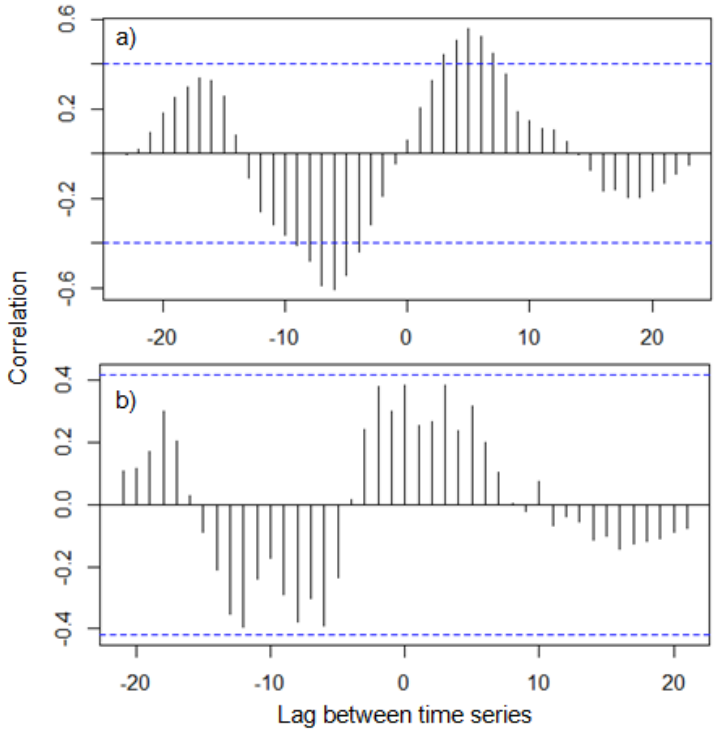

Figure 9.5: Graphical results of cross correlation on 200 year time series temperature anomaly data for Yanou Lake and a) JRI (Mulvaney *et al*., 2012) and b) Canal Wide (Caniupán *et al*., 2014) since c. 4300 cal. yr B.P. Results outside of the blue dashed line are statistically significant at the 95% level.

	Fan Lake	Yanou Lake	Palmer Deep	James Ross Island	EPICA Dome C	Canal Wide
Fan Lake		*0.477*	*0.534*	*0.002*	*0.328*	*0.013*
Yanou Lake	0.16		*0.484*	*0.395*	*0.768*	*0.077*
Palmer Deep	-0.10	-0.16		*0.003*	*0.026*	*0.135*
James Ross Island	0.45	0.19	-0.43		*0.986*	*0.004*
EPICA Dome C	0.15	-0.07	0.34	0.00		*0.677*
Canal Wide	0.52	0.39	-0.33	0.59	0.09	

Table 9.1: The correlations between GDGT-temperatures from Fan Lake and Yanou Lake, SST reconstructions from Palmer Deep (Shevenell *et al*., 2011) and Canal Wide (Caniupán *et al*., 2014) and ice core temperature reconstructions from JRI (Mulvaney *et al*., 2012) and Dome C (Stenni *et al*., 2010) since c. 4300 cal. yr B.P. The table gives r values to the bottom left and *p* values to the top right.

During the mid-Holocene, between c. 4300 and 2600 cal. yr B.P., the strongest and most statistically significant correlation was seen between Palmer Deep and JRI where r = 0.49 and $p = 0.045$. The Chilean record from Canal Wide indicated no significant relationships with all records from Antarctica other than JRI during the mid-Holocene warm period (Table 9.2). Nevertheless, cross correlation also showed no evidence of any statistically significant leads or lags between the Canal Wide and Fan Lake or Yanou Lake (Fig. 9.6.a & b).

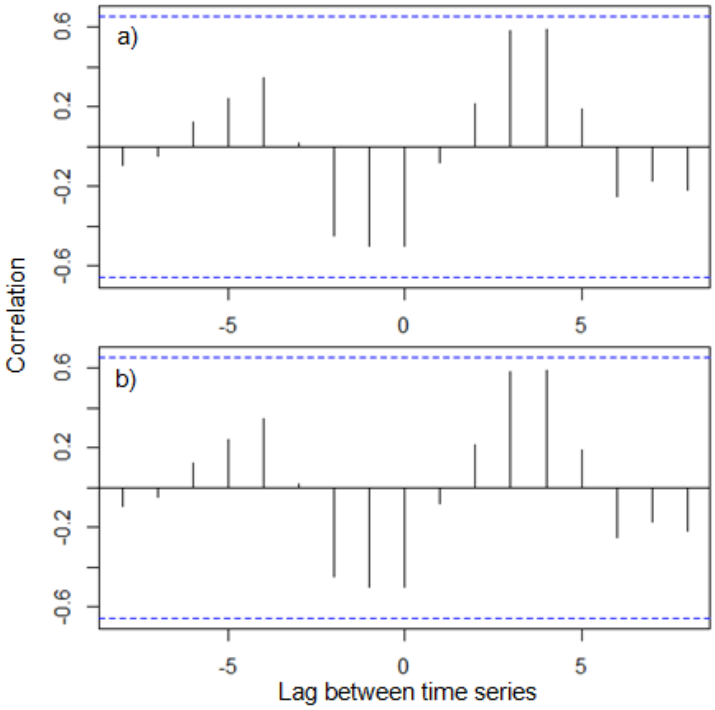

Figure 9.6: Graphical results of cross correlation on 200 year time series temperature anomaly data for Canal Wide (Caniupán *et al*., 2014) and a) Fan Lake and b) Yanou Lake between c. 4300 and 2600 cal. yr B.P. Results outside of the blue dashed line are statistically significant at the 95% level.

	Fan Lake	Yanou Lake	Palmer Deep	James Ross Island	EPICA Dome C	Canal Wide
Fan Lake		*0.400*	*0.788*	*0.175*	*0.561*	*0.174*
Yanou Lake	-0.32		*0.888*	*0.684*	*0.687*	*0.318*
Palmer Deep	-0.07	0.06		*0.045*	*0.999*	*0.719*
James Ross Island	-0.35	-0.16	0.49		*0.591*	*0.346*
EPICA Dome C	0.15	-0.16	0.00	-0.14		*0.422*
Canal Wide	-0.50	-0.38	-0.14	0.36	-0.31	

Table 9.2: The correlations between GDGT-temperatures from Fan Lake and Yanou Lake, SST reconstructions from Palmer Deep (Shevenell *et al*., 2011) and Canal Wide (Caniupán *et al*., 2014) and ice core temperature reconstructions from JRI (Mulvaney *et al*., 2012) and Dome C (Stenni *et al*., 2010) between c. 4300 and 2600 cal. yr B.P. The table gives r values to the bottom left and *p* values to the top right.

Pearson's correlation coefficient indicated that the last 2000 years showed the strongest and most significant relationships throughout the record. Fan Lake showed strong and statistically significant positive correlations with Yanou Lake, Palmer Deep and Jacaf Fjord and a significant negative relationship with JRI (Table 9.3). Yanou Lake also showed a strong positive relationship with Canal Wide, r = 0.62, $p = 0.041$. The most statistically significant relationship during the last 2000 years was seen between Fan Lake and Jacaf Fjord (r = 0.55, $p < 0.001$). Not surprisingly, due to the strong relationships found, cross correlation indicated no clear evidence of any leads or lags since c. 2000 cal. yr B.P.

	Fan Lake	Yanou Lake	Palmer Deep	James Ross Island	EPICA Dome C	Canal Wide	Jacaf Fjord
Fan Lake		*0.078*	*0.034*	*0.031*	*0.734*	*0.404*	*< 0.001*
Yanou Lake	0.55		*0.692*	*0.692*	*0.663*	*0.041*	*0.576*
Palmer Deep	0.46	-0.14		*0.043*	*0.058*	*0.891*	*0.113*
James Ross Island	-0.47	0.27	-0.45		*0.636*	*0.607*	*0.833*
EPICA Dome C	0.08	0.15	0.42	0.11		*0.183*	*0.016*
Canal Wide	0.28	0.62	-0.05	0.19	0.46		0.*654*
Jacaf Fjord	0.55	-0.20	0.38	-0.05	0.54	-0.16	

Table 9.3: The correlations between GDGT-temperatures from Fan Lake and Yanou Lake, SST reconstructions from Palmer Deep (Shevenell *et al*., 2011), Canal Wide (Caniupán *et al*., 2014) and Jacaf Fjord (Sepúlveda *et al*., 2009) and ice core temperature reconstructions from JRI (Mulvaney *et al*., 2012) and Dome C (Stenni *et al*., 2010) since c. 2000 cal. yr B.P. The table gives r values to the bottom left and *p* values to the top right. The Sepúlveda *et al*. (2009) record only dates to c. 1750 cal. yr B.P.

9.3. Discussion

9.3.1. The mid-Holocene warm period

9.3.1.1. Comparison of South Georgia and the South Shetland Islands

The GDGT-derived summer temperature reconstructions from Fan Lake and Yanou Lake indicated that the mid-Holocene warm period started later at the SSI than South Georgia (Fig. 9.2). Cross correlation between the records showed further evidence of this delay recording a c. 400 year lag between the records in which Yanou Lake lags Fan Lake (Fig. 9.3). One other notable difference between the mid-Holocene warm period in the two records was the more abrupt nature of the warming in Yanou Lake than Fan Lake.

The c. 400 year delay in the onset of the mid-Holocene warm period at Yanou Lake may have been longer than the GDGT-temperature records alone suggest. As discussed in Chapter 7, Section 7.5.2, in Fan Lake meltwater input might have dampened the onset of the mid-Holocene warm period in the GDGT-temperature record meaning the mid-Holocene warm period began earlier on South Georgia than the Fan Lake GDGT-temperature record alone suggests. Assuming there was no similar meltwater input into Yanou Lake, for which there was no evidence seen in Chapter 8, Section 8.5.2, this could mean the delay between the records was greater than c. 400 years. Other records from the SSI (e.g., Björck *et al*., 1991; 1993) and South Georgia (e.g., Rosqvist and Schuber, 2003; Van der Putten *et al*., 2004; 2009) showed the timing of the mid-Holocene warm period to be consistent with the GDGT-temperature reconstructions from Yanou Lake and Fan Lake respectively (Chapter 7 & 8). Therefore, suggesting that, within the dating uncertainties of the records, the Yanou Lake and Fan Lake records accurately recording the timing of the mid-Holocene warm period and the delay between the records is real.

The earlier onset of the mid-Holocene warm period at more northerly South Georgia could be a result of a southerly migration of the warmer conditions. Consequently, South Georgia at 54 °S could warm before the SSI at 62 °S. If there was a southerly migration of the warming it could be expected that Chilean records would also show evidence of an earlier onset of the mid-Holocene warm period. Caniupán *et al*. (2014) recorded warming in Canal Wide, Chile at 50 °S between c. 6000 and 4000 cal. yr B.P. predating the South Georgian mid-Holocene warm period. Furthermore, Jones *et al*.

(2000) and Hodgson and Convey (2005) reconstructed the onset of mid-Holocene warm period on Signy Island at 60 °S, north of the SSI, at c. 3300 and 3800 cal. yr B.P. respectively similar to the timing of the mid-Holocene warm period at Yanou Lake. The evidence from these records suggests that a southern migration of warmer conditions could explain the disparities between the records, however, at JRI at 64 °S, similar to the SSI, but on the eastern Antarctic Peninsula Björck *et al*. (1996) recorded an earlier onset of the mid-Holocene warming at c. 4200 cal. yr B.P. Not only would this discount a southerly migration it would also suggest a climatic differential between the western and eastern sides of the Antarctic Peninsula. Previous records have also noted such a differential as seen during the early Holocene climate optimum (Bentley *et al*., 2009) and recent warming over the last 50 years (Turner *et al*., 2005a). Nevertheless, a more recent study by Mulvaney *et al*. (2012) reconstructed a peak in temperature c. 3000 cal. yr B.P. which could be more closely related to the Yanou Lake record. The discrepancy between the two JRI records is most likely due to the Björck *et al*. (1996) reconstruction being an indirect qualitative reconstruction opposed to the Mulvaney *et al*. (2012) quantitative ice core temperature record.

Another theory, discussed briefly in Chapter 8, is that the mid-Holocene warm period was delayed on the SSI due to localised storms during the summer season as a result of reduced sea ice in Maxwell Bay between c. 5900 and 4750 cal. yr B.P. Previous research has shown that sea ice is a key factor in western Antarctic Peninsula climates and a positive feedback exists between sea ice and air temperatures (Vaughan *et al*., 2001; 2003; Bentley *et al*., 2009). As temperatures increased in the western Antarctic Peninsula during the mid-Holocene warm period evidence from Maxwell Bay, SSI (Milliken *et al*., 2009) and Marguerite Bay, further south on the Antarctic Peninsula, (Hodgson *et al*., 2013) suggests reduced summer sea ice.

Although in their sea ice reconstruction from Maxwell Bay Milliken *et al*. (2009) recorded an increase in sea ice from c. 5900 cal. yr B.P., it remained relatively sporadic until increasing rapidly at c. 3000 cal. yr B.P. to a peak at c. 2600 cal. yr B.P. as the mid-Holocene warm period ended in the Yanou Lake GDGT-temperature record. Furthermore, Milliken *et al*. (2009) suggested that between c. 5900 and 2600 cal. yr B.P. there was significant seasonal variability in the sea ice, evidenced by diverse diatom assemblages and low $\delta^{13}C$ and $\delta^{15}N$. Therefore, Maxwell Bay was likely to have been ice free in the summer season during this period.

A reduction in summer sea ice coupled with an intensification of the SWW, seen through the presence of *Nothofagus* pollen, common in South America, at the SSI (Björck *et al*., 1991; 1993), may have had the potential to generate increased wave activity and stormier climates. Similar conditions have been noted on the west Antarctic Peninsula during the 1980s and 1990s, when reduced sea ice occurred concurrently with increased wind speed, cloudiness (Van den Broeke, 2000) and precipitation (Turner *et al*., 2005b) indicative of more stormy conditions (Stammerjohn *et al*., 2008). Furthermore, Stammerjohn *et al*. (2008) also noted that a reduction in sea ice duration could lead to an increase in ocean heat flux to the atmosphere during winter, thus increasing winter air temperatures. Such changes would be reflected in records of annual air temperatures, i.e. ice core temperature trends, however, may not be recorded in the GDGT summer temperature record.

Evidence of stormier conditions can also be seen on King George Island where Watcham *et al*. (2011) recorded an increase in sea spray in Ardley and Belén Lakes between c. 5900 and 4750 cal. yr B.P. Stormier climatic conditions during the summer season at the SSI could have led to increased snow cover or extended the length of both seasonal snow and lake ice cover causing a reduction in air and lake temperatures at the start of the mid-Holocene warm period. As sea ice cover in Maxwell Bay increased at c. 3000 cal. yr B.P. (Milliken *et al*., 2009) the climate became more stable allowing temperatures at Yanou Lake to peak rapidly at c. 3120 cal. yr B.P. (Fig 9.2). Therefore, the reduction in summer sea ice has the potential to not only explain the later onset of the mid-Holocene warm period in Yanou Lake, and other reconstructions from the SSI, but also the more abrupt nature of the warming.

9.3.1.2. Synthesis of the mid-Holocene warm period in Antarctica and Chile

A comparison of the GDGT-derived summer temperature records from Fan Lake and Yanou Lake have shown varying degrees of correlation with other temperature records from elsewhere on the Antarctic Peninsula, East Antarctic and Chile (Fig. 9.4, Table 9.1 & 9.2). In East Antarctica neither the EPICA Dome C (Stenni *et al*., 2010) or Vostok (Vimeux *et al*., 2002) ice core temperature reconstructions demonstrated clear evidence of the mid-Holocene warm period consistent with Fan and Yanou Lakes (Fig. 9.4.c & d). Furthermore, no statistically significant relationships were found between EPICA Dome C and Fan Lake or Yanou Lake during the mid-Holocene warm period, $r = -0.16$, $p = 0.687$ and $r = 0.15$, $p = 0.561$ respectively (Table 9.2). A difference in the

temperature trends between the Antarctic Peninsula and East Antarctica is not surprising as modern temperature records from the Antarctic Peninsula and East Antarctic have shown different climatic trends (Turner *et al*., 2005a).

Moreover, recent comparisons between the western and eastern Antarctic Peninsula have shown evidence of differential climates on either side of the Peninsula, with warming over the last 50 years confined to a region from Faraday (65°15'S, 64°16'W) to just north of the tip of the peninsula (Turner *et al*., 2005a). These differences are likely due to the influence of the SWW on the western side bringing in warm air masses (Bentley *et al*., 2009). Nevertheless, the JRI ice core temperature anomaly data indicated a peak in temperature on JRI c. 3000 cal. yr B.P. which is consistent with the GDGT-temperature records from Fan Lake and Yanou Lake (Fig. 9.4).

Southern Chile is located within the influence of both the ACC and SWW (Kaiser *et al*., 2005) both of which are thought to be drivers of climate on the western Antarctic Peninsula. Therefore, Southern Chile climates may be more closely related to the western Antarctic Peninsula than East Antarctica, or even the eastern Antarctic Peninsula. In addition, temperature records from Southern Chile may help identify the causal factors affecting climate change in the Antarctic Peninsula region. Tight correlation of the western Antarctic Peninsula and Chilean records could potentially be used as an indicator of a southern shift in the SWW bringing warm air masses from South America to the western Antarctic Peninsula (Bentley *et al*., 2009).

Fan Lake and Yanou Lake reconstructed a period of mid-Holocene warmth between c. 4300 and 2500 cal. yr B.P. and c. 3400 and 2700 cal. yr B.P. respectively. Where the mid-Holocene warm period was recorded in lacustrine and marine records from Chile it tends to predate that of Fan Lake and Yanou Lake. For example, SST reconstructions from JPC-42, Canal Wide (49°55′ S, 74°23′W) showed evidence of warm summer temperatures between c. 6000 and 4000 cal. yr B.P. (Caniupán *et al*., 2014). The earlier mid-Holocene warming at Canal Wide resulted in negative relationships between JPC-42 and Fan Lake and Yanou Lake between c. 4200 and 2600 cal. yr B.P., r = -0.50, p = 0.174 and r= -0.38, p = 0.318 respectively (Table 9.2). Nonetheless, cross correlation indicated no clear evidence of a lag between the records (Fig. 9.5.b), however, longer records which predate c. 4300 cal. yr B.P. from Fan Lake and Yanou Lake may be required for a lag to be seen.

Further north, Bertrand *et al*. (2008) reconstructed Holocene changes in temperature, light and nutrient supply in Lago Puyehue, Chile (40°40'S, 72°28'W) through changes in productivity. Between c. 6000 and 3500 cal. yr B.P. they recorded a period of large variability in palaeoproductivity. This coincided with a decrease in diatom abundance between c. 4750 and 3000 cal. yr B.P. from which Sterken *et al*. (2008) cautiously infer a period of decreased wind, precipitation and / or increased temperatures. Therefore, although not all Chilean records demonstrated evidence of the mid-Holocene warm period, there was some indication of warming in Chile around the time of the mid-Holocene warm period in the Antarctic Peninsula region. Coupled with the presence of South American pollen, e.g. *Nothofagus,* in lake records from the SSI (e.g., Björck *et al*., 1991; 1993) this could be interpreted as a southern shift and / or increased intensity of the SWW. Nevertheless, *Nothofagus* was not found in Fan Lake, South Georgia during the mid-Holocene warm period, but did appear as temperatures dropped at c. 2400 cal. yr B.P. (Strother *et al*., 2015). This implies that during the mid-Holocene warm period the position of the SWW may have been south of South Georgia consistent with climate models of the SWW which suggest a poleward shift in the position of the SWW during warm periods (Bentley *et al*., 2009; Lamy *et al*, 2001; Toggweiler *et al*., 2006; Varma *et al*., 2011; 2012).

In addition to the SWW, the ACC could also have played a key role in the warming of the western Antarctic Peninsula during the mid-Holocene warm period. The ACC flows clockwise around Antarctica passing along the western side of the Antarctic Peninsula before the southern edge of the ACC passes through Drake Passage, while the northern part transports cold, nutrient-rich Antarctic waters to Chile (Bentley *et al*., 2009). A poleward shift in the SWW, as described above, has the potential to strengthen the ACC (Bentley *et al*., 2009). Increased surface mixing, as a consequence of this strengthening, could reduce sea ice extent as evident at the west Antarctic Peninsula during the mid-Holocene (Milliken *et al*., 2009; Hodgson *et al*., 2013). In Palmer Deep some records do not show warming during the mid-Holocene (e.g., Domack, 2002; Shevenell *et al*., 2011; Etourneau *et al*., 2013) hence there was no correlation between TEX_{86} Palmer Deep record and Fan, r = -0.07, $p = 0.788$, or Yanou r = 0.06, $p = 0.888$ during the mid-Holocene warm period (Table 9.2). Nevertheless, the increased TOC and decreased IRD in Lallemand Fjord (67 °S, 66 °W) could be indicative of higher productivity, reduced sea ice extent and warmer conditions between c. 4900 and 2700 cal. yr B.P. (Shevenell *et al*., 1996).

Concerns have been raised regarding the use of TEX_{86} index, as done by Shevenell *et al*. (2011), in sub-polar and polar regions (Ho *et al*., 2014). Ho *et al*. (2014) tested the appropriateness of both TEX_{86} and TEX_{86}^{L} in surface sediments and found large residuals between actual and reconstructed temperature. Therefore, even though there was no evidence of warming in the GDGT-temperature record, the TOC and IRD evidence of the mid-Holocene warm period should not be discounted. Such a warming in the Palmer Deep region could indicate a potential increase in the ACC as a driver of the mid-Holocene warm period alongside increased SWW.

The comparison of Antarctic Peninsula climate records during the mid-Holocene warm period with other records from Antarctica and Chile has allowed the evaluation of potential mechanisms of this warming. There is considerable evidence of an increase in intensity of the SWW in the sub-polar latitudes as a result of a poleward shift in the position of the SWW. Furthermore, the decrease in sea ice extent in the region at this time could be indicative of an intensification of ACC bringing warmer waters to the surface (Bentley *et al*., 2009). Other mechanisms of the Southern Annular Mode (SAM), which also impacts sea ice extent are wind-derived advection of heat, moisture and momentum (Stammerjohn *et al*., 2008). The complementary nature and positive feedbacks of these mechanisms means that together they have the potential to have significantly increased temperatures in the western Antarctic Peninsula during the mid-Holocene warm period.

9.3.2. The Medieval Climate Anomaly and Little Ice Age

After the termination of the mid-Holocene warm period, at c. 2600 and 2700 cal. yr B.P. in Fan Lake and Yanou Lake respectively, both showed cooling trends in the GDGT-derived temperatures (Fig. 9.2). The Fan Lake and Yanou Lake records both showed similar broad trends post c. 3000 cal. yr B.P. with cross correlation between the two after c. 3200 cal. yr B.P. indicating no lag and a strong positive correlation ($r = 0.66$, $p = 0.004$). In Fan Lake the cooling trend was punctuated by two peaks in temperature at c. 1680 and 580 cal. yr B.P. while in Yanou Lake peaks in temperature were also seen at c. 1660 and 740 cal. yr B.P. The timing of the latter could relate to the 'Medieval Climate Anomaly' (MCA). Following the MCA both records show a cooling event, at c. 300 cal. yr B.P. in Fan Lake and c. 500 cal. yr B.P. in Yanou Lake, which could be representing the 'Little Ice Age' (LIA) (Fig. 9.2).

In Chapter 7, the presence of the MCA and LIA in Fan Lake was used to suggest that over the last 1000 years the climate on South Georgia had potentially become de-coupled from Antarctic climates and is more representative of hemispheric trends. A change in position of the SWW was interpreted as a factor in this change in climate regime due to small peaks in long distance pollen in Fan Lake, e.g. *Nothofagus*, between c. 2210 and 1670 cal. yr B.P. (Strother *et al*., 2015). If this is the case, the tight correlation between the Fan Lake and Yanou Lake records could indicate that the western Antarctic Peninsula may no longer be representing broader Antarctic climates. However, there was no evidence of long distance pollen in lake records from Livingstone Island (Björck *et al*., 1991; 1993) thus, suggesting a reduction or shift in the SWW post the mid-Holocene warm period. Another possible explanation for the absence of long distance pollen in the Livingstone Island lakes might be an increase in ice cover meaning windblown pollen might not be able to enter the lakes. This is supported by Björck *et al*.'s (1993) suggestion that Lake Åsa was ice covered year round between c. 2000 and 1400 cal. yr B.P.

Other records from the Antarctic Peninsula, such as the Shevenell *et al*. (2011) TEX_{86} SST record from Palmer Deep, also showed evidence of the MCA and LIA (Fig. 9.4.f). Shevenell *et al*. (2011) reconstructed a peak in temperature to 3.9 °C at c. 850 cal. yr B.P. and colder conditions between c. 300 and 100 cal. yr B.P. During the last 2000 years the Shevenell *et al*. (2011) TEX_{86} SST record and the Fan Lake record showed a strong positive correlation r = 0.46 and $p = 0.034$ but Yanou Lake temperature record showed no relationship r = -0.14 and $p = 0.692$ with the TEX_{86} record (Table 9.3). The lack of correlation between Yanou Lake and Palmer Deep could be due to the sampling resolution at Yanou Lake of 150 years since c. 2000 cal. yr B.P. not being sufficient to capture these smaller scale climatic events and a higher resolution record is required.

The JRI ice core (Mulvaney *et al*., 2012) also recorded some evidence of colder conditions in the temperature anomaly data between c. 550 and 450 cal. yr B.P. which could relate to the LIA (Fig. 9.4.e). However, JRI showed a negative correlation with Fan Lake since c. 2000 cal. yr B.P., r = -0.47, $p = 0.031$ (Table 9.3), most likely due to Fan Lake not recording the recent warming seen in JRI since c. 600 cal. yr B.P. Alternatively, Yanou Lake showed no statistically significant relationship with JRI since c. 2000 cal. yr B.P., r = 0.27, $p = 0.692$ (Table 9.3), again likely due to the lack of recent warming in the Yanou Lake GDGT-temperature record.

It is difficult to say whether these Antarctic Peninsula records are representative of a wider Antarctic occurrence of the MCA and LIA. Firstly, there are few records that give late Holocene temperature reconstructions at high enough resolution to identify the presence or absence of these events across continental Antarctica for comparison. Secondly, it could be that the western Antarctic Peninsula and East Antarctica represented different climatic trends during the MCA and LIA, as seen in instrumental records over the last 50 years (Turner *et al*., 2005a). During this period the western Antarctic Peninsula has warmed rapidly while some areas of East Antarctica, both at the coast at Halley, Neumayer and Mawson and in central Antarctica at Amundsen-Scott, have cooled (Turner *et al*., 2005a). Therefore, if the western Antarctic Peninsula and East Antarctic were out of phase during the last 1000 years the MCA and LIA might not have been present in East Antarctica. The MCA and LIA, however, are well documented in South America in lake sediment records (e.g., Moy *et al*., 2008; Kastner *et al*., 2010) and marine records (e.g., Sepúlveda *et al*., 2009; Caniupán *et al*., 2014) and often associated with changes in El Niño Southern Oscillation (ENSO) activity and the position and / or strength of the SWW (e.g., Moy *et al*., 2008; Sepúlveda *et al*., 2009). This supports the theory that South Georgia, and potentially the SSI, were representing more hemispheric climate trends over the last 1000 years thus becoming decoupled with Antarctic trends (Chapter 7; Van Nieuwenhuyze *et al*., in prep).

Caniupán *et al*.'s (2014) alkenone SST data from between 50 and 53 °S reconstructed a c. 1 – 2 °C drop in temperature between c. 600 and 250 cal. yr B.P., consistent with the timing of the LIA, but showed no evidence of warming during the MCA (Fig. 9.4.a). The lack of the MCA warming might be why there is little correlation between Fan Lake and Canal Wide ($r = 0.23$, $p = 0.404$) but there was a significant positive correlation between Yanou Lake and Canal Wide since c. 2000 cal. yr B.P., $r = 0.62$, $p = 0.041$ (Table 9.3). The stronger relationship between Yanou Lake and Canal Wide is likely due to a less prominent MCA at Yanou Lake compared to Fan Lake. Also in Jacaf Fjord, 44 °S Sepúlveda *et al*. (2009) showed evidence of warmer and drier conditions during the MCA which terminated at c. 950 cal. yr B.P. and wetter and colder conditions between c. 450 and 250 cal. yr B.P. (Fig 9.4.b). As a result, Jacaf Fjord showed a strong and significant correlation with Fan Lake, $r = 0.55$, $p < 0.001$ since c. 2000 cal. yr B.P. (Table 9.3).

Increased precipitation during the LIA may be indicative of a northern location of the SWW, as this is the main source of precipitation in the region, which could also suggest

a period of high ENSO activity (Sepúlveda *et al*., 2009). On the other hand, weak ENSO variability is thought to have contributed to the changes in climate during the MCA (Rein *et al*., 2004; Sepúlveda *et al*., 2009). Further evidence of changes in the strength and position of the SWW as a causal factor of both the MCA and LIA was identified by Moy *et al*. (2008) and Kastner *et al*. (2010). Both Moy *et al*. (2008) and Kastner *et al*. (2010) reconstructed a period of aridity during the MCA suggesting a southern shift and decrease in SWW intensity. This is consistent with current understanding of the SWW, where a more southerly position is often related to warmer Antarctic Peninsula conditions, such as the mid-Holocene warm period and the MCA. Higher resolution pollen records in Fan Lake and a pollen record for Yanou Lake may help identify if there was increased intensity of the SWW during either the MCA or the LIA through the presence or absence of long distance pollen.

9.3.3. Recent Rapid Warming

The GDGT-derived summer temperature records from Fan Lake and Yanou Lake did not show evidence of the recent rapid warming seen over the last 50 years on the west Antarctic Peninsula (Turner *et al*., 2005a) and recorded in other Antarctic Peninsula temperature reconstructions such as the JRI ice core since c. 600 cal. yr B.P. (Mulvaney *et al*., 2012). As a result, both the Fan Lake and Yanou Lake temperature records have a negative correlation with JRI over the last 1000 years, $r = -0.69$, $p = 0.019$ and $r = -0.85$, $p = 0.033$ respectively. Nevertheless, although the Palmer Deep TEX_{86} temperature record (Shevenell *et al*., 2011) showed a recent increase in temperature over the last 100 years, the tight coupling of the TEX_{86} record and the Fan Lake and Yanou lake records prior to this warming meant they showed a positive correlation over the last 1000 years, particularly Fan Lake where $r = 0.69$, $p = 0.034$.

The absence of recent warming at Yanou Lake could be due to slower sediment accumulations rates meaning a lower resolution record. Therefore, the GDGT-temperature record might not be at high enough resolution to identify the full extent of the warming. Nonetheless, the surface sample, dated 2007 AD, should capture the warming but it reconstructed a c. 2.3 °C fall in temperature since c. 250 cal. yr B.P. It could be that errors in the age-depth model are contributing to the absence of the recent warming. However, there was tight coupling between the ages of the tephra layers in Yanou Lake and nearby Ardley Lake using independent age models (Roberts pers. comm.), thus providing confidence in the Yanou age-depth model. Moreover, the record

for the last 100 years in Fan Lake was at much higher resolution and well-dated, using ^{210}Pb dating, yet the GDGT-derived temperatures still showed no evidence of the recent rapid warming with a reduction in temperature reconstructed during this period.

Dating inaccuracies become more problematic when reconstructing small scale climatic changes. Uncertainties in the age-depth model for Yanou Lake were greater as it relies solely on radiocarbon ages, whereas ^{210}Pb and ^{137}Cs dating was also undertaken on the top 11 cm of the Fan Lake core (Strother *et al*., 2015), giving greater confidence, and reduced 95% error ranges, in the most recent part of the Fan Lake age-depth model. Moreover, although ice cores are often considered to be more accurately dated, through the counting of annual layers, the dating of the JRI ice core, which does exhibit the recent warming, was not based on layer counting and was grounded through correlating 14 tephra layers with radiocarbon dates of tephra deposits in regional lake and marine sediment cores (Mulvaney *et al*., 2012).

Another possible cause for the absence of recent warming in Fan Lake and Yanou Lake is that the GDGT-derived temperatures are a reconstruction of summer temperatures rather than the mean annual air temperatures as reconstructed in other records i.e. ice cores. Consequently, if the recent warming was equally spread throughout the year annual records may reflect a greater change than seasonal records. Moreover, if there was a winter bias in recent warming then the GDGT-derived summer temperatures may misrepresent this warming. Turner *et al*. (2005a) analysed regional Antarctic climate change for the last 50 years finding that on the west Antarctic Peninsula, although there was an annual increase in temperature, there was a bias towards winter warming. Moreover, Bellingshausen Station, King George Island, showed its greatest warming during the winter months (June – August), but there was still a small 0.30 ± 0.20 °C increase in summer temperatures, not evident in the Yanou Lake GDGT-temperature record (Table 1 Turner *et al*., 2005a). Due to an incomplete instrumental temperature record at Grytviken, South Georgia, during the 1980s and 1990s it was not possible to calculate whether the recent warming on South Georgia was seasonal in nature or an annual warming.

In Fan Lake, although temperature did not increase over the last 100 years an increase in primary productivity was seen as noted by Nieuwenhuyze *et al*. (in prep) through small increases in TOC, sediment accumulation rate and chlorophyll and carotenoid flux (Fig. 7.5). They interpret this as an indicator of warmer conditions yet this was not visible in

the GDGT-temperature record where the last 100 years showed some of the coldest summer temperatures at Fan Lake c. 3.7 °C (Fig. 9.2). Perhaps primary productivity increases prior to increased temperature. During the mid-Holocene warm period primary productivity in Fan Lake increased before temperature and again during the MCA (Fig. 7.5). This suggests that productivity may be more closely related to other climatic and environmental factors such as ice cover. Therefore, although air temperatures were warming, the greatest impact of recent climatic warming on lakes was as a result of changes in lake ice cover duration. Only once the ice free period reaches a critical length will lake temperatures increase. The relationship between productivity and temperature is discussed further in Section 9.3.4.

9.3.4. The relationship between productivity and temperature

In Chapter 7 a disparity between primary productivity proxies, i.e. diatom, carotenoid and chlorophyll flux, and GDGT-temperature was noted in Fan Lake at the beginning of the mid-Holocene warm period c. 4200 cal. yr B.P. (Section 7.5.2; Fig. 7.5). Primary productivity proxies increased c. 400 years before the main temperature increase at c. 3800 cal. yr B.P., by which time productivity was decreasing again (Fig. 7.5). The offset was attributed to a delay in temperature increase due to meltwater inputs from the catchment (Chapter 7). Similar patterns, but on a smaller scale, were also seen in Yanou Lake (Chapter 8; Section 8.5.2) during the mid-Holocene warm period however, in Yanou Lake there was limited evidence of any large meltwater inputs. In Yanou Lake carotenoid and chlorophyll fluxes showed a small increase prior to the mid-Holocene warming but, more interestingly, did not increase during the GDGT-temperature maximum (Fig. 8.4 & 8.5). The near absence of pigments during the mid-Holocene warm period in Yanou Lake was attributed to a reduction in lake level (Chapter 8; Section 8.5.2).

Primary productivity appears to be indirectly related to air temperature rather than water temperature in that, an increase in air temperature causes an increase in ice free conditions which increases light availability. For example, Karlsson *et al*. (2005) and Reuss *et al*. (2010) both showed that in sub-Arctic lakes the length of ice free conditions was a major control on primary production due to light and nutrient availability. However, as discussed in Chapter 7, increased air temperature in polar and sub-polar environments can lead to increased meltwater input into lakes, thus cooling water temperatures, meaning GDGT-derived temperatures are unlikely to increase.

Furthermore, a meltwater input has the potential to increase the supply of nutrients and ions from the catchment hence causing increased productivity, as seen in sub-Arctic lakes from northern Sweden by Reuss *et al*. (2010). All of these factors might provide an explanation as to why primary productivity in Fan Lake increased before lake temperature during the mid-Holocene warm period.

Although longer ice free conditions, thus an extended growth season, could explain the increased diatom, carotenoid and chlorophyll flux in Fan Lake at c. 4200 cal. yr B.P., both Fan and Yanou Lakes showed low carotenoid and chlorophyll flux during the peak GDGT-temperatures of the mid-Holocene warm period. One possible explanation is that temperatures had become sufficiently high that the lakes were annually ice free, thus light penetration within the lake would be at a maximum. In addition, increased evaporation, hence reduced lake levels, could have further increased light availability at the bed of the lakes. Although light is required for within-lake productivity, pigments are known to be highly sensitive to light degradation (Leavitt and Hodgson, 2001). Most pigment degradation occurs within the water column thus is controlled by the light availability at the lake bed (Leavitt and Hodgson, 2001). Increased light penetration could lead to increased pigment degradation as seen through an increase in unidentifiable pigments, particularly in Yanou Lake. Such increased light degradation could explain why carotenoid and chlorophyll flux decreased in Fan Lake and pigments were almost absent in Yanou Lake during the warmest part of the mid-Holocene.

Total organic content (TOC) is also often used as an indicator of productivity, and thus to indirectly infer temperature, in both lake cores (e.g., Rosén, 2005; Ji *et al*., 2005) and marine cores (e.g., Domack *et al*., 2003; Michalchuk *et al*., 2009). While in mid-low latitude settings TOC may be related to temperature, in Antarctic environments TOC is often more appropriately correlated to the extent or duration of ice cover (e.g., Shevenell *et al*., 1996; Hodgson *et al*., 2013). In Narrows Lake, Marguerite Bay, Hodgson *et al*. (2013) interpret high TOC (>7.5%) as an indicator of increased summer ice free conditions hence, increased within-lake productivity through an extended growth season. In Fan Lake TOC does not peak during the highest temperatures, and associated ice free conditions, of the mid-Holocene. Rather, the one peak in the record to 9.8% occurred at the end of the warm period at c. 3000 cal. yr B.P. Moreover, in Yanou Lake there was a weak but not statistically significant negative correlation between TOC and GDGT-temperature ($r = -0.25$, $p = 0.121$). Consequently, while there may be a relationship between TOC and ice free duration, there is no apparent

relationship between lake GDGT-derived temperature and TOC in Fan Lake or Yanou Lake. Therefore, to interpret TOC with regards to temperature, in particular in polar and sub-polar regions, the driver of ice free conditions must be established

9.5. Conclusions

A comparison of Fan Lake and Yanou Lake with other records from the Antarctic Peninsula, East Antarctica and Chile showed periods of coherence between records alongside periods of inconsistency. Comparing Fan Lake and Yanou Lake solely showed good correlation between the records after c. 3200 cal. yr B.P. The most notable difference between the two records was that the mid-Holocene warm period started c. 400 years earlier in Fan Lake. The later onset at Yanou Lake was possibly due to stormier conditions in the area perhaps as a result of a reduction in summer sea ice. The occurrence of the mid-Holocene warm period in Chilean records, alongside the presence of long distance pollen in lakes from South Georgia and the SSI, suggested a potential poleward shift in the SWW during the mid-Holocene warm period.

After the mid-Holocene warm period a general cooling of climates was evident in both the GDGT-temperature records and other previously published temperature reconstructions. During the last 1000 years two events noted in records from the Antarctic Peninsula and Chile, however not in East Antarctica, were the MCA and LIA. The warming of the MCA may be correlated to a poleward shift in the SWW as ENSO weakened, whereas, during the LIA SWW were likely to be in a more northerly position consistent with increased ENSO activity. The reconstructed changes in the SWW, shifting polewards during warmer periods and north during colder phases, agree with previous reconstructions and model simulations of the SWW.

Recent rapid warming, reconstructed in previously published temperature records from the Antarctic Peninsula, i.e. JRI and Lallemand Fjord, as well as in the instrumental records were not represented in the GDGT-temperature record from either Fan Lake or Yanou Lake. Although a higher resolution record may be required at Yanou Lake to see this warming, Fan Lake was a much higher resolution record of c. 20 years compared to c. 150 years at Yanou Lake. The instrumental record from Bellingshausen, King George Island, indicated a large winter component in recent warming, which may be misrepresented by the summer temperature reconstruction from the GDGT record. Due to missing data in the recent Grytviken temperature record the same cannot be said for South Georgia however, productivity did increase during the last 100 years at Fan Lake.

Productivity increased before temperature in both the Fan and Yanou Lake records, most notably prior to the mid-Holocene warm period in Fan Lake. It is likely that productivity was more closely related to ice cover hence the duration of the growth season. Ice free conditions and increased meltwater also allowed the input of nutrient and ions from the catchment, thus could further increase primary productivity. There was no statistically significant relationship found between TOC and temperature in Fan Lake or Yanou Lake, therefore, it appears that the driver of changes in ice extent is crucial. Consequently, the use of primary productivity proxies to indirectly infer temperature should be undertaken with great caution in polar and sub-polar environments.

Chapter 10: Conclusions

Summary

The major findings of this research are concluded in this chapter in terms of the research aims and objectives previously outlined in Chapter 1:

1. Develop the use of glycerol dialkyl glycerol tetraethers (GDGTs) as indicators of palaeotemperature in Antarctic lakes.
2. Reconstruct changes in mid-late Holocene temperatures in Antarctic lakes.
3. Compare records along the Polar Frontal Zone (PFZ) transect to reconstruct changes in the position of the PFZ during the Holocene and how variations in the PFZ relate to climatic changes.
4. Compare temperature records from Antarctic Lakes with indicators of primary productivity to identify if temperature is the main driver of primary productivity in these environments.

The potential for expanding the use of the Antarctic and sub-Antarctic GDGT-temperature calibration and other future research prospects are also considered.

10.1. Key Findings

10.1.1. Develop the use of glycerol dialkyl glycerol tetraethers (GDGTs) as indicators of palaeotemperature in Antarctic lakes

In Chapter 6, surface samples (top 0 – 2 cm) from 32 Antarctic, sub-Antarctic and Chilean lakes were used to investigate the environmental controls on branched GDGT (brGDGT) composition in these environments with a view to developing a GDGT-temperature calibration. The lakes were selected to give a sufficient range in temperature to enable a statistical assessment of the effects of temperature on brGDGT composition and statistical analysis identified mean summer air temperature (MSAT) as the primary environmental control on brGDGT composition. Best subsets regression selected a model with optimal predictive properties for MSAT using four brGDGT compounds, GDGT-Ib, GDGT-II, GDGT-III and GDGT-IIIb. These are the same three compounds as used in the Pearson *et al*. (2011) global brGDGT-temperature calibration for lakes, with the addition of GDGT-IIIb. The addition of this compound significantly improved the model's performance accounting for a statistically significant fraction of variance in temperature. This was one of the key discoveries of this research. Notably,

although previously identified in lacustrine brGDGT studies, this is the first time GDGT-IIIb has been incorporated into a calibration model further showing its importance in the Antarctic and sub-Antarctic environment, and potentially other cold environments.

10.1.2. Reconstruct changes in mid-late Holocene temperatures in Antarctic lakes

The first application of the Antarctic and sub-Antarctic GDGT-temperature calibration on a low resolution c. 4000 year record from Fan Lake was completed in Chapter 6 to assess its applicability downcore. Following this, the calibration was applied at higher resolution in Fan Lake in Chapter 7 and in Yanou Lake in Chapter 8. This application successfully provided the first mid-late Holocene quantitative temperature record from lake archives on South Georgia and the South Shetland Islands respectively. The temperature record from Fan Lake dates back to c. 4300 cal. yr B.P., prior to which the lake was heavily influenced by a deglaciating catchment, and in Yanou Lake to c. 6050 cal. yr B.P. Key warm periods, highlighted in previous research, such as the mid-Holocene warm period, were identified in both Fan Lake between c. 3800 and 3200 cal. yr B.P. and Yanou Lake between c. 3400 and 2700 cal. yr B.P. when reconstructed temperatures peaked at 14.0 °C and 13.8 °C respectively. In Fan Lake the GDGT-temperature record showed the mid-Holocene warm period to start later than the records of primary productivity would indicate. Closer analysis suggested that, a meltwater input may be affecting lake temperatures through an input of cold freshwater into the lake as air temperature increased (see Section 7.5.2 for details). Finally, temperatures of c. 14 °C during the mid-Holocene warm period appear high, especially in more southern Yanou Lake. However, with a persistent warming and a reduction in lake volume significant temperature increases could occur, as noted previously at Signy Island (see Section 8.5.2 for details).

The higher resolution record from Fan Lake allowed the identification of both the Medieval Climate Anomaly (MCA) and Little Ice Age (LIA) at c.1000 – 500 cal. yr B.P. and c. 300 – 100 cal. yr B.P. respectively. A peak in temperature in Yanou Lake was also noted at c. 740 cal. yr B.P., consistent with the timing of the MCA. Moreover, a reduction of c. 3 °C at c. 570 cal. yr B.P. may correlate with the LIA. Neither Fan Lake nor Yanou Lake reconstructed the recent rapid warming seen in other proxy records and instrumental data from the region over the last 100 years, despite the higher 15 year resolution surface core record from Fan Lake. This could again be linked to

meltwater inputs into the lake or a bias in warming which might not be reflected in the GDGT summer temperature record.

10.1.3. Compare records along the Polar Frontal Zone (PFZ) transect to reconstruct changes in the position of the PFZ during the Holocene and how variations in the PFZ relate to climatic changes

A comparison of Fan Lake and Yanou Lake with other records from Antarctica and Chile was made in Chapter 9. The comparison between the Fan Lake and Yanou Lake records indicated that the most significant difference between the records was the timing of the mid-Holocene warm period, which commenced c. 400 years later in Yanou Lake. The later onset at Yanou Lake was possibly due to stormier conditions in the area as a result of a reduction in summer sea ice.

Focusing on the strength and position of the PFZ during the mid-late Holocene the records suggest that during warmer periods the core of the PFZ shifts polewards and during colder periods it lies in a more northerly position. Whether this is a shift of the whole PFZ or purely a shift in intensity cannot be differentiated. Evidence supporting the theory of a poleward shift in the PFZ was first seen in the mid-late Holocene, identified through the presence of the mid-Holocene warm period in some Chilean records alongside Antarctic records. Further evidence for this poleward shift was also indicated through the presence of long distance pollen in lakes from South Georgia and the South Shetland Islands. Furthermore, the close relationship between Fan Lake and the Chilean palaeoclimate records over the last 1000 years suggests that the PFZ may be located in a more southerly location causing a climatic barrier between South Georgia and continental Antarctica.

10.1.4. Comparison of temperature records from Antarctic Lakes with indicators of primary productivity: is temperature the main driver of primary productivity in these environments?

Primary productivity indicators and the GDGT-temperature record for both Fan Lake and Yanou Lake were compared in Chapter 9. In both records productivity can be seen to increase prior to the mid-Holocene warm period, most notably in Fan Lake. This suggests that in Fan Lake and Yanou Lake, and perhaps other Antarctic lakes, lake temperature may not be the main driver of primary production. Primary productivity could be more closely related to ice cover, hence the duration of the growth season. Ice

free conditions and increased meltwater also allowed the input of nutrients and ions from the catchment, thus further increasing productivity. Notably, no statistical significant relationship was found between total organic carbon (TOC) and GDGT-derived temperature in Fan Lake or Yanou Lake therefore, caution must be taken when using TOC as a proxy for temperature in these environments.

10.2. Wider implications and Future Research

10.2.1. Implications of GDGT-IIIb

The development of the Antarctic and sub-Antarctic GDGT-temperature model was the first GDGT-temperature model for lacustrine environments to incorporate samples from below 1.5 °C. The relationship between GDGT-IIIb and MSAT in these cold environments should be further investigated. Two focuses for further research into GDGT-IIIb should consider; (1) if the relationship between GDGT-IIIb and MSAT, seen in Antarctic and sub-Antarctic lakes, holds true in other cold environments including the Arctic and high altitude settings; (2) if there is a cut-off temperature below which GDGT-IIIb is no longer produced, as suggested in the Antarctic dataset. One way to assess both of these points would be to collect surface sediments from Arctic lakes, in particular focusing on areas where MSAT is below c. 3 °C and analyse the distribution of GDGT-IIIb in these lakes and its relationship with MSAT. Finally, an extension of the Antarctic dataset to include more 'cold' sites would also help identify if there is a cut-off temperature below which GDGT-IIIb is not produced.

10.2.2. Further downcore application of the Antarctic and sub-Antarctic GDGT-temperature model

The development of the Antarctic and sub-Antarctic GDGT-temperature model has unlocked the potential to reconstruct temperature in Antarctica quantitatively without the complicating factors of changing ocean currents (which limit the application of marine-based palaeothermometry) and high altitudes (which affect most ice core reconstructions). Further application of this calibration model will enable more palaeotemperature reconstructions to be made.

The application of the GDGT-temperature calibration model in other lakes from Antarctica would provide a greater insight into Holocene temperature changes in Antarctica. Applying the calibration downcore in one of the Beak Island lakes, perhaps Beak 2, or lakes from Signy Island, would be of particular interest as it would give an

insight into cross peninsula variations throughout the Holocene, which are not potentially confounded by the comparison of two different types of record i.e. comparing lake cores and ice cores, or any proxy bias.

Finally, although the Antarctic and sub-Antarctic GDGT-temperature model has currently only been applied in Antarctic and sub-Antarctic environments, it may be applicable in other cold environments, such as the Arctic or high altitude lakes.

10.2.3. Further research within the region of the Polar Frontal Zone

In addition to further GDGT-temperature reconstructions in lakes from the region, as discussed above, palynological analysis of lakes from the South Shetland Islands, such as Yanou, will further the current knowledge regarding the strength of the southern westerly winds. This is of particular interest during the mid-Holocene warm period to help better understand the position of the PFZ during these warmer conditions.

Appendix A: Environmental and Water Chemistry Data for all Antarctic and sub-Antarctic Lake Studied

Lake Name	Region	Latitude (°)	Longitude (°)	Elevation (m)	Depth (m)	MAAT (°C)	MSAT (°C)	pH	Cond (mS/cm)	Source
Cannonball	Alexander Island	-71.783	-68.250	98.0	5.6	-4.9	0.3	6.67	0.058	BAS field report (2001)
AB1	Campbell Island	-52.587	169.188	268.0	0.9	4.8	7.0	4.46	0.117	NZ Government (2013) & Saunders *et al.* (2015)
FR2	Campbell Island	-52.412	169.154	300.0	1.2	4.5	6.7	4.68	0.283	NZ Government (2013) & Saunders *et al.* (2015)
HO2	Campbell Island	-52.572	169.190	379.0	0.9	3.8	6.0	5.03	0.266	NZ Government (2013) & Saunders *et al.* (2015)
NE2	Campbell Island	-52.513	169.178	377.0	1.0	3.8	6.0	5.07	0.287	NZ Government (2013) & Saunders *et al.* (2015)
Ardley	Fildes Peninsula	-62.213	-58.939	18.0	6.1	-2.4	1.1	7.71	0.013	BAS field report (2008) & Watcham *et al.* (2011)
Belen	Fildes Peninsula	-62.229	-58.982	19.9	7.0	-2.4	1.1	7.72	0.081	BAS field report (2008) & Watcham *et al.* (2011)
Gaoshan	Fildes Peninsula	-62.221	-58.965	34.5	7.0	-2.5	1.0	8.07	0.074	BAS field report (2008) & Watcham *et al.* (2011)
Long	Fildes Peninsula	-62.205	-58.967	15.0	5.6	-2.4	1.1	8.05	0.177	BAS field report (2008) & Watcham *et al.* (2011)
Yanou	Fildes Peninsula	-62.221	-58.960	14.5	5.3	-2.4	1.1	7.53	0.094	BAS field report (2008) & Watcham *et al.* (2011)
Heart	Larsemann Hills	69.400	-76.383	5.0	4.5	-11.2	-1.6	6.30	1.649	Hodgson *et al.* (2001) & Verleyen *et al.* (2003)
Progress	Larsemann Hills	69.383	-76.400	65.0	38.0	-11.8	-2.2	6.70	0.261	Hodgson *et al.* (2001; 2005; 2006), Verleyen *et al.* (2003) & Sabbe *et al.* (2004)
Pup Lagoon	Larsemann Hills	69.408	-76.050	5.0	4.6	-11.2	-1.6	6.40	0.985	Hodgson *et al.* (2001) & Verleyen *et al.* (2003)
Reid	Larsemann Hills	69.385	-76.375	30.0	3.8	-11.5	-1.9	7.10	7.380	Hodgson *et al.* (2005)
Narrows Lake	Marguerite Bay	-67.601	-67.207	19.4	6.1	-4.5	0.7	6.54	0.131	BAS field report (2003) & Bentley *et al.* (2005)
MI10	Marion Island	-46.8623	37.8481	95.0	0.9	4.6	6.7	6.46	0.064	Ghent University field report (2011)
MI4	Marion Island	-46.8610	37.8469	71.0	1.0	4.8	6.8	7.85	0.061	Ghent University field report (2011)
MI7	Marion Island	-46.8623	37.8457	98.0	1.0	4.6	6.7	6.71	0.069	Ghent University field report (2011)
GPS15	Potter Peninsula	-62.241	-58.678	21.0	2.2	-1.8	1.1	6.40	0.050	Pearson (Pers. Comm.) & Roberts (Pers. Comm.)
Matias	Potter Peninsula	-62.245	-58.664	35.0	5.6	-1.9	1.0	6.17	0.050	Pearson (Pers. Comm.) & Roberts (Pers. Comm.)
Fan	South Georgia	-54.497	-37.053	94.0	18.0	1.6	4.4	8.07	0.038	BAS field report (2005), Hodgson (2009) & Pearson *et al.* (2011)
Lago Bulnes	Southern Chile	-53.603	-70.952	3.0	17.0	6.1	10.3	8.64	0.301	BAS field report (2008)
Laguna Pato	Southern Chile	-51.300	-72.679	50.0	4.4	5.8	10.0	8.81	0.246	BAS field report (2008) & Pearson *et al.* (2011)
Mago Ike	Syowa Oasis	-69.474	39.612	5.0	5.8	-10.7	-2.0	8.95	0.484	BAS field report (2007) & Kimura *et al.* (2010)
West Ongul 2	Syowa Oasis	-69.025	39.568	0.1	2.2	-10.7	-2.0	7.78	0.451	BAS field report (2007)
Higashi-ura Ike (WO6)	Syowa Oasis	-69.034	39.520	-10.0	5.0	-10.6	-1.9	7.64	0.668	BAS field report (2007)
Nishi Ike (WO8)	Syowa Oasis	-69.031	39.514	-4.0	6.0	-10.6	-1.9	7.76	0.273	BAS field report (2007)
Beak 1	Trinity Penisula	-63.611	-57.339	11.0	24.0	-5.2	0.3	7.37	0.172	BAS field report (2006) & Roberts *et al.* (2011)
Beak 2	Trinity Penisula	-63.614	-57.354	2.5	4.0	-5.1	0.4	8.60	0.188	BAS field report (2006), Roberts *et al.* (2011) & Sterken *et al.* (2012)
Beak 4	Trinity Penisula	-63.613	-57.365	6.0	0.5	-5.2	0.3	9.80	0.470	BAS field report (2006) & Sterken *et al.* (2012)
Viewpoint 7	Trinity Penisula	-63.552	-57.410	134.0	15.0	-5.9	-0.4	8.15	0.035	BAS field report (2006)

Appendix B: Different GDGT Extraction Methods Used in Previous Studies

Study	Aliquot Size (g)	Sediment preparation	Extraction method and solvent used	Column and solvent used	Final dilution solvent	Filter size (µm)	Standard used
Hopmans *et al*., 2000		Freeze-dried	Ultrasonic, 3 times with DCM:MeOH (1:1) and 3 times with DCM		Hexane:IPA (99:1)	0.45	
Schouten *et al*., 2000	1 – 5	Freeze-dried	Ultrasonic, 3 times with 5ml MeOH and 3 times with 5ml DCM:MeOH (1:1)		Hexane:IPA (99:1)	0.45	
Schouten *et al*., 2002		Freeze-dried	Ultrasonic, 3 times with MeOH for 1 minute and 3 times with DCM:MeOH (1:1) for 1 minute	Al_2O_3 (DCM: MeOH 1:1)	Hexane:IPA (99:1)	0.45	
Sinninghe Damsté *et al*., 2002			Soxhlet DCM:MeOH (9:1)	Al_2O_3 (DCM: MeOH 1:1)	Hexane:IPA (99:1)	0.45	
Hopmans *et al*., 2004			Ultrasonic, 3 times with DCM:MeOH (1:1) and 3 times with DCM	Al_2O_3 (DCM: MeOH 1:1)	Hexane:IPA (99:1)	0.45	
Powers *et al*., 2004	5 – 10	Freeze-dried Homogenised	Soxhlet DCM:MeOH (2:1)	Al_2O_3 (DCM: MeOH 1:1)	Hexane:IPA (99:1)		
Powers *et al*., 2005	1 – 3	Freeze-dried Homogenised	Soxhlet or ASE DCM:MeOH (2:1)	Al_2O_3 (DCM: MeOH 1:1)	Hexane:IPA (99:1)		
Weijers *et al*., 2006b		Freeze-dried	ASE DCM: MeOH (9:1) Flushed 3 times at 5 minute intervals 100°C and $7.6x10^6$ Pa	Al_2O_3 (DCM: MeOH 1:1)	Hexane:IPA (99:1)	0.45	
Weijers *et al*., 2007a		Freeze-dried Homogenised	ASE DCM: MeOH (9:1) Flushed 3 times at 5 minute intervals 100°C and $7.6x10^6$ Pa	Al_2O_3 (DCM: MeOH 1:1)	Hexane:IPA (99:1)	0.45	
Blaga *et al*., 2009	1.5 – 2	Freeze-dried Homogenised	Ultrasonic, 3 times with DCM:MeOH and 3 times with DCM followed by ASE DCM: MeOH (9:1) Flushed 3 times at 5 minute intervals 120°C and $7.6x10^6$ Pa	Na_2SO_4 (DCM: MeOH 1:1)	Hexane:IPA (99:1)	0.45	
Tierney and Russell, 2009		Freeze-dried Homogenised	ASE DCM: MeOH (9:1)	Al_2O_3 (DCM: MeOH 1:1)	Hexane:IPA (99:1)	0.45	C_{46}
Bechtel *et al*., 2010	2 – 6		MAE at 70°C for 7 minutes DCM: MeOH (9:1)		Hexane:IPA (99:1)	0.45	C_{46}
Blaga *et al*., 2010			ASE DCM: MeOH (9:1) Flushed 3 times at 5 minute intervals 100°C and $7.6x10^6$ Pa	Al_2O_3 (DCM: MeOH 1:1)	Hexane:IPA (99:1)	0.45	
Kim *et al*., 2010	1 – 5	Freeze-dried Homogenised	ASE DCM: MeOH (9:1) 120°C and $7.6x10^6$ Pa	Al_2O_3 (DCM: MeOH 1:1)	Hexane:IPA (99:1)	0.4	
Powers *et al*., 2010	1 – 5	Freeze-dried Homogenised	Soxhlet or ASE DCM:MeOH (2:1)	Al_2O_3 (DCM: MeOH 1:1)	Hexane:IPA (99:1)	0.4	
Loomis *et al*., 2011			ASE DCM: MeOH (9:1)	Al_2O_3 (DCM: MeOH 1:1)	Hexane:IPA (99:1)		C_{46}

Pearson *et al*., 2011	0.1 – 2		MAE temperature ramps to 70°C in 2 minutes and holds at 70°C for 5 minutes 15ml DCM:MeOH (3:1) Samples are also saponified in 6% KOH:Hexane		Hexane:IPA (99:1)	0.45	
Sun *et al*., 2011		Freeze-dried Homogenised	ASE DCM: MeOH (9:1) Flushed 3 times at 5 minute intervals 100°C and $7.6x10^6$ Pa	Al_2O_3 (DCM: MeOH 1:1)	Hexane:Propanol (98:2)	0.45	
Zink *et al*., 2011			ASE DCM: MeOH (1:1) Flushed 2 times 65°C and 50 bar	Al_2O_3 (DCM: MeOH 1:1)	Hexane:IPA (99:1)	0.45	
Loomis *et al*., 2012	0.02 – 2.2	Freeze-dried Homogenised	ASE DCM: MeOH (9:1)				C_{46}
Sinninghe Damsté *et al*., 2012	1 – 3	Freeze-dried Homogenised	ASE				
Shanahan *et al*., 2013	1 – 5	Freeze-dried	ASE DCM: MeOH (9:1)		Hexane:IPA (99:1)		
Woltering *et al*., 2014	1 – 5	Freeze-dried	ASE DCM: MeOH (9:1)	Al_2O_3 (DCM: MeOH 1:1)	Hexane:IPA (99:1)	0.45	

MAE – Microwave Assisted Extraction ASE – Accelerated Solvent Extraction
DCM – Dichloromethane MeOH – Methanol IPA – Isopropanol

Appendix C: The Affinity and Interpretation of different Lacustrine Pigments

Affinity	Pigment	Reference
Plantae	Chlorophyll *a*	Leavitt, 1993; Leavitt and Hodgson, 2001; Mikomägi and Punning, 2007
	Chlorophyll *b*	Leavitt and Hodgson, 2001
	Lutein	Leavitt and Hodgson, 2001; Mikomägi and Punning, 2007
	β, β-carotene	Leavitt, 1993; Leavitt and Hodgson, 2001; Buchaca and Catalan, 2007; Mikomägi and Punning, 2007
Photosynthetic algae	Chlorophyll *a*	Verleyen *et al.*, 2004; Hodgson *et al.*, 2003; 2005
Macrophytes	Chlorophyll *a*	Waters *et al.*, 2010
	Chlorophyll *b*	Waters *et al.*, 2010
	Lutein	Waters *et al.*, 2010
Chrysophytes – golden algae	Chlorophyll *b*	Leavitt, 1993
	Fucoxanthin	Leavitt, 1993, Leavitt *et al.*, 1999; Leavitt and Hodgson, 2001; Hodgson *et al.*, 2003; 2005; Verleyen *et al.*, 2004; Buchaca and Catalan, 2007; Waters *et al.*, 2010; Huguet *et al.*, 2011; Sterken *et al.*, 2012
	Diadinoxanthin	Buchaca and Catalan, 2007
	Myxoxanthin	Hodgson *et al.*, 2005; Mikomägi and Punning, 2007
	Diatoxanthin	Leavitt and Hodgson, 2001; Hodgson *et al.*, 2003; 2005; Verleyen *et al.*, 2004; Buchaca and Catalan, 2007; Mikomägi and Punning, 2007; Matsumoto *et al.*, 2010
Pyrrophyta	Chlorophyll *b*	Leavitt, 1993
Chlorophyta - green algae	Chlorophyll *b*	Leavitt and Hodgson, 2001; Hodgson *et al.*, 2003; 2005; 2006; Verleyen *et al.*, 2004; Waters *et al.*, 2010
	Antheraxanthin	Hodgson *et al.*, 2005
	Zeaxanthin	Verleyen *et al.*, 2004; Hodgson *et al.*, 2005; 2006; Buchaca and Catalan, 2007; Matsumoto *et al.*, 2010
	Lutein	Leavitt, 1993; Leavitt and Hodgson, 2001; Verleyen *et al.*, 2004; Hodgson *et al.*, 2003; 2005; Buchaca and Catalan, 2007; Mikomägi and Punning, 2007; Waters *et al.*, 2010
	β, β-carotene	Hodgson *et al.*, 2003; Verleyen *et al.*, 2004; Hodgson *et al.*, 2005; Sterken *et al.*, 2012
	Fucoxanthin	Matsumoto *et al.*, 2010
	Violaxanthin	Wright and Jeffery, 2006
	Diatoxanthin	Matsumoto *et al.*, 2010
Euglenophyta	Chlorophyll *b*	Leavitt and Hodgson, 2001; Verleyen *et al.*, 2004
Bacillariophyta - Diatoms	Chlorophyllide *a*	Leavitt, 1993; Buchaca and Catalan, 2007
	Pheophorbide *a*	Leavitt, 1993; Verleyen *et al.*, 2004; Hodgson *et al.*, 2003; 2005
	Chlorophyll *c*2	Hodgson *et al.*, 2005

Bacillariophyta - Diatoms (cont.)	Fucoxanthin	Leavitt, 1993, Hodgson *et al.,* 1997; Leavitt *et al.,* 1999; Leavitt and Hodgson, 2001; Hodgson *et al.,* 2003; 2005; Verleyen *et al.,* 2004; Reuss and Conley, 2005; Buchaca and Catalan, 2007; Matsumoto *et al.,* 2010; Waters *et al.,* 2010; Huguet *et al.,* 2011; Sterken *et al.,* 2012
	Diatoxanthin	Leavitt *et al.,* 1999; Leavitt and Hodgson, 2001; Hodgson *et al.,* 2003*;* 2005; Verleyen *et al.,* 2004; Reuss and Conley, 2005; Buchaca and Catalan, 2007; Mikomägi and Punning, 2007; Matsumoto *et al.,* 2010; Waters *et al.,* 2010
	Diadinoxanthin	Leavitt, 1993; Buchaca and Catalan, 2007
	Zeaxanthin	Buchaca and Catalan, 2007
Cyanophyta – cyanobacteria	Scytonemin reduced	Hodgson *et al.,* 2005
	Scytonemin	Leavitt and Hodgson, 2001; Verleyen *et al.,* 2004; Hodgson *et al.,* 2005; Fulton *et al.,* 2012
	Fucoxanthin	Waters *et al.,* 2010
	Myxoxanthin	Leavitt, 1993; Leavitt and Hodgson, 2001; Verleyen *et al.,* 2004; Buchaca and Catalan, 2007; Waters *et al.,* 2010
	Diatoxanthin	Matsumoto *et al.,* 2010
	Zeaxanthin	Leavitt, 1993; Leavitt and Hodgson, 2001; Verleyen *et al.,* 2004; Hodgson *et al.,* 2005; 2006; Buchaca and Catalan, 2007; Mikomägi and Punning, 2007; Matsumoto *et al.,* 2010; Waters *et al.,* 2010
	Canthaxanthin	Leavitt, 1993; Leavitt and Hodgson, 2001; Verleyen *et al.,* 2004; Hodgson *et al.,* 2005; Buchaca and Catalan, 2007; Waters *et al.,* 2010
	Echinenone	Leavitt, 1993; Leavitt and Hodgson, 2001; Verleyen *et al.,* 2004; Hodgson *et al.,* 2005; 2006; Buchaca and Catalan, 2007; Mikomägi and Punning, 2007; Waters *et al.,* 2010
	β, β-carotene	Hodgson *et al.,* 2005; Buchaca and Catalan, 2007; Sterken *et al.,* 2012
UV radiation	Scytonemin	Sabbe *et al.,* 2004; Verleyen *et al.,* 2004; 2005; Hodgson *et al.,* 2005*;* 2006a; Buchaca and Catalan, 2007
Some *Dinophyta* - Dinoflagellates	Fucoxanthin	Leavitt *et al.,* 1999; Leavitt and Hodgson, 2001; Reuss and Conley, 2005; Matsumoto *et al.,* 2010; Waters *et al.,* 2010
	Dinoxanthin	Leavitt and Hodgson, 2001; Verleyen *et al.,* 2004
	Diatoxanthin	Leavitt and Hodgson, 2001; Hodgson *et al.,* 2003; 2005; Verleyen *et al.,* 2004; Reuss and Conley, 2005; Mikomägi and Punning, 2007; Matsumoto *et al.,* 2010
Chromophtye algae - Brown seaweeds	Chlorophyll *c*2	Hodgson *et al.,* 2003
	β, β-carotene	Hodgson *et al.,* 2003; 2005; Verleyen *et al.,* 2004
Prymnesiophytes - Haptophytes	Diatoxanthin	Hodgson *et al.,* 2003; Verleyen *et al.,* 2004
	Fucoxanthin	Hodgson *et al.,* 2003; Verleyen *et al.,* 2004; Huguet *et al.,* 2011
Raphidophytes	Fucoxanthin	Hodgson *et al.,* 2003; Verleyen *et al.,* 2004
Chromatiaceae - purple sulphur bacteria	Okenone	Leavitt, 1993; Vincent *et al.,* 1993; Buchaca and Catalan, 2007

Oscillatoriaceae	Oscillaxanthin	Leavitt, 1993; Leavitt *et al*., 1999
Zooplankton - crustacean	Astaxanthin	Buchaca and Catalan, 2007
	Canthaxanthin	Buchaca and Catalan, 2007
	Echinenone	Buchaca and Catalan, 2007
Mosses	Chlorophyll *b*	Hodgson *et al.*, 2005; 2006a
	Zeaxanthin	Hodgson *et al.*, 2006a
	Lutein	Hodgson *et al.*, 2006a
Euglenophytes	Lutein	Leavitt, 1993; Leavitt and Hodgson, 2001; Mikomägi and Punning, 2007
Tracheophytes	Lutein	Leavitt, 1993
Red seaweeds	Lutein	Hodgson *et al.*, 2003
Herbivore tissues	Canthaxanthin	Leavitt, 1993; Leavitt and Hodgson, 2001; Verleyen *et al.*, 2004; Hodgson *et al.*, 2005

Environmental Interpretation	**Pigments**	**References**
Relative production	Chlorophyll *a*	Hodgson *et al.*, 2003; 2005
	β, β-carotene	Hodgson *et al.*, 2003; 2005; Reuss and Conley, 2005
Total algal abundance	Chlorophyll *a*	Reuss and Conley, 2005; Mikomägi and Punning, 2007
	Pheophytin *a*	Reuss and Conley, 2005; Mikomägi and Punning, 2007
	β, β-carotene	Hodgson *et al.*, 2003; 2005; Reuss and Conley, 2005; Mikomägi and Punning, 2007
Preservation	Chlorophyll *a*	Buchaca and Catalan, 2007
Oxygenic photoautotroph	Pheophorbide *a*	Squier *et al.*, 2002
	Pheophytin *a*	Squier *et al.*, 2002
lake eutrophication	Pheophytin *a*	Mikomägi and Punning, 2007
	Alloxanthin	Mikomägi and Punning, 2007
	Lutein	Mikomägi and Punning, 2007
	Zeaxanthin	Mikomägi and Punning, 2007
	Myxoxanthin	Mikomägi and Punning, 2007
Photoprotective pigment	Violaxanthin	Wright and Jeffery, 2006
	Antheraxanthin	Wright and Jeffery, 2006
	Diatoxanthin	Wright and Jeffery, 2006
	Zeaxanthin	Leavitt, 1993; Wright and Jeffery, 2006
Photosynthetic	Lutein	Matsumoto *et al.*, 2010
	Chlorophyll *a*	Verleyen *et al.*, 2004; Hodgson *et al.*, 2003; 2005
	Scytonemin	Buchaca and Catalan, 2007
	Okenone	Buchaca and Catalan, 2007
Animal-specific pigment	Canthaxanthin	Leavitt, 1993
Positive relationship with lake depth	Canthaxanthin	Buchaca and Catalan, 2007
	Echinenone	Buchaca and Catalan, 2007

Appendix D: Previous Analysis Undertaken on the Fan and Yanou Lake Sediment Cores

Sedimentological and chronological analysis had previously been carried out on the sediment cores from both Fan Lake and Yanou Lake. Some details regarding the analysis of Yanou Lake have previously been published by Watcham *et al*. (2011) and of Fan Lake by Strother *et al*. (2015). The XRF scanning method outlined here is currently unpublished but is included within this thesis with permission (Roberts pers. comm.).

Prior to chronological analysis, or the application of any other destructive analytical techniques, Fan Lake and Yanou Lake sediment cores were X-rayed at NDT Services (East Midlands Airport). These images allowed a contrast between organic and minerogenic sediments to be seen. X-ray images of the frozen cores were taken at 70 kV, with a 30 second exposure to radiation at 10 mA.

Munsell colour charts were used as part of a detailed core log of changes in sediment colour. GEOTEK core logging was also undertaken at 2 mm intervals. Both whole core gamma (bulk) density (2 mm aperture gamma ray attenuation sensor) and magnetic susceptibility (MS) (Barrington Instruments MS2G loop sensor (1 cm sensor, 10 second measurement time) were recorded using the standard calibration procedures of GeoTek (2000) and Gunn and Best (1998).

Micro-XRF (μ-XRF) geochemical core scanning using the ITRAX scanner at Aberystwyth University was undertaken by Stephen Roberts. Scanning was completed in 2008 on defrosted intact half cores using a Molybedenum (Mo) anode X-ray, tube, settings: 30kV, 50 mA, count time 10 seconds at 1 or 2 mm intervals. During scanning, digital X-ray images were taken using the ITRAX radiographic imaging system (50 kV, 50 mA, 200 ms). The cores were re-scanned, again by Stephen Roberts, in 2011 at 100 or 200μm intervals with both Mo and Chromium (Cr) tubes to give a more detailed analysis of finely laminated core sections. Mo settings: as previously and Cr settings: 40 kV, 40 mA, count time 10 seconds.

Results for the Mo-tube were calculated as measurable element counts per second data (cps) normalised by total scatter counts (incoherent+coherent) and given as a percentage of total normalised element and scatter counts per second (cps) thus accounting for closed-sum effects and downcore changes in organic and water content (Kylander *et al*.,

2011; Löwemark *et al*., 2012; Davies *et al*., 2015; Roberts pers. comm.). Only through scatter-normalisation can a fair comparison be made between wet sediment μ-XRF scan data and standard whole-rock composition μ-XRF data, where water and carbon were removed prior to analysis (Roberts pers. comm.). Here scan data were not calibrated by subsample analysis as interest in both cores focused on wet, and sometimes, organic-rich material. Data are given as a percentage of measureable elements, not whole rock equivalents (Roberts pers. comm.). The Statistical analysis used to interpret the ITRAX scan data are outlined in Section 5.6.2.

Existing particle size analysis undertaken at Durham University was also made available and is used with permission (Watcham *et al*., 2011; Roberts pers. comm.). Particle sizes of the <2 mm (sand–silt–clay) fraction were determined at 4 or 8 cm intervals for Fan Lake and at 1 cm intervals for Yanou Lake using a Coulter Particle Size Analyser LS230 (range 0.4 μm–2 mm). Grain size distributions were modelled using the Fraunhofer model and Udden–Wentworth geometric grain size divisions of Tucker (1981), interpolated with v. 3.01 of the Coulter LS Control software. Further statistical analysis was undertaken using GRADISTAT v5 (Blott and Pye, 2001; Roberts pers. comm.). Finally, the >8 mm fraction was used to determine changes in the coarse-fraction provenance following Roberts *et al*. (2008).

Loss on ignition (LOI) for Yanou Lake at 1 cm intervals was undertaken by Watcham *et al*. (2011). One dry porcelain crucible per sample was weighed and the dried sediment sample added to the crucible. The dry weight of each sample was calculated. Crucibles were heated to 550 °C in a furnace then held at 550 °C for 2 hours to estimate changes in organic carbon. Once cooled samples were re-weighed and the LOI calculated as a percentage of the original pre-combustion dry weight using the following equation:

$$LOI_{550} = ((DW_{150} - DW_{550}) / DW_{150}) \times 100$$

where DW_{150} (in grams) is the pre-combustion weight and DW_{550} (in grams) the post-combustion weight. Samples were further heated the samples to 950 °C for 4 hours to estimate change in carbonate. The same methodology was followed by Van Nieuwenhuyze *et al*. (in prep) for Fan Lake at 1 cm intervals.

Carbon and nitrogen isotope analysis, undertaken at NIGL for both cores, is used with permission (Roberts pers. comm.). Freeze-dried, hand-crushed and homogenised samples were treated in 5% HCl for 24 hours prior to analysis. Samples were then

washed and dried to remove any carbonate. A Carlo Erba 1500 on-line to a VG Triple Trap and Optima dual-inlet mass spectrometer was used to determine total organic carbon (TOC), total nitrogen (TN) and bulk organic carbon isotopic ratios ($\delta^{13}C_{org}$). Finally, $\delta^{13}C_{org}$ values were calculated to the VPDB scale using a within-run laboratory standard calibrated against NBS-19 and NBS-22. Replicates were run and gave a precision of ± 0.1 (per mil) for $\delta^{13}C_{org}$ and 10% for C/N.

Existing chronological data, for both Fan Lake and Yanou Lake cores, was made available (Roberts pers. comm.). Lead-210 (^{210}Pb) and Ceasium-137 (^{137}Cs) dating was undertaken on dried and homogenised samples from the Fan Lake core as detailed in Strother *et al*. (2015). Prior to analysis, samples were stood for at least 21 days so ^{226}Ra and ^{214}Pb could reach equilibrium. Measurements were taken using an Ortec J-shape ultra-low background germanium well detector with remote preamplifier. Appleby's (2001) standard analytical and modelling procedures were followed. Unsupported ^{210}Pb age estimates were derived from both the constant initial concentration (CIC) and constant rate of supply (CRS) method (Appleby and Oldfield, 1978) (Table 1; Strother *et al*. 2015).

Radiocarbon dating via Accelerator Mass Spectrometry (AMS) was undertaken on both cores. Radiocarbon ages were calibrated in OXCAL (version 4.2; Bronk-Ramsey, 2009) using the SHCal13 Southern Hemisphere calibration curve (Hogg *et al*., 2013). Post-bomb samples were corrected using $^{13}C/^{12}C$ isotopic ratios from a measured percentage of modern carbon (pMC) to calculate the absolute pMC, where 'modern' pMC (1950 AD) is 100% and 2010 AD pMC is 107.5% (Roberts, pers. comm.). Calibration was achieved using the SHCal13 SH Zone 1 – 2 Bomb curve in CALIBomb (Hua *et al*., 2013; Reimer and Reimer, 2004). Radiocarbon ages were rounded to the nearest five years.

Radiocarbon, and for Fan Lake ^{210}Pb, ages were used to generate a master age-depth model in BACON v.2.2 (Bayesian) age-depth modelling software in R v3.1 (Blaauw, 2010; Blaauw and Christen, 2011; Strother *et al*., 2015; Roberts pers. comm.). The BACON age-depth model allowed ages to be interpolated from the best-fit age. For Fan Lake, outside of the ^{210}Pb data, ages were rounded to 10 years or 50 years after c. 3000 years to give a fair reflection of the 95% confidence interval (Roberts pers. comm.). For Yanou Lake, ages were rounded to the nearest 10 years or 50 years after c. 1000 years.

References

Abbott, M. R., Richman, J. G., Nahorniak, J. S. and Barksdale, B. S. 2001. Meanders in the Antarctic polar frontal zone and their impact on phytoplankton. *Deep-Sea Research Part Ii-Topical Studies in Oceanography.* 48 (19–20) 3891–3912. DOI:10.1016/S0967-0645(01)00073-X.

Abram, N. J., Mulvaney, R., Vimeux, F., Phipps, S. J., Turner, J. and England, M. H. 2014. Evolution of the Southern Annular Mode during the past millennium. *Nature Climate Change*. 4 (7) 564–569. DOI:10.1038/nclimate2235.

Adams, M. S., Guilizzoni, P. and Adams, S. 1978. Sedimentary pigments and recent primary productivity in northern Italian lakes. *Mem. Ist. Ital. Idrobiol*. 36, 267–285.

Ajioka, T., Yamamoto, M. and Murase, J. 2014. Branched and isoprenoid glycerol dialkyl glycerol tetraethers in soils and lake/river sediments in Lake Biwa basin and implications for MBT/CBT proxies. *Organic Geochemistry*. 73, 70–82. DOI:10.1016/j.orggeochem.2014.05.009.

Anderson, L., Abbott, M. B., Finney, B. P. 2001. Holocene climate inferred from oxygen isotope ratios in lake sediments, central Brooks Range, Alaska. *Quaternary Research*. 55, 313–321. DOI:10.1006/qres.2001.2219.

Anderson, R. F., Ali, S., Bradtmiller, L. I., Nielsen, S. H. H., Fleisher, M. Q., Anderson, B. E. and Burckle, L. H. 2009. Wind-Driven Upwelling in the Southern Ocean and the Deglacial Rise in Atmospheric CO_2. *Science*. 323 (5920) 1443–1448. DOI: 10.1126/science.1167441.

Appleby, P. G. 2001. Chronostratigraphic techniques in recent sediments. In: *Tracking Environmental Change Using Lake Sediments*. Edited by Last, W.M. and Smol, J. P. Springer, Dordrecht. pp. 171–203.

Appleby, P. G. and Oldfield, F. 1978. The calculation of lead-210 dates assuming a constant rate of supply of unsupported ^{210}Pb to the sediment. *Catena.* 5, 1–8. DOI:10.1016/S0341-8162(78)80002-2.

Barnard, A., Wellner, J. S. and Anderson, J. B. 2014. Late Holocene climate change recorded in proxy records from a Bransfield Basin sediment core, Antarctic Peninsula. *Polar Research.* 3, 17236, http://dx.doi.org/10.3402/polar.v33.17236.

Battarbee, R. W. and Kneen, M. J. 1982. The use of electronically counted microspheres in absolute diatom analysis. *Limnology and Oceanography.* 27 (1) 184 –188. DOI: 10.4319/lo.1982.27.1.0184.

Bechtel, A., Smittenberg, R. H., Bernasconi, S. M. and Schubert, C.J. 2010. Distribution of branched and isoprenoid tetraether lipids in an oligotrophic and a eutrophic Swiss lake: Insights into sources and GDGT-based proxies. *Organic Geochemistry*. 41 (8) 822 –832. DOI:10.1016/j.orggeochem.2010.04.022.

Bendle, J. A., Weijers, J. W. H., Maslin, M. A., Sinninghe Damsté, J. S., Schouten, S., Hopmans, E. C., Boot, C. S. and Pancost, R. D. 2010. Major changes in glacial and Holocene terrestrial temperatures and sources of organic carbon recorded in the Amazon fan by tetraether lipids. *Geochemistry, Geophysics, Geosystems*. 11 (12) DOI:10.1029/2010GC003308.

Bennett, K. D. 1996. Determination of the number of zones in a biostratigraphical sequence. *New Phytologist.* 132 (1) 155 –170. DOI: 10.1111/j.1469-8137.1996.tb04521.x.

Bentley, M. J., Evans, D. J. A., Fogwill, C. J., Hansom, J. D., Sugden, D. E. and Kubik, P. W. 2007. Glacial geomorphology and chronology of deglaciation, South Georgia, sub-Antarctic. *Quaternary Science Reviews*. 26 (5 – 6) 644 – 677. DOI:10.1016/j.quascirev.2006.11.019.

Bentley, M. J., Hodgson, D. A., Smith, J. A., Cofaigh, C. Ó., Domack, E. W., Larter, R. D., Roberts, S. J., Brachfeld, S., Leventer, A., Hjort, C., Hillenbrand, C. D. and Evans, J. 2009. Mechanisms of Holocene palaeoenvironmental change in the Antarctic Peninsula region. *The Holocene*. 19 (1) 51 – 69. DOI:10.1177/0959683608096603.

Bentley, M. J., Hodgson, D. A., Sugden, D. E., Roberts, S. J., Smith, J. A., Leng, M. J. and Bryant, C. 2005. Early Holocene retreat of the George VI Ice Shelf, Antarctic Peninsula. *Geology*. 33 (3) 173 –176. DOI:10.1130/G21203.1.

Bertler, N. A. N., Mayewski, P. A. and Carter, L. 2011. Cold conditions in Antarctica during the Little Ice Age - Implications for abrupt climate change mechanisms. *Earth and Planetary Science Letters*. 308 (1 – 2) 41–51. DOI:10.1016/j.epsl.2011.05.021.

Bertrand, S., Castiaux, J. and Juvigné, E. 2008. Tephrostratigraphy of the late glacial and Holocene sediments of Puyehue Lake (Southern Volcanic Zone, Chile, 40°S). *Quaternary Research*. 70, 343–357. DOI:10.1016/j.yqres.2008.06.001.

Bestic, K., Duncan, R., McGlone, M. S., Wilmshurst, J. M. and Meurk, C. 2005. Population age structure and recent Dracophyllum spread on subantarctic Campbell Island. *New Zealand Journal of Ecology.* 29, 291–297.

Bird, B. W., Abbott, M. B., Vuille, M., Rodbell, D. T., Stansell, N. D. and Rosenmeier, M. F. 2011. A 2,300-year-long annually resolved record of the South American summer monsoon from the Peruvian Andes. *Proceedings of the National Academy of Sciences of the United States of America*. 108 (21) 8583–8. DOI:10.1073/pnas.1003719108.

Birks, H. H., Aarnes, I., Bjune, A. E., Brooks, S. J., Bakke, J., Kühl, N. and Birks, J. B. 2014. Lateglacial and early-Holocene climate variability reconstructed from multi-proxy records on Andøya, northern Norway. *Quaternary Science Reviews*. 89, 108–122. DOI:10.1016/j.quascirev.2014.01.018.

Birnie, J. 1990. Holocene environmental-change in South Georgia - evidence from lake-sediments. *Journal of Quaternary Science.* 5 (3) 171–187. DOI:10.1002/jqs.3390050302.

Björck, S. and Wohlfarth, B. 2001. ^{14}C Chronostratigraphic Techniques in Paleolimnology In: *Tracking Environmental Change Using Lake Sediments Developments in Paleoenvironmental Research Volume 1; Basin Analysis, Coring, and Chronological Techniques.* Edited by Last, W. M. And Smol, J. P. Springer, Netherlands. Pages 205-245.

Björck, S., Hakansson, H., Olsson, S., Barnekow, L. and Janssens, J. 1993. Palaeoclimatic studies in South Shetland Islands, Antarctica, based on numerous stratigraphic variables in lake sediments. *Journal of Paleolimnology*. 8 (3) 233–272. DOI:10.1007/BF00177858.

Björck, S., Håkansson, H., Zale, R., Karlen, W. and Jonsson, B. L. 1991. A late Holocene lake sediment sequence from Livingston Island, South Shetland Islands, with palaeoclimatic implications. *Antarctic* Science. 3 (1) 61–72. DOI:10.1017/S095410209100010X.

Björck, S., Olsson, S., Ellis-Evans, C., Håkansson, H., Humlum, O. and de Lirio, J. M. 1996. Late Holocene palaeoclimatic records from lake sediments on James Ross Island, Antarctica. *Palaeogeography, Palaeoclimatology, Palaeoecology*. 121 (3–4) 195–220. DOI:10.1016/0031-0182(95)00086-0.

Blaauw, M. 2010. Methods and code for 'classical' age-modelling of radiocarbon sequences. *Quaternary Geochronology*. 5 (5) 512–518. DOI:10.1016/j.quageo.2010.01.002.

Blaauw, M. and Christen, J. A. 2011. Flexible Paleoclimate Age-Depth Models Using an Autoregressive Gamma Process. *Bayesian Analysis.* 6 (3) 457–474. DOI:10.1214/11-BA618.

Blaga, C. I., Reichart, G. J., Heiri, O. and Sinninghe Damsté, J. S. 2009. Tetraether membrane lipid distributions in water-column particulate matter and sediments: a study of 47 European lakes along a north–south transect. *Journal of Paleolimnology*. 41 (3) 523–540. DOI:10.1007/s10933-008-9242-2.

Blaga, C. I., Reichart, G. J., Schouten, S., Lotter, A. F., Werne, J. P., Kosten, S., Mazzeo, N., Lacerot, G. and Sinninghe Damsté, J. S. 2010. Branched glycerol dialkyl glycerol tetraethers in lake sediments: Can they be used as temperature and pH proxies? *Organic Geochemistry*. 41 (11) 1225–1234. DOI:10.1016/j.orggeochem.2010.07.002.

Blott, S. J. and Pye, K. 2001. GRADISTAT: a grain size distribution and statistics package for the analysis of unconsolidated sediments. *Earth Surface Processes and Landforms.* 26 (11) 1237–1248. DOI: 10.1002/esp.261.

Blyth, A. J. and Schouten, S. 2013. Calibrating the glycerol dialkyl glycerol tetraether temperature signal in speleothems. *Geochimica et Cosmochimica Acta.* 109, 312–328. DOI:10.1016/j.gca.2013.02.009.

Blyth, A. J., Jex, C. N., Baker, A., Khan, S. J. and Schouten, S. 2014. Contrasting distributions of glycerol dialkyl glycerol tetraethers (GDGTs) in speleothems and associated soils. *Organic Geochemistry.* 69, 1–10. DOI:10.1016/j.orggeochem.2014.01.013.

Bockheim, J. G. and Hall, K. J. 2002. Permafrost, active-layer dynamics and periglacial environments of continental Antarctica. *South African Journal of Science*. 98 (1–2) 82–90.

Bond, G., Showers, W., Cheseby, M., Lotti, R., Almasi, P., deMenocal, P., Priore, P., Cullen, H., Hajdas, I. and Bonani, G., 1997. A pervasive millenial-scale cycle in North Atlantic Holocene and glacial climates. *Science*. 278 (5341) 1257–1266. DOI:10.1126/science.278.5341.1257.

Böning, C. W., Dispert, A., Visbeck, M., Rintoul, S. R. and Schwarzkopf, F. U. 2008. The response of the Antarctic Circumpolar Current to recent climate change. *Nature Geoscience*. 1 (12) 864–869. DOI:10.1038/ngeo362.

Borcard, D., Gillet, F., and Legendre, P. 2011. *Numerical Ecology with R.* Springer, Dordrecht.

Borcard, D., Legendre, P. and Drapeau, P. 1992. Partialling out the Spatial Component of Ecological Variation. *Ecology.* 73, 1045–1055. DOI: 10.2307/1940179.

Braun, M., Saurer, H. and Goßmann, H. 2004. Climate, energy fluxes and ablation rates on the ice cap of King George Island. *Pesquisa Antártica Brasileira*. 4, 87–103.

British Antarctic Survey, 2002. *Scientific Report – Sledge Bravo 2001-2002 (Ref. R/2001/NT1).* British Antarctic Survey, Cambridge.

British Antarctic Survey. 2003. *Scientific Report – Sledge Bravo 2002-2003 (Ref. AD6/2R/2002/NT3).* British Antarctic Survey, Cambridge.

British Antarctic Survey. 2006. *Field Report – Sledge Uniform 2005-2006 (Ref. R/2005NT3).* British Antarctic Survey, Cambridge.

British Antarctic Survey, 2007 *MERLIN Field Report - A joint research expedition between the Japanese REGAL project, the BAS CACHE-PEP program and the Belgian HOLANT and AMBIO projects.* British Antarctic Survey, Cambridge.

British Antarctic Survey. 2008. *Field Report – Sledge Bravo 2006-2007 and CACHE-PEP South America 2007-2008.* British Antarctic Survey, Cambridge.

Brochier-Armanet, C., Boussau, B., Gribaldo, S. and Forterre, P. 2008. Mesophilic Crenarchaeota: proposal for a third Archaeal phylum, the Thaumarchaeota. *Nature Reviews Microbiology*. 6 (3) 245–52. DOI:10.1038/nrmicro1852.

Bronk-Ramsey, C. 2009. Bayesian analysis of radiocarbon dates. *Radiocarbon.* 51 (1) 337–360.

Brown, E. T., Johnson, T. C., Scholz, C. A., Cohen, A. S. and King, J. W. 2007. Abrupt change in tropical African climate linked to the bipolar seesaw over the past 55,000 years. *Geophysical Research Letters.* 34 (L20702) DOI:10.1029/2007GL031240.

Buchaca, T. and Catalan, J. 2007. Factors influencing the variability of pigments in the surface sediments of mountain lakes. *Freshwater Biology*. 52, 1365–1379. DOI: 10.1111/j.1365-2427.2007.01774.x.

Buckles, L. K., Weijers, J. W. H., Tran, X. -M., Waldron, S. and Sinninghe Damsté, J. S. 2014. Provenance of tetraether membrane lipids in a large temperate lake (Loch Lomond, UK): implications for glycerol dialkyl glycerol tetraether (GDGT)-based palaeothermometry. *Biogeosciences*. 11, 5539–5563. DOI:10.5194/bg-11-5539-2014.

Burman, P., Chow, E. and Nolan, D. 1994. A cross-validatory method for dependent data. *Biometrika.* 81, 351–358.

Cane, M. A. 2005. The evolution of El Niño, past and future. *Earth and Planetary Science Letters.* 230 (3–4) 227–240. DOI: 10.1016/j.epsl.2004.12.003.

Caniupán, M., Lamy, F., Lange, C. B., Kaiser, J., Kilian, R., Arz, H. W., León, T., Mollenhauer, G., Sandoval, S., De Pol-Holz, R., Pantoja, S., Wellner, J. and Tiedemann, R. 2014. Holocene sea-surface temperature variability in the Chilean fjord region. *Quaternary Research.* 82 (2) 342–353. DOI:10.1016/j.yqres.2014.07.009.

Cantonati, M., Guella, G., Komárek, J. and Spitale, D. 2014. Depth distribution of epilithic cyanobacteria and pigments in a mountain lake characterized by marked water-level fluctuations. *Freshwater Science.* 33 (2) 537–547. DOI: 10.1086/675930.

Castañeda, I. S. and Schouten, S. 2011. A review of molecular organic proxies for examining modern and ancient lacustrine environments. *Quaternary Science Reviews.* 30, 2851–2891. DOI:10.1016/j.quascirev.2011.07.009.

Catalan, J., Barbieri, M. G., Bartumeus, F., Bitušík, P., Botev, I., Brancelj, A., Cogălniceanu, D., Manca, M., MArchetto, A., Ognjanova-Rumenova, N., Pla, S., Rieradevall, M., Sorvari, S., Štefková, E., Stuchlík, E. and Ventura, M. 2009. Ecological thresholds in European alpine lakes. *Freshwater Biology*. 54, 2494–2517. DOI:10.1111/j.1365-2427.2009.02286.x

Chalie, F. 1995. Paleoclimates of the southern Tanganyika Basin over the last 25–thousand years—Quantitative reconstruction from the statistical treatment of pollen data. *C. R. Acad. Sci., Ser. II*. 320, 205–210.

Chapori, N. G., Chiessi, C. M., Bickert, T. and Laprida, C. 2015. Sea-surface temperature reconstruction of the Quaternary western South Atlantic: New planktonic foraminiferal correlation function. *Palaeogeography, Palaeoclimatology, Palaeoecology*. 425, 67–75. DOI:10.1016/j.palaeo.2015.02.027.

Chown, S. L. and Convey, P. 2007. Spatial and temporal variability across life's hierarchies in the terrestrial Antarctic. *Philosophical Transactions of the Royal Society B-Biological Sciences*. 362 (1488) 2307–2331. DOI: 10.1098/rstb.2006.1949.

Clapperton, C. M., Sugden, D. E., Birnie, J. and Wilson, M. J. 1989. Late-Glacial and Holocene glacier fluctuations and environmental-change on South Georgia, Southern-Ocean. *Quaternary Research.* 31 (2) 210–228. DOI: 10.1016/0033-5894(89)90006-9.

Colcord, D. E., Cadieux, S. B., Brassell, S. C., Castañeda, I. S., Pratt, L. M. and White, J. R. 2015. Assessment of branched GDGTs as temperature proxies in sedimentary records from several small lakes in southwestern Greenland. *Organic Geochemistry.* 82, 33–41. DOI: 10.1016/j.orggeochem.2015.02.005.

Collins D. 2000 Annual temperature summary: Australia records warmest decade. *Climate Change Newsletter*. 12 (1) 6.

Cook, A. J., Fox, A. J., Vaughan, D. G. and Ferrigno, J. G. 2005. Retreating glacier fronts on the Antarctic Peninsula over the past half-century. *Science*. 308 (5721) 541–544. DOI:10.1126/science.1104235.

Cook, A. J., Poncet, S., Cooper, A. P. R., Herbert, D. J. and Christie, D. 2010. Glacier retreat on South Georgia and implications for the spread of rats. *Antarctic Science.* 22 (03) 255–263. DOI:10.1017/S0954102010000064.

Davies, S. J., Lamb, H. F. and Roberts, S. 2015. Micro-1 XRF core scanning in palaeolimnology: recent developments. In: *Micro-XRF Studies of Sediment Cores: Applications of a non-destructive tool for the environmental sciences*. Edited by: Croudace, I. W. and Rothwell, R. G. Springer, Netherlands. pp 189-226.

De Jonge, C., Hopmans, E. C., Stadnitskaia, A., Rijpstra, W. I. C., Hofland, R., Tegelaar, E. and Sinninghe Damsté, J. S. 2013. Identification of novel penta- and hexamethylated branched glycerol dialkyl glycerol tetraethers in peat using HPLC–MS^2, GC–MS and GC–SMB-MS. *Organic Geochemistry*. 54, 78–82. DOI:10.1016/j.orggeochem.2012.10.004.

De Jonge, C., Hopmans, E. C., Zell, C. I., Kim, J-H., Schouten, S. and Sinninghe Damsté, J. S. 2014b. Occurrence and abundance of 6-methyl branched glycerol dialkyl glycerol tetraethers in soils: Implications for palaeoclimate reconstruction. *Geochimica et Cosmochimica Acta.* 141, 97–112. DOI:10.1016/j.gca.2014.06.013.

De Jonge, C., Stadnitskaia, A., Hopmans, E. C., Cherkashov, G., Fedotov, A. and Sinninghe Damsté, J. S. 2014a. In situ produced branched glycerol dialkyl glycerol tetraethers in suspended particulate matter from the Yenisei River, Eastern Siberia. *Geochimica et Cosmochimica Acta*. 125, 476–491. DOI:10.1016/j.gca.2013.10.031.

De Rosa, M. and Gambacorta, A. 1988. The Lipids of Archaebacteria. *Progress in Lipid Research*. 27, 153–175.

Deconto, R., Pollard, D. and Harwood, D. 2007. Sea ice feedback and Cenozoic evolution of Antarctic climate and ice sheets. *Palaeoceanography*. 22 (PA3214) DOI:10.1029/2006PA001350.

Del Valle, R. A., Montalti, D. and Inbar, M. 2002. Mid-Holocene macrofossil-bearing raised marine beaches at Potter Peninsula, King George Island, South Shetland Islands. *Antarctic Science.* 14 (3) 263–269. DOI:10.1017/S0954102002000081.

Department of Conservation, New Zealand Government. 2013. *Offshore islands and conservation - Campbell Island.* http://www.doc.govt.nz/conservation/land-and-freshwater/offshore-islands/new-zealands-subantarctic-islands/campbell-island/ (Accessed 17/04/13).

Diaz, H. F., Trigo, R., Hughes, M. K., Mann, M. E., Xoplaki, E. and Barriopedro, D. 2011. Spatial and Temporal Characteristics of Climate in Medieval Times Revisited. *Bulletin of the American Meteorological Society*. 92 (11) 1487–1500. DOI:10.1175/BAMS-D-10-05003.1.

Domack, E.W. 2002. A synthesis for site 1098: Palmer Deep. In: *Proceedings of the ocean drilling program, scientific results, Volume 178*. Edited by Barker, P.F., Camerlenghi, A., Acton, G.D. and Ramsay, A.T.S. Ocean Drilling Program, Texas A&M University.

Domack, E. W., Leventer, A., Root, S., Ring, J., Williams, E., Carlson, D., Hirshorn, E., Wright, W., Gilbert, R. and Burr, G. 2003. Marine sedimentary record of natural environmental variability and recent warming in the Antarctic Peninsula. In: *Antarctic Peninsula climate variability: historical and paleoenvironmental perspectives. Antarctic Research Series 79.* Edited by Domack, E.W., Leventer, A., Burnett, A., Bindschadler, R., Convey, P. and Kirby, M. American Geophysical Union, 205–22.

Dray, S., Legendre, P., and Peres-Neto, P.R. 2006. Spatial modelling: a comprehensive framework for principal coordinate analysis of neighbour matrices (PCNM). *Ecological Modelling.* 196, 483–493. DOI:10.1016/j.ecolmodel.2006.02.015.

Ducklow, H. W., Baker, K., Martinson, D. G., Quetin, L. B., Ross, R. M., Smith, R. C., Stammerjohn, S. E., Vernet, M. and Fraser, W. 2007. Marine pelagic ecosystems: The West Antarctic Peninsula. *Philosophical Transactions of the Royal Society B-Biological Sciences*. 362 (1477) 67–94. DOI:10.1098/rstb.2006.1955.

Edinger, J., Dutterweiler, D. and Geyer, J. 1968. The response of water temperatures to meteorological conditions. *Water Resources Research.* 4 (5) 1137–1143. DOI:10.1029/WR004i005p01137.

Elderfield, H. and Ganssen, G. 2000. Past temperature and delta18O of surface ocean waters inferred from foraminiferal Mg/Ca ratios. *Nature*. 405, 442–445. DOI:10.1038/35013033.

Esposito, R. M. M., Horn, S. L., McKnight, D. M., Cox, M. J., Grant, M. C., Spaulding, S. A., Doran, P. T. and Cozzetto, K. D. 2006. Antarctic climate cooling and response of diatoms in glacial meltwater streams. *Geophysical Research Letters*. 33 (7) L07406. DOI:10.1029/2006GL025903.

Etourneau, J., Collins, L. G., Willmott, V., Kim, J.-H., Barbara, L., Leventer, A., Schouten, S., Sinninghe Damsté, J. S., Bianchini, A., Klein, V., Crosta, X. and Massé, G. 2013. Holocene climate variations in the western Antarctic Peninsula: evidence for sea ice extent predominantly controlled by changes in insolation and ENSO variability. *Climate of the Past*. 9 (4) 1431–1446. DOI:10.5194/cp-9-1431-2013.

Farmer, E. J., Chapman, M. R. and Andrews, J. E. 2008. Centennial-scale Holocene North Atlantic surface temperatures from Mg/Ca ratios in Globigerina bulloides. *Geochemistry Geophysics Geosystems.* 9 (12) Q12029. DOI:10.1029/2008GC002199.

Fernandez-Carazo, R. Verleyen, E., Hodgson, D. A., Roberts, S. J., Waleron, K., Vyverman, W. and Wilmotte, A. 2013. Late Holocene changes in cyanobacterial community structure in maritime Antarctic lakes. *Journal of Paleolimnology*. 50, 15–31. DOI:10.1007/s10933-013-9700-3.

Fletcher, M. S. and Moreno, P. I. 2011. Zonally symmetric changes in the strength and position of the Southern Westerlies drove atmospheric CO2 variations over the past 14 k.y. *Geology*. 39 (5) 419–422. DOI:10.1130/G31807.1.

Fletcher, M. S. and Moreno, P. I. 2012. Have the Southern Westerlies changed in a zonally symmetric manner over the last 14,000 years? A hemisphere-wide take on a controversial problem. *Quaternary International.* 253 (0) 32–46. DOI:10.1016/j.quaint.2011.04.042

Fretwell, P. T., Hodgson, D. A., Watcham, E. P., Bentley, M. J. and Roberts, S. J. 2010. Holocene isostatic uplift of the South Shetland Islands, Antarctic Peninsula, modelled from raised beaches. *Quaternary Science Reviews*. 29 (15–16) 1880–1893. DOI:10.1016/j.quascirev.2010.04.006.

Fulton, J. M., Arthur, M. A. and Freeman, K. H.2012. Subboreal aridity and scytonemin in the Holocene Black Sea. *Organic Geochemistry*. 49, 47–55. DOI:10.1016/j.orggeochem.2012.05.008.

Gillieson, D. S. 1991. An environmental history of two freshwater lakes in the Larsemann Hills, Antarctica. *Hydrobiologia*. 214 (1) 327–331. DOI:10.1007/BF00050967.

Gliozzi, A., Paoli, G., De Rosa, M., and Gambacorta, A. 1983. Effect of isoprenoid cyclization on the transition temperature of lipids in thermophilic archaebacteria. *Biochimica* et Biophysica Acta. 735, 234–242. DOI:10.1016/0005-2736(83)90298-5.

Goosse, H., Crespin, E., de Montety, A., Mann, M. E., Renssen, H. and Timmermann, A. 2010. Reconstructing surface temperature changes over the past 600 years using climate model simulations with data assimilation. *Jounral of Geophysical Research.* 115, D09108, DOI:10.1029/2009JD012737.

Gordon, J. E., Haynes, V. M., and Hubbard, A. 2008. Recent glacier changes and climate trends on South Georgia. *Global and Planetary Change*. 60 (1–2) 72–84. DOI:10.1016/j.gloplacha.2006.07.037.

Gordon, J. E., Tlmmls, R. J., Wood, G. and Stevenage, R. 1992. Glacier fluctuations on South Georgia during the 1970s and early 1980s, *Antarctic Science.* 4 (2) 215–226. DOI:10.1017/S0954102092000336.

Grimm, E. C. 1987. CONISS: A FORTRAN 77 program for stratigraphically constrained cluster analysis by the method of incremental sum of squares. *Computers & Geosciences.* 13, 13‑35. DOI:10.1016/0098-3004(87)90022-7.

Guilizzoni, P., Bonomi, G., Galanti, G. and Ruggiu, D. 1982. Basic trophic status and recent development of some Italian Lakes as revealed by plant pigments and other chemical components in sediment cores. *Mem Ist Ital Idrobiol*. 40, 79–98.

Guilizzoni, P., Bonomi, G., Galanti, G. and Ruggiu, D. 1983. Relationship between sedimentary pigments and primary production: evidence from core analysis of twelve Italian lakes. *Hydrobiologia*. 103. 103–106. DOI:10.1007/978-94-009-7290-2_17.

Gunn, D. E. and Best, A. I. 1998. A new automated non-destructive system for high resolution multi sensor core logging of open sediment cores. *Geo-Marine Letters.* 18, 70‑77. DOI: 10.1007/s003670050054.

Günther, F., Thiele, A., Gleixner, G., Xu, B., Yao, T. and Schouten, S. 2014. Distribution of bacterial and archaeal ether lipids in soils and surface sediments of Tibetan lakes: Implications for GDGT-based proxies in saline high mountain lakes. *Organic Geochemistry*. 67, 19–30. DOI:10.1016/j.orggeochem.2013.11.014.

Hall, B. L. 2010. Holocene relative sea-level changes and ice fluctuations in the South Shetland Islands. *Global and Planetary Change.* 74 (1) 15–26. DOI:10.1016/j.gloplacha.2010.07.007.

Hall, K., Meiklejohn, I. and Bumby, A. 2011. Marion Island volcanism and glaciation. *Antarctic Science.* 23 (2) 155–163.

Hass, H. C., Kuhn, G., Monien, P., Brumsack, H. -J. and Forwick, M. 2010. Climate fluctuations during the past two millennia as recorded in sediments from Maxwell Bay, South Shetland Islands, West Antarctica. *Geological Society, London, Special Publications*. 344, 243–260. DOI: 10.1144/SP344.17.

Hatté, C., Rousseau, D.-D. and Guiot, J. 2009. Climate reconstruction from pollen and $\delta^{13}C$ records using inverse vegetation modeling – Implication for past and future climates. *Climate of the Past.* 5, 147–156. DOI:10.5194/cp-5-147-2009.

Hayward, R. J. C. 1983. Glacier fluctuations in South-Georgia, 1883–1974. B*ritish Antarctic Survey Bulletin*. 52, 47–61.

Heroy, D. C., Sjunneskog, C. and Anderson, J. B. 2008. Holocene climate change in the Bransfield Basin, Antarctic Peninsula: evidence from sediment and diatom analysis. *Antarctic Science*. 20 (1) 69–87. DOI:10.1017/S0954102007000788.

Heyng, A. M., Mayr, C., Lücke, A., Moschen, R., Wissel, H., Striewski, B. and Bauersachs, T. In press. Middle and Late Holocene paleotemperatures reconstructed from oxygen isotopes and GDGTs of sediments from Lake Pupuke, New Zealand. *Quaternary International*. DOI:10.1016/j.quaint.2014.12.040.

Ho, S. L., Mollenhauer, G., Fietz, S., Martínez-Garcia, A., Lamy, F., Rueda, G., Schipper, K., Méheust, M., Rosell-Melé, A., Stein, R. and Tiedemann, R. (2014). Appraisal of TEX86 and thermometries in subpolar and polar regions. *Geochimica et Cosmochimica Acta.* 131, 213–226. DOI:10.1016/j.gca.2014.01.001.

Hodgson, D. A. 2009. Changes in the sub-Antarctic in the modern era of science and environmental consciousness. *Papers and Proceedings of the Royal Society of Tasmania.* 143 (1) 19–24.

Hodgson, D. A. and Convey, P. 2005. A 7000-year Record of Oribatid Mite Communities on a Maritime-Antarctic Island: Responses to Climate Change. *Arctic, Antarctic, and Alpine Research.* 37 (2) 239–245.

Hodgson, D. A. and Sime, L. C. 2010. Palaeoclimate Southern westerlies and CO2. *Nature Geoscience.* 3 (10) 666–667. DOI:10.1038/ngeo970.

Hodgson, D. A., Bentley, M. J., Roberts, S. J., Smith, J. A., Sugden, D. E. and Domack, E. W. 2006b. Examining Holocene stability of Antarctic Peninsula ice shelves. *Eos Trans. AGU.* 87 (31) 305–312. DOI:10.1029/2006EO310001.

Hodgson, D. A., McMinn, A., Kirkup, H., Cremer, H., Gore, D., Melles, M., Roberts, D. and Montiel, P. 2003. Colonization, succession, and extinction of marine floras during a glacial cycle: A case study from the Windmill Islands (east Antarctica) using biomarkers. *Paleoceanography,* 18 (3) DOI:10.1029/2002PA000775.

Hodgson, D. A., Noon, P., Vyverman, W., Bryant, C., Gore, D. B., Appleby, P., Gilmour, M., Verleyen, E., Sabbe, K., Jones, V. J., Ellis-Evans, J. C. and Wood, P. 2001. Were the Larsemann Hills ice-free through the Last Glacial Maximum? *Antarctic Science*. 13 (4) 440–454. DOI:10.1017/S0954102001000608.

Hodgson, D. A., Roberts, S. J., Smith, J. A., Verleyen, E., Sterken, M., Labarque, M., Sabbe, K., Vyverman, W., Allen, C. S., Leng, M. J. and Bryant, C. 2013. Late Quaternary environmental changes in Marguerite Bay, Antarctic Peninsula, inferred from lake sediments and raised beaches. *Quaternary Science Reviews.* 68, 216–236. DOI:10.1016/j.quascirev.2013.02.002.

Hodgson, D. A., Verleyen, E., Sabbe, K., Squier, A. H., Keely, B. J., Leng, M. J., Saunders, K. M. and Vyverman, W. 2005. Late Quaternary climate-driven environmental change in the Larsemann Hills, East Antarctica, multi-proxy evidence from a lake sediment core. *Quaternary Research, 64*(1), 83–99. DOI:10.1016/j.yqres.2005.04.002.

Hodgson, D. A., Verleyen, E., Squier, A. H., Sabbe, K., Keely, B. J., Saunders, K. M. and Vyverman, W. 2006a. Interglacial environments of coastal east Antarctica: comparison of MIS 1 (Holocene) and MIS 5e (Last Interglacial) lake-sediment records. *Quaternary Science Reviews.* 25 (1–2) 179–197. DOI:10.1016/j.quascirev.2005.03.004.

Hodgson, D.A., Wright, S. W. and Davies, N. 1997. Mass spectrometry and reverse phase HPLC techniques for the identification of degraded fossil pigments in lake sediments and their application in palaeolimnology. *Journal of Paleolimnology*. 18, 335–350. DOI:10.1023/A:1007943119392.

Hoefs, M. J. L., Versteegh, G. J. M., Rijpstra, W. I. C., de Leeuw, J. W. And Sinninghe Damsté, J. S. 1998. Postdepositional oxic degradation of alkenones: Implications for the measurement of palaeo sea surface temperatures. *Paleoceanography*. 13 (1) 42. DOI:10.1029/97PA02893.

Hogg, A., Hua, Q., Blackwell, P. G., Niu, M., Buck, C. E., Guilderson, T. P., Heaton, T. H., Palmer, J. G., Reimer, P. J., Reimer, R. W., Turney, C. S. M. and Zimmerman, S. R. H. 2013. SHCal13 Southern Hemisphere Calibration, 0–50,000 Years cal BP. *Radiocarbon*. 55 (4) 1889–1903. DOI:10.2458/azu_js_rc.55.16783.

Holmgren, K., Lee-Thorp, J. A., Cooper, G. R. J, Lundblad, K., Partridge, T. C., Scott, L., Sithaldeen, R., Talma, A. S. and Tyson P. D. 2003. Persistent millenial-scale climatic variability over the past 25,000 years in Southern Africa, *Quaternary Science Reviews.* 22, 2311–2326. DOI:10.1016/S0277-3791(03)00204-X.

Hopmans, E. C., Schouten, S., Pancost, R. D., Van der Meer, M. T. and Sinninghe Damsté, J. S. 2000. Analysis of intact tetraether lipids in Archaeal cell material and sediments by high performance liquid chromatography/atmospheric pressure chemical ionization mass spectrometry. *Rapid communications in mass spectrometry*. 14 (7) 585–589. DOI: 10.1002/(SICI)1097-0231(20000415)14:7<585::AID-RCM913>3.0.CO;2-N.

Hopmans, E. C., Weijers, J. W.., Schefuß, E., Herfort, L., Sinninghe Damsté, J. S. and Schouten, S. 2004. A novel proxy for terrestrial organic matter in sediments based on branched and isoprenoid tetraether lipids. *Earth and Planetary Science Letters.* 224 (1–2). 107–116. DOI:10.1016/j.epsl.2004.05.012.

Hua, Q, Barbetti, M. and Rakowski, A. Z. 2013. Atmospheric radiocarbon for the period 1950‑2010. *Radiocarbon.* 55 (4) 2059–2072. DOI:10.2458/azu_js_rc.v55i2.16177.

Hughes, L. 2003. Climate change and Australia: Trends, projections and impacts. *Austral* Ecology. 28, 423–443. DOI:10.1046/j.1442-9993.2003.01300.x.

Huguet, C., Fietz, S., Stockhecke, M., Sturm, M., Anselmetti, F. S., and Rosell-Melé, A. 2011. Biomarker seasonality study in Lake Van, Turkey. *Organic Geochemistry*. 42 (11) 1289–1298. DOI:10.1016/j.orggeochem.2011.09.007.

Huguet, A., Fosse, C., Laggoun-Défarge, F., Toussaint, M. L. and Derenne, S. 2010b. Occurrence and distribution of glycerol dialkyl glycerol tetraethers in a French peat bog. *Organic Geochemistry*. 41 (6) 559–572. DOI:10.1016/j.orggeochem.2010.02.015.

Huguet, C., Hopmans, E. C., Febo-Ayala, W., Thompson, D. H., Sinninghe Damsté, J. S. and Schouten, S. 2006. An improved method to determine the absolute abundance of glycerol dibiphytanyl glycerol tetraether lipids. *Organic Geochemistry*. 37 (9) 1036–1041. DOI:10.1016/j.orggeochem.2006.05.008.

Huguet, C., Martens-Habbena, W., Urakawa, H., Stahl, D. A. and Ingalls, A. E. 2010a. Comparison of extraction methods for quantitative analysis of core and intact polar glycerol dialkyl glycerol tetraethers (GDGTs) in environmental samples. *Limnology and Oceanography: Methods*. 8, 127–145. DOI:10.4319/lom.2010.8.127.

Huguet, C., Schimmelmann, A., Thunell, R., Lourens, L. J., Sinninghe Damsté, J. S. and Schouten, S. 2007. A study of the TEX86 paleothermometer in the water column and sediments of the Santa Barbara Basin, California. *Paleoceanography*. 22, PA3203, DOI:10.1029/2006PA001310.

Jenkyns, H. C., Forster, A., Schouten, S. and Sinninghe Damsté, J. S. 2004. High temperatures in the late Cretaceous Arctic Ocean. *Nature*. 432, 888–892. DOI:10.1038/nature03143.

Ji, S., Xingqi, L., Sumin, W. and Matsumoto, R. 2005. Palaeoclimatic changes in the Qinghai Lake area during the last 18,000 years. *Quaternary International*. 136, 131–140. DOI:10.1016/j.quaint.2004.11.014.

Jia, G., Zhang, J., Chen, J., Peng, P. and Zhang, C. L. Archaeal tetraether lipids record subsurface water temperature in the South China Sea. *Organic Geochemistry*. 50, 68–77. DOI:10.1016/j.orggeochem.2012.07.002.

Jian, Z., Wang, L., Kienast, M., Sarnthein, M., Kuhnt, W., Lin, H. and Wang, P. 1999. Benthic foraminiferal paleoceanography of the South China Sea over the last 40,000 years. *Marine Geology*. *156*, 159–186. DOI:10.1016/S0025-3227(98)00177-7.

Jiang, Q., Ji, J., Shen, J., Matsumoto, R., Tong, G., Qian, P., Ren, X. and Yan, D. 2013. Holocene vegetational and climatic variation in westerly dominated areas of Central Asia inferred from the Sayram Lake in northern Xinjiang, China. *Science China Earth Sciences.* 56 (3) 339–353. DOI: 10.1007/s11430-012-4550-9.

Johnson, J. S., Everest, J. D., Leat, P. T., Golledge, N. R., Rood, D. H. and Stuart, F. M. 2012. The deglacial history of NW Alexander Island, Antarctica, from surface exposure dating. *Quaternary Research*. 77 (2) 273–280. DOI:10.1016/j.yqres.2011.11.012.

Jones, V. J., Hodgson, D. A. and Chepstow-Lusty, A. 2000. Palaeolimnological evidence for marked Holocene environmental changes on Signy Island, Antarctica. *Holocene*. 10 (1) 43–60. DOI:10.1191/095968300673046662.

Juggins, S. 2014 rioja: Analysis of Quaternary Science Data, R package version (0.9–3). (http://cran.r-project.org/package=rioja).

Kaiser, J., Lamy, F. and Hebbeln, D. 2005. A 70-kyr sea surface temperature record off southern Chile (Ocean Drilling Program Site 1233). *Paleoceanography*. 20 (4) PA4009. DOI:10.1029/2005PA001146.

Karlsson, J., Jonsson, A. and Jansson, M. 2005. Productivity of high-latitude lakes: Climate effect inferred from altitude gradient. *Global Change Biology*. 11, 710–715. DOI:10.1111/j.1365-2486-2005.00945.x.

Kastner, S., Enters, D., Ohlendorf, C., Haberzettl, T., Kuhn, G., Lücke, A., Mayr, C., Reyss, J-L., Wastegård, S. and Zolitschka, B. 2010. Reconstructing 2000 years of hydrological variation derived from laminated proglacial sediments of Lago del Desierto at the eastern margin of the South Patagonian Ice Field, Argentina. *Global and Planetary Change.* 72, 201–214. DOI: 10.1016/j.gloplacha.2010.04.007.

Kaup, E. and Burgess, J. S. 2002. Surface and subsurface flows of nutrients in natural and human impacted lake catchments on Broknes, Larsemann Hills, Antarctica. *Antarctic Science*. 14 (4) 343–352. DOI:10.1017/S0954102002000123.

Kim, J-H., Crosta, X., Michel, E., Schouten, S., Duprat, J. and Sinninghe Damsté, J. S. 2009. Impact of lateral transport on organic proxies in the Southern Ocean. *Quaternary Research*. 71 (2) 246–250. DOI:10.1016/j.yqres.2008.10.005.

Kim, J-H., Crosta, X., Willmott, V., Renssen, H., Bonnin, J., Helmke, P., Schouten, S. and Sinninghe Damsté, J. S. 2012. Holocene subsurface temperature variability in the eastern Antarctic continental margin. *Geophysical Research Letters*. 39, L06705, DOI:10.1029/2012GL051157.

Kim, J-H., Van der Meer, J., Schouten, S., Helmke, P., Willmott, V., Sangiorgi, F., Koç, N., Hopmans, E. C. and Sinninghe Damsté, J. S. 2010. New indices and calibrations derived from the distribution of crenarchaeal isoprenoid tetraether lipids: Implications for past sea surface temperature reconstructions. *Geochimica et Cosmochimica Acta.* 74 (16) 4639–4654. DOI:10.1016/j.gca.2010.05.027.

Kimura, S., Ban, S., Imura, S., Kudoh, S. and Matsuzaki, M. 2010. Limnological characteristics of vertical structure in the lakes of Syowa Oasis, East Antarctica. *Polar Science*. 3 (4) 262–271. DOI:10.1016/j.polar.2009.08.002.

Kornilova, O. and Rosell-Melé, A. 2003. Application of microwave-assisted extraction to the analysis of biomarker climate proxies in marine sediments. *Organic Geochemistry*. 34 (11) 1517–1523. DOI:10.1016/S0146-6380(03)00155-4.

Krossa, V. R., Moros, M., Blanz, T., Jansen, E. and Schneider, R 2015. Late Holocene Baltic Sea outflow changes reconstructed using C37:4 content from marine cores. *Boreas*. 44, 81–93. DOI:10.1111/bor.12093.

Kulbe, T., Melles, M., Verkulich, S. R. and Pushina, Z. V. 2001. East Antarctic climate and environmental variability over the last 9400 years inferred from marine sediments of the Bunger Oasis. *Arctic, Antarctic and Alpine Research.* 33, 223–30.

Kylander, M. E., Ampel, L., Wohlfarth, B. and Veres, D. 2011. High-resolution X-ray fluorescence core scanning analysis of Les Echets (France) sedimentary sequence: new insights from chemical proxies. *Journal of Quaternary Science.* 26 (1) 109–117. DOI:10.1002/jqs.1438.

Lami, A., Musazzi, S., Marchetto, A., Buchaca, T., Kernan, M., Jeppesen, E. and Guilizzoni, P. 2009. Sedimentary pigments in 308 alpine lakes and their relation to environmental gradients. *Advances in Limnology*. 62, 247–268.

Lamy, F., Kilian, R., Arz, H. W., Francois, J.-P., Kaiser, J., Prange, M. and Steinke, T. 2010. Holocene changes in the position and intensity of the southern westerly wind belt. *Nature Geoscience*. 3 (10) 695–699. DOI:10.1038/ngeo959.

Lamy, F., Hebbeln, D., Röhl, U. and Wefer, G. 2001. Holocene rainfall variability in Southern Chile: A marine record of latitudinal shifts of the Southern Westerlies. *Earth and Planetary Science Letters.* 185, 369–382. DOI:10.1016/S0012-821X(00)00381-2.

Larocque, I., Hall, R. I. and Grahn, E. 2001. Chironomids as indicators of climate change: A 100-lake training set from a subarctic region of northern Sweden (Lapland). *Journal of Paleolimnology*. 26, 307–322. DOI:10.1023/A:1017524101783.

Larocque, S.J. and Smith, D.J. 2003 Little Ice Age glacial activity in the Mt. Waddington area, British Columbia Coast Mountains, *Canada. Canadian Journal of Earth Sciences.* 40, 1413–36. DOI: 10.1139/e03-053.

Leavitt, P. R. 1993. A review of factors that regulate carotenoid and chlorophyll deposition and fossil pigment abundance. *Journal of Paleolimnology*. 9 (2) 109–127. DOI:10.1007/BF00677513.

Leavitt, P. R. and Hodgson, D. A. 2001. Sedimentary pigments. In: *Developments in Paleoenvironmental Research. Volume 3, Tracking environmental changes using lake sediments: Terrestrial algal and siliceous indicators*. Edited by Smol, J. P., Birks, H. J. B. and Last, W. M. pp. 295–325.

Leavitt, P.R., Findlay, D., Hall, R., and Smol, J. 1999. Algal responses to dissolved organic carbon loss and pH decline during whole-lake acidification: Evidence from paleolimnology. *Limnology and Oceanography*. 44, 757–773. DOI:10.4319/lo.1999.44.3_part_2.0757.

Ledru, M.-P., Jomelli, V., Samaniego, P., Vuille, M., Hidalgo, S., Herrera, M. and Ceron, C. 2013. The Medieval Climate Anomaly and the Little Ice Age in the eastern Ecuadorian Andes. *Climate of the Past*. 9 (1) 307–321. DOI:10.5194/cp-9-307-2013.

Leventer, A., Domack, E., Dunbar, R., Pike, J., Stickley, C., Maddison, E., Brachfeld, S., Manley, P. and McClennen, C. 2006. Marine sediment record from the East Antarctic margin reveals dynamics of ice sheet recession. *GSA Today.* 16 (12) 4–10. DOI:0.1130/GSAT01612A.1.

Li, D., Zhao, M., Tian, J. and Li, L. 2013. Comparison and implication of TEX86 and UK’37 temperature records over the last 356 kyr of ODP Site 1147 from the northern South China Sea. *Palaeogeography, Palaeoclimatology, Palaeoecology*. 376, 213–223. DOI:10.1016/j.palaeo.2013.02.031.

Liew, P. M., Lee, C. Y. and Kuo, C. M. 2006. Holocene thermal optimal and climate variability of East Asian monsoon inferred from forest reconstruction of a subalpine pollen sequence, Taiwan. *Earth and Planetary Science Letters*. 250 (3–4) 596–605. DOI:10.1016/j.epsl.2006.08.002.

Linnert, C., Robinson, S. A., Lees, J. A., Bown, P. R., Pérez-Rodríguez, I., Petrizzo, M. R., Falzoni, F., Littler, K., Arz, J. A. and Russell, E. E. 2014. Evidence for global cooling in the Late Cretaceous. *Nature Communications.* 5. DOI:10.1038/ncomms5194.

Lipp, J. S., Morono, Y., Inagaki, F, and Hinrichs, K-U. 2008. Significant contribution of Archaea to extant biomass in marine subsurface sediments. *Nature*. 454 (7207) 991–994. DOI:10.1038/nature07174.

Livingstone, D. and Dokulil, M. 2001. Eighty years of spatially coherent Austrian lake surface temperatures and their relationship to regional air temperature and the North Atlantic Oscillation. *Limnology and Oceanography.* 46 (5) 1220–1227. DOI:10.4319/lo.2001.46.5.1220.

Ljungqvist, F. C. 2010. A New Reconstruction of Temperature Variability in the Extra-Tropical Northern Hemisphere During the Last Two Millennia. *Geografiska Annaler: Series A, Physical Geography.* 92 (3) 339–351. DOI: 10.1111/j.1468-0459.2010.00399.x.

Loomis, S. E., Russell, J. M., Eggermont, H., Verschuren, D. and Sinninghe Damsté, J. S. 2014a. Effects of temperature, pH and nutrient concentration on branched GDGT distributions in East African lakes: Implications for paleoenvironmental reconstruction. *Organic Geochemistry*. 66, 25–37. DOI:10.1016/j.orggeochem.2013.10.012.

Loomis, S. E., Russell, J. M., Heureux, A. M., D'Andrea, W. J. and Sinninghe Damsté, J. S. 2014b. Seasonal variability of branched glycerol dialkyl glycerol tetraethers (brGDGTs) in a temperate lake system. *Geochimica et Cosmochimica Acta*. 144, 173–187. DOI:10.1016/j.gca.2014.08.027.

Loomis, S. E., Russell, J. M., Ladd, B., Street-Perrott, F. A. and Sinninghe Damsté, J. S. 2012. Calibration and application of the branched GDGT temperature proxy on East African lake sediments. *Earth and Planetary Science Letters*. 357–358, 277–288. DOI:10.1016/j.epsl.2012.09.031.

Loomis, S. E., Russell, J. M. and Sinninghe Damsté, J. S. 2011. Distributions of branched GDGTs in soils and lake sediments from western Uganda: Implications for a lacustrine paleothermometer. *Organic Geochemistry*. 42 (7) 739–751. DOI:10.1016/j.orggeochem.2011.06.004.

Lopes dos Santos, R. A., Prange, M., Castañeda, I. S., Schefuß, E., Mulitza, S., Schulz, M., Niedermeyer, E. M., Sinninghe Damsté, J. S. and Schouten, S. 2010. Glacial–interglacial variability in Atlantic meridional overturning circulation and thermocline adjustments in the tropical North Atlantic. *Earth and Planetary Science Letters*. 300, 407–414. DOI:10.1016/j.epsl.2010.10.030.

Löwemark, W., O'Regan, M., Hanebuth, T. J. J. and Jakobsson, M. 2012. Late Quaternary spatial and temporal variability in Arctic deep-sea bioturbation and its relation to Mn cycles. *Palaeogeography, Palaeoclimatology, Palaeoecology.* 365–366, 192–208. DOI:10.1016/j.palaeo.2012.09.028.

Lumley, T. 2009. Leaps: regression subset selection. R Package version 2.9. http://cran.r-project.org/web/packages/leaps/index.html.

Magand, O., Frezzotti, M., Pourchet, M., Stenni, B., Genoni, L. and Fily, M. 2004. Climate variability along latitudinal and longitudinal transects in East Antarctica. *Annals of Glaciology*. 39, 351–358. DOI:10.3189/172756404781813961

Mann, M. E., Zhang, Z., Rutherford, S., Bradley, R. S., Hughes, M. K., Shindell, D., Ammann, C., Faluvegi, G. and Ni, F. 2009. Global Signatures and Dynamical Origins of the Little Ice Age and Medieval Climate Anomaly. *Science.* 326, 1256–1260. DOI:10.1126/science.1177303.

Marchant, R., Kefford, B. J., Wasley, J., King, C. K., Doube, J. and Nugegoda, D. 2011. Response of stream invertebrate communities to vegetation damage from overgrazing by exotic rabbits on subantarctic Macquarie Island. *Marine and Freshwater Research.* 62 (4) 404–413. DOI:10.1071/MF10317.

Marcott, S. A., Shakun, J. D., Clark, P. U. and Mix, A. C. 2013. A Reconstruction of Regional and Global Temperature for the Past 11,300 Years. *Science.* 339 (6124) 1198–1201. DOI:10.1126/science.1228026.

MARGO Project Members. 2009. Constraints on the magnitude and patterns of ocean cooling at the Last Glacial Maximum. *Nature Geoscience.* 2, 127–132. DOI:10.1038/ngeo411

Masson, V., Vimeux, F., Jouzel, J., Morgan, V., Delmotte, M., Ciais, P., Hammer, C., Johnsen, S., Lipenkov, V. Y., Mosley-Thompson, E., Petit, J. R., Steig, E. J., Stievenard, M. and Vaikmae, R. 2000. Holocene climate variability in Antarctica based on 11 ice-core isotopic records. *Quaternary Research.* 54 (3) 348–358. DOI:10.1006/qres.2000.2172.

Masson-Delmotte, V., Buiron, D., Ekaykin, A., Frezzotti, M., Gallée, H., Jouzel, J., Krinner, G., Landais, A., Motoyama, H., Oerter, H., Pol, H., Pollard, D., Ritz, C., Schlosser, E., Sime, L. C. Sodemann, H., Stenni, B., Uemura, R. and Vimeux, F. 2011. A comparison of the present and last interglacial periods in six Antarctic ice cores. *Climate of the Past.* 7, 397–423. DOI:10.5194/cp-7-397-2011.

Matsumoto, G. I., Tani, Y., Seto, K., Tazawa, T., Yamamuro, M., Watanabe, T., Nakamura, T., Takemura, T., Imura, S. and Kanda, H. 2010. Holocene paleolimnological changes in Lake Skallen Oike in the Syowa Station area of Antarctica inferred from organic components in a sediment core (Sk4C-02). *Journal of Paleolimnology.* 44 (2) 677–693. DOI:10.1007/s10933-010-9448-y.

Mayewski, P. A., Rohling, E. E., Curt Stager, J., Karlén, W., Maasch, K. A., David Meeker, L., Meyerson, E. A., Gasse, F., van Kreveld, S., Holmgren, K., Lee-Thorp, J., Rosqvist, G., Rack, F., Staubwasser, M., Schneider, R. R. and Steig, E. J. 2004. Holocene climate variability. *Quaternary Research*. 62 (3) 243–255. DOI:10.1016/j.yqres.2004.07.001.

McClymont, E. L., Ganeshram, R. S., Pichevin, L. E., Talbot, H. M., van Dongen, B. E., Thunell, R. C., Haywood, A. M., Singarayer, J. S. and Valdes, P. J. 2012. Sea-surface temperature records of Termination 1 in the Gulf of California: Challenges for seasonal and interannual analogues of tropical Pacific climate change. *Paleoceanography*. 27, PA2202, DOI:10.1029/2011PA002226.

McDougall, I., Verwoerd, W. and Chevallier, L. 2001. K-Ar geochronology of Marion Island, Southern Ocean. *Geological Magazine*. 138 (1) 1–17.

McGlone, M. S., Turney, C. S. M., Wilmshurst, J. M., Renwick, J. and Pahnke, K. 2010. Divergent trends in land and ocean temperature in the Southern Ocean over the past 18,000 years. *Nature Geoscience.* 3 (9) 622–626. DOI:10.1038/ngeo931.

McGowan, S. 2007. Pigment studies. In: *Encyclopedia of Quaternary Science*. Edited by Elias, S. A. pp. 2062–2074.

Meeker, L. D. and Mayewski, P. A. 2002. A 1400-year high-resolution record of atmospheric circulation over the North Atlantic and Asia. *The Holocene*. 12 (3) 257–266. DOI:10.1191/0959683602hl542ft.

Met READER. 2015. Antarctic Climate Data, Results from the SCAR READER project. http://www.antarctica.ac.uk/met/READER/ Accessed 07/01/15.

Michalchuk, B. R., Anderson, J. B., Wellner, J. S., Manley, P. L., Majewski, W. and Bohaty, S. 2009. Holocene climate and glacial history of the northeastern Antarctic Peninsula: the marine sedimentary record from a long SHALDRIL core. *Quaternary Science Reviews.* 28, 3049–3065. DOI:10.1016/j.quascirev.2009.08.012.

Mikomägi, A., and Punning, J. 2007. Fossil pigments in surface sediments of some Estonian lakes. *Proc. Estonian Acad. Sci. Biol. Ecol*. 56 (3) 239–250.

Milliken, K. T., Anderson, J. B., Wellner, J. S., Bohaty, S. M. and Manley, P. L. 2009. High resolution climate record from Maxwell Bay, South Shetland Islands, Antarctic. *Geological Society of America Bulletin.* 121 (11/12) 1711–1725. DOI:10.1130/B26478.1.

Morellón, M., Valero-Garcés, B., González-Sampériz, P., Vegas-Vilarrúbia, T., Rubio, E., Rieradevall, M., Delgado-Huertas, A., Mata, P., Romero, O., Engstrom, D. R., López-Vicente, M., Navas, A. and Soto, J. 2011. Climate changes and human activities recorded in the sediments of Lake Estanya (NE Spain) during the Medieval Warm Period and Little Ice Age. *Journal of Paleolimnology*. 46 (3) 423–452. DOI:10.1007/s10933-009-9346-3.

Moreno, P. I., Francois, J. P., Moy, C. M. and Villa-Martinez, R. 2010. Covariability of the Southern Westerlies and atmospheric CO(2) during the Holocene. *Geology*. 38 (8) 727–730. DOI:10.1130/G30962.1.

Moy, C. M., Dunbar, R. B., Moreno, P. I., Francois, J-P., Villa-Martínez, R., Mucciarone, D. M., Guilderson, T. P. and Garreaud, R. D. 2008. Isotopic evidence for hydrologic change related to the westerlies in SW Patagonia, Chile, during the last millennium. *Quaternary Science Reviews*. 27 (13–14) 1335–1349. DOI:10.1016/j.quascirev.2008.03.006.

Mulvaney, R., Abram, N. J., Hindmarsh, R. C. A., Arrowsmith, C., Fleet, L., Triest, J., Sime, L. C., Alemany, O. and Foord, S. 2012. Recent Antarctic Peninsula warming relative to Holocene climate and ice-shelf history. *Nature.* 489 (7414) 141–204. DOI:10.1038/nature11391.

Naeher, S., Peterse, F., Smittenberg, R. H., Niemann, H., Zigah, P. K. and Schubert, C. J. 2014. Sources of glycerol dialkyl glycerol tetraethers (GDGTs) in catchment soils, water column and sediments of Lake Rotsee (Switzerland) – Implications for the application of GDGT-based proxies for lakes. *Organic Geochemistry*. 66, 164–173. DOI:10.1016/j.orggeochem.2013.10.017.

Neukom, R., Gergis, J., Karoly, D. J., Wanner, H., Curran, M., Elbert, J., Gonzalez-Rouco, F., Linsley, B. K., Moy, A. D., Mundo, I., Raible, C. C., Steig, E. J., van Ommen, T., Vance, T., Villalba, R., Zinke, J. and Frank, D. 2014. Inter-hemispheric temperature variability over the past millennium. *Nature Climate Change*. 4 (5) 362–367. DOI:10.1038/nclimate2174.

Neukom, R., Luterbacher, J., Villalba, R., Küttel, M., Frank, D., Jones, P. D., Grosjean, M., Wanner, H., Aravena, J.-C., Black, D. E., Christie, D. A., D'Arrigo, R., Lara, A., Morales, M., Soliz-Gamboa, C., Srur, A., Urrutia, R. and von Gunten, L. 2010. Multiproxy summer and winter surface air temperature field reconstructions for southern South America covering the past centuries. *Climate Dynamics*. 37 (1–2) 35–51. DOI:10.1007/s00382-010-0793-3.

Niemann, H., Stadnitskaia, A., Wirth, S. B., Gilli, A., Anselmetti, F. S., Sinninghe Damsté, J. S., Schouten, S., Hopmans, E. C. and Lehmann, M. F. 2012. Bacterial GDGTs in Holocene sediments and catchment soils of a high Alpine lake: application of the MBT/CBT-paleothermometer. *Climate of the Past*. 8 (3) 889–906. DOI:10.5194/cp-8-889-2012.

Noon, P. E., Leng, M. J. and Jones, V. J. 2003. Oxygen-isotope (δ18O) evidence of Holocene hydrological changes at Signy Island, maritime Antarctica. *The Holocene*. 13 (2) 251–263. DOI:10.1191/0959683603hl611rp.

Oksanen, J., Blanchet, F. G., Kindt, R., Legendre, P., Minchin, P. R., O'Hara, R.B., Simpson, G. L., Solymos, P., Stevens, H. M. H. and Wagner H. 2014. Vegan: Community Ecology Package. R package version 2.3-0. http://cran.r-project.org/web/packages/vegan/index.html.

Oppermann, B. I., Michaelis, W., Blumenberg, M., Frerichs, J., Schulz, H. M., Schippers, A., Beaubien, S. E. and Krüger, M. 2010. Soil microbial community changes as a result of long-term exposure to a natural CO2 vent. *Geochimica et Cosmochimica Acta*. 74, 2697–2716. DOI:10.1016/j.gca.2010.02.006

Parkinson, C. L. 2002. The puzzle of polar sea-ice changes. *AAAS Annual Meeting and Science Innovation Exposition.* 168, A24.

Pearson, E. J., Juggins, S. and Farrimond, P. 2008. Distribution and significance of long-chain alkenones as salinity and temperature indicators in Spanish saline lake sediments. *Geochimica et Cosmochimica Acta*. 72 (16) 4035–4046. DOI:10.1016/j.gca.2008.05.052.

Pearson, E. J., Juggins, S., Talbot, H. M., Weckstrom, J., Rosen, P., Ryves, D. B., Roberts, S. J. and Schmidt, R. 2011. A lacustrine GDGT-temperature calibration from the Scandinavian Arctic to Antarctic: Renewed potential for the application of GDGT-paleothermometry in lakes. *Geochimica Et Cosmochimica Acta*. 75 (20) 6225–6238. DOI:10.1016/j.gca.2011.07.042.

Peters, K.E., Walters, C.C. and Moldowan, J.M. 2005. *The Biomarker Guide: Biomarkers and Isotopes in Petroleum Exploration and Earth History.* Cambridge University Press, New York.

Peterse, F., Hopmans, E. C., Schouten, S., Mets, A., Rijpstra, W. I. C. and Sinninghe Damsté, J. S. 2011. Identification and distribution of intact polar branched tetraether lipids in peat and soil. *Organic Geochemistry.* 42 (9) 1007–1015. DOI:10.1016/j.orggeochem.2011.07.006

Peterse, F., Kim, J-H., Schouten, S., Kristensen, D. K., Koç, N. and Sinninghe Damsté, J. S. 2009a. Constraints on the application of the MBT/CBT palaeothermometer at high latitude environments (Svalbard, Norway). *Organic Geochemistry*. 40 (6) 692–699. DOI:10.1016/j.orggeochem.2009.03.004.

Peterse, F., Schouten, S., van der Meer, J., ven der Meer, M. T. J. and Sinninghe Damsté, J. S. 2009c. Distribution of branched tetraether lipids in geothermally heated soils: Implications for the MBT/CBT temperature proxy. *Organic Geochemistry*. 40 (2) 201-205. DOI:10.1016/j.orggeochem.2008.10.010.

Peterse, F., van der Meer, J., Schouten, S., Jia, G., Ossebaar, J., Blokker, J. and Sinninghe Damsté, J. S. 2009b. Assessment of soil *n*-alkane *δD* and branched tetraether membrane lipid distributions as tools for paleoelevation reconstruction. *Biogeosciences Discuss*. 6, 8609–8631.

Peterse, F., van der Meer, J., Schouten, S., Weijers, J. W. H., Fierer, N., Jackson, R. B., Kim, J-H. Sinninghe Damsté, J. S. 2012. Revised calibration of the MBT–CBT paleotemperature proxy based on branched tetraether membrane lipids in surface soils. *Geochimica et Cosmochimica Acta*. 96, 215–229. DOI: 10.1016/j.gca.2012.08.011.

Peterse, F., Vonk, J., Holmes, M., Giosan, L., Zimov, N. and Eglinton, T. I. 2014. Branched glycerol dialkyl glycerol tetraethers in Arctic lake sediments: Sources and implications for paleothermometry at high latitudes. *Journal of Geophysical Research, Biogeosciences*. 119, 1738–1754. DOI:10.1002/2014JG002639.

Peterson, L. C., Haug, G. H., Hughen, K. A. and Röhl, U. 2000. Rapid Changes in the Hydrologic Cycle of the Tropical Atlantic During the Last Glacial. *Science.* 290 (5498) 1947–1951. DOI:10.1126/science.290.5498.1947.

Pitcher, A., Hopmans, E. C., Schouten, S. and Sinninghe Damsté, J. S. 2009. Separation of core and intact polar Archaeal tetraether lipids using silica columns: Insights into living and fossil biomass contributions. *Organic Geochemistry*. 40 (1) 12–19. DOI:10.1016/j.orggeochem.2008.09.008.

Placzek, C., Quade, J. and Patchett, P. J. 2006. Geochronology and stratigraphy of late Pleistocene lake cycles on the southern Bolivian Altiplano: Implications for causes of tropical climate change. *Geological Society of America Bulletin.* 118 (5–6) 515–532. DOI:10.1130/B25770.1.

Powers, L. A., Johnson, T. C., Werne, J. P. and Castañeda, I. S. 2005. Large temperature variability in the southern African tropics since the Last Glacial Maximum. *Geophysical Research Letters.* 32 (L08706). DOI:10.1029/2004GL022014.

Powers, L. A., Werne, J. P., Johnson, T. C., Hopmans, E. C., Damsté, J. S. S. and Schouten, S. 2004. Crenarchaeotal membrane lipids in lake sediments: A new paleotemperature proxy for continental paleoclimate reconstruction? *Geology*. 32 (7) 613–616. DOI:10.1130/G20434.1.

Powers, L. A., Werne, J. P., Vanderwoude, A. J., Sinninghe Damsté, J. S., Hopmans, E. C. and Schouten, S. 2010. Applicability and calibration of the TEX_{86} paleothermometer in lakes. *Organic Geochemistry*. 41 (4) 404–413. DOI:10.1016/j.orggeochem.2009.11.009.

Prinsloo, L. C., Colomban, P., Brink, J. D. and Meiklejohn, I. 2010. A Raman spectroscopic study of the igneous rocks on Marion Island: a possible terrestrial analogue for the geology on Mars. *Journal of Raman Spectroscopy*. 42 (4) 626–632. DOI:10.1002/jrs.2756.

Pritchard, H. D. and Vaughan, D. G. 2007. Widespread acceleration of tidewater glaciers on the Antarctic Peninsula. *Journal of Geophysical Research*. 112 (F03S29) DOI:10.1029/2006JF000597.

Pudsey, C. J., Murray, J. W., Appleby, P. and Evans, J. 2006. Ice shelf history from petrographic and foraminiferal evidence, Northeast Antarctic Peninsula. *Quaternary Science Reviews.* 25 (17–18) 2357–2379. DOI:10.1016/j.quascirev.2006.01.029.

Putnam, A. E., Denton, G. H., Schaefer, J. M., Barrell, D. J. A., Andersen, B. G., Finkel, R. C., Schwartz, R., Doughty, A. M., Kaplan, M. R. and Schluechter, C. 2010. Glacier advance in southern middle-latitudes during the Antarctic Cold Reversal. *Nature Geoscience*. 3 (10) 700–704. DOI:10.1038/ngeo962.

Quayle, W. C., Peak, L. S., Peat, H., Ellis-Evans. J. C. and Harrigan, P. R. 2002. Extreme Responses to Climate Change in Antarctic Lakes. *Science*. 295, 645. DOI:10.1126/science.1064074.

R Core Team (2014). R: A language and environment for statistical computing. R Foundation for Statistical Computing, Vienna, Austria. URL http://www.R-project.org/.

Reimer, R. and Reimer, P. 2004. *CALIBomb – Calibration of postbomb C-14 data*. Available at: http://www.calib.org.

Reimer, P. J., Bard, E., Bayliss, A., Beck, J. W., Blackwell, P. G., Bronk-Ramsey, C., Buck, C. E., Cheng, H., Edwards, R. L., Friedrich, M., Grootes, P. M., Guilderson, T. P., Haflidason, H., Hajdas, I., Hatté, C., Heaton, T. J., Hoffmann, D. L., Hogg, A. G., Hughen, K. A., Kaiser, K. F., Kromer, B., Manning, S. W., Niu, M., Reimer, R. W., Richards, D. A., Scott, E. M., Southon, J. R., Staff, R. A., Turney, C. S. M. and van der Plicht, J. 2013. INTCAL13 and MARINE13 Radiocarbon Age Calibration Curves 0–50,000 Years Cal BP. *Radiocarbon*. 55 (4) 1869–1887.

Rein, B., Lückge, A. and Sirocko, F. 2004. A major Holocene ENSO anomaly during the Medieval period. *Geophysical Research Letters*. 31 (17), 2–5. DOI:10.1029/2004GL020161.

Reinemann, S. A., Porinchu, D. F. and Mark, B. G. 2014. Regional Climate Change Evidenced by Recent Shifts in Chironomid Community Composition in Subalpine and Alpine Lakes in the Great Basin of the United States. Arctic, Antarctic, and Alpine Research. 46 (3) 600–615. DOI: 10.1657/1938-4246-46.3.600.

Renssen, H., Goosse, H., Fichefet, T., Masson-Delmotte, V. and Koc, N. 2005. Holocene climate evolution in the high-latitude Southern Hemisphere simulated by a coupled atmosphere-sea ice-ocean-vegetation model. *The Holocene*. 15 (7) 951–964. DOI:10.1191/0959683605hl869ra.

Reuss, N., and Conley, D. 2005. Effects of sediment storage conditions on pigment analyses. *Limnology and Oceanography: Methods*. 3, 477–487. DOI:10.4319/lom.2005.3.477.

Reuss, L., Leavitt, P. R., Hall, R. I., Bigler, C. and Hammarlund, D. 2010. Development and application of sedimentary pigments for assessing effects of climatic and environmental changes on subarctic lakes in northern Sweden. *Journal of Paleolimnology*. 43, 149–169. DOI:10.1007/s10933-009-9323-x.

Roberts, D., McMinn, A., Cremer, H., Gore, D. B. and Melles, M. 2004. The Holocene evolution and palaeosalinity history of Beall Lake, Windmill Islands (East Antarctica) using an expanded diatom-based weighted averaging model. *Palaeogeography Palaeoclimatology Palaeoecology*. 208 (1–2) 121–140. DOI:10.1016/j.palaeo.2004.02.032.

Roberts, S. J., Hodgson, D. A., Bentley, M. J., Sanderson, D. C. W., Milne, G., Smith, J.A., Verleyen, E. and Balbo, A. 2009. Holocene relative sea-level change and deglaciation on Alexander Island, Antarctic Peninsula, from elevated lake deltas. *Geomorphology.* 112 (1–2) 122–134. DOI:10.1016/j.geomorph.2009.05.011.

Roberts, S. J., Hodgson, D. A., Bentley, M. J., Smith, J. A., Millar, I. L., Olive, V. and Sugden, D. E. 2008. The Holocene history of George VI Ice Shelf, Antarctic Peninsula from clast-provenance analysis of epishelf lake sediments. *Palaeogeography Palaeoclimatology Palaeoecology*. 259 (2–3) 258–283. DOI:10.1016/j.palaeo.2007.10.010.

Roberts, S. J., Hodgson, D. A., Shelley, S., Royles, J., Griffiths, H. J., Deen, T. J. and Thorne, M. A. S. 2010. Establishing Lichenometric Ages For Nineteenth- And Twentieth-Century Glacier Fluctuations On South Georgia (South Atlantic). *Geografiska Annaler: Series A, Physical Geography*. 92 (1) 125–139. DOI:10.1111/j.1468-0459.2010.00382.x.

Roberts, S. J., Hodgson, D. A., Sterken, M., Whitehouse, P. L., Verleyen, E., Vyverman, W., Sabbe, K., Balbo, A., Bentley, M. J. and Moreton, S. G. 2011. Geological constraints on glacio-isostatic adjustment models of relative sea-level change during deglaciation of Prince Gustav Channel, Antarctic Peninsula. *Quaternary Science Reviews.* 30 (25–26) 3603–3617. DOI:10.1016/j.quascirev.2011.09.009.

Rojas, M., Moreno, P., Kageyama, M., Crucifix, M., Hewitt, C., Abe-Ouchi, A., Ohgaito, R., Brady, E. C. and Hope, P. 2009. The Southern Westerlies during the last glacial maximum in PMIP2 simulations. *Climate Dynamics*. 32 (4) 525–548. DOI:10.1007/s00382-008-0421-7.

Rolland, N., Larocque, I., Francus, P., Pienitz, R., Laperriere, L., 2009. Evidence for a warmer period during the 12th and 13th centuries AD from chironomid assemblages in Southampton Island, Nunavut, Canada. *Quaternary Research.* 72, 27–37. DOI:10.1016/j.yqres.2009.03.001.

Rosén, P. 2005. Total organic carbon (TOC) of lake water during the Holocene inferred from lake sediments and near-infrared spectroscopy (NIRS) in eight lakes from northern Sweden. *Biogeochemistry.* 76, 503–516. DOI:10.1007/s10533-005-8829-1.

Rosqvist, G. C. and Schuber, P. 2003. Millennial-scale climate changes on South Georgia, Southern Ocean. *Quaternary Research.* 59 (3) 470–475. DOI:10.1016/S0033-5894(03)00036-X.

Rosqvist, G., Rietti-Shati, M. and Shemesh, A. 1999. Late glacial to middle Holocene climatic record of lacustrine biogenic silica oxygen isotopes from a Southern Ocean island. *Geology.* 27 (11) 967–970. DOI:10.1130/0091-7613(1999).

Rouault, M., Melice, J. L., Reason, C. J. C. and Lutijeharms, J. R. E. 2005. Climate variability at Marion Island, Southern Ocean, since 1960. *Journal of Geophysical Research.* 110 (C05007) DOI:10.1029/2004JC002492.

Sabbe, K., Hodgson, D. A., Verleyen, E., Taton, A., Wilmotte, A., Vanhoutte, K., and Vyverman, W. 2004. Salinity, depth and the structure and composition of microbial mats in continental Antarctic lakes. Freshwater Biology. 49, 296–319. DOI: 10.1111/j.1365-2427.2004.01186.x.

Sasaki, M., Endoh, N., Imura, S., Kudoh, S., Yamanouchi, T., Morimoto, S. and Hashida, G. 2010. Air-lake exchange of methane during the open water season in Syowa Oasis, East Antarctica. *Journal of Geophysical Research*. 115 (D16313) DOI:10.1029/2010JD013822.

Saunders, K. M., Hodgson, D. A., McMurtrie, S. and Grosjean, M. 2015. A diatom–conductivity transfer function for reconstructing past changes in the Southern Hemisphere westerly winds over the Southern Ocean. *Journal of Quaternary Scicence.* 30 (5) 464-477. DOI: 10.1002/jqs.2788.

Saunders, K. M., Hodgson, D. A. and McMinn, A. 2009. Quantitative relationships between benthic diatom assemblages and water chemistry in Macquarie Island lakes and their potential for reconstructing past environmental changes. *Antarctic Science.* 21 (1) 35–49. DOI:10.1017/S0954102008001442.

Schoon, P. L., de Kluijver, A., Middelburg, J. J., Downing, J. A., Sinninghe Damsté, J. S. and Schouten, S. 2013. Influence of lake water pH and alkalinity on the distribution of core and intact polar branched glycerol dialkyl glycerol tetraethers (GDGTs) in lakes. *Organic Geochemistry*. 60, 72–82. DOI:10.1016/j.orggeochem.2013.04.015.

Schouten, S., Hopmans, E. C., Pancost, R. D. and Sinninghe Damsté, J. S. 2000. Widespread occurrence of structurally diverse tetraether membrane lipids: evidence for the ubiquitous presence of low-temperature relatives of hyperthermophiles. *Proceedings of the National Academy of Sciences of the United States of America.* 97 (26) 14421–14426. DOI:10.1073/pnas.97.26.14421.

Schouten, S., Hopmans, E. C., Schefuß, E. and Sinninghe Damsté, J. S. 2002. Distributional variations in marine crenarchaeotal membrane lipids: a new tool for reconstructing ancient sea water temperatures? *Earth and Planetary Science Letters.* 204, 265–274. DOI:10.1016/S0012-821X(02)00979-2.

Schouten, S., Hopmans, E. C. and Sinninghe Damsté, J. S. 2013. The organic geochemistry of glycerol dialkyl glycerol tetraether lipids: A review. *Organic Geochemistry. 54*, 19–61. DOI:10.1016/j.orggeochem.2012.09.006.

Schouten, S., Rijpstra, W. I. C., Durisch-Kaiser, E., Schubert, C. J. and Sinninghe Damsté, J. S. 2012. Distribution of glycerol dialkyl glycerol tetraether lipids in the water column of Lake Tanganyika. *Organic Geochemistry*. 53, 34–37. DOI:10.1016/j.orggeochem.2012.01.009.

Scott, J. J. and Kirkpatrick, J. B. 2013. Changes in the cover of plant species associated with climate change and grazing pressure on the Macquarie Island coastal slopes, 1980–2009. *Polar Biology.* 36 (1) 127–136. DOI: 10.1007/s00300-012-1243-y.

Seki, O., Schmidt, D. N., Schouten, S., Hopmans, E. C., Sinninghe Damsté, J. S. and Pancost, R. D. 2012. Paleoceanographic changes in the Eastern Equatorial Pacific over the last 10 Myr. *Paleoceanography*. 27, PA3224, DOI:10.1029/2011PA002158.

Sepúlveda, J., Pantoja, S., Hughen, K. a., Bertrand, S., Figueroa, D., León, T., Drenzek, N. J. and Lange, C. 2009. Late Holocene sea-surface temperature and precipitation variability in northern Patagonia, Chile (Jacaf Fjord, 44°S). *Quaternary Research*. 72 (3) 400–409. DOI:10.1016/j.yqres.2009.06.010.

Shakun, J. D. and Carlson, A. E. 2010. A global perspective on Last Glacial Maximum to Holocene climate change. *Quaternary Science Reviews*. 29 (15–16) 1801–1816. DOI:10.1016/j.quascirev.2010.03.016.

Shanahan, T. M., Hughen, K. A. and Van Mooy, B. A. S. 2013. Temperature sensitivity of branched and isoprenoid GDGTs in Arctic lakes. *Organic Geochemistry*. 64, 119–128. DOI:10.1016/j.orggeochem.2013.09.010.

Shevenell, A., Domack, E. W. and Kernan, G. M. 1996. Record of Holocene palaeoclimate change along the Antarctic Peninsula: evidence from glacial marine sediments, Lallemand Fjord. *Papers and Proceedings of the Royal Society of Tasmania*. 130 (2) 55–64.

Shevenell, A., Ingalls, A., Domack, E. W. and Kelly, C. 2011. Holocene Southern Ocean surface temperature variability west of the Antarctic Peninsula. *Nature*. 470 (7333) 250–254. DOI:10.1038/nature09751.

Sime, L. C., Risi, C., Tindall, J. C., Sjolte, J., Wolff , E. W., Masson-Delmotte, V. and Capron, E. 2013. Warm climate isotopic simulations: what do we learn about interglacial signals in Greenland ice cores? *Quaternary Science Reviews*. 67, 59–80. DOI:10.1016/j.quascirev.2013.01.009

Sinninghe Damsté, J. S., Hopmans, E. C., Pancost, R. D., Schouten, S. and Geenevasen, J. A. J. 2000. Newly discovered non-isoprenoid glycerol dialkyl glycerol tetraether lipids in sediments. *Chemical Communications*. 17, 1683–1684. DOI:10.1039/B004517I.

Sinninghe Damsté, J. S., Ossebaar, J., Abbas, B., Schouten, S. and Verschuren, D. 2009. Fluxes and distribution of tetraether lipids in an equatorial African lake: Constraints on the application of the TEX86 palaeothermometer and BIT index in lacustrine settings. *Geochimica et Cosmochimica Acta*. 73 (14) 4232–4249. DOI:10.1016/j.gca.2009.04.022.

Sinninghe Damsté, J. S., Ossebaar, J., Schouten, S. and Verschuren, D. 2012. Distribution of tetraether lipids in the 25-ka sedimentary record of Lake Challa: extracting reliable TEX_{86} and MBT/CBT palaeotemperatures from an equatorial African lake. *Quaternary Science Reviews*. 50, 43–54. DOI:10.1016/j.quascirev.2012.07.001

Sinninghe Damsté, J. S., Schouten, S., Hopmans, E. C., Van Duin, A. C. T. and Geenevasen, J. A. J. 2002. Crenarchaeol: the characteristic core glycerol dibiphytanyl glycerol tetraether membrane lipid of cosmopolitan pelagic Crenarchaeota. *The Journal of Lipid Research.* 43 (10) 1641–1651. DOI:10.1194/jlr.M200148-JLR200.

Smith, D. A, and Klinck, J. M. 2002. Water properties on the west Antarctic Peninsula continental shelf: a model study of effects of surface fluxes and sea ice. *Deep Sea Research Part II: Topical Studies in Oceanography*. 49, 4863–4886. DOI:10.1016/S0967-0645(02)00163-7.

Smith, D. A., Hofmann, E. E., Klinck, J. M. and Lascara, C. M. 1999. Hydrography and circulation of the West Antarctic Peninsula Continental Shelf. *Deep-Sea Research Part I: Oceanographic Research Papers.* 46, 925–949. DOI:10.1016/S0967-0637(98)00103-4.

Smith, J. A., Bentley, M. J., Hodgson, D. A., Roberts, S. J., Leng, M. J., Lloyd, J. M., Barrett, M. S., Bryant, C. and Sugden, D. E. 2007. Oceanic and atmospheric forcing of early Holocene ice shelf retreat, George VI Ice Shelf, Antarctica Peninsula. *Quaternary Science Reviews*. 26 (3–4) 500–516. DOI:10.1016/j.quascirev.2006.05.006.

Smith, V. R. 2002. Climate change in the sub-Antarctic: An illustration from Marion Island. *Climatic Change.* 52 (3) 345–357. DOI:10.1023/A:1013718617277.

Spang, A., Hatzenpichler, R., Brochier-Armanet, C., Rattei, T., Tischler, P., Spieck, E., Streit, W., Stahl, D. A., Wagner, M. and Schleper, C. 2010. Distinct gene set in two different lineages of ammonia-oxidizing Archaea supports the phylum *Thaumarchaeota. Trends in microbiology.* 18 (8) 331–340. DOI:10.1016/j.tim.2010.06.003.

Spaulding, S., McKnight, D., Stoermer, E. and Doran, P. T. 1997. Diatoms in sediments of perennially ice-covered Lake Hoare, and implications for interpreting lake history in the McMurdo Dry Valleys of Antarctica. *Journal of Paleolimnology*. 17, 403–420. DOI:10.1023/A:1007931329881.

Spero, H. J., Bijma, J., Lea, D. W. and Bemis, B. E. 1997. Effect of seawater carbonate concentration on foraminiferal carbon and oxygen isotopes. *Nature*. 390, 497–500. DOI:10.1038/37333.

Squier, A. H., Hodgson, D. A., and Keely, B. J. 2002. Sedimentary pigments as markers for environmental change in an Antarctic lake. *Organic Geochemistry*. 33 (12) 1655–1665. DOI:10.1016/S0146-6380(02)00177-8.

Stammerjohn, S. E., Martinson, D. G., Smith, R. C., Yuan, X. and Rind, D. 2008. Trends in Antarctic annual sea ice retreat and advance and their relation to El Niño–Southern Oscillation and Southern Annular Mode variability. *Journal of Geophysical Research.* 113 (C3) C03S90. DOI:10.1029/2007JC004269.

Stenni, B., Buiron, D., Frezzotti, M., Albani, S., Barbante, C., Bard, E., Barnola, J. M., Baroni, M., Baumgartner, M., Bonazza, M., Capron, E., Castellano, E., Chappellaz, J., Delmonte, B., Falourd, S., Genoni, L., Iacumin, P., Jouzel, J., Kipfstuhl, S., Landais, A., Lemieux-Dudon, B., Maggi, V., Masson-Delmotte, V., Mazzola, C., Minster, B., Montagnat, M., Mulvaney, R., Narcisi, B., Oerter, H., Parrenin, F., Petit, J. R., Ritz, C., Scarchilli, C., Schilt, A., Schüpbach, S., Schwander, J., Selmo, E., Severi, M., Stocker, T. F. and Udisti, R. 2010. Expression of the bipolar see-saw in Antarctic climate records during the last deglaciation. *Nature Geoscience*. 4 (1) 46–49. DOI:10.1038/ngeo1026.

Sterken, M., Roberts, S. J., Hodgson, D. A., Vyverman, W., Balbo, A. L., Sabbe, K., Moreton, S. G. and Verleyen, E. 2012. Holocene glacial and climate history of Prince Gustav Channel, northeastern Antarctic Peninsula. *Quaternary Science Reviews.* 31, 93–111. DOI:10.1016/j.quascirev.2011.10.017.

Sterken, M., Verleyen, E., Sabbe, K., Terryn, G., Charlet, F., Bertrand, S., Boës, X., Fagel, N., De Batist, M, and Vyverman, W. 2008. Late Quaternary climatic changes in southern Chile, as recorded in a diatom sequence of Lago Puyehue (40°40′ S). *Journal of Paleolimnology*. 39, 219–235. DOI:10.1007/s10933-007-9114-1.

Strother, S. L. Salzmann, U., Roberts, S. J. Hodgson, D. A., Woodward, J., Van Nieuwenhuyze, W., Verleyen, E., Vyverman, W. and Moreton, S. G. 2015. Holocene vegetation and change of westerly winds reconstructed from a high-resolution sub-Antarctic pollen record at Fan Lake, South Georgia. *The Holocene.* 25 (2) 263–279. DOI: 10.1177/0959683614557576.

Summerhayes, C. 2009. The Antarctic Environment in the Global System. In: *Antarctic Climate Change and the Environment.* Edited by: Turner, J., Bindschadler, R., Convey, P., di Prisco, G., Fahrbach, E., Gutt, J., Hodgson, D. A., Mayewski, P. and Summerhayes, C. Scientific Committee on Antarctic Research, Cambridge. Pages 1–32.

Sun, Q., Chu, G., Liu, M., Xie, M., Li, S., Ling, Y., Wang, X., Shi, L., Jia, G. and Lü, H. 2011. Distributions and temperature dependence of branched glycerol dialkyl glycerol tetraethers in recent lacustrine sediments from China and Nepal. *Journal of Geophysical Research*. 116 (G01008) DOI:10.1029/2010JG001365.

Sutton, P. A. and Rowland, S. J. 2012. High temperature gas chromatography-time-of-flight-mass spectrometry (HTGC-ToF-MS) for high-boiling compounds. *Journal of chromatography A*. 1243, 69–80. DOI:10.1016/j.chroma.2012.04.044.

Tan, Z., Han, Y., Cao, J., Huang, C. C. and An, Z. 2015. Holocene wildfire history and human activity from high-resolution charcoal and elemental black carbon records in the Guanzhong Basin of the Loess Plateau, China. *Quaternary Science Reviews*. 109, 76–87. DOI:10.1016/j.quascirev.2014.11.013.

Taylor, F., Whitehead, J. and Domack, E. 2001. Holocene paleoclimate change in the Antarctic Peninsula: evidence from the diatom, sedimentary and geochemical record. *Marine Micropaleontology*. 41 (1–2) 25–43. DOI:10.1016/S0377-8398(00)00049-9.

Telford, R. J. and Birks, H. J. B. 2005. The secret assumption of transfer functions: problems with spatial autocorrelation in evaluating model performance. *Quaternary Science Reviews*. 24 (20–21) 2173–2179. DOI:10.1016/j.quascirev.2005.05.001.

Thomas, E. R., Wolff, E. W., Mulvaney, R., Steffensen, J. P., Johnsen, S. J., Arrowsmith, C., White, J. W. C., Vaughn, B. and Popp, T. 2007. The 8.2 ka event from Greenland ice cores. *Quaternary Science Reviews*. 26 (1–2) 70–81. DOI:10.1016/j.quascirev.2006.07.017.

Thompson, L. G., Mosley-Thompson, E., Davis, M. E., Henderson, K. A., Brecher, H. H., Zagorodnov, V. S., Mashiotta, T. A., Lin, P. N., Mikhalenko, V. N., Hardy, D. R. and Beer, J. 2002. Kilimanjaro ice core records: Evidence of Holocene climate change in tropical Africa. *Science*. 298 (5593) 589–593. DOI:10.1126/science.1073198.

Tierney, J. E. and Russell, J. M. 2007. Abrupt climate change in southeast tropical Africa influenced by Indian monsoon variability and ITCZ migration. *Geophysical Research Letters.* 34 (L15709) DOI:10.1029/2007GL029508.

Tierney, J. E. and Russell, J. M. 2009. Distributions of branched GDGTs in a tropical lake system: Implications for lacustrine application of the MBT/CBT paleoproxy. *Organic Geochemistry*. 40 (9) 1032–1036. DOI:10.1016/j.orggeochem.2009.04.014.

Tierney, J. E. and Tingley, M. P. 2014. A Bayesian, spatially-varying calibration model for the TEX_{86} proxy. *Geochimica et Cosmochimica Acta.* 127, 83–106. DOI:10.1016/j.gca.2013.11.026.

Tierney, J. E., Russell, J. M., Eggermont, H., Hopmans, E. C., Verschuren, D. and Sinninghe Damsté, J. S. 2010a. Environmental controls on branched tetraether lipid distributions in tropical East African lake sediments. *Geochimica et Cosmochimica Acta* .74 (17) 4902–4918. DOI:10.1016/j.gca.2010.06.002.

Tierney, J. E., Russell, J. M. and Huang, Y. 2010b. A molecular perspective on Late Quaternary climate and vegetation change in the Lake Tanganyika basin, East Africa. *Quaternary Science Reviews.* 29 (5–6) 787–800. DOI:10.1016/j.quascirev.2009.11.030.

Tierney, J. E, Russell, J. M., Huang, Y., Sinninghe Damsté, J. S., Hopmans, E. C. and Cohen, A. 2008. Northern hemisphere controls on tropical southeast African climate during the past 60,000 years. *Science*. 322 (5899) 252–255. DOI:10.1126/science.1160485.

Tierney, J. E., Schouten, S., Pitcher, A., Hopmans, E. C. and Sinninghe Damsté, J. S. 2012. Core and intact polar glycerol dialkyl glycerol tetraethers (GDGTs) in Sand Pond, Warwick, Rhode Island (USA): Insights into the origin of lacustrine GDGTs. *Geochimica et Cosmochimica Acta*. 77, 561–581. DOI:10.1016/j.gca.2011.10.018.

Tinner, W. and Lotter, A. F. 2001. Central European vegetation response to abrupt climate change at 8.2 ka. *Geology*. 29 (6) 551–554. DOI:10.1130/0091-7613(2001)029<0551:CEVRTA>2.0.CO;2

Toggweiler, J. R. 2009. Shifting Westerlies. *Science*. 323 (5920) 1434–1435.

Toggweiler, J. R., Russell, J. L. and Carson, S. R. 2006. Midlatitude westerlies, atmospheric CO_2, and climate change during the ice ages. *Paleoceanography*. 21 (2) 1–15. DOI:10.1029/2005PA001154.

Toney, J. L., Huang, Y., Fritz, S. C., Baker, P. A., Grimm, E. and Nyren, P. 2010. Climatic and environmental controls on the occurrence and distributions of long chain alkenones in lakes of the interior United States. *Geochimica et Cosmochimica Acta*. 74 (5) 1563–1578. DOI:10.1016/j.gca.2009.11.021.

Toney, J. L., Leavitt, P. R. and Huang, Y. 2011. Alkenones are common in prairie lakes of interior Canada. *Organic Geochemistry*. 42 (7) 707–712. DOI:10.1016/j.orggeochem.2011.06.014.

Trathan, P. N., Brandon, M. A. and Murphy, E. J. 1997. Characterization of the Antarctic Polar Frontal Zone to the north of South Georgia in summer 1994. *Journal of Geophysical Research*. 102 (C5) 10483–10497. DOI:10.1029/97JC00381.

Trusel, L. D., Frey, K. E. and Das, S. B. 2012. Antarctic surface melting dynamics: Enhanced perspectives from radar scatterometer data. *Journal of Geophysical Research*. 117 (F2) F02023. DOI:10.1029/2011JF002126.

Tucker, M.E., 1981. *An Introduction to Sedimentary Petrology*. Blackwell, Oxford.

Turich, C. Schouten, S., Thunell, R. C., Varela, R. Astor, Y. and Wakeham, S. G. 2013. Comparison of TEX86 and UK'37 temperature proxies in sinking particles in the Cariaco Basin. *Deep-Sea Research I.* 78, 115–133. DOI:10.1016/j.dsr.2013.02.008.

Turner, J., Colwell, S. R., Marshall, G. J., Lachlan-Cope, T. A., Carleton, A. M., Jones, P. D., Lagun, V., Reid, Phil A. and Iagovkina, S. 2005a. Antarctic climate change during the last 50 years. *International Journal of Climatology*. 25 (3) 279–294. DOI:10.1002/joc.1130.

Turner, J., Lachlan-Cope, T., Colwell, S. and Marshall, G. J. 2005b. A positive trend in western Antarctic Peninsula precipitation over the last 50 years reflecting regional and Antarctic-wide atmospheric circulation changes. *Annals of Glaciology*. 41 (1) 85–91. DOI:10.3189/172756405781813177.

Uda, I., Sugai, A, Itoh, Y. H. and Itoh, T. 2001. Variation in molecular species of polar lipids from thermoplasma acidophilum depends on growth temperature. *Lipids.* 36 (1) 103–5. DOI: 10.1007/s11745-001-0914-2.

Van Asch, N., Lutz, A. F., Duijkers, M. C. H., Heiri, O., Brooks, S. J., and Hoek, W. Z. 2012. Rapid climate change during the Weichselian Lateglacial in Ireland: Chironomid-inferred summer temperatures from Fiddaun, Co. Galway. *Palaeogeography, Palaeoclimatology, Palaeoecology*. 315–316, 1–11. DOI:10.1016/j.palaeo.2011.11.003.

Van den Broeke, M. 2000. The Semi-Annual Oscillation and Antarctic Climate. Part 4: A Note on Sea Ice Cover in the Amundsen and Bellingshausen Seas. *International Journal of Climatology*. 20, 455–462. DOI: 10.1002/(SICI)1097-0088(20000330)20:4<455::AID-JOC482>3.0.CO;2-M.

Van der Putten, N., Mauquoy, D., Verbruggen, C. and Bjorck, S. 2012. Subantarctic peatlands and their potential as palaeoenvironmental and palaeoclimatic archives. *Quaternary International*. 268, 65–76. DOI:10.1016/j.quaint.2011.07.032.

Van der Putten, N., Stieperaere, H., Verbruggen, C. and Ochyra, R. 2004. Holocene palaeoecology and climate history of South Georgia (sub-Antarctica) based on a macrofossil record of bryophytes and seeds. *The Holocene.* 14 (3) 382–392 .DOI:10.1191/0959683604hl714rp.

Van der Putten, N., Verbruggen, C., Ochyra, R., Spassov, S., de Beaulieu, J.-L., De Dapper, M., Hus, J. and Thouveny, N. 2009. Peat bank growth, Holocene palaeoecology and climate history of South Georgia (sub-Antarctica), based on a botanical macrofossil record. *Quaternary Science Reviews*. 28 (1–2) 65–79. DOI:10.1016/j.quascirev.2008.09.023.

Van Nieuwenhuyze' W., Roberts, S. J., Verleyen, E., Hodgson, D.A., Sterken, M., Strother, S. L., Salzmann, U., Van der Putten, N., Leng, M., Moreton, S., Balbo, A., Emmings, J., Sabbe, K. and Vyverman, W. In prep. Mid to late Holocene climate change on South Georgia from lake sediment and peat records.

Van Zinderen Bakker, E.M., Coetzee, J.A., 1972. A re-appraisal of late-Quaternary climatic evidence from tropical Africa. *Palaeoecology of Africa*. 7, 151–181.

Varma, V., Prange, M., Lamy, F., Merkel, U. and Schulz, M. 2011. Solar-forced shifts of the Southern Hemisphere Westerlies during the Holocene. *Climate of the Past*. 7 (2) 339–347. DOI:10.5194/cp-7-339-2011.

Varma, V., Prange, M., Merkel, U., Kleinen, T., Lohmann, G., Pfeiffer, M., Renssen, H., Wagner, A., Wagner, S. and Schulz, M. 2012. Holocene evolution of the Southern Hemisphere westerly winds in transient simulations with global climate models. *Climate of the Past.* 8, 391–402. DOI:10.5194/cp-8-391-2012.

Vaughan, D. G. 2006. Recent trends in melting conditions on the Antarctic Peninsula and their implications for ice-sheet mass balance and sea level. *Arctic, Antarctic and Alpine Research*. 38 (1) 147–152.

Vaughan, D. G., Marshall, G. J., Connolley, W. M., King, J. C. and Mulvaney, R. 2001. Devil in the Detail. *Science*. 293 (5536) 1777–1779. DOI:10.1126/science.1065116.

Vaughan, D. G., Marshall, G. J., Connolley, W. M., Parkinson, C., Mulvaney, R., Hodgson, D. A., King, J. C., Pudsey, C. J. and Turner, J. 2003. Recent rapid regional climate warming on the Antarctic Peninsula. *Climatic Change*. 60 (3) 243–274. DOI:10.1023/A:1026021217991.

Verleyen, E., Hodgson, D. A., Gibson, J., Imura, S., Kaup, E., Kudoh, S., De Wever, A., Hoshino, T., McMinn, A., Obbels, D., Roberts, D., Roberts, S., Sabbe, K., Souffreau, C., Tavernier, I., van Nieuwenhuyze, W., van Ranst, E., Vindevogel, N. and Vyverman, W. 2012. Chemical limnology in coastal East Antarctic lakes: monitoring future climate change in centres of endemism and biodiversity. *Antarctic Science*. 24 (1) 23–33. DOI:10.1017/S0954102011000642.

Verleyen, E., Hodgson, D. A., Sabbe, K., Cremer, H., Emslie, S. D., Gibson, J., Hall, B., Imura, S., Kudoh, S., Marshall, G. J., McMinn, A., Melles, M., Newman, L., Roberts, D., Roberts, S. J., Singh, S. M., Sterken, M., Tavernier, I., Verkulich, S., Van de Vyver, E., Van Nieuwenhuyze, W., Wagner, B. and Vyverman, W. 2011. Post-glacial regional climate variability along the East Antarctic coastal margin-Evidence from shallow marine and coastal terrestrial records. *Earth-Science Reviews*. 104 (4) 199–212. DOI:10.1016/j.earscirev.2010.10.006.

Verleyen, E., Hodgson, D. A., Sabbe, K., Vanhoutte, K., and Vyverman, W. 2004. Coastal oceanographic conditions in the Prydz Bay region (East Antarctica) during the Holocene recorded in an isolation basin. *The Holocene*. 14 (2) 246–257. DOI:10.1191/0959683604hl702rp.

Verleyen, E., Hodgson, D. A., Sabbe, K., and Vyverman, W. 2005. Late Holocene changes in ultraviolet radiation penetration recorded in an East Antarctic lake. *Journal of Paleolimnology*. 34 (2) 191–202. DOI:10.1007/s10933-005-4402-0.

Verleyen, E., Hodgson, D. A., Vyverman, W., Roberts, D., McMinn, A., Vanhoutte, K. and Sabbe, K. 2003. Modelling diatom responses to climate induced fluctuations in the moisture balance in continental Antarctic lakes. *Journal of Paleolimnology.* 30 (2) 195–215. DOI:10.1023/A:1025570904093.

Verleyen, E. and Van Nieuwenhuyze, W. 2011. *Marion Island Field Report*. Ghent University, Belgium.

Vimeux, F., Cuffey, K. M. and Jouzel, J. 2002. New insights into Southern Hemisphere temperature changes from Vostok ice cores using deuterium excess correction. *Earth and* Planetary Science Letters. 203, 829–843. DOI:10.1016/S0012-821X(02)00950-0.

Vincent, W., Downes, M., Castenholz, R., and Howard-Williams, C. 1993. Community structure and pigment organisation of cyanobacteria-dominated microbial mats in Antarctica. *European Journal of Phcology*. 28 (4) 213–221. DOI:10.1080/09670269300650321.

Vinebrooke, R. D., Hall, R. I., Leavitt, P. R. and Cumming, B. F. 1998. Fossil pigments as indicators of phototrophic response to salinity and climatic change in lakes of western Canada. *Canadian Journal of Fisheries and Aquatic Sciences*. 55 (3) 668–681. DOI:10.1139/f97-263.

Vinocur, A. and Pizarro, H. 2000. Microbial mats of twenty-six lakes from Potter Peninsula, King George Island, Antarctica. Hydrobiologia. 437, 171–185. DOI:10.1023/A:1026511125146.

Vinocur, A. and Maidana, N. I. 2010. Spatial and temporal variations in moss-inhabiting summer diatom communities from Potter Peninsula (King George Island, Antarctica). *Polar Biology.* 33, 443–455. DOI:10.1007/s00300-009-0719-x.

Wagner, B., Ortlepp, S., Doran, P. T., Kenig, F., Melles, M. and Burkemper, A. 2011. The Holocene environmental history of Lake Hoare, Taylor Valley, Antarctica, reconstructed from sediment cores. *Antarctic Science*. 23 (3) 307–319. DOI:10.1017/S0954102011000125.

Wagner, S., Widmann, M., Jones, J., Haberzettl, T., Lücke, A., Mayr, C., Ohlendorf, C., Schäbitz, F. and Zolitschka, B. 2007. Transient simulations, empirical reconstructions and forcing mechanisms for the Mid-holocene hydrological climate in southern Patagonia. Climate Dynamics. 29 (4) 333–355. DOI:10.1007/s00382-007-0229-x.

Wang, X., Auler, A. S., Edwards, R. L., Cheng, H., Cristalli, P. S., Smart, P. L., Richards, D. A. and Shen, C. C. 2004. Wet periods in northeastern Brazil over the past 210 kyr linked to distant climate anomalies. *Nature.* 432 (7018) 740–743. DOI:10.1038/nature03067.

Wang, Y. J., Cheng, H., Edwards, R.L., An, Z. S., Wu, J. Y., Shen, C. C. and Dorale, J. A. 2001. A high-resolution absolute-dated late Pleistocene Monsoon record from Hulu Cave, China. *Science.* 294 (5550) 2345–8. DOI:10.1126/science.1064618.

Wanner, H., Beer, J., Buetikofer, J., Crowley, T. J., Cubasch, U., Flueckiger, J., Goosse, H., Grosjean, M., Joos, F., Kaplan, J. O., Kuettel, M., Mueller, S. A., Prentice, I. C., Solomina, O., Stocker, T. F., Tarasov, P., Wagner, M. and Widmann, M. 2008. Mid- to Late Holocene climate change: an overview. *Quaternary Science Reviews*. 27 (19–20) 1791–1828. DOI:10.1016/j.quascirev.2008.06.013.

Wanner, H., Mercolli, L., Grosjean, M. and Ritz, S. P. 2014. Holocene climate variability and change; a data-based review. *Journal of the Geological Society*. Published online October 17, 2014. DOI:10.1144/jgs2013-101.

Wanntorp, L., Vajda, V. and Raine, J. I. 2011. Past diversity of Proteaceae on subantarctic Campbell Island, a remote outpost of Gondwana. *Cretaceous Research.* 32 (3) 357–367. DOI:10.1016/j.cretres.2011.01.007.

Watcham, E. P., Bentley, M. J., Hodgson, D. A., Roberts, S. J., Fretwell, P. T., Lloyd, J. M., Larter, R. D., Whitehouse, P. L., Leng, M. J., Monien, P. and Moreton, S. G. 2011. A new Holocene relative sea level curve for the South Shetland Islands, Antarctica. *Quaternary Science Reviews*. 30 (21–22) 3152–3170. DOI:10.1016/j.quascirev.2011.07.021.

Waters, M. N., Piehler, M. F., Smoak, J. M., and Martens, C. S. 2010. The development and persistence of alternative ecosystem states in a large, shallow lake. *Freshwater Biology.* 55 (6) 1249–1261. DOI:10.1111/j.1365-2427.2009.02349.x.

Watson, A. J. and Naveira Garabato, A. C. 2006. The role of Southern Ocean mixing and upwelling in glacial-interglacial atmospheric CO_2 change. *Tellus.* 58 (1) 73–87. DOI:10.1111/j.1600-0889.2005.00167.x.

Weatherly, J. W. 2004. Sensitivity of Antarctic Precipitation to Sea Ice Concentrations in a General Circulation Model. *Journal of Climate*. 17, 3214–3223. DOI:10.1175/1520-0442(2004)017<3214:SOAPTS>2.0.CO;2.

Webb, B. and Nobilis, F. 1997. Long-term Perspective on the Nature of the Air-Water Temperature Relationship: A Case Study. *Hydrological Processes.* 11, 137–147. DOI: 10.1002/(SICI)1099-1085(199702)11:2<137::AID-HYP405>3.0.CO;2-2.

Weijers, J. W. H., Panoto, E., van Bleijswijk, J., Schouten, S., Rijpstra, I. C., Balk, M., Stams, A. J. M. and Sinninghe Damsté, J. S. 2009. Constraints on the Biological Source(s) of the Orphan Branched Tetraether Membrane Lipids. *Geomicrobiology Journal.* 26 (6) 402-414. DOI:10.1080/01490450902937293.

Weijers, J. W. H., Schefuß, E., Schouten, S. and Sinninghe Damsté, J. S. 2007b. Coupled thermal and hydrological evolution of tropical Africa over the last deglaciation. *Science*. 315 (5819) 1701–1704. DOI:10.1126/science.1138131.

Weijers, J. W. H., Schouten, S., Hopmans, E. C., Geenevasen, J. A. J., David, O. R. P., Coleman, J. M., Pancost, R. D. and Sinninghe Damsté, J. S. 2006a. Membrane lipids of mesophilic anaerobic bacteria thriving in peats have typical Archaeal traits. *Environmental microbiology*. 8 (4) 648–657. DOI:10.1111/j.1462-2920.2005.00941.x.

Weijers, J. W. H., Schouten, S., Spaargaren, O. C. and Sinninghe Damsté, J. S. 2006b. Occurrence and distribution of tetraether membrane lipids in soils: Implications for the use of the TEX86 proxy and the BIT index. *Organic Geochemistry*. 37 (12) 1680–1693. DOI:10.1016/j.orggeochem.2006.07.018.

Weijers, J. W. H., Schouten, S., Van den Donker, J. C., Hopmans, E. C. and Sinninghe Damsté, J. S. 2007a. Environmental controls on bacterial tetraether membrane lipid distribution in soils. *Geochimica et Cosmochimica Acta*. 71 (3) 703–713. DOI:10.1016/j.gca.2006.10.003.

Weijers, J. W. H., Steinmann, P., Hopmans, E. C., Schouten, S. and Sinninghe Damsté, J. S. 2011. Bacterial tetraether membrane lipids in peat and coal: Testing the MBT-CBT temperature proxy for climate reconstruction. *Organic Geochemistry*. 42 (5) 477–486. DOI:10.1016/j.orggeochem.2011.03.013.

Woltering, M., Atahan, P., Grice, K., Heijnis, H., Taffs, K. and Dodson, J. 2014. Glacial and Holocene terrestrial temperature variability in subtropical east Australia as inferred from branched GDGT distributions in a sediment core from Lake McKenzie. *Quaternary Research*. 82 (1) 132–145. DOI:10.1016/j.yqres.2014.02.005.

Wright, S. W. and Jeffery S. W. 2006. Pigment Markers for Phytoplankton Production. In: *The Handbook of Environmental Chemistry. Volume 24, Marine Organic Matter: Biomarkers, Isotopes and DNA*. Edited by Volkman, J. K. pp. 71–104.

Wu, X., Dong, H., Zhang, C. L., Liu, X., Hou, W., Zhang, J. and Jiang, H. 2013. Evaluation of glycerol dialkyl glycerol tetraether proxies for reconstruction of the paleo-environment on the Qinghai-Tibetan Plateau. *Organic Geochemistry*. 61, 45–56. DOI:10.1016/j.orggeochem.2013.06.002.

Wu, Y. and Zhu, L. 2008. The response of lake-glacier variations to climate change in Nam Co Catchment, central Tibetan Plateau, during 1970–2000. *Journal of Geographical Sciences*. 18 (2) 177–189. DOI:10.1007/s11442-008-0177-3.

Yang, G., Zhang, C. L., Xie, S., Chen, Z., Gao, M., Ge. Z. and Yang, Z. 2013. Microbial glycerol dialkyl glycerol tetraethers from river water and soil near the Three Gorges Dam on the Yangtze River. *Organic Geochemistry*. 56, 40-50. DOI:10.1016/j.orggeochem.2012.11.014

Yang, H., Ding, W., Zhang, C. L., Wu, X., Ma, X., He, G., Huang, J. and Xie, S. 2011. Occurrence of tetraether lipids in stalagmites: Implications for sources and GDGT-based proxies. *Organic Geochemistry*. 42 (1) 108–115. DOI:10.1016/j.orggeochem.2010.11.006.

Yoon, H. I., Park, B.-K., Kim, Y. and Kim, D. 2000. Glaciomarine sedimentation and its paleoceanographic implications along the fjord margins in the South Shetland Islands, Antarctica during the last 6000 years. *Palaeogeography, Palaeoclimatology, Palaeoecology*. 157 (3–4) 189–211. DOI:10.1016/S0031-0182(99)00165-0.

Zachos, J. C., Schouten, S., Bohaty, S., Quattlebaum, T., Sluijs, A., Brinkhuis, H., Gibbs, S. J. and Bralower, T. J. 2006. Extreme warming of mid-latitude coastal ocean during the Paleocene-Eocene Thermal Maximum: Inferences from TEX86 and isotope data. *Geology*. 34 (9) 737–740. DOI:10.1130/G22522.1.

Zapata, M., Rodríguez, F. and Garrido, J. 2000. Separation of chlorophylls and carotenoids from marine phytoplankton: a new HPLC method using a reversed phase C_8 column and pyridine-containing mobile. *Marine Ecology Progress Series.* 195, 29–45. DOI:10.3354/meps195029.

Zell, C., Kim, J.-H., Moreira-Turcq, P., Abril, G., Hopmans, E. C., Bonnet, M.-P., Lima Sobrinho, R. and Sinninghe Damsté, J. S. 2013. Disentangling the origins of branched tetraether lipids and crenarchaeol in the lower Amazon River: Implications for GDGT-based proxies. *Limnology and Oceanography.* 58 (1) 343–353. DOI:10.4319/lo.2013.58.1.0343.

Zhu, C., Weijers, J. W. H., Wagner, T., Pan, J.-M., Chen, J.-F., and Pancost, R. D. 2011. Sources and distributions of tetraether lipids in surface sediments across a large river-dominated continental margin. *Organic Geochemistry.* 42 (4) 376–386. DOI:10.1016/j.orggeochem.2011.02.002.

Zink, K. G., Vandergoes, M. J., Mangelsdorf, K., Dieffenbacher-Krall, A. C. and Schwark, L. 2010. Application of bacterial glycerol dialkyl glycerol tetraethers (GDGTs) to develop modern and past temperature estimates from New Zealand lakes. *Organic Geochemistry*. 41 (9) 1060–1066. DOI:10.1016/j.orggeochem.2010.03.004.